Arbeitsbericht NAB 20-08

TBO Bülach-1-1: Data Report

Dossier V
Structural Geology

February 2021

National Cooperative
for the Disposal of
Radioactive Waste

Hardstrasse 73
P.O. Box 280
5430 Wettingen
Switzerland
Tel. +41 56 437 11 11

www.nagra.ch

nagra.

Arbeitsbericht NAB 20-08

TBO Bülach-1-1: Data Report

Dossier V Structural Geology

February 2021

A. Ebert[1], L. Gregorczyk[1],
E. Hägerstedt[1] & M. Gysi[2]

[1] Geologiegemeinschaft Strukturgeologie-Experten
Nagra Tiefbohrungen
[2] Nagra

Keywords:
Bülach-1-1, Bülach-1-1B, BUL1-1, BUL1-1B, Nördlich Lägern, TBO, deep drilling campaign, structural geology, goniometry, drill core

National Cooperative for the Disposal of Radioactive Waste

Hardstrasse 73
P.O. Box 280
5430 Wettingen
Switzerland
Tel. +41 56 437 11 11

www.nagra.ch

Nagra Arbeitsberichte NAB ("Working Reports") present the results of work in progress that have not necessarily been subject to a comprehensive review. They are intended to provide rapid dissemination of current information.

This NAB aims at reporting drilling results at an early stage. Additional borehole-specific data will be published elsewhere.

In the event of inconsistencies between dossiers of this NAB, the dossier addressing the specific topic takes priority. In the event of discrepancies between Nagra reports, the chronologically later report is generally considered to be correct. Data sets and interpretations laid out in this NAB may be revised in subsequent reports. The reasoning leading to these revisions will be detailed there.

This Dossier was prepared by a project team consisting of:
A. Ebert (core description, core photograph picking, writing and QC)
L. Gregorczyk (core description, core photograph picking, core goniometry, writing and QC)
E. Hägerstedt (core description, core photograph picking)
K. Decker (QC)
M. Gysi (project management, conceptualisation and QC)

Editorial work: Geomecon, M. Storz and M. Unger

The Dossier has greatly benefitted from technical discussions with, and reviews by, external and internal experts. Their input and work are very much appreciated!

"Copyright © 2021 by Nagra, Wettingen (Switzerland) / All rights reserved.
All parts of this work are protected by copyright. Any utilisation outwith the remit of the copyright law is unlawful and liable to prosecution. This applies in particular to translations, storage and processing in electronic systems and programs, microfilms, reproductions, etc."

Table of Contents

Table of Contents I

List of Tables II

List of Figures III

List of Appendices VIII

1 Introduction 1
1.1 Context 1
1.2 Location and specifications of the borehole 2
1.3 Documentation structure for the BUL1-1 borehole 5
1.4 Scope and objectives of this dossier 6
1.5 Petrophysical logs and preliminary log analysis available 7
1.6 Borehole deviation 8

2 Methodology 9
2.1 Core goniometry 9
2.1.1 Introduction 9
2.1.2 Workflow 9
2.1.3 Dip picking and dip type classification 11
2.1.4 Dip data for non-oriented drill cores 13
2.1.5 Goniometry confidence assessment and uncertainties 15
2.2 Structural work 19
2.3 Geo-statistical evaluation 26

3 Inventory of structure types 29
3.1 Examples of fault planes 29
3.2 Examples of fault zones 36
3.3 Examples of joints 39
3.4 Examples of veins / tension gashes 41
3.5 Examples of stylolites 43
3.6 Examples of open pores 46
3.7 Drilling-induced fractures 49
3.8 Folding 52

4 Geo-statistical evaluation: results 55
4.1 Entire cored borehole section (535 – 1'370.14 m MD log depth) 55
4.1.1 Basic structural dip evaluation 55
4.1.2 Natural structural discontinuities 59
4.1.3 Fracture density (P32) 69
4.1.4 Kinematic indicators 69
4.2 Malm 74

4.2.1 «Felsenkalke» / «Massenkalk» 74
4.2.2 Schwarzbach Formation 81
4.2.3 Villigen Formation 87
4.2.4 Wildegg Formation 94
4.3 Dogger 99
4.3.1 'Brauner Dogger' (Wutach Formation – «Murchisonae-Oolith Formation») 99
4.3.2 Opalinus Clay 105
4.4 Lias (Staffelegg Formation) 108
4.5 Keuper 113
4.5.1 Klettgau Formation 113
4.5.2 Bänkerjoch Formation 118
4.6 Muschelkalk 123
4.6.1 Schinznach Formation 123
4.6.2 Upper and Middle Zeglingen Formation («Dolomitzone» – «Salzlager») 130
4.6.3 Lowermost Zeglingen Formation («Untere Sulfatzone») 135
4.6.4 Kaiseraugst Formation 138
4.7 Buntsandstein and Rotliegend (Early Triassic to Permian, Dinkelberg Formation to Weitenau Formation) 143

5 Main structural findings 149
5.1 Fault zone within the «Felsenkalke» / «Massenkalk» 149
5.2 Faulting within the 'Brauner Dogger' 155
5.3 The deformed Zeglingen Formation 157

6 References 161

List of Tables

Tab. 1-1: General information about the BUL1-1 borehole 2
Tab. 1-2: List of dossiers included in NAB 20-08 5
Tab. 2-1: Core goniometry confidence assessment 15
Tab. 2-2: Types of structural discontinuities identified in this study 20
Tab. 2-3: Systematically recorded parameters for the investigated structures 23
Tab. 4-1: Mean orientation values for bedding planes and structural discontinuities 55
Tab. 4-2: List of interpreted fault zones and associated FDC (fracture density class) 61
Tab. 4-3: List of all kinematic indicators in oriented and non-oriented cores 70

List of Figures

Fig. 1-1: Tectonic overview map with the three siting regions under investigation 1
Fig. 1-2: Overview map of the investigation area in the Nördlich Lägern siting region with the location of the BUL1-1 borehole and the existing Weiach-1 borehole 3
Fig. 1-3: Lithostratigraphic profile and casing scheme for the BUL1-1 borehole 4
Fig. 1-4: Borehole deviation within the cored section..... 8
Fig. 2-1: Using a goniometer to determine kinematic indicators along faults..... 11
Fig. 2-2: Symbols for dip types, fracture density classes and kinematic data used for this study..... 12
Fig. 2-3: Fault plane at 660.75 m MD log depth..... 13
Fig. 2-4: Dip data in a non-oriented core section displayed with hollow tadpoles..... 14
Fig. 2-5: Short interval without 360° core photographs..... 14
Fig. 2-6: Core – FMI / UBI correlation for a fault at 767.27 m MD log depth..... 16
Fig. 2-7: Core – FMI correlation in the Bänkerjoch Formation from 1'102.50 – 1'103.20 m MD..... 17
Fig. 2-8: Core – FMI correlation in the case of flat bedding..... 18
Fig. 2-9: The five main groups of structural discontinuities 20
Fig. 2-10: Completed DIN A3 sheet of primary record of the structural core analysis..... 25
Fig. 3-1: Fault plane 29
Fig. 3-2: Fault plane 30
Fig. 3-3: Fault plane 31
Fig. 3-4: Fault planes..... 32
Fig. 3-5: Mirror-like fault plane 33
Fig. 3-6: Mirror-like fault plane 34
Fig. 3-7: Stylolitic fault plane..... 35
Fig. 3-8: Fault zone with FDC 2..... 36
Fig. 3-9: Fault zone with FDC 3..... 36
Fig. 3-10: Fault zone with FDC 4..... 37
Fig. 3-11: Dynamic recrystallisation within a fault zone 38
Fig. 3-12: Joint 39
Fig. 3-13: Joint 40
Fig. 3-14: Joint 40
Fig. 3-15: Vein / tension gash..... 41
Fig. 3-16: Vein / tension gash..... 41
Fig. 3-17: Vein / tension gash..... 42
Fig. 3-18: Stylolites..... 43

Fig. 3-19: Stylolites 44
Fig. 3-20: Stylolites 45
Fig. 3-21: Stylolites 45
Fig. 3-22: Open pore 46
Fig. 3-23: Open pores 46
Fig. 3-24: Open pores 47
Fig. 3-25: Open pores 48
Fig. 3-26: Petal fractures 49
Fig. 3-27: Petal fractures 50
Fig. 3-28: Discing 50
Fig. 3-29: Discing surface 51
Fig. 3-30: Folding 52
Fig. 3-31: Folding 53
Fig. 3-32: Folding 54
Fig. 4-1: Stereogram and depth plot for bedding planes (n = 316) for the entire cored borehole section 56
Fig. 4-2: Azimuth rose diagram, dip histogram and depth plot for bedding planes (n = 316) for the entire cored borehole section 57
Fig. 4-3: Vector azimuth plot for bedding-related planes (n = 316) of picked core dips 58
Fig. 4-4: Overview plot showing P32 fracture densities along the borehole 60
Fig. 4-5: Stereogram and depth plot of fault planes in the entire cored interval 63
Fig. 4-6: Azimuth rose diagram, dip histogram and depth plot for fault planes in the entire cored interval 64
Fig. 4-7: Stereogram and depth plot for tension gashes / veins, fractures and joints in the entire cored interval 65
Fig. 4-8: Azimuth rose diagram of tension gashes / veins, fractures and joints in the entire cored interval 66
Fig. 4-9: Stereogram and depth plot of stylolites along the borehole in the entire cored interval 67
Fig. 4-10: Azimuth rose diagram and depth plot for stylolites in the entire cored interval 68
Fig. 4-11: Dip direction of striations along fault planes in the entire cored interval 70
Fig. 4-12: Stereogram with all oriented fault planes and associated kinematic data 71
Fig. 4-13: Stereogram with all striations of thrust / reverse fault planes 71
Fig. 4-14: Stereogram with all normal fault planes and associated striations 72
Fig. 4-15: Stereogram with all strike-slip fault planes and associated striations 72
Fig. 4-16: Stereogram for all fault planes with unknown shear sense 73
Fig. 4-17: Stereogram and depth plot of fault planes («Felsenkalke» / «Massenkalk») 74

Fig. 4-18: Azimuth rose diagram, dip histogram and depth plot of fault planes («Felsenkalke» / «Massenkalk») 75
Fig. 4-19: Stereogram and depth plot of fractures, tension gashes / veins and joints («Felsenkalke» / «Massenkalk») 76
Fig. 4-20: Azimuth rose diagram, dip histogram and depth plot of fractures, tension gashes / veins and joints («Felsenkalke» / «Massenkalk»)..... 77
Fig. 4-21: Stereogram and depth plot of stylolites («Felsenkalke» / «Massenkalk», n = 283)..... 78
Fig. 4-22: Azimuth rose diagram, dip histogram and depth plot of stylolites («Felsenkalke» / «Massenkalk», n = 283) 79
Fig. 4-23: Stereogram of faults («Felsenkalke» / «Massenkalk», n = 173)..... 80
Fig. 4-24: Stereogram and depth plot of fault planes (Schwarzbach Formation)..... 81
Fig. 4-25: Azimuth rose diagram, dip histogram and depth plot of fault planes (Schwarzbach Formation)..... 82
Fig. 4-26: Stereogram and depth plot for fractures, tension gashes / veins and joints (Schwarzbach Formation)..... 83
Fig. 4-27: Stereogram and depth plot of stylolites (Schwarzbach Formation, n = 12)..... 84
Fig. 4-28: Azimuth rose diagram, dip histogram and depth plot of stylolites (Schwarzbach Formation, n = 12) 85
Fig. 4-29: Stereogram of faults (Schwarzbach Formation, n = 15)..... 86
Fig. 4-30: Stereogram and depth plot of fault planes (Villigen Formation)..... 87
Fig. 4-31: Azimuth rose diagram, dip histogram and depth plot of fault planes (Villigen Formation)..... 88
Fig. 4-32: Stereogram and depth plot of fractures, tension gashes / veins and joints (Villigen Formation)..... 89
Fig. 4-33: Azimuth rose diagram, dip histogram and depth plot of fractures, tension gashes / veins and joints (Villigen Formation) 90
Fig. 4-34: Stereogram and depth plot of stylolites (Villigen Formation, n = 171)..... 91
Fig. 4-35: Azimuth rose diagram, dip histogram and depth plot of stylolites (Villigen Formation, n = 171)..... 92
Fig. 4-36: Stereogram of faults (Villigen Formation, n = 130) 93
Fig. 4-37: Stereogram and depth plot of fault planes (Wildegg Formation) 94
Fig. 4-38: Azimuth rose diagram, dip histogram and depth plot of faults (Wildegg Formation) 95
Fig. 4-39: Stereogram and depth plot of stylolites (Wildegg Formation, n = 16) 96
Fig. 4-40: Azimuth rose diagram, dip histogram and depth plot of stylolites (Wildegg Formation, n = 16)..... 97
Fig. 4-41: Stereogram of faults (Wildegg Formation, n = 27) 98
Fig. 4-42: Stereogram and depth plot of fault planes ('Brauner Dogger') 99

Fig. 4-43: Azimuth rose diagram, dip histogram and depth plot of fault planes ('Brauner Dogger') 100
Fig. 4-44: Stereogram and depth plot of fractures, tension gashes / veins and joints ('Brauner Dogger') 101
Fig. 4-45: Stereogram and depth plot of stylolites ('Brauner Dogger', n = 76) 102
Fig. 4-46: Azimuth rose diagram, dip histogram and depth plot of stylolites ('Brauner Dogger', n = 76) 103
Fig. 4-47: Stereogram of faults ('Brauner Dogger', n = 58)..... 104
Fig. 4-48: Stereogram and depth plot of fault planes (Opalinus Clay)..... 105
Fig. 4-49: Azimuth rose diagram, dip histogram and depth plot of fault planes (Opalinus Clay)..... 106
Fig. 4-50: Stereogram of lineations (Opalinus Clay, n = 4) 107
Fig. 4-51: Stereogram and depth plot of fault planes (Lias)..... 108
Fig. 4-52: Azimuth rose diagram, dip histogram and depth plot of fault planes (Lias) 109
Fig. 4-53: Stereogram and depth plot of fractures, tension gashes / veins and joints (Lias)..... 110
Fig. 4-54: Stereogram and depth plot of stylolites (Lias, n = 1)..... 111
Fig. 4-55: Stereogram of fault planes (Lias, n = 11) 112
Fig. 4-56: Stereogram and depth plot of faults (Klettgau Formation)..... 113
Fig. 4-57: Azimuth rose diagram, dip histogram and depth plot of faults (Klettgau Formation) 114
Fig. 4-58: Stereogram and depth plot of fractures, tension gashes / veins and joints (Klettgau Formation) 115
Fig. 4-59: Azimuth rose diagram, dip histogram and depth plot of fractures, tension gashes / veins and joints (Klettgau Formation) 116
Fig. 4-60: Stereogram and depth plot of stylolites (Klettgau Formation, n = 6) 117
Fig. 4-61: Stereogram of lineations (Klettgau Formation, n = 40)..... 117
Fig. 4-62: Stereogram and depth plot of faults (Bänkerjoch Formation) 118
Fig. 4-63: Azimuth rose diagram, dip histogram and depth plot of faults (Bänkerjoch Formation)..... 119
Fig. 4-64: Stereogram and depth plot of fractures, tension gashes / veins and joints (Bänkerjoch Formation)..... 120
Fig. 4-65: Azimuth rose diagram, dip histogram and depth plot of fractures, tension gashes / veins and joints (Bänkerjoch Formation)..... 121
Fig. 4-66: Stereogram of fault planes (Bänkerjoch Formation, n = 85) 122
Fig. 4-67: Stereogram and depth plot of fault planes (Schinznach Formation)..... 123
Fig. 4-68: Azimuth rose diagram, dip histogram and depth plot of fault planes (Schinznach Formation)..... 124
Fig. 4-69: Stereogram and depth plot of fractures, tension gashes / veins and joints (Schinznach Formation)..... 125

Fig. 4-70: Azimuth rose diagram, dip histogram and depth plot of fractures, tension gashes / veins and joints (Schinznach Formation) 126
Fig. 4-71: Stereogram and depth plot of stylolites (Schinznach Formation, n = 164) 127
Fig. 4-72: Azimuth rose diagram, dip histogram and depth plot of stylolites (Schinznach Formation, n = 164) 128
Fig. 4-73: Stereogram of fault planes (Schinznach Formation, n = 15) 129
Fig. 4-74: Stereogram and depth plot of fault planes («Dolomitzone» – «Salzlager») 130
Fig. 4-75: Azimuth rose diagram, dip histogram and depth plot of fault planes («Dolomitzone» – «Salzlager») 131
Fig. 4-76: Stereogram and depth plot of fractures, tension gashes / veins and joints («Dolomitzone» – «Salzlager») 132
Fig. 4-77: Stereogram and depth plot of stylolites («Dolomitzone» – «Salzlager», n = 5) ... 133
Fig. 4-78: Stereogram of faults («Dolomitzone» – «Salzlager», n = 47) 134
Fig. 4-79: Stereogram and depth plot of fault planes («Untere Sulfatzone») 135
Fig. 4-80: Stereogram and depth plot of fractures, tension gashes / veins and joints («Untere Sulfatzone») 136
Fig. 4-81: Stereogram of fault planes («Untere Sulfatzone», n = 5) 137
Fig. 4-82: Stereogram and depth plot of fault planes (Kaiseraugst Formation) 138
Fig. 4-83: Azimuth rose diagram, dip histogram and depth plot of fault planes (Kaiseraugst Formation) 139
Fig. 4-84: Stereogram and depth plot of fractures, tension gashes / veins and joints (Kaiseraugst Formation) 140
Fig. 4-85: Stereogram and depth plot of stylolites (Kaiseraugst Formation, n = 2) 141
Fig. 4-86: Stereogram of fault planes (Kaiseraugst Formation, n = 29) 142
Fig. 4-87: Stereogram and depth plot of fault planes (Dinkelberg Formation to Weitenau Formation) 143
Fig. 4-88: Azimuth rose diagram, dip histogram and depth plot of fault planes (Dinkelberg Formation to Weitenau Formation) 144
Fig. 4-89: Stereogram and depth plot of fractures, tension gashes / veins and joints (Dinkelberg Formation to Weitenau Formation) 145
Fig. 4-90: Stereogram and depth plot for stylolites (Dinkelberg Formation to Weitenau Formation, n = 3) 146
Fig. 4-91: Stereogram of fault planes (Dinkelberg Formation to Weitenau Formation, n = 75) 147
Fig. 5-1: Structures observed in cores within the fault zone 150
Fig. 5-2: Structural overview plot for the from 535 – 560 m MD log depth 151
Fig. 5-3: Stereogram and depth plot of fault zone from 537.66 to 554.00 m MD log depth 152
Fig. 5-4: Azimuth rose diagram and dip histogram for the fault zone from 537.66 to 554.00 m MD log depth 153

Fig. 5-5: Stereogram of fault planes in the fault zone from 537.66 to 554.00 m MD log depth 154

Fig. 5-6: Azimuth rose diagram and dip histogram for striations in the fault zone from 537.50 to 554.00 m MD log depth..... 154

Fig. 5-7: Core scan example for fault zones in the 'Brauner Dogger'..... 155

Fig. 5-8: Fault zone within the 'Brauner Dogger' observed in cores 156

Fig. 5-9: Schematic structural overview of the Zeglingen Formation (1'205 – 1'240 m MD log depth) 158

Fig. 5-10: Schematic structural overview of the Zeglingen Formation (1'240 – 1'275 m MD log depth) 159

List of Appendices

App. A: Lithostratigraphy profile Bülach-1-1 and Bülach-1-1B, 1:2'500, 0.00 m to 1'370.19 m MD core depth

App. B: Structural geology profile Bülach-1-1 and Bülach-1-1B, 1:1'000, 500.00 m to 1'370.14 m MD log depth

App. C-1: Structural geology profile Bülach-1-1 and Bülach-1-1B, 1:100, 525.00 m to 800.00 m MD log depth

App. C-2: Structural geology profile Bülach-1-1 and Bülach-1-1B, 1:100, 775.00 m to 1'050.00 m MD log depth

App. C-3: Structural geology profile Bülach-1-1 and Bülach-1-1B, 1:100, 1'025.00 m to 1'300.00 m MD log depth

App. C-4: Structural geology profile Bülach-1-1 and Bülach-1-1B, 1:100, 1'275.00 m to 1'370.14 m MD log depth

App. D-1: Overview plot of stereograms and rose diagrams: «Felsenkalke» / «Massenkalk» to Staffelegg Fm.

App. D-2: Overview plot of stereograms and rose diagrams: Klettgau to Weitenau Fm.

App. E-1: Core goniometry depth shift table

App. E-2: Core goniometry rotation angle table

App. F: Lithostratigraphy patterns, colours, weathering index and symbols for lithostratigraphy

Note: In the digital version of this report the appendices can be found under the paper clip symbol.

1 Introduction

1.1 Context

To provide input for site selection and the safety case for deep geological repositories for radioactive waste, Nagra has drilled a series of deep boreholes in Northern Switzerland. The aim of the drilling campaign is to characterise the deep underground of the three remaining siting regions located at the edge of the Northern Alpine Molasse Basin (Fig. 1-1).

In this report, we present the results from the Bülach-1-1 borehole.

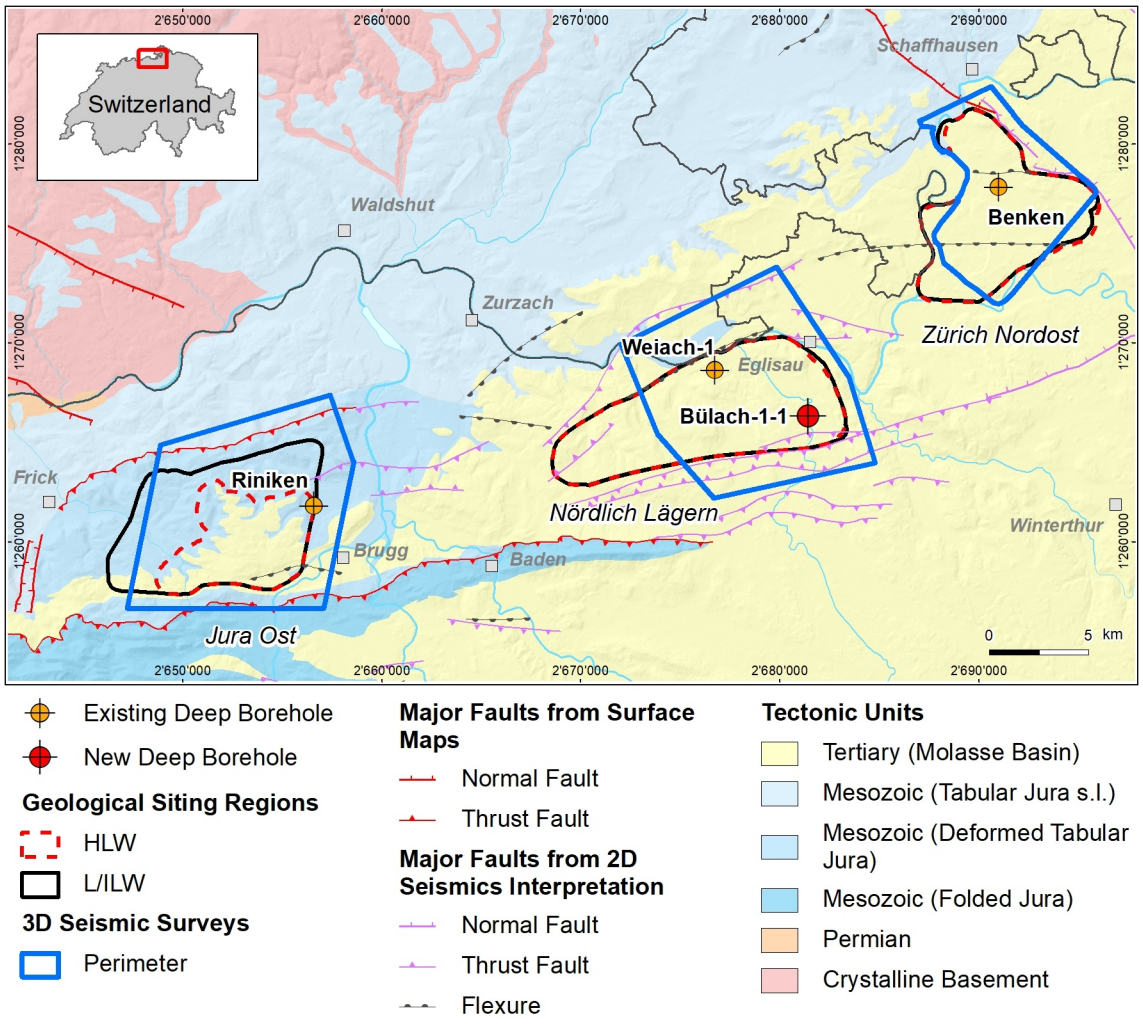

Fig. 1-1: Tectonic overview map with the three siting regions under investigation

1.2 Location and specifications of the borehole

The Bülach-1-1 (BUL1-1) exploratory borehole is the first deep borehole drilled within the framework of the TBO project. BUL1-1 is a vertical borehole. The drill site is located in the south-eastern part of the Nördlich Lägern siting region (Fig. 1-2). The borehole specifications are provided in Tab. 1-1. The lithostratigraphic profile and the casing scheme are shown in Fig. 1-3. Due to instabilities, the borehole was plugged back from 1'043.00 m to 918.70 m (*cf.* Dossier I). Resuming coring operations, a sidetrack was initiated with a kickoff point at 995.85 m. This sidetrack was labelled Bülach-1-1B (BUL1-1B). BUL1-1B reached the final depth of 1'370.19 m (measured depth MD core depth)[1]. For easier communication and labelling, the name BUL1-1 is generally used for the complete vertical borehole unless stated otherwise. Fig. 1-3 shows the combined lithostratigraphic profile of BUL1-1.

Tab. 1-1: General information about the BUL1-1 borehole

Location	Bülach (Canton Zurich / ZH), Switzerland
Siting region	Nördlich Lägern
Coordinates	2'681'446.028 / 1'266'298.472
Elevation	389.62 m asl (top of rig cellar)
Borehole depth	1'370.19 m MD core depth
Drilling period	15 April 2019 – 27 November 2019 (spud – rig release)
Drilling company	Daldrup & Söhne AG
Drilling rig	Wirth B 152t
Drilling fluid	Water-based mud with varying amounts of Pure-Bore®, Pure-Bore® ULV, soda ash, sodium bicarbonate, xanthan gum

[1] *Measured depth (MD)* below top rig cellar along borehole trajectory. In all dossiers, depth refers to MD unless stated otherwise.

MD core depth refers to the depth marked on the cores. Note that petrophysical logs have not been shifted to core depth, hence MD log depth differs from MD core depth. The depth shift between core depth and log depth is documented in Dossier V, Appendix E-1.

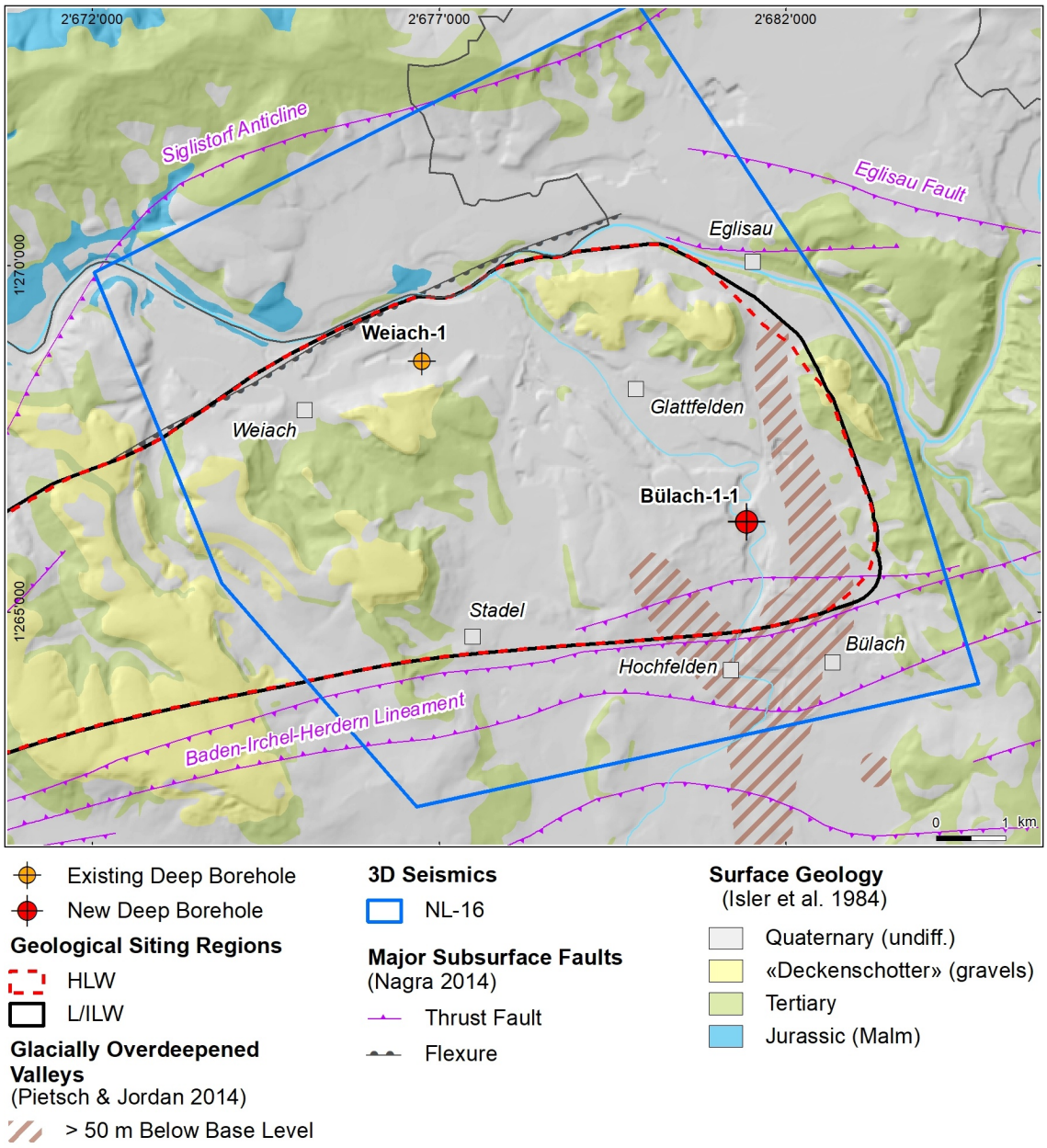

Fig. 1-2: Overview map of the investigation area in the Nördlich Lägern siting region with the location of the BUL1-1 borehole and the existing Weiach-1 borehole

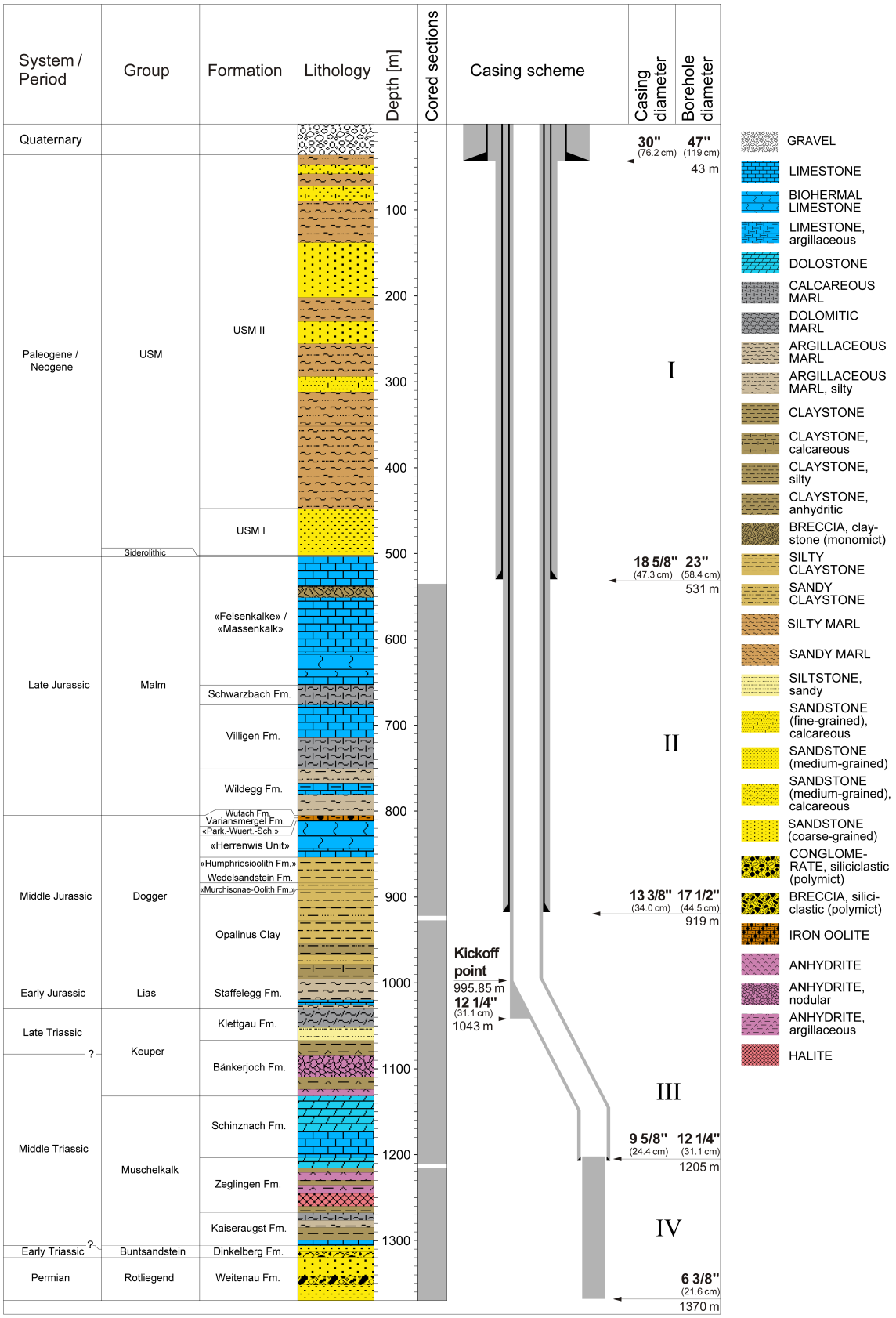

Fig. 1-3: Lithostratigraphic profile and casing scheme for the BUL1-1 borehole

1.3 Documentation structure for the BUL1-1 borehole

NAB 20-08 documents the majority of the investigations carried out in the BUL1-1 borehole, including laboratory investigations on core material. The NAB comprises a series of stand-alone dossiers addressing individual topics and a final dossier with a summary composite plot (Tab. 1-2).

This borehole documentation aims at early publication of the data collected in the BUL1-1 borehole. It includes the majority of the data available approximately one year after completion of the borehole. Some analyses are still ongoing (e.g. diffusion experiments, analysis of veins, hydrochemical interpretation of water samples) and will be published in separate reports.

The current borehole report will provide an important basis for the integration of datasets from different boreholes. The integration and interpretation of the results in the wider geological context will be documented later in separate geoscientific reports.

Tab. 1-2: List of dossiers included in NAB 20-08

Black marks the dossier at hand.

Dossier	Title	Authors
I	TBO Bülach-1-1: Drilling	M. Ammen & P.-J. Palten
II	TBO Bülach-1-1: Core Photography	D. Kaehr & M. Gysi
III	TBO Bülach-1-1: Lithostratigraphy	P. Jordan, H. Naef, P. Schürch, M. Schwarz, T. Ibele, R. Felber & M. Gysi
IV	TBO Bülach-1-1: Microfacies, Bio- and Chemostratigraphic Analysis	S. Wohlwend, H.R. Bläsi, S. Feist-Burkhardt, B. Hostettler, U. Menkveld-Gfeller, V. Dietze & G. Deplazes
V	TBO Bülach-1-1: Structural Geology	A. Ebert, L. Gregorczyk, E. Hägerstedt & M. Gysi
VI	TBO Bülach-1-1: Wireline Logging and Microhydraulic Fracturing	R. Garrard, J. Gonus, J. Desroches & E. Bailey
VII	TBO Bülach-1-1: Hydraulic Packer Testing	R. Schwarz, L. Schlickenrieder & T. Vogt
VIII	TBO Bülach-1-1: Rock Properties, Porewater Characterisation and Natural Tracer Profiles	M. Mazurek, L. Aschwanden, L. Camesi, T. Gimmi, A. Jenni, M. Kiczka, U. Mäder, D. Rufer, H. N. Waber, P. Wanner, P. Wersin & D. Traber
IX	TBO Bülach-1-1: Rock-mechanical and Geomechanical Laboratory Testing	E. Crisci, L. Laloui & S. Giger
X	TBO Bülach-1-1: Petrophysical Log Analysis	S. Marnat & J.K. Becker
	TBO Bülach-1-1: Summary Plot	Nagra

1.4 Scope and objectives of this dossier

The dossier at hand (Dossier V) documents the work of the structural geology experts. The objectives of the report are:

- core goniometry to reset drill cores to the correct depth and original orientation based on high resolution borehole images and high resolution 360° core photographs (Appendices E-1 and E-2)
- structural discontinuities identification on high resolution 360° core photographs and drill cores
- true dip and dip azimuth analysis of structures and bedding planes on high resolution 360° photographs in TerraStation II and / or manual measurements with a geological compass on drill cores.
- documentation of recorded structures and their relevant parameters
- visualisation of structural geology data as profiles and overview plots:
  - profile 1:1'000: Appendix B
  - profile 1:100: Appendices C-1 to C-4
  - overview plot of stereograms and rose diagrams: Appendices D-1 and D-2

As the cores of the sidetrack BUL1-1B were not sampled in the Lias and having a full suite of petrophysical logs available for this sidetrack, it was decided to use the structural analysis of the entire BUL1-1B section as the base for the combined structural geological profile. The structural analysis from 995 m to 1'043.00 m of BUL1-1 are therefore neither documented in this report nor included in the profiles.

The level of detail in this dossier is limited by the data availability at data cut-off two months after the end of drilling operations. The lithostratigraphic subdivision used in this report are in line with the finding in Dossier III.

1.5 Petrophysical logs and preliminary log analysis available

The petrophysical logs and preliminary log analysis listed below were available at the data-freeze and considered as a supplementary source of information for this report (for more details, see Dossier VI).

- total natural gamma ray borehole corrected (GR)
- caliper / radius (RD1 to RD6)
- near / array corrected limestone porosity (APLC)
- high resolution formation density (RHO8)
- high resolution formation photoelectric factor (PEF8)
- array laterolog apparent resistivity from computed focusing mode 0 to 5 (RLA1 to RLA5)
- formation micro imager (FMI)
- ultrasonic borehole image (UBI)
- borehole breakouts and centreline fractures analysis based on FMI and UBI images

1.6 Borehole deviation

The borehole BUL1-1 and the sidetrack BUL1-1B are almost vertical down to a depth of 995 m MD log depth. Due to the sidetrack starting at 996.01 m MD log depth, there is a slight deviation towards the west. The maximum borehole deviation is 1.4° from 1'215 to 1'217 m MD log depth. This leads to a maximum deviation of approximately 8 m to the west at TD (total depth; see Fig. 1-4).

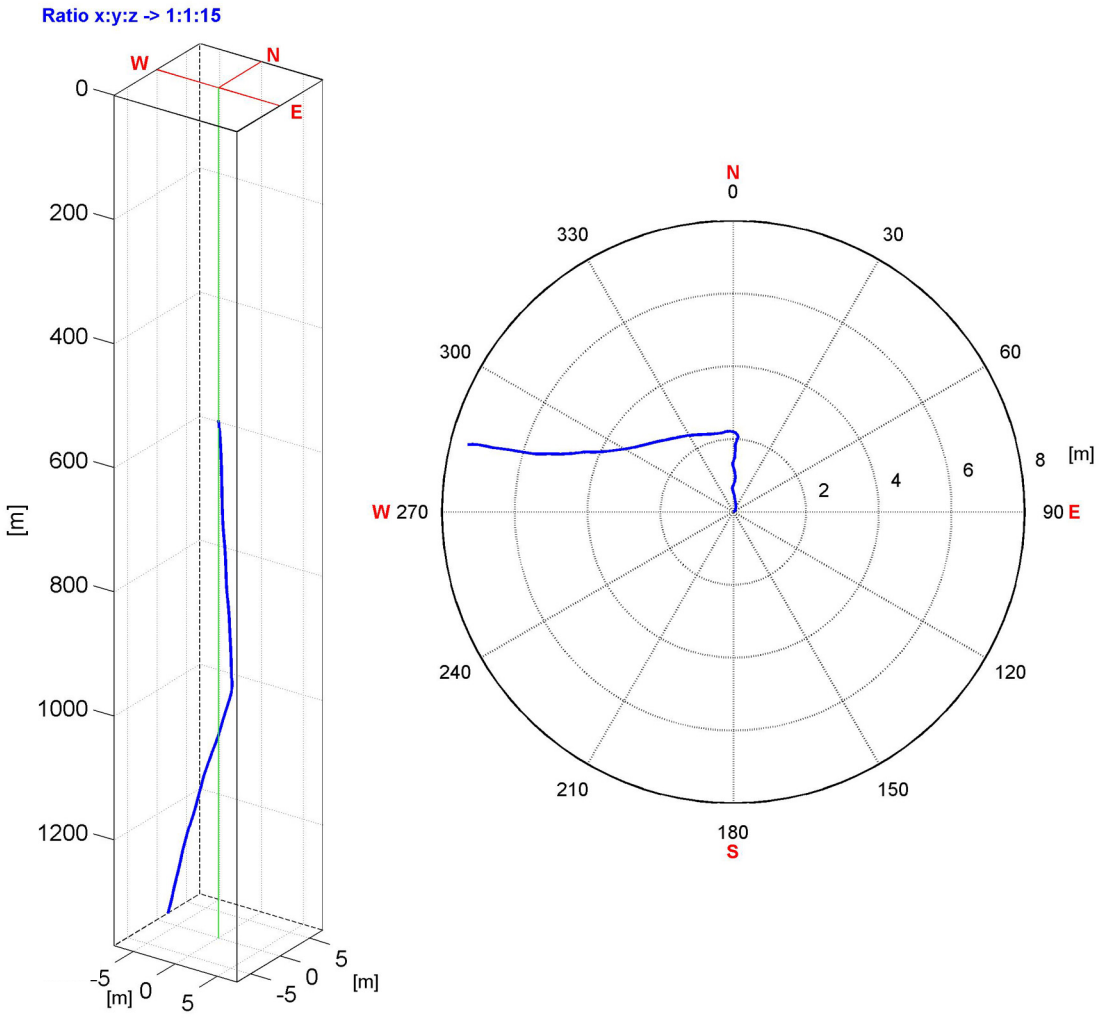

Fig. 1-4: Borehole deviation within the cored section

The sidetrack BUL1-1B is visible below 996.01 m MD log depth. The left image visualises the borehole path in 3D with a compressed z-axis. The borehole azimuth is shown on the right.

2 Methodology

2.1 Core goniometry

2.1.1 Introduction

A structural core analysis was performed on drill cores along with circumferential and planar drill core photographs. Using the reference line on the core surface, positioned at an azimuth of 0° during core photography, most drill core could be oriented using borehole image logs.

For this study, high-resolution 360° and planar photographs were available for most of the cored interval from 535 to 1'370.14 m MD log depth. The data were delivered as 1'244 circumferential and 1'301 planar photographs in TIF format. The original photographs, with a resolution of 10 pixels/mm, however, were too big to be handled within TerraStation II (TERRASCIENCES Inc.). Therefore, the original photographs were compressed by 25 % exported with a resolution of 300 dpi. In addition, formation micro image (FMI) and ultrasonic borehole image (UBI) logs were available. Both data sets were of good to excellent quality. Further relevant data included auxiliary borehole data, core orientation line and core section listings, lithostratigraphic tops and petrophysical logs.

2.1.2 Workflow

This section describes the methodology used for extracting the directional information from 360° core photographs. The following steps were tailored for efficient core goniometry using TerraStation II software:

1. Quality control of core photographs:

   Prior to loading the data, it was ensured that the core orientation line (red) on the 360° core photographs was set to 0°.

   Note: the core orientation line (COL) represents a continuous reference line set to an azimuth of 0° to fix the relative orientation of drill cores. The COL was drawn on the core surface immediately after core retrieval at the drill site. The line lengths vary widely from a few centimetres up to several metres and therefore sometimes continue over several core sections. It depends on whether each individual core section could be fitted together along the core edges or not. If core sections could not be merged, a new COL was determined. The coherent COL was then used to orient the drill core using borehole image logs.

2. Data loading:

   All 360° core photographs were loaded as mirror images in order to simulate the borehole image log. A constant value of 95 mm (3.74") was added as image diameter.

   The processed FMI and UBI logs as well as the auxiliary petrophysical logs were imported into TerraStation II. It was checked that the depth of the petrophysical logs, especially the first GR (gamma ray) run, matched the depth of the FMI data.

3. Depth shifting:

   The 360° core photographs were shifted to FMI logs using distinct, correlated planar and / or non-planar features. For the purpose of simplicity and consistency, only one shift value was applied for each individual core section (generally 3 m per section). This resulted in minor data gaps and / or overlaps at core section boundaries of a few centimetres maximum. In total, 286 distinct depth shift values were applied for the core sections of the entire cored borehole; these varied from 0 to ± 31 cm. The defined values are listed in Appendix E-1.

4. Core orientation:

   The core was oriented using correlated geological features (e.g. faults / fractures, inclined / deformed bedding, nodules, etc.) which were matched with the orientation on the FMI by rotating the 360° core photographs clockwise around the borehole axis.

   The obtained angle of rotation was then applied to the entire core section with a continuous COL. Simultaneously, the validity across other geological features was checked. Note that the length of a linked COL segment was highly variable and could continue across several core sections. All COLs and the applied angles of rotation of the individual COLs are listed in Appendix E-2. To highlight the uncertainties related to core orientation, an uncertainty assessment was carried out and visualised in three confidence classes.

5. Quality control of core goniometry:

   Prior to the structural recording of the drill cores, the depth shifts, the core correlation with the FMI / UBI combination and the core orientations were reviewed by Michael Gysi (Nagra).

The following steps do not belong to classical core goniometry. However, they played a key role in the coherent workflow of the structural core analysis and are thus mentioned here:

6. Dip picking on oriented 360° core photographs:

   Bedding-related planes were picked manually for a structural dip evaluation. Structural elements on drill cores were picked manually and characterised in detail with respect to relevant parameters.

7. Recording of kinematic features:

   Kinematic indicators along fault surfaces such as slickensides, striations, shear sense indicators and (fault) offsets were identified and measured on the drill cores. To determine the lineation azimuth and plunge and / or planes not visible in the photographs, a goniometer constructed by Geo Explorers was used. The drill core was placed in the goniometer facing up-hole and rotated around the vertical axis by the angle of rotation determined from the core orientation line. Subsequently, the azimuth and plunge of the striation were measured using a geological compass (Fig. 2-1).

8. Examination of angular differences:

   Using the TectonicsFP software, the angular differences between the striation azimuths / plunges and the orientation of associated fault planes were checked. In cases the angular offset exceeded 15°, the fault plane and lineation were remeasured.

9. Quality control:

   A final quality control was performed by Dr. Kurt Decker with the main focus on consistency (between TerraStation project, primary records of structural core analysis and the structural inventory metadata), completeness of records and the accurate characterisation of the recorded tectonic features.

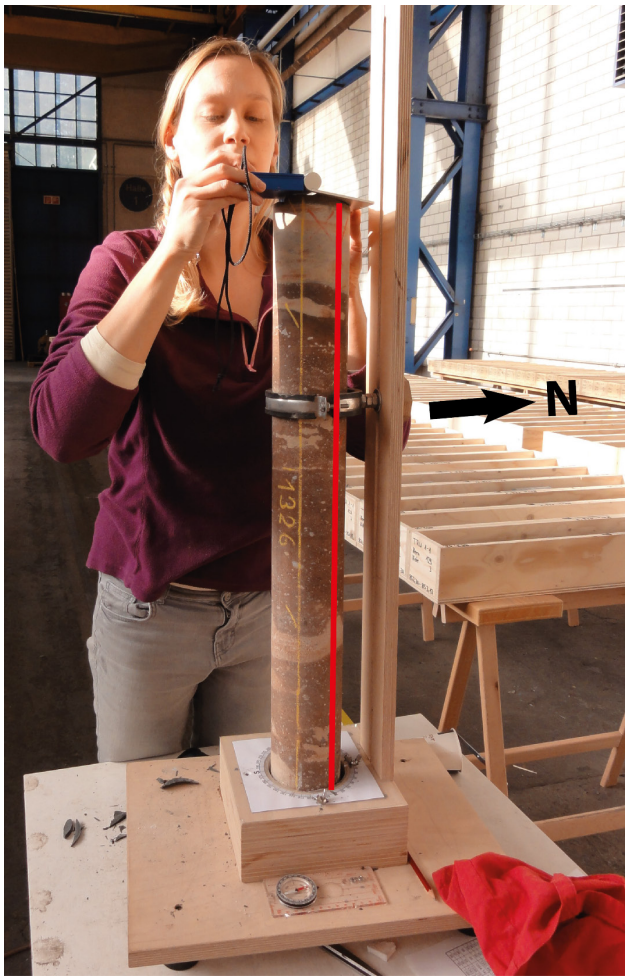

Fig. 2-1: Using a goniometer to determine kinematic indicators along faults

Note the red core orientation line defining the position of the drill core in the goniometer.

2.1.3 Dip picking and dip type classification

Due to a higher accuracy and reliability compared to automated methods, a manual sinusoid method and a point-to-point method were used to pick all relevant features on the 360° core photographs. In a cylindrical borehole, a perfect plane will appear as a sine wave on the circumferential core photograph and its amplitude reflects the dip relative to the borehole axis.

Different dip classes were defined for the different structure types. For this study, a total of 15 different dip types were defined in TerraStation II (Fig. 2-2).

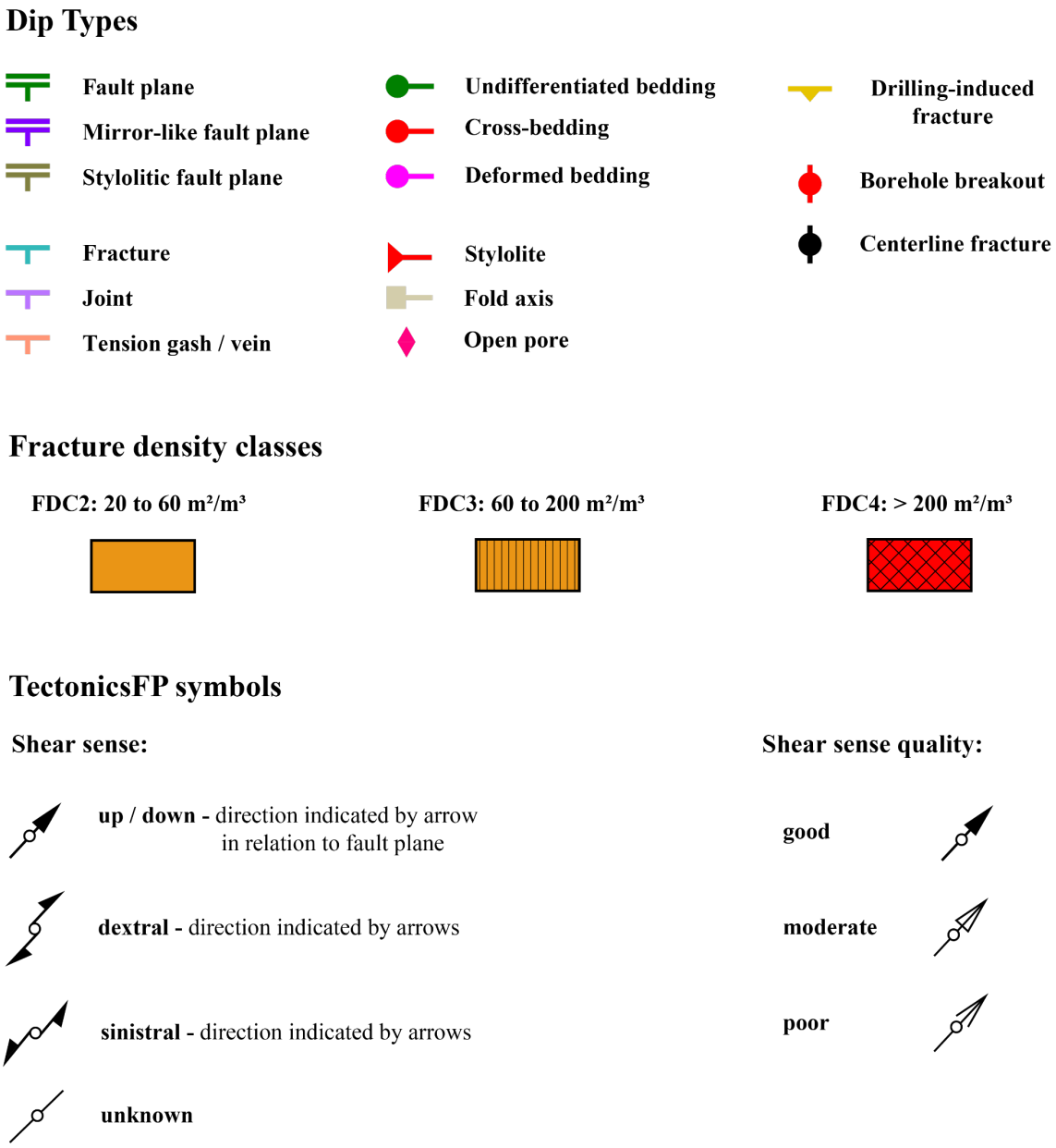

Fig. 2-2: Symbols for dip types, fracture density classes and kinematic data used for this study

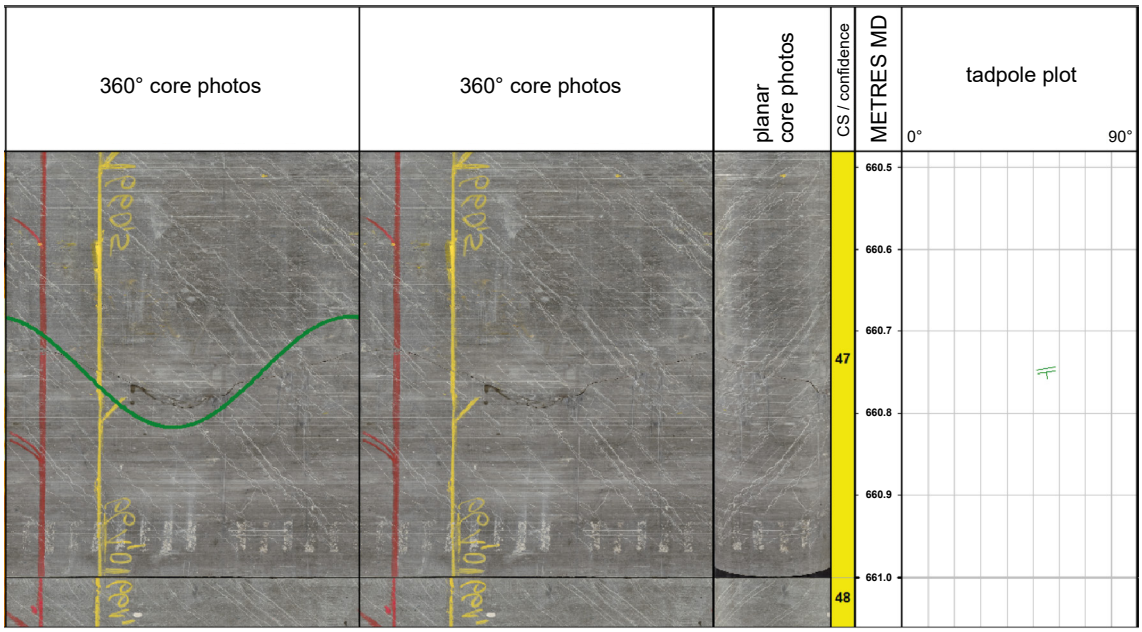

Fig. 2-3: Fault plane at 660.75 m MD log depth

From left to right: Shifted and oriented 360° core photograph with (left) and without (right) picked sine waves, followed by depth-shifted planar core photographs, core section numbering in the coloured bar displaying the goniometry confidence ranking, depth track showing the position and length of the currently displayed window, tadpole plot. Note that the displayed sine wave does not fit with the visible (dark) fault trace as the orientation was obtained from geological compass measurement.

Some structures were only visible on planes not outcropping at the rim of the core and were not visible on the 360° core photographs. The orientation of these structures was obtained with a geological compass and the data were subsequently imported into the digital dip dataset. Consequently, the associated dip sine waves did not fit with any visible traces and / or were simply not visible at this depth level, as exemplified in Fig. 2-3.

2.1.4 Dip data for non-oriented drill cores

Due to a lack of correlated features and / or poor data quality, approximately 182 m of the available drill core remained non-oriented, although 260 bedding planes and about 200 structures could be observed within these non-oriented drill cores. The structural planes were nevertheless manually measured with a geological compass and included into TerraStation II, or digitally picked on 360° core photographs. In case of non-oriented drill cores and core photographs, the red core orientation line was set to 0°. As the dip measurement of these features are correct but the dip azimuth measurements are affected by the lack of orientation, the non-oriented data set can only be used for fracture density calculations.

To highlight that the dip azimuth measurements of these features are incorrect, a quality indicator of 0 was assigned and hollow tadpoles used for visualisation (Fig. 2-4). A quality indicator of 1 was assigned to all correctly oriented features.

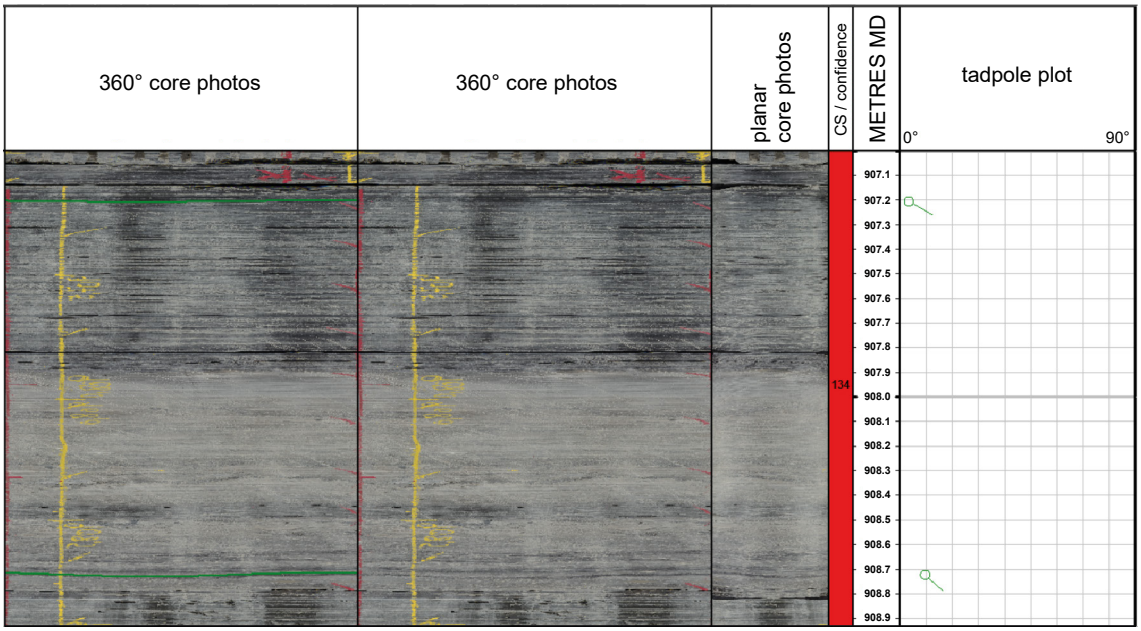

Fig. 2-4: Dip data in a non-oriented core section displayed with hollow tadpoles

The goniometry confidence is set to not oriented (red).

For intervals where 360° core photographs were missing, short drill core sections could still be oriented using the coherent core orientation line, which sometimes continued across several cores. The depth and orientation of the structures were then measured on the core and the dip data were subsequently imported into the digital database of TerraStation (Fig. 2-5).

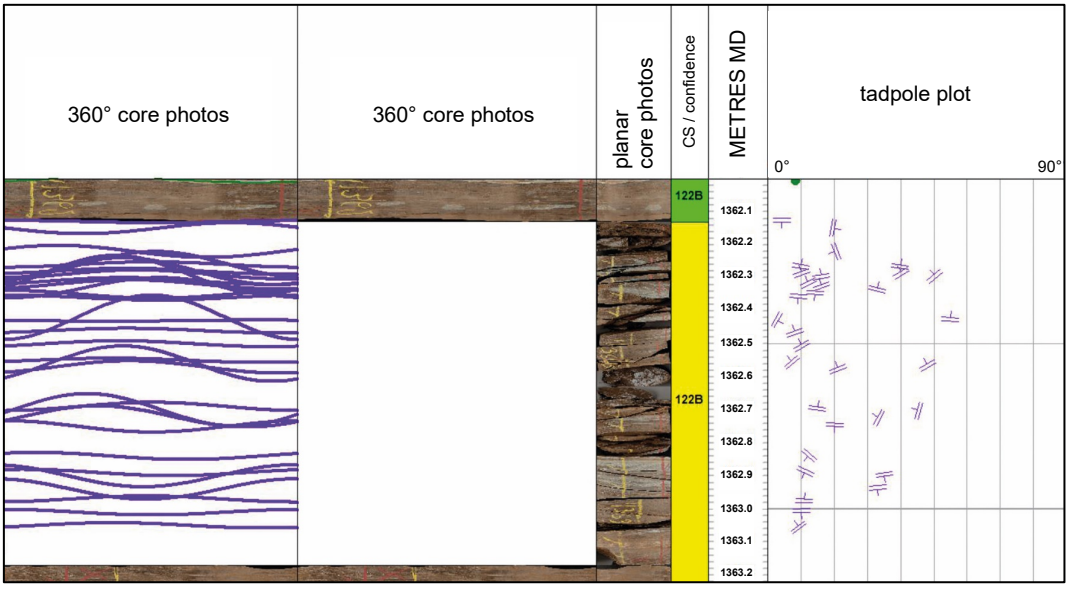

Fig. 2-5: Short interval without 360° core photographs

In this example from 1'362.00 to 1'363.22 m MD log depth, the core goniometry and structural analysis were performed directly on the drill core and the orientation data were determined with a geological compass and subsequently imported into the digital dip database of TerraStation II. The goniometry confidence is set to moderate (yellow).

2.1.5 Goniometry confidence assessment and uncertainties

Goniometry confidence ranking

To visualise the uncertainties related to the core goniometry, the reliability of the core orientation was classified using a confidence ranking scheme. The assessment was carried out for each connected core orientation line and depended particularly on the number of reliably correlated features within these intervals. Features with a moderate to steep (> 15°) dip generally provided a higher confidence and resulted in lower angular uncertainties than e.g. shallow structures (< 15°). Examples of the correlated features between the FMI and the core are presented in Figs. 2-6, 2-7 and 2-8.

There are three confidence levels for the goniometry illustrated as coloured fields in the structural composite plots (Appendix B and C). The confidence level depends on the number of evident structures found within each coherent core orientation line:

- high is defined by three or more distinct, preferably moderately inclined to steep (> 15°) planar and / or non-planar features (Figs. 2-6 and 2-7) resulting in a high angular accuracy
- moderate is associated with one or two correlated (non-)planar structures with shallow to moderate dip angles (< 15°; Fig. 2-8). Thus, the core orientation bears some uncertainty and is less accurate
- not oriented is characterised by a lack of obvious indicators for the core orientation. These cores are not oriented.

Tab. 2-1 gives an overview of the core goniometry confidence assessment. The procedure described in Section 2.1.2 resulted in a successful orientation of 651 m out of the total 833 m of drill cores (78 %).

Tab. 2-1: Core goniometry confidence assessment

Interval			**Goniometry confidence**								
Top	**Bottom**	**Core length**	**High**			**Moderate**			**Not oriented**		
[m]			[m]	[%]	No. of COLs	[m]	[%]	No. of COLs	[m]	[%]	No. of COLs
535	1370.19	833	330	40	35	321	38	63	182	22	79

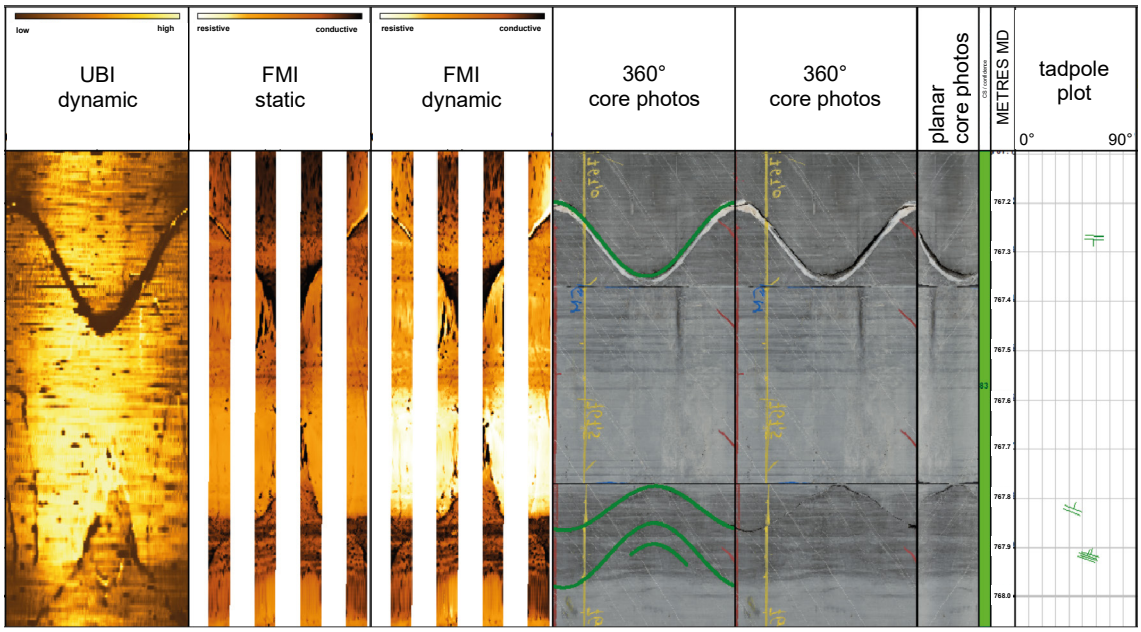

Fig. 2-6: Core – FMI / UBI correlation for a fault at 767.27 m MD log depth

This prominent 58° dipping fault was unequivocally correlated across the UBI / FMI log and the core photograph and therefore represents a high-confidence indicator for the core orientation. From left to right: acoustic UBI image log, dynamic and static normalised FMI, shifted and oriented 360° core photographs with (left) and without (right) sine waves, followed by shifted planar core photographs. The core section numbering is shown in the coloured bar displaying the goniometry confidence ranking. The depth track shows the position and length of the currently displayed window. A tadpole plot with true orientation of manually picked planes is also displayed.

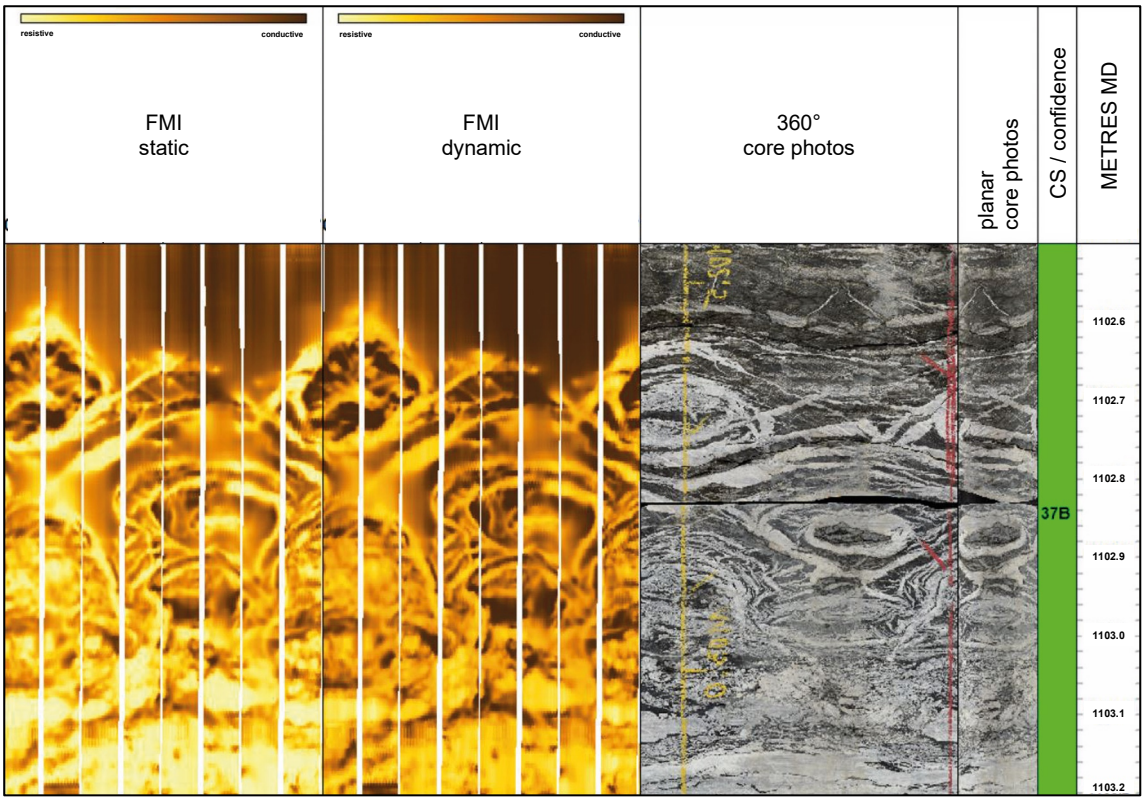

Fig. 2-7: Core – FMI correlation in the Bänkerjoch Formation from 1'102.50 – 1'103.20 m MD

These unique structures represent bullseyes related to folding and were used to orient the core Section 37B. They are considered as robust indicators for the core goniometry and assigned to the high confidence level (green).

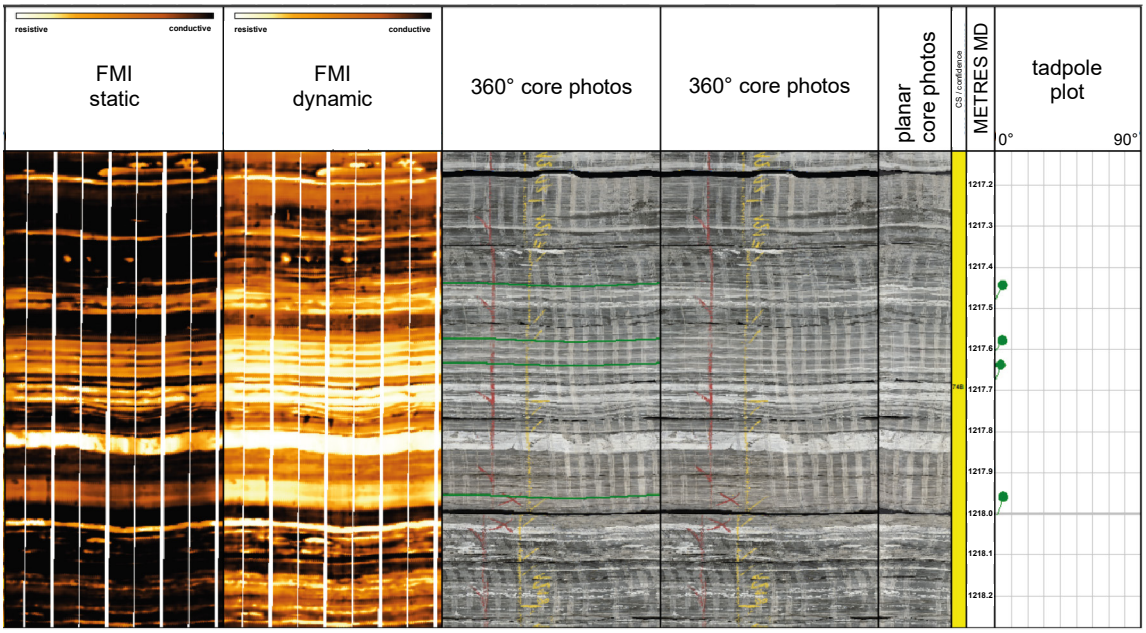

Fig. 2-8: Core – FMI correlation in the case of flat bedding

The FMI and the core photograph match with the well-bedded strata in the Zeglingen Formation from 1'217.10 - 1'218.30 m MD log depth. Although the bedding planes are clearly visible on FMI and cores, the relatively low dip angles (< 15°) imply some angular uncertainty and are therefore considered as moderate indicators for core goniometry.

Project-specific uncertainties

A number of unavoidable limitations and uncertainties were associated with the work performed and may have affected the accuracy of the results. These factors are evaluated below:

- angular uncertainty is associated with the core goniometry and is reflected by the confidence scheme. It particularly implies an angular error for the azimuth

- errors related to geological compass measurements on drill cores: to explore the measurement-related error, multiple measurements of the same structure were performed by different users. The reproducibility was ~ 5° for the dip magnitudes and 5 – 10° for the dip azimuths. Considering that most geological compasses have an error margin within 2° for dip azimuth and magnitude, it can be concluded that the above-mentioned goniometer has an acceptable error margin and can safely be used for accurate structural core analysis

- dip picking on 360° photographs: the pixel resolution of the screen defines the angular uncertainty of the dip picks in 3D space and is 1 to 2° for the dip angle and 2 to 4° for the dip azimuth

  - core photographs: although the derived 360° core photographs covered almost the entire studied interval (535 – 1'370.14 m MD log depth), minor data gaps occurred, e.g. at around 545 m, 1'038 m and 1111 m MD log depth. These gaps are mainly related to disintegrated drill cores which were not suitable for circumferential photography

  - FMI / UBI logs: due to borehole instabilities there was a gap in the FMI / UBI data between 943 and 995 m MD core depth, resulting in non-oriented drill cores

- in some core intervals the core orientation line was discontinuous. This was mainly related to uncertainties in the assemblage of individual core pieces / sections at the drill site. In such cases the non-coherent core sections were treated separately
- due to the presence of steel in Nagra's core storage facility in Würenlingen, a site-specific magnetic field disturbance was recognised. Consequently, the goniometer needed to be carefully aligned towards relative north to obtain the correct orientations of the geological features (mainly lineations) measured with a compass. This always had to be kept in mind when moving the equipment across the core store

2.2 Structural work

This section describes (A) how the structural recording and characterisation of drill cores was carried out, (B) which structure types were distinguished, and (C) which structure parameters were defined. Details with regard to the structural core analysis are given in the structural analysis manual and enclosed fact sheets and templates (Ebert & Decker 2019).

A) After the core goniometry was finalised, all deformation structures were recorded on the drill cores.

The overall core quality was excellent. Only cores from clay-rich lithologies (especially Dogger) were strongly affected by progressive discing but were still suitable for structural analysis. Due to approximately 350 samples with lengths of up to 50 cm being taken at the drill site there were gaps within the core sections. Samplers were strictly advised not to sample core intervals containing tectonic structures. The completeness of structural record is therefore not biased or limited by sampling. Furthermore, it can be assumed that the complete structural inventory was recorded because high-resolution core photographs were taken from all cores, including the sampled core sections.

Most of the structural work was performed by two people. A structural geology expert defined all visible structure types along with their relevant parameters for each core section, which was usually 3 m long. At the same time the other colleague manually picked the structure on the 360° core photographs in TerraStation II. The structures and their parameters such as mineralisation, thickness or shear sense were documented on a DIN A3 template with content previously defined in Ebert & Decker (2019). The log depth was determined in metres MD along with the true orientation of the structures on oriented 360° core photographs. The difference in depth between the core and log depth mostly varied by only a few centimetres and depended on the dynamic depth shift of the core photos with regard to the FMI used as the main depth reference data. Striations on slickensides recognised on surfaces of broken cores were measured with a geological compass (Fig. 2-1). As soon as a core section was completely analysed, all entries from the DIN A3 template were digitised and data QC was carried out.

B) Depending on rock rheology and the type and degree of deformation, different types of structural discontinuities may develop. Based on this, the structures were subdivided into five main groups of structural discontinuities (Fig. 2-9). In total, 20 types of structures were distinguished in this study (Tab. 2-2) and are illustrated with numerous examples in Chapter 3. Detailed definitions and information on the origin of the structures can be found in the structural manual of Ebert & Decker (2019).

C) Additionally, parameters such as mineralisation, shear sense and thickness listed in Tab. 2-3 were determined and documented for each individual structure on the DIN A3 template (Fig. 2-10). In addition, each structure was sketched and labelled with a consecutive number on the designed grid with a scale of 1:10.

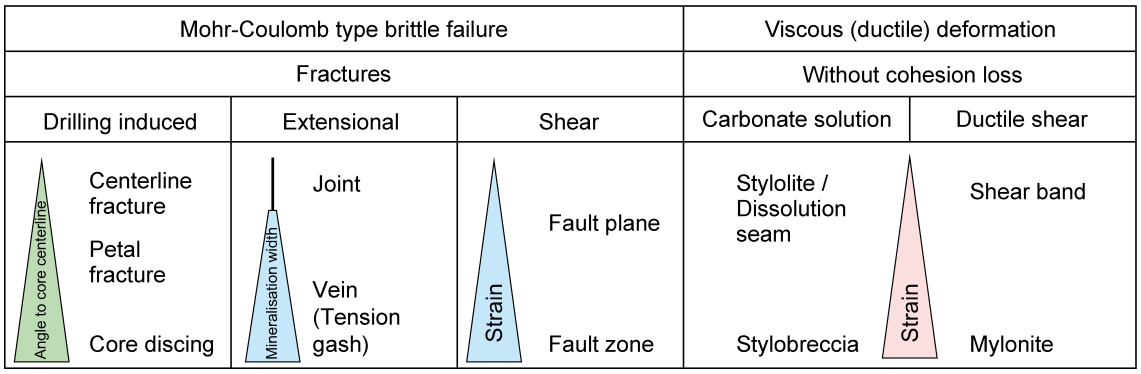

Fig. 2-9: The five main groups of structural discontinuities

Tab. 2-2: Types of structural discontinuities identified in this study

For more details see Ebert & Decker (2019).

Discontinuity group	**Structure type**	**Characteristics**
Brittle structures with shear indications	Fault plane	Planes of shear failure, i.e. planes along which there has been movement parallel to the plane (Peacock et al. 2016). Single, thin, planar and sharp structural discontinuities with shear indications (e.g. striation or slickenfibres).
	Mirror-like fault plane	A fault plane with a smoothed, polished or shiny slip surface.
	Stylolitic fault plane	A fault plane with dissolution seams and stylolites-bearing columns which are oblique or parallel to the plane (modified from Hancock 1985).
	Fault zone	A fault zone is defined as a zone with a volume which includes interacting and linked fault segments, densely fractured rock and / or fault rocks; zones are typically bounded by sub-parallel margins or fault planes (modified from Peacock et al. 2016).

Tab. 2-2: continued

Discontinuity group	**Structure type**	**Characteristics**
Brittle structures without shear or slip indications	Joint	A barren, closed fracture on which there is no measurable slip or dilatation at the scale of observation. If any mineral fill, including crystal growth fibres, is visible, the structure is better called a vein (Hancock 1985).
	Vein	Extensional fracture filled by secondary mineral crystallisation.
	Tension gash	Vein formed by dilatation; tension gashes may be fully cemented (vein), partly cemented (partly open) or open (Passchier & Trouw 1996).
Structure without preserved evidence for the mode of fracturing	Fracture	General term for a structure without preserved evidence for the mode of fracturing, i.e. it is applicable to structures formed by extension or shear; fractures can include close-to-planar discontinuities such as dykes, faults, joints and veins. (Peacock et al. 2016).
Structures caused by dissolution	Stylolites	Stylolites are irregular seams of insoluble residues with dark, "mountainous" rough teeth formed by pressure solution (Passchier & Trouw 1996).
	Open pores	Isolated open volumes in the rock mass, resulting e.g. from incomplete cementation of veins, dissolution, or preserved cavities in fossils.
	Karst	Open networks resulting from dissolution of carbonates. These cm to m wide cavities may have been refilled later.
Fabrics without cohesion loss, e.g. caused by ductile deformation	Shear bands	Minor planar shear zones in which the progressive deformation is non-coaxial (Passchier & Trouw 1996).
	Mylonites	Strongly deformed rock from a ductile shear zone with a planar foliation and usually with a stretching lineation (Passchier & Trouw 1996).
	Schistosity	Secondary foliation defined by preferred orientation of equant fabric elements in a medium- to coarse-grained rock. Individual foliation-defining elements (e.g. micas) are visible with the naked eye (Passchier & Trouw 1996).
	Dynamic recrystallisation	Dynamically recrystallised, smaller and elongated crystals.

Tab. 2-2: continued

Discontinuity group	**Structure type**	**Characteristics**
Drilling-induced fractures (DIF)	Drilling-induced fractures	Collective term for fractures created by forces associated with drilling and coring procedures. Depending on load on drill bit, mud weight and rock properties, drilling-induced fractures develop during drilling or shortly thereafter. Based on the aperture, fracture surface and geometric relationships, drilling-induced fractures can be distinguished from natural fractures. Drilling-induced fractures are always open and never mineralised.
	Petal fracture	Drilling-induced fracture with convex-up geometry cutting a core downwards starting from its perimeter. Petal fractures form immediately ahead of the drill bit as a result of excessive bit weight during coring. They propagate downhole.
	Centreline fracture	Drilling-induced fracture that typically splits a core approximately in half.
	Core discing	The formation of discs of relatively uniform thickness which fracture on surfaces approximately normal to the axis of the core
Additional features / dip types	Undifferentiated bedding	Planar surface representing either the boundary between two different lithological units or internal bedding. Thought to reflect original horizontal and planar surfaces.
	Deformed bedding	Bedding planes occurring in narrow zones in any lithology with moderate to steep dip angles (> 15°) which differ from the general structural dip. They have been subject to deformation due to faulting and / or folding.
	Cross-bedding	Inclined foreset surfaces in sandstone occurring in sets and bounded by set boundaries. These sedimentary features may be used as paleocurrent indicators. Upper truncation by the next set is diagnostic.
	Fold (axis)	One or a stack of originally flat and planar surfaces, such as sedimentary rocks, that are bent or curved due to applied external stress. Folds appear in various scales and shapes.
	Fracture density	Numerical value that reflects a quantitative measure of the abundance of fractures in rock mass (e.g. fractures per metre, fracture area per rock volume).

Tab. 2-3: Systematically recorded parameters for the investigated structures

Parameter	**Definition of parameters and procedure for defining parameters**
Depth	All types of structures are recorded quantitatively along the scanline of the core axis. The depth of the structure is measured at the point where it cuts the core axis. For steeply dipping planes, depth should be determined half-way between the top and the base of the intersection ellipse of the structure. If a zone is recorded (e.g. fault zone, shear band, fracture density class), the top (Top MD) and the base (Bottom MD) of the zone are specified in the corresponding columns.
Core orientation line number	After the extraction of the core from the inner tube, the core pieces are juxtaposed whenever possible. Continuous sections without drilling breaks, demarcated by grinding, crushed or core loss zones, are marked with a core orientation line and denoted with a consecutive number. This number enables linking of the recorded structure with the key structure of this orientation line section that was identified on the borehole image.
Depth shift between core and FMI	The depth shift is defined using correlated structures visible on both the FMI and core.
Correlation with log	Assessment whether each individual structure can be clearly identified on FMI / UBI and core. “yes” indicates that the structure can be correlated with the image log, and “no” indicates structures which cannot be correlated, or which are not shown by the image log. In addition, a correlation quality ranking is carried out (1 – good, 2 – moderate, 3 – no correlation).
Dip direction and dip	Measured dip direction and dip of the structure.
Structure type	The abbreviations of structure types according to Tab. 2-2 are entered into the paper template.
Length of structure	The length of the long axis of the intersection ellipse should be measured for structures which cut the core axis at acute angles (dipping with more than about 70°) and structures which do not cut through the entire core diameter. The measured length will be used for the calculation of fracture density P32. Measurements are required to reduce the inaccuracy resulting from calculating fracture areas solely from the angle between the structure and the core axis.
Azimuth and plunge of lineations	Measured dip azimuth and plunge of the lineation observed on the measured plane.
Shear sense and quality	Shear sense of fault planes and shear bands using up (reverse fault), down (normal fault), dex (dextral strike slip) or sin (sinistral strike slip), and reliability indicators (good, fair, poor) of the shear sense observation.
Mineralisation / fault rock type	Any type of filling, mineralisation or fault rock associated with the structure (e.g. CC for calcite of a vein filling, synCC for mineralisation of slickenfibres).

Tab. 2-3: continued

Parameter	**Definition of parameters and procedure for defining parameters**
Open / closed and width / length of open structures	Information on whether a tension gash / vein is open (displaying a continuous aperture), partly open (displaying a discontinuous aperture) or closed at the observation scale (i.e. the naked eye), including the width of the aperture and the observed lengths of open streaks for partly open structures.
Roughness	Roughness classification of a structure using the joint roughness coefficient (JRC). The JRC gives a picture of the classification of fracture smoothness and waviness (planarity) along 10 cm length of the fracture (Barton 1976, Barton & Choubey 1977). The scale of the JRC is from 0 (very smooth and planar) to 20 (very rough and wavy).
Fracture condition	Specifies whether the core is broken naturally or artificially at the structure under consideration or intact. If it cannot be specified whether the break occurred naturally or artificially, broken should be used.
Fracture density class (FDC)	In cases where cores or parts of a core are heavily disintegrated and order cannot be restored, the density of natural fractures cannot be calculated accurately. Fracture density should be estimated using the classification scheme of Bauer et al. (2016): fracture density class 2 (spacing of fractures = 5 – 10 cm), fracture density class 3 (spacing of fractures = 1 – 5 cm) or fracture density class 4 (spacing of fractures < 1 cm).
Additional remarks	Offsets or displacements as well as crosscutting relations are documented under "remarks". Further remarks are e.g. karstification, the shape and length of the teeth of stylolites, alterations, recrystallisation phenomena, or whether a structure is of synsedimentary origin.

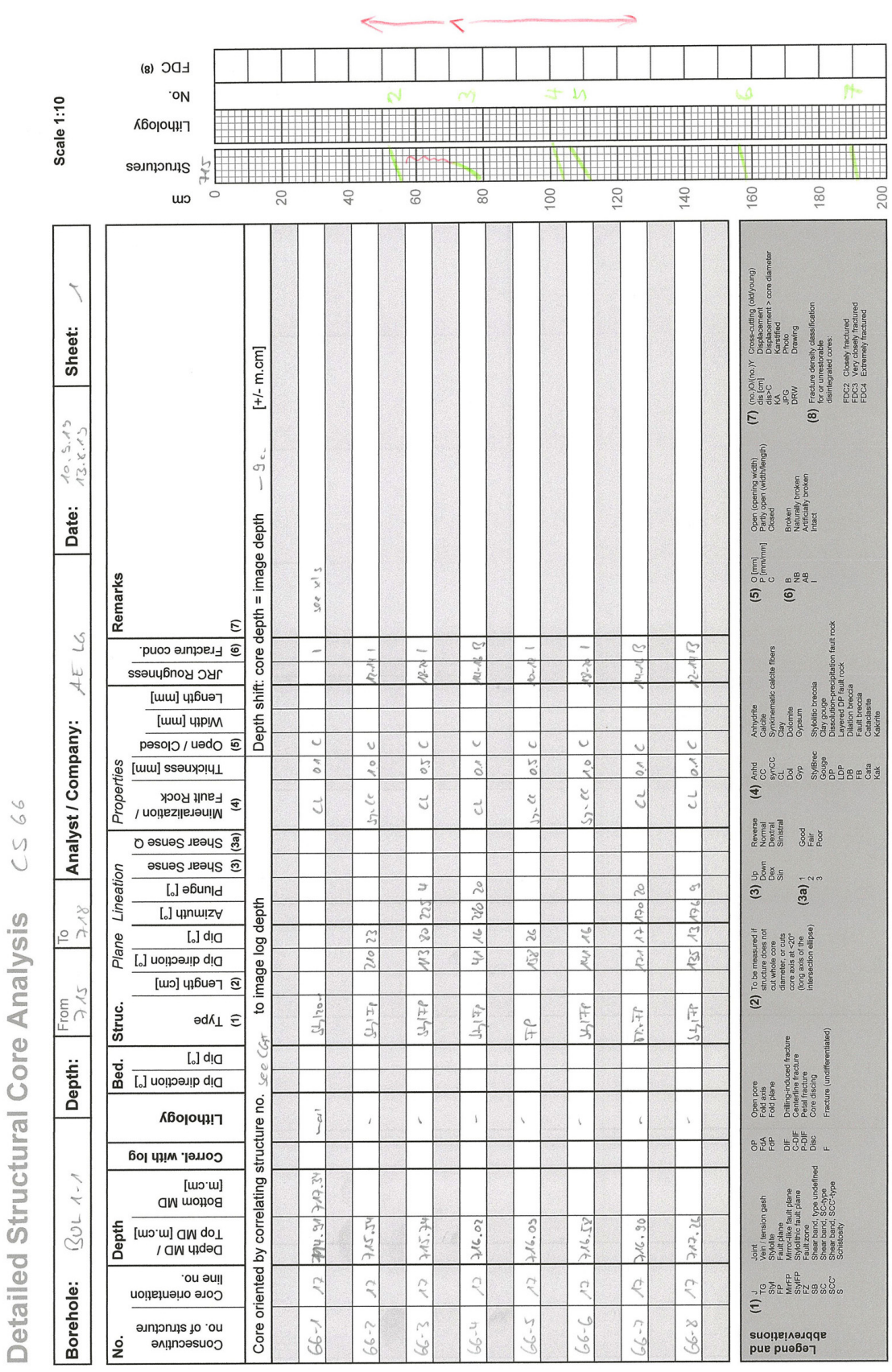

Fig. 2-10: Completed DIN A3 sheet of primary record of the structural core analysis

2.3 Geo-statistical evaluation

For the geo-statistical evaluation presented in Chapter 4, different structural tools and techniques were applied to analyse the available dip dataset. Most of the work was performed with TerraStation II. This provides several advanced modules for the import, processing, visualisation and analysis of all types of available borehole data such as petrophysical logs, borehole images, core data and stratigraphic information.

For the structural evaluation of the different lithostratigraphic units and the different types of structural discontinuities, a series of figures was compiled:

- stereograms (Schmidt projection, lower hemisphere):
  - poles of the planes were displayed to examine the spatial orientation of bedding and structural planes
  - azimuth rose diagrams were compiled for planar features (bedding and fractures). The diagrams show the dip azimuth of the planes under consideration. The rose diagram is a circular histogram summarising orientation measurements. The radius of each segment of a rose diagram is proportional to the number of observations that occur within the angular range of that segment. Azimuth rose diagrams are displayed with cumulative petals resulting in staked petals for different dip categories. For the directional statistics a minimum threshold of ten structures was set for the rose diagrams
- dip histograms visualise the dip angle distribution and clustering for a given dip dataset
- vector means for representative clusters of the different structure types were calculated in stereograms
- the vector azimuth plot (dip walkout plot) reflects the along-borehole dip variations and was compiled for bedding-related dips only (deformed dips and crossbedding were excluded). Here, the azimuth of a plane was plotted in a nose-to-tail fashion pointing in the direction of dip. The length of an interval is related to the number of dips and not to the thickness of lithostratigraphic units
- fracture density (P32 curves) reflects the fracture area per unit of rock volume (m^2/m^3). The algorithm computes the area of each fracture and creates a sum of the areas across the defined window of 1 m core length and steps of 0.1524 m. The lengths of sub-vertical fractures are incorporated whereas truncated parts of fractures are discarded. The computation of the area accounts for borehole ellipticity. The total area of fractures is then divided by the borehole volume (or volume of the rock mass) of the selected window. See Ebert & Decker (2019) and the literature therein for a more detailed discussion on P32 fracture density calculation. For this study, P32 fracture densities were calculated for all structural discontinuities as well as for each individual group:
  - fault-planes, mirror-like fault planes and stylolitic fault plane
  - fractures, joints and tension gashes / veins
  - stylolites

The recorded kinematic indicators were analysed using TectonicsFP software. The available fault and kinematic data were plotted in stereographic Angelier projection where the symbols and colours reflect the different shear senses (up, down, sinistral or dextral) and the observed shear sense reliability (good, moderate, poor). Please be aware that all Angelier plots in this report show corrected data sets, where the data points of the lineations are projected on the great circle of the corresponding fault plane, even though they may have an angular offset < 15°.

3 Inventory of structure types

The different structure types identified in the drill cores from BUL1-1 and BUL1-1B and their most important characteristics were described in Section 2.2. In this Chapter, these structures are visualised with examples. The diameter of the cores in the following figures is 95 mm (Figs. 3-1 to 3-32).

3.1 Examples of fault planes



Fig. 3-1: Fault plane

Characteristics: Left: Example of a prominent fault plane with striation and cm-thick syn-kinematic calcite. Shear sense is top up (reverse fault).

Right: 360° core photograph view of the same structure with a high amplitude sine wave indicating a steep dip angle (image width is 30 cm).

Formation: Wildegg Formation, Depth: 780.39 m MD core depth.

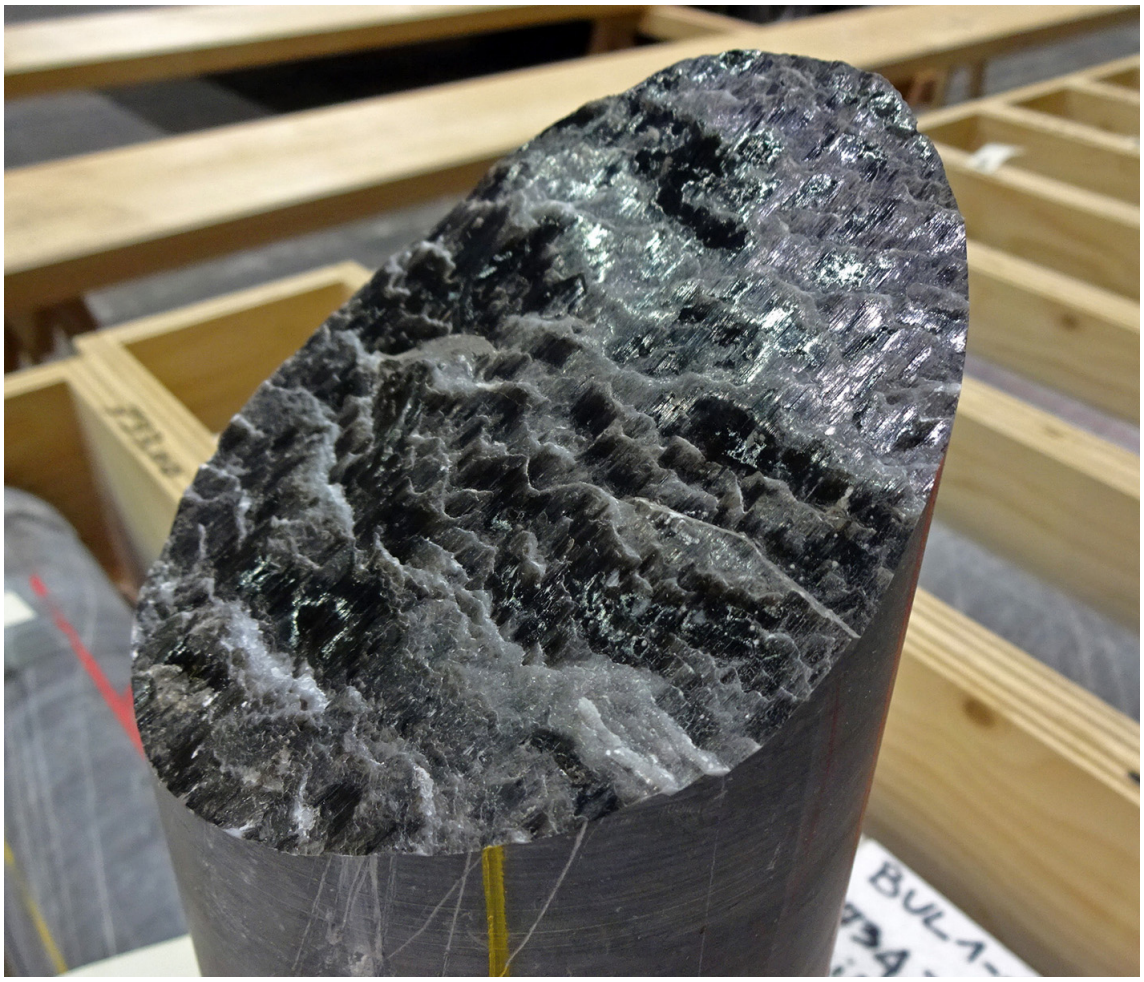

Fig. 3-2: Fault plane

Characteristics: A discrete, planar and sharp fault plane. The striation shows dip-parallel slip formed by striation and slickenfibres with synkinematic calcite. Shear sense is top up (reverse fault).

Formation: Villigen Formation, Depth: 733.27 m MD core depth.



Fig. 3-3: Fault plane

360° core photograph view of the fault plane presented in Fig. 3-2 (image width = 30 cm). Note the typical, jagged sine wave visible on the core surface.



Fig. 3-4: Fault planes

Characteristics: Left: Example of a horizontal fault plane.

Right: An oblique fault plane with a sub-horizontal striation. Both striations are directed N-S and are associated with synkinematic calcite mineralisation.

Formation: «Felsenkalke» / «Massenkalk», Depth: 554.60 m MD core depth (left), 556.84 m MD core depth (right).

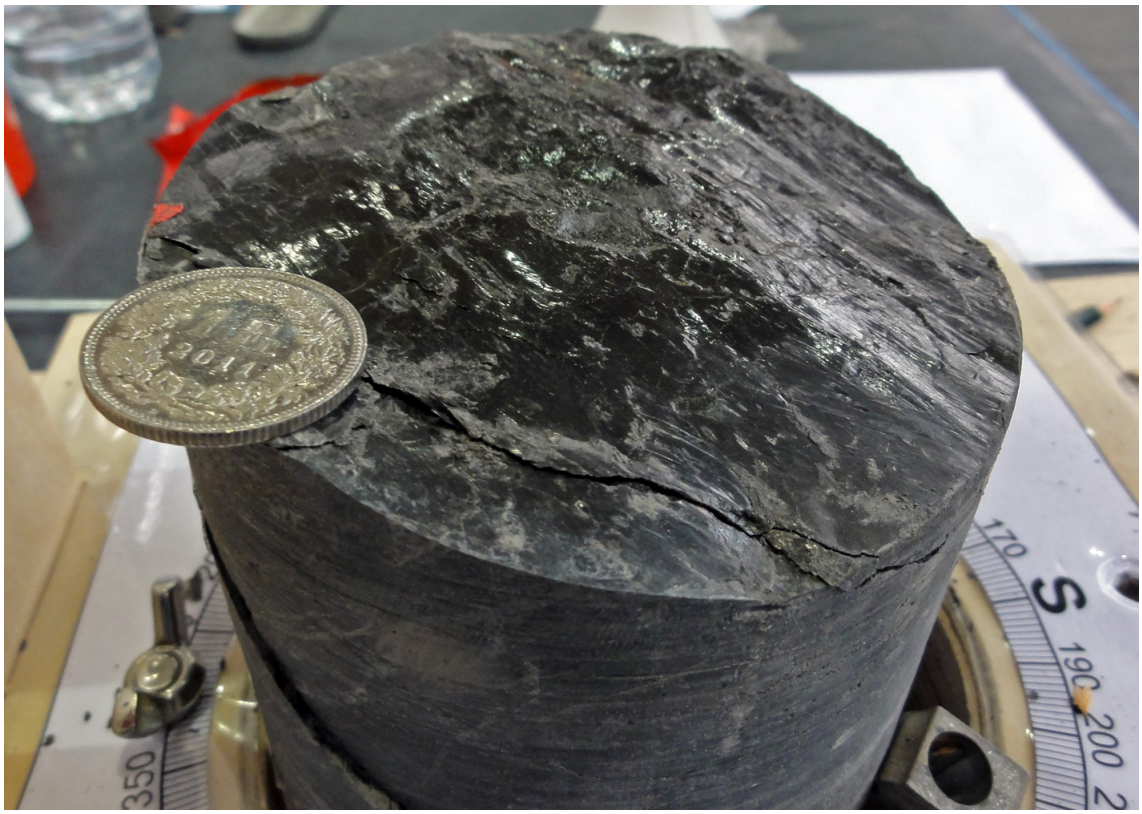

Fig. 3-5: Mirror-like fault plane

Characteristics: A sharp fault plane with a polished, mirror-like slip surface and striation.

Formation: 'Brauner Dogger', Depth: 890.16 m MD core depth.



Fig. 3-6: Mirror-like fault plane

Characteristics: Example of a sharp fault plane with a smooth, polished mirror-like slip surface.

Formation: Zeglingen Formation, Depth: 1'238.22 m MD core depth.



Fig. 3-7: Stylolitic fault plane

Characteristics: Example of a steep fault plane with an oblique striation generated by stylolitic dissolution sub-parallel to the plane. Strike-slip fault with an oblique, reverse fault shear sense. (Left: core; right: 360° core photograph with width 30 cm).

Formation: «Felsenkalke» / «Massenkalk», Depth: 612.25 m MD core depth.

3.2 Examples of fault zones

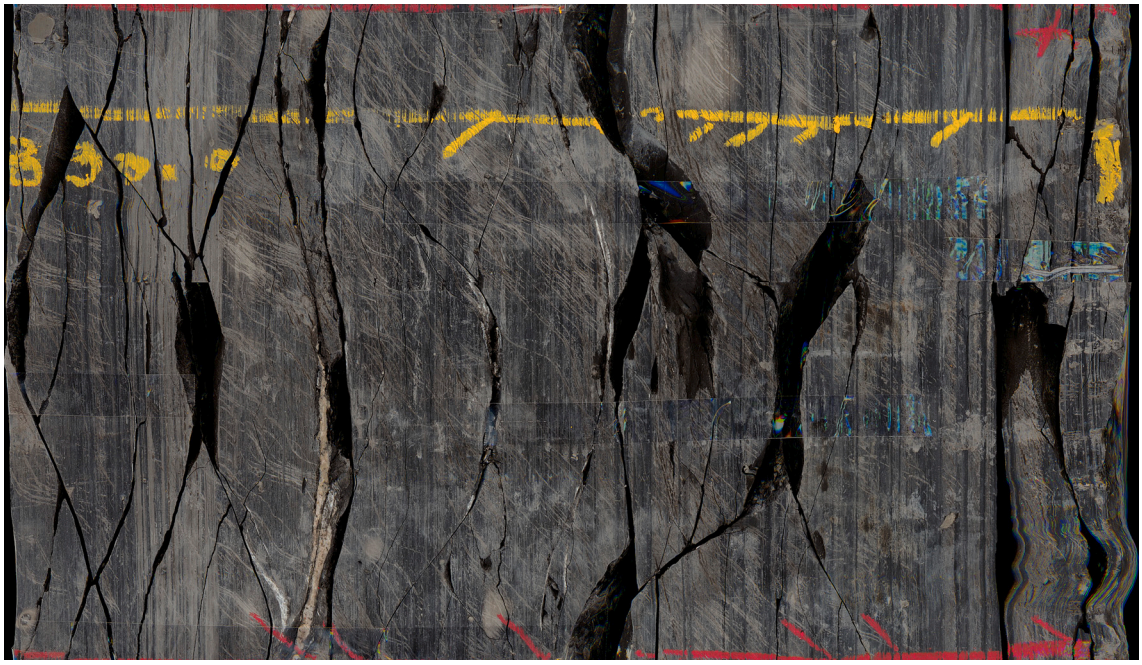

Fig. 3-8: Fault zone with FDC 2

Characteristics: Example of a fault zone with numerous discrete and intersecting mirror-like fault planes and fault planes with synkinematic calcite. The core disintegration level corresponds to fracture density class 2. 360° core photograph with an image height of 30 cm.

Formation: 'Brauner Dogger', Depth: 890.02 – 890.37 m MD core depth.



Fig. 3-9: Fault zone with FDC 3

Characteristics: Example of a fault zone with numerous intersecting mirror-like fault planes. The abundance of faults corresponds to fracture density class 3.

Formation: Klettgau Formation, Depth: 1'041.36 – 1'041.86 m MD core depth.

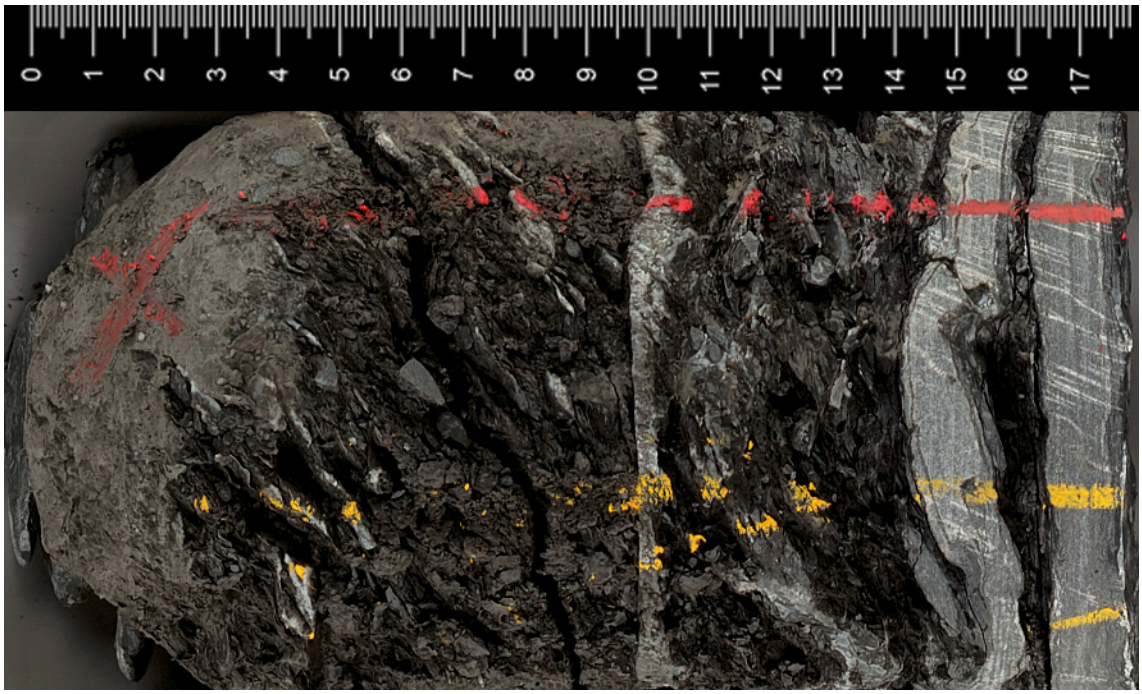

Fig. 3-10: Fault zone with FDC 4

Characteristics: Example of a fault zone revealing a network of mirror-like fault planes with mm spacing. The core disintegration level corresponds to fracture density class 4.

Formation: Klettgau Formation, Depth: 1'087.04 – 1'087.23 m MD core depth.

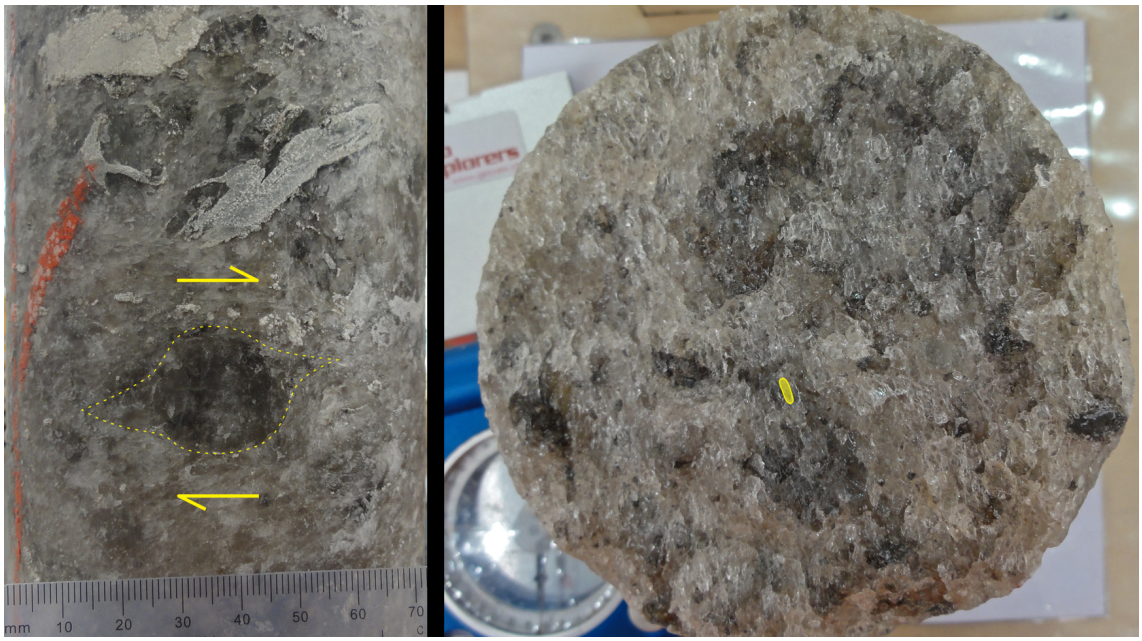

Fig. 3-11: Dynamic recrystallisation within a fault zone

Characteristics: Example of a shear zone in the salt layers of the Zeglingen Formation. The zone is characterised by dynamic recrystallisation of salt resulting in smaller, elongated (recrystallised) salt crystals (right image, example crystal marked in yellow). In addition, sigmoidal salt clasts were found in the partly recrystallised matrix (left image, inferred shear sense indicated in yellow).

Formation: Zeglingen Formation, Depth: 1'251.13 m MD core depth (left), 1'255.70 m MD core depth (right).

3.3 Examples of joints

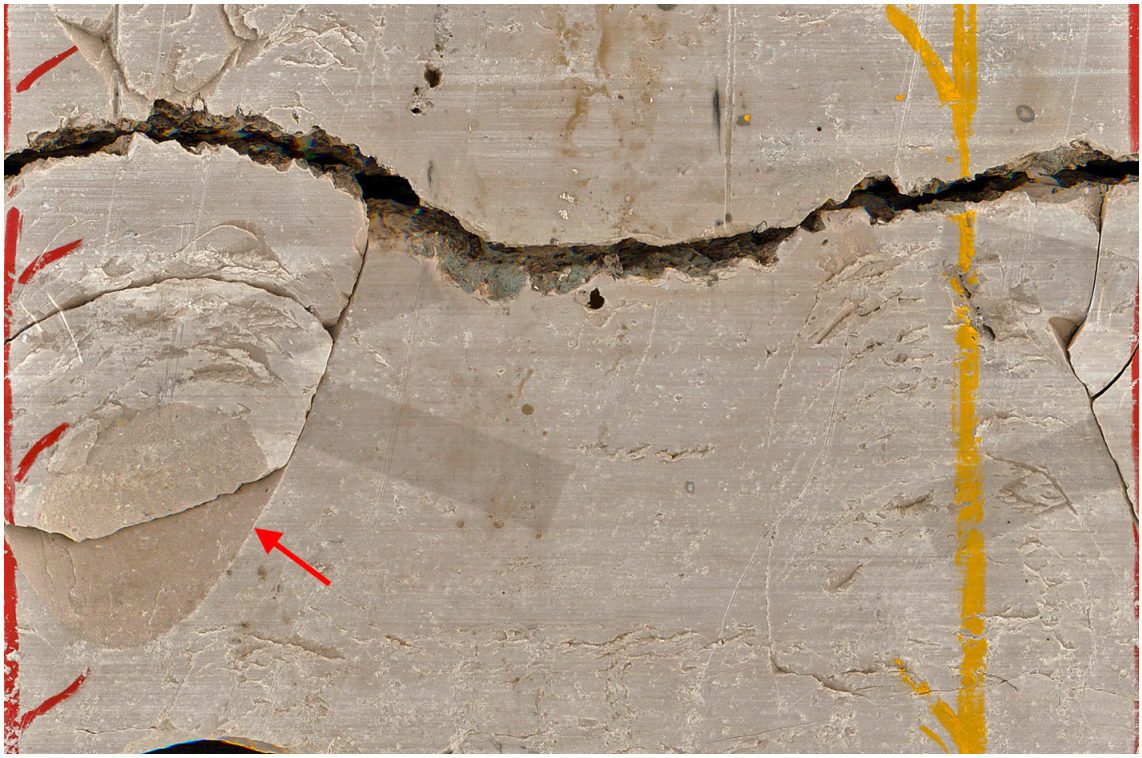

Fig. 3-12: Joint

Characteristics: Example of a planar fracture without lineation or slip indications. The joint (marked with a red arrow) terminates on a sub-horizontal stylolite. 360° core photograph (image width = 30 cm).

Formation: «Felsenkalke» / «Massenkalk», Depth: 585.91 m MD core depth.



Fig. 3-13: Joint

Characteristics: Example of fracture without any lineation or slip indications. Microscopic calcite crystals are visible on the core surface.

Formation: «Felsenkalke» / «Massenkalk», Depth: 600.71 m MD core depth.

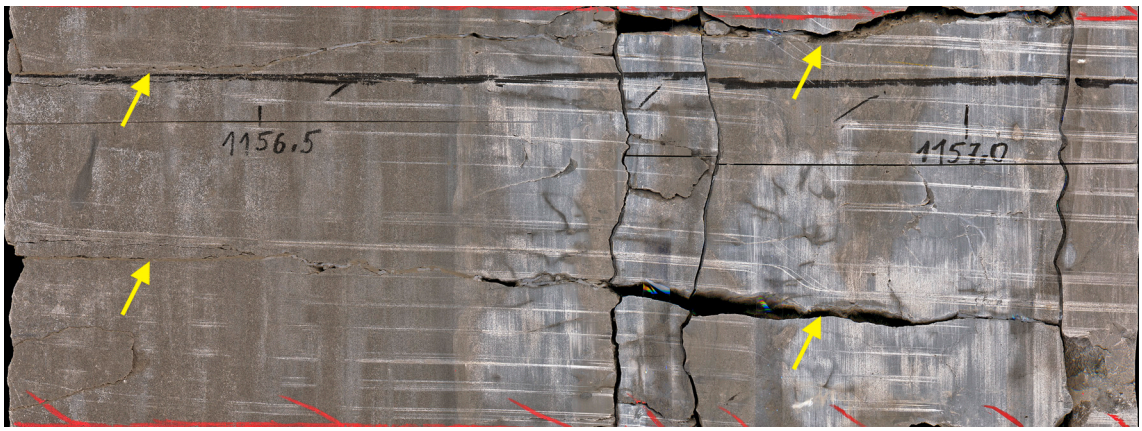

Fig. 3-14: Joint

Characteristics: A 4 m long, sub-vertical joint which was traceable over several core sections (marked with yellow arrows). It is characterised by the absence of lineations and slip indications. Partial filling with drilling mud indicates an open character. 360° core photograph (image height = 30 cm).

Formation: Schinznach Formation, Depth: 1'156.32 – 1'157.13 m MD core depth.

3.4 Examples of veins / tension gashes



Fig. 3-15: Vein / tension gash

Characteristics: Example of a sharp sub-vertical vein with blocky calcite cement filling of an extension fracture. 360° core photograph (image height = 30 cm).

Formation: Villigen Formation, Depth: 725.71 m MD core depth.

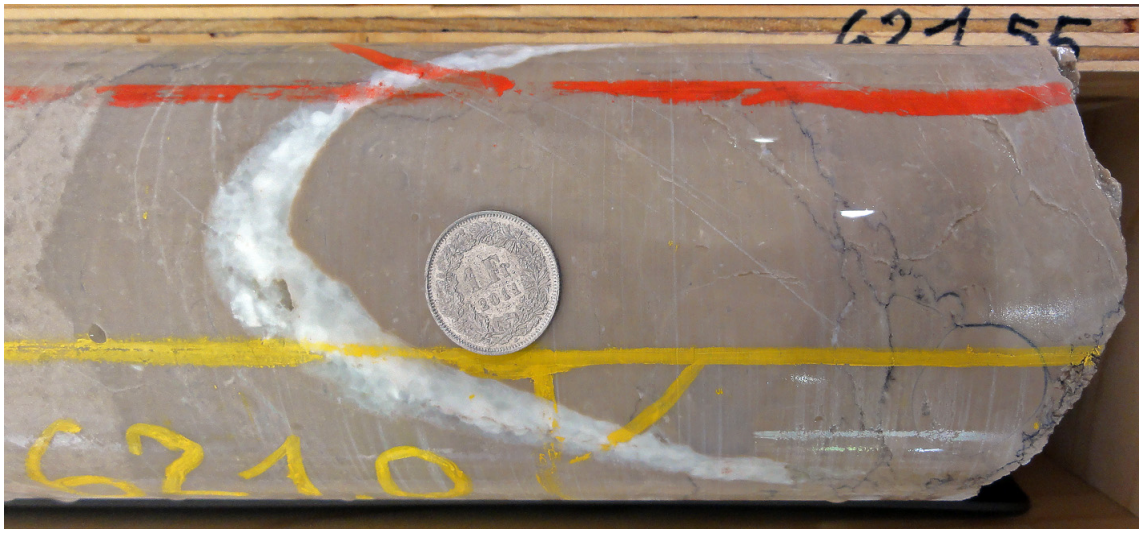

Fig. 3-16: Vein / tension gash

Characteristics: Example of a thick vein with blocky calcite filling.

Formation: «Felsenkalke» / «Massenkalk», Depth: 621.05 m MD core depth.

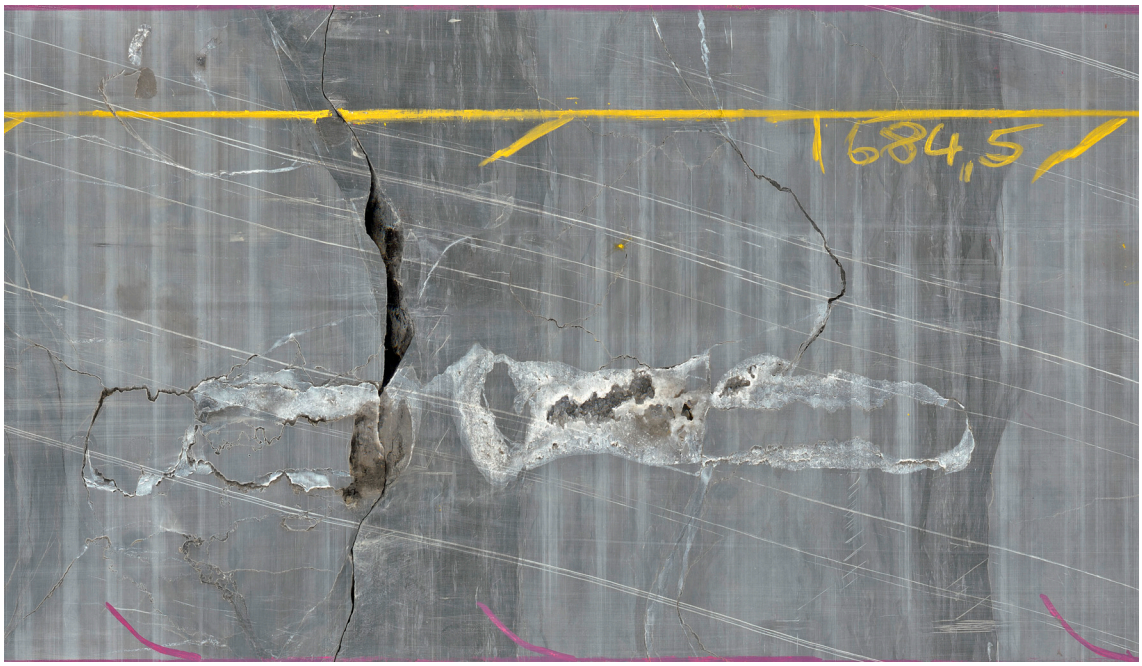

Fig. 3-17: Vein / tension gash

Characteristics: Example of a sub-vertical calcite vein. The vein is partly open with druse-like calcite crystals in its centre. 360° core photograph (image height = 30 cm).

Formation: Villigen Formation, Depth: 684.28 m MD core depth.

3.5 Examples of stylolites



Fig. 3-18: Stylolites

Characteristics: Example of a stylolite with cm-long sub-vertical teeth (image height = core diameter = 95 mm).

Formation: «Felsenkalke» / «Massenkalk», Depth: 586.49 m MD core depth.



Fig. 3-19: Stylolites

Characteristics: Examples of sub-horizontal stylolites with small vertical teeth (dark lines marked with red arrows) on a 360° core photograph (image width = 30 cm).

Formation: Left: «Felsenkalke» / «Massenkalk», Depth: 593.07 – 593.63 m MD core depth.
Right: Schinznach Formation, Depth: 1'141.34 - 1'141.73 m MD core depth.



Fig. 3-20: Stylolites

Characteristics: Example of the surface of a stylolite with cm-long sub-vertical teeth.
Formation: Schinznach Formation, Depth: 1'141.03 m MD core depth.

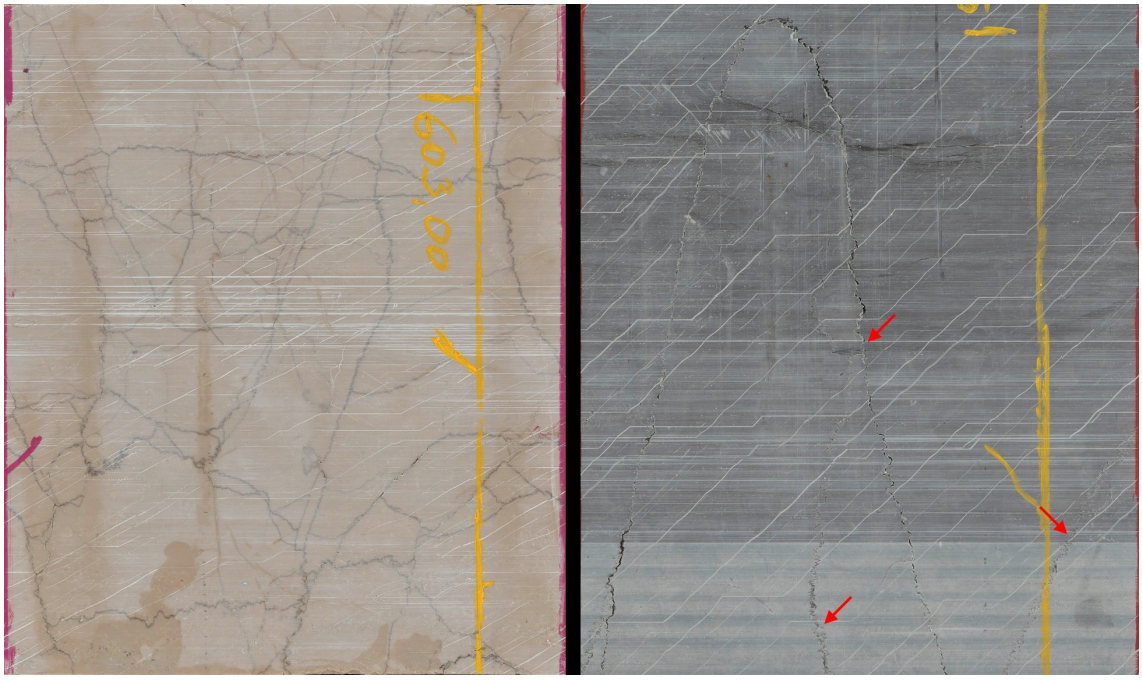

Fig. 3-21: Stylolites

Characteristics: Network of stylolites (left) and sub-vertical stylolites with sub-horizontal teeth (right). 360° core photograph (image width = 30 cm).
Formation: Left: «Felsenkalke» / «Massenkalk», Depth: 602.95 – 603.31 m MD core depth.
Right: Villigen Formation, Depth: 715.48 m – 603.83 m MD core depth.

3.6 Examples of open pores



Fig. 3-22: Open pore

Characteristics: Example of large open pores with druse-like, idiomorphic calcite crystals.

Formation: 'Brauner Dogger', Depth: 833.37 m MD core depth



Fig. 3-23: Open pores

Characteristics: Example of a medium-sized open pore that is partly mineralised with calcite crystals (image height = 30 cm).

Formation: «Felsenkalke» / «Massenkalk», Depth: 572.30 m MD core depth.

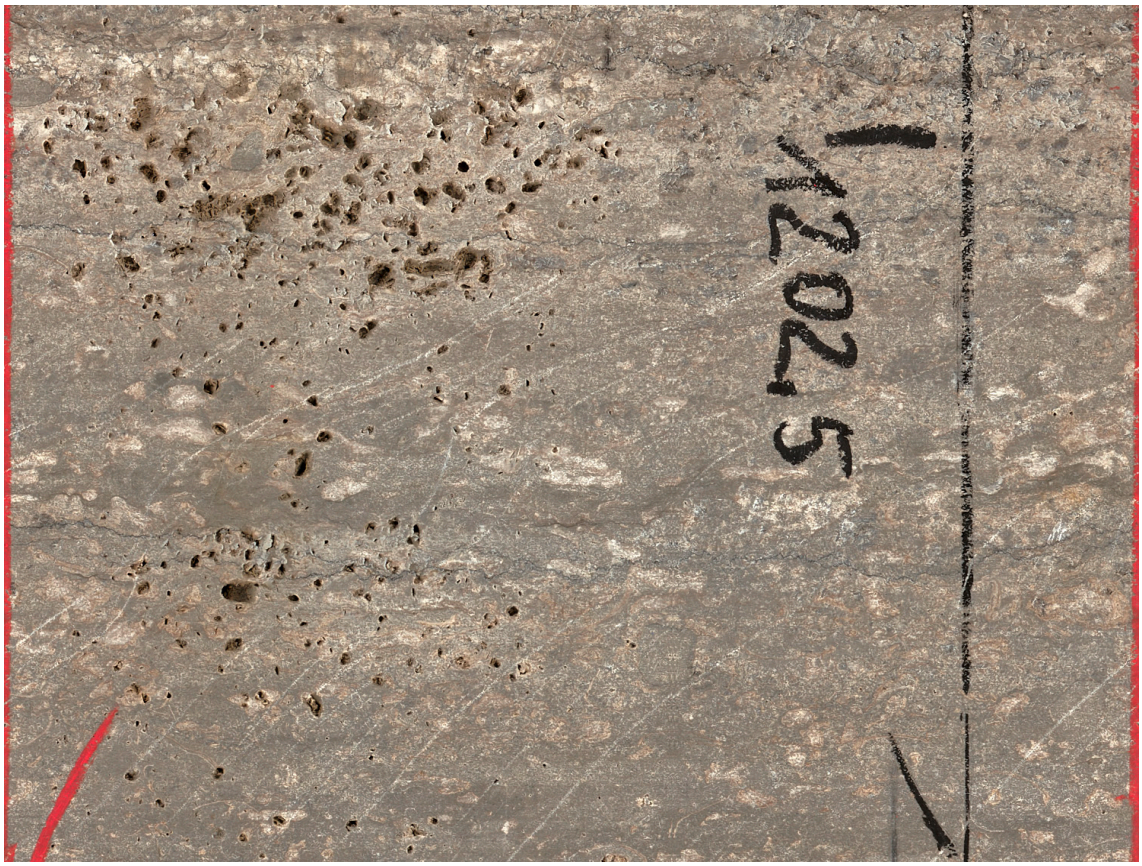

Fig. 3-24: Open pores

Characteristics: Example of small-sized open pores. Typical layer found in the Schinznach Formation with a dense network of mm-sized pores without mineralisation (image width = 30 cm).

Formation: Schinznach Formation, Depth: 1'202.40 – 1'202.76 m MD core depth.

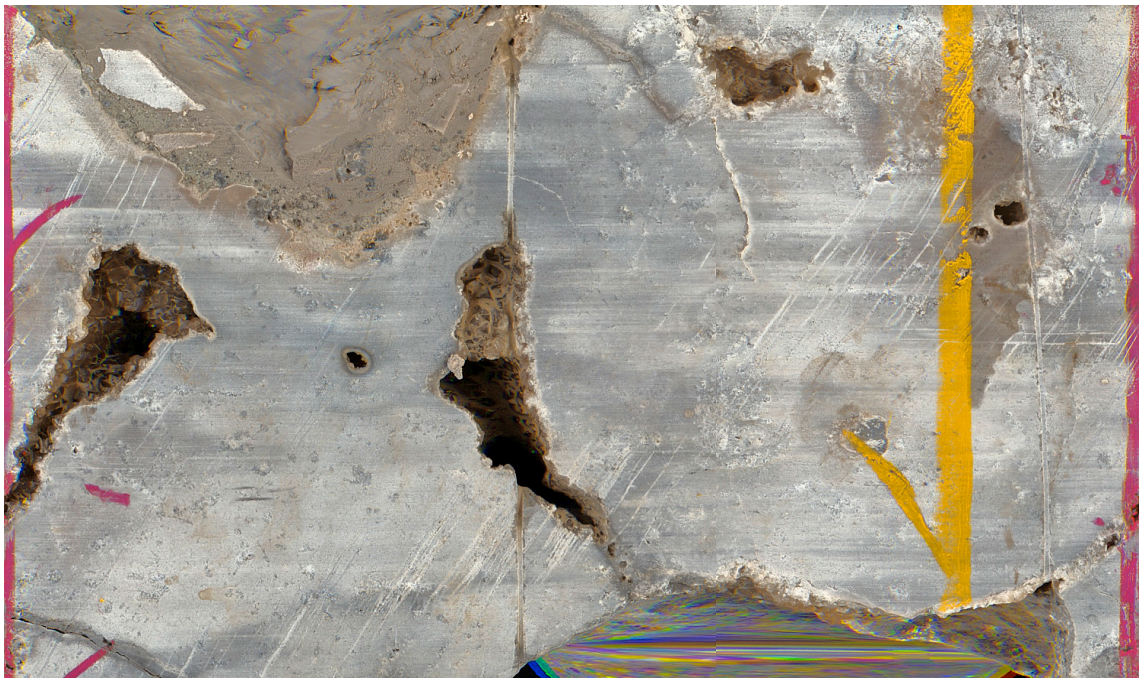

Fig. 3-25: Open pores

Characteristics: Example of open karst cavities formed due to rock dissolution (image width = 30 cm).

Formation: «Felsenkalke» / «Massenkalk», Depth: 625.73 m MD core depth.

3.7 Drilling-induced fractures

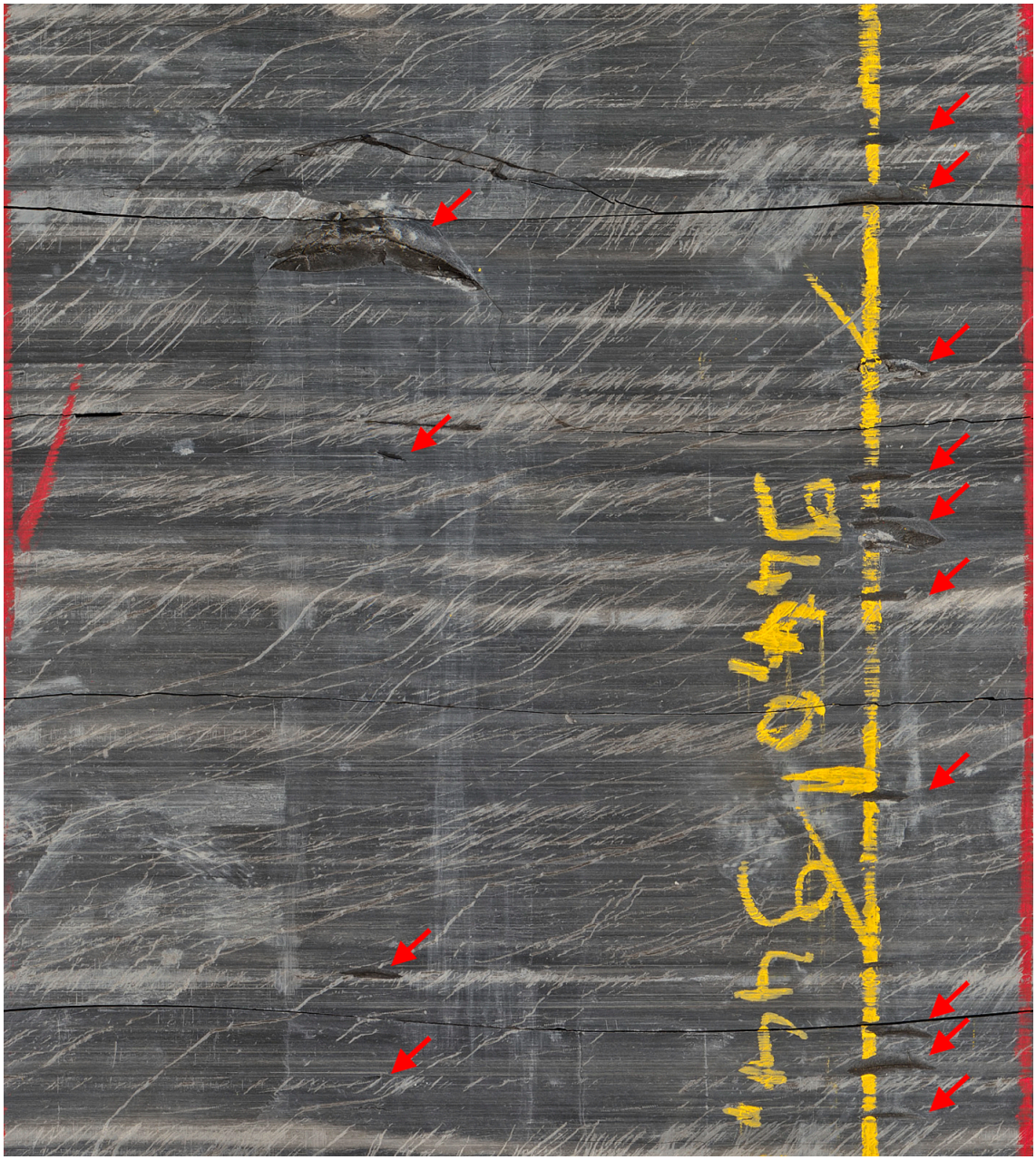

Fig. 3-26: Petal fractures

Characteristics: In claystones, pairs of petal fractures were visible as two opposite facing, parallel sets of small, curved and broken core pieces. The strike of both sets was NNE-SSW and the mean dip directions were around 110° and 300° (image width = 30 cm).

Formation: Opalinus Clay, Depth: 943.77 – 944.13 m MD core depth.

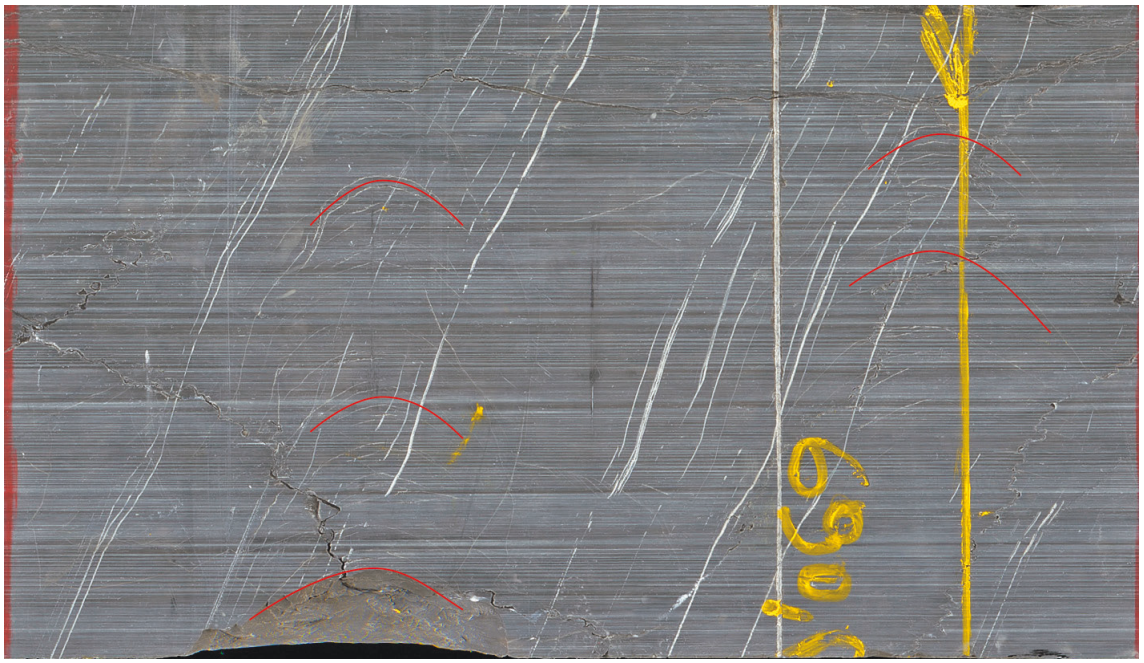

Fig. 3-27: Petal fractures

Characteristics: Sharp fissures that bend down-dip into the core from the core rim. Usually occur in multiples and in succession. Two sets of opposing PDIFs (petal drilling-induced fractures) were visible. The strike of both sets was NNE-SSW and the dip directions were around 100° and 280° (image width = 30 cm).

Formation: Villigen Formation, Depth: 689.83 – 690.00 m MD core depth.

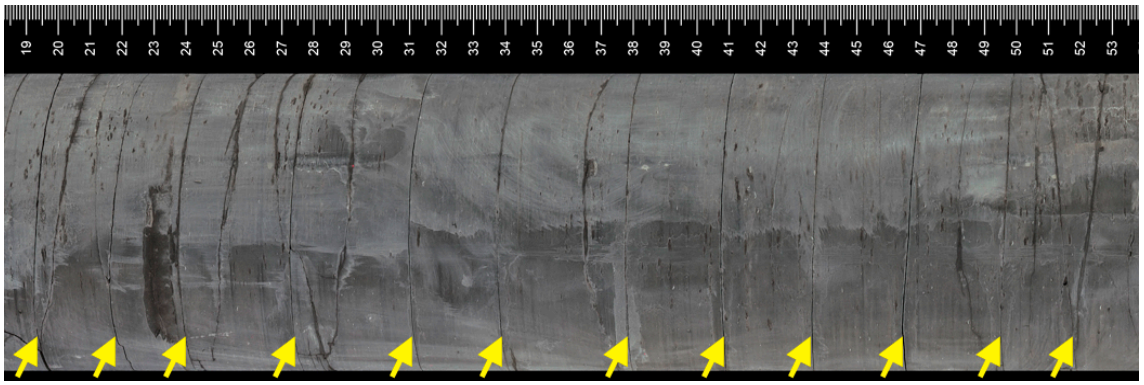

Fig. 3-28: Discing

Characteristics: Example of discing in claystone splitting the core into several discs with typical parallel fractures. Discs were perpendicular to the core axis and parallel to the bedding (marked with yellow arrows).

Formation: Opalinus Clay, Depth: 991.26 – 991.60 m MD core depth.



Fig. 3-29: Discing surface

Characteristics: Example of a discing surface with plume structure nucleating from the core centre.

Formation: Opalinus Clay, Depth: 888.72 m MD core depth.

3.8 Folding

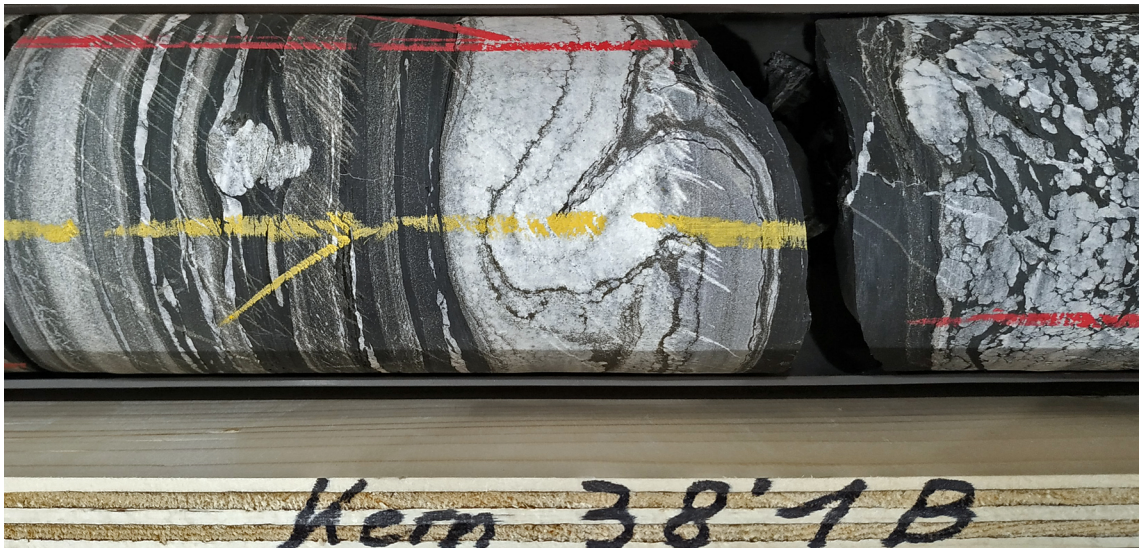

Fig. 3-30: Folding

Characteristics: Example of a folded anhydrite layer.
Formation: Bänkerjoch Formation, Depth: 1'105.35 m MD core depth.

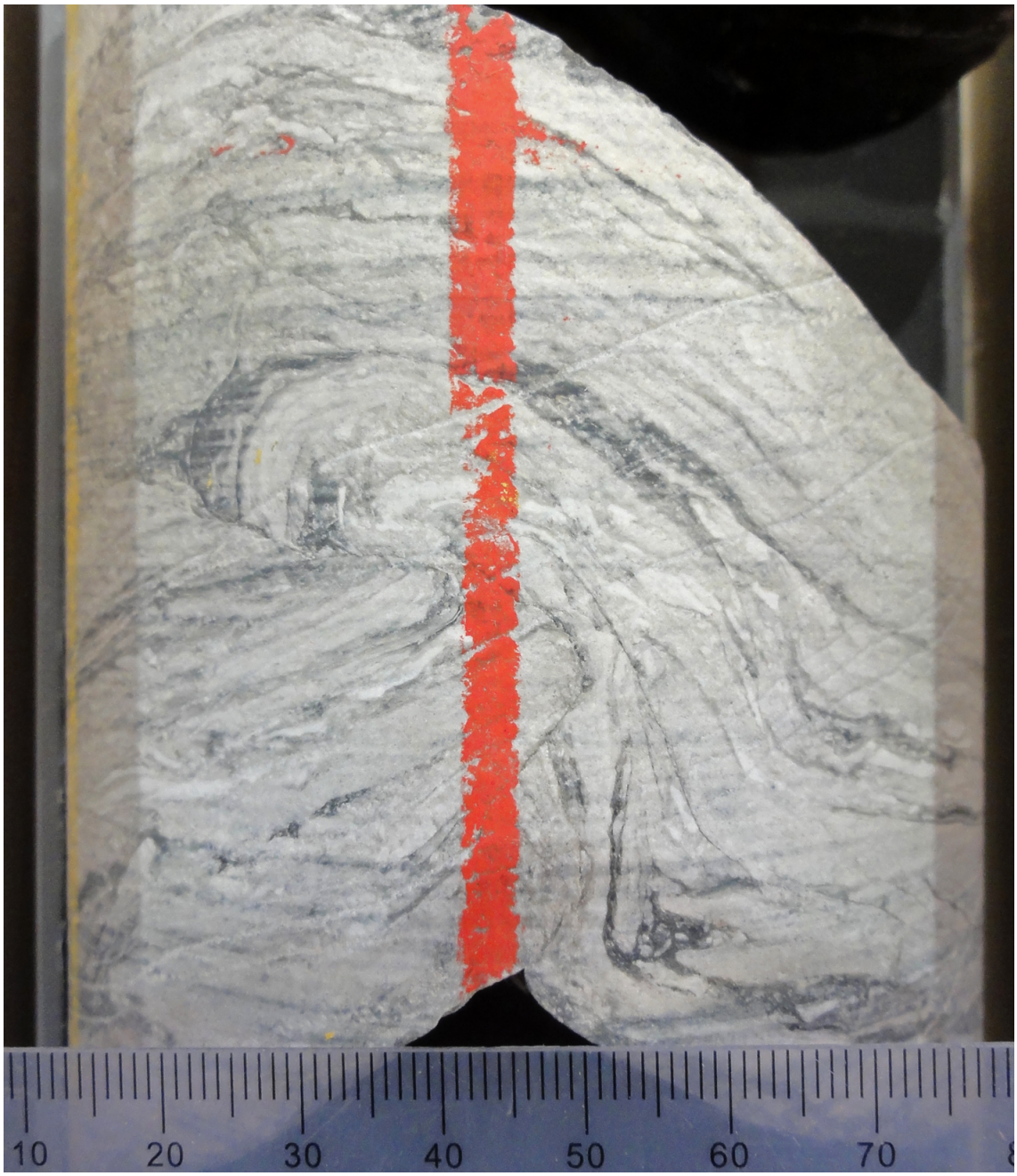

Fig. 3-31: Folding

Characteristics: Example of a folded anhydrite layer. Note the fault propagation folding governing the ramp anticline / reverse fault with 1 cm displacement.

Formation: Zeglingen Formation, Depth: 1'241.29 m MD core depth.



Fig. 3-32: Folding

Characteristics: Example of a box-like fold in an anhydrite layer associated with fault propagation folding and reverse faulting causing 1 cm displacement (image width = 30 cm).

Formation: Zeglingen Formation, Depth: 1'240.14 – 1'240.48 m MD core depth.

4 Geo-statistical evaluation: results

Vector means orientation values (dip direction and dip angle) of bedding planes and structural discontinuities were calculated for different data clusters in a stereogram projection (Tab. 4-1). Bedding dips and structural discontinuities recorded in non-oriented cores (n = 176) were excluded from the following stereographic evaluation. However, they were included into the fracture density calculations (P32 curves) presented in Section 4.1.3.

Tab. 4-1: Mean orientation values for bedding planes and structural discontinuities

	Cluster 1 (Main)			**Cluster 2 (Subordinate)**			**Cluster 3 (Subordinate)**		
	Azim	**Dip**	**No.**	**Azim**	**Dip**	**No.**	**Azim**	**Dip**	**No.**
Bedding	164	05	183	323	06	94			
Faults	163	07	660	180	43	90			
Tension gashes, joints, fractures	102	05	101	270	73	72			
Stylolites	127	03	352	183	77	63	001	77	46

4.1 Entire cored borehole section (535 – 1'370.14 m MD log depth)

A total of 3'254 individual planar and non-planar features were identified during the core analysis and manual dip picking of the 835 m of drill core (535 – 1'370.14 m MD log depth). The results of the structural analysis are described in the following section.

4.1.1 Basic structural dip evaluation

Bedding dips, particularly in lithologies with a plane-parallel bedding such as in claystone, marl and siltstone sequences, are the best indicators for structural dip. The dip variations along the borehole are well reflected in the stereograms of Figs. 4-1 and 4-2 and in the vector azimuth plot in Fig. 4-3.

The interpreted borehole interval from 535 to 1'319.24 m MD (Malm to Triassic) reveals a stable sub-horizontal to shallow (1 – 10º) structural dip towards the SSE (overall mean: 164/05 [dip direction / dip angle]; n = 183; Tab. 4-1). An obvious change in dip orientation was observed within the Weitenau Formation below 1'319.46 m MD, showing a 5 – 15º N dip. This dip change is assumed to be associated with an angular unconformity at the Permian-Triassic boundary at 1'319.46 m MD. However, the amount of sedimentary dips within the sand-rich Weitenau Formation is uncertain. Further, local dip anomalies were observed within the Zeglingen Formation in the depth interval from 1'224 to 1'267 m MD. The latter is characterised by moderately inclined to steep bedding governed by small-scale folding.

There were several further dip breaks along the studied borehole. Some of these dip changes are indicated with question marks in Fig. 4-3 as the data analysis did not reveal the cause of the change in structural dip.

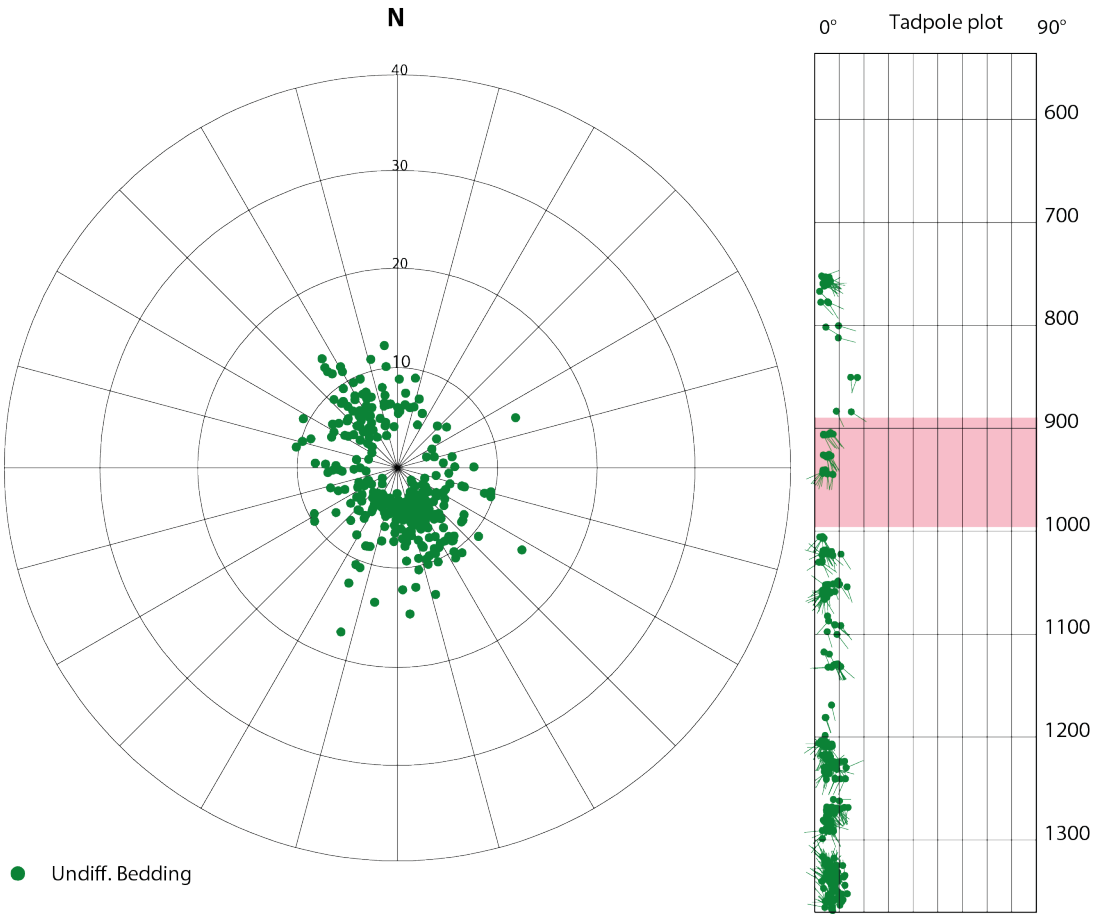

Fig. 4-1: Stereogram and depth plot for bedding planes (n = 316) for the entire cored borehole section

Note the predominance of 0 – 10° SE dips with an overall mean of 164/05 (n = 183). The rim of the stereogram is restricted to 40°. Depth range is 535 – 1'370.14 m MD log depth. The Opalinus Clay interval is indicated in red in the tadpole plot.

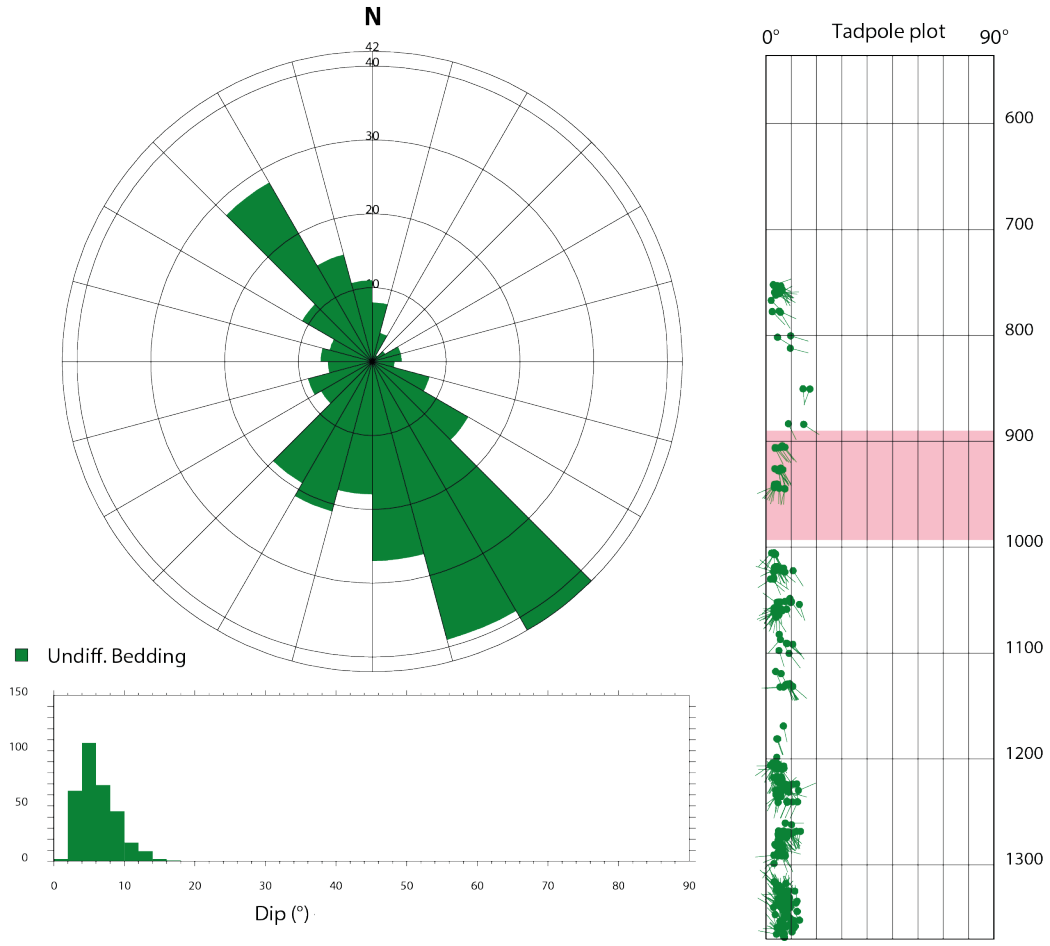

Fig. 4-2: Azimuth rose diagram, dip histogram and depth plot for bedding planes (n = 316) for the entire cored borehole section

Note the predominance of dip directions towards the SE. Depth range is 535 – 1'370.14 m MD log depth. The Opalinus Clay interval is indicated in red in the tadpole plot.

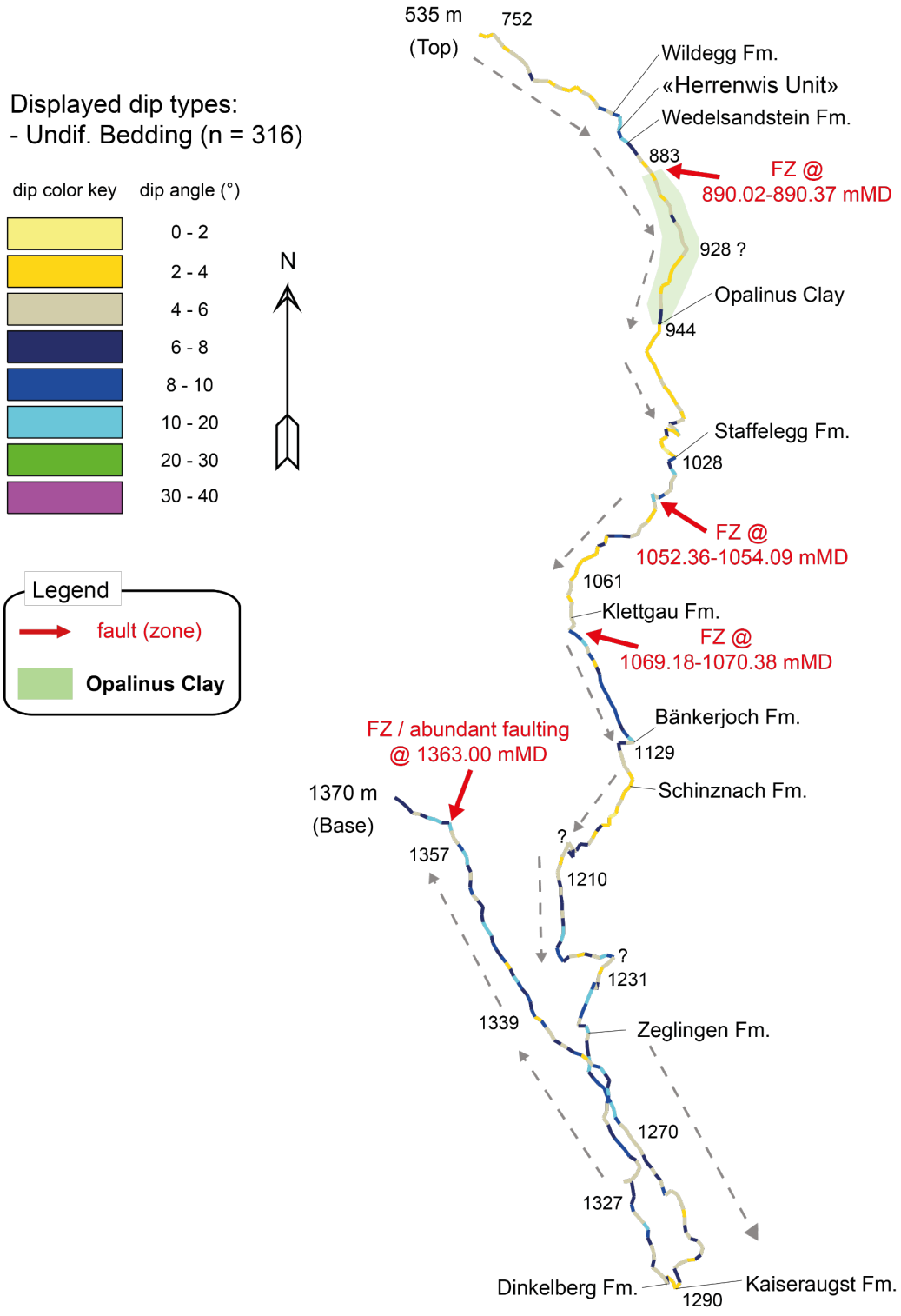

Fig. 4-3: Vector azimuth plot for bedding-related planes (n = 316) of picked core dips

The colour coding reflects the dip magnitude, while question marks indicate prominent dip changes. The horizontal distance has no meaning and represents only the amount of bedding in the corresponding section. Grey arrows point in the direction of the mean overall dip direction. Lithostratigraphic formation boundaries are marked. Deformed bedding dips and non-oriented dip data are excluded from this plot. Depth range is 535 – 1'370.14 m MD log depth.

4.1.2 Natural structural discontinuities

Fault planes

The majority of the interpreted structures are faults, with a total of 1'332 observed individual fault planes. Faults are planes of shear failure, i.e. planes with plane-parallel movement (Ebert & Decker 2019). Depending on their appearance in the core, three types were distinguished: fault planes (n = 467), mirror-like fault planes (n = 474) and stylolitic fault planes (391). Out of all recorded faults, 1'182 (89 %) were detected in oriented cores and are included in this evaluation.

Several structurally complex intervals along the studied borehole were categorised as fault zones. They are commonly associated with profound fracturing and high fracture densities. The latter correspond to the different fracture density classes (FDC) defined by Ebert & Decker (2019). A total of 50 individual fault zones (up to 4.04 m thick) were defined for the entire cored interval along with their FDC for each zone (Tab. 4-2).

Faults are unevenly distributed along the borehole as shown in Fig. 4-4 and discussed in Section 4.1.4. At certain depths, faults are absent, whereas at other depths they occur as countless swarms causing heavily fractured and disintegrated rock (fault zones and FDC).

The orientations of all fault planes observed in the borehole are displayed in the stereograms of Fig. 4-5 and 4-6. Two orientation clusters were determined, revealing similar dip directions towards the SSE and S, but with variable dip magnitudes (Tab. 4-1). These clusters consist of a main cluster dipping 1 – 30° (mean of 163/07; n = 660) and a subordinate cluster dipping 30 – 65° (mean of 180/43; n = 90). However, faults with scattered orientations were also observed. Striations could be observed on 715 fault planes. The observations and interpretations regarding the striations of the fault planes can be found in Section 4.1.4.

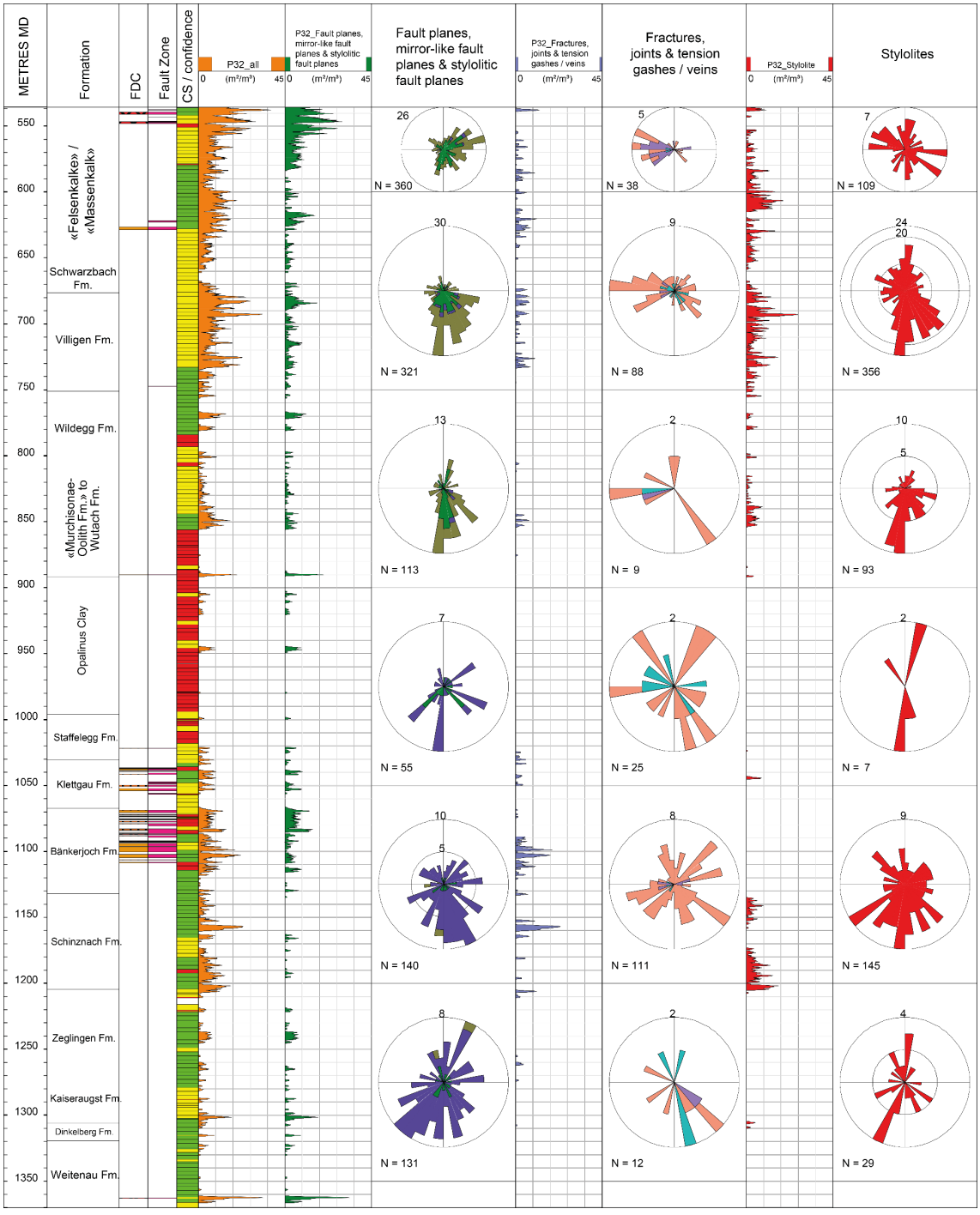

Fig. 4-4: Overview plot showing P32 fracture densities along the borehole

In addition, lithostratigraphic subdivision, core sections and goniometry confidence as well as fault zones associated with intense fracturing (expressed by fracture density classes; see Tab. 4-2) are shown. For colour legend see Fig. 2-2. Note that the stereograms with the respective number of planes are displayed for 150 m intervals.

Tab. 4-2: List of interpreted fault zones and associated FDC (fracture density class)

Fault zones				**FDC**			
Top [m MD log depth]	**Bottom** [m MD log depth]	**Thickness** [m]	**Type**	**Top** [m MD log depth]	**Bottom** [m MD log depth]	**Thickness** [m]	**FDC**
535.18	535.27	0.09	Fault zone				
537.66	537.83	0.17	Fault zone				
539.56	541.21	1.65	Fault zone	539.56	541.21	1.65	FDC 4
543.55	543.58	0.03	Fault zone				
546.28	546.31	0.03	Fault zone				
546.74	548.13	1.39	Fault zone	546.74	548.13	1.39	FDC 4
621.93	622.75	0.82	Fault zone				
626.64	628.71	2.07	Fault zone	626.64	628.71	2.07	FDC 2
747.15	747.70	0.55	Fault zone				
890.02	890.37	0.35	Fault zone	890.02	890.37	0.35	FDC 2
890.71	890.83	0.12	Fault zone	890.71	890.83	0.12	FDC 2
1'021.77	1'021.91	0.14	Fault zone	1'021.77	1'021.91	0.14	FDC 3
1'036.74	1'036.93	0.19	Fault zone	1'036.74	1'036.93	0.19	FDC 3
1'037.50	1'038.55	1.05	Fault zone	1'037.50	1'038.55	1.05	FDC 2
1'039.34	1'039.50	0.16	Fault zone	1'039.34	1'039.50	0.16	FDC 3
1'040.68	1'041.71	1.03	Fault zone	1'041.30	1'041.71	0.41	FDC 3
1'047.28	1'048.03	0.75	Fault zone				
1'048.14	1'049.05	0.91	Fault zone				
1'049.75	1'050.88	1.13	Fault zone	1'049.75	1'050.88	1.13	FDC 3
1'052.36	1'054.09	1.73	Fault zone	1'052.36	1'054.09	1.73	FDC 2
1'055.89	1'056.73	0.84	Fault zone				
1'068.74	1'068.93	0.19	Fault zone	1'068.74	1'068.93	0.19	FDC 3
1'069.18	1'070.38	1.20	Fault zone	1'069.18	1'070.38	1.20	FDC 2
1'070.93	1'070.99	0.06	Fault zone	1'070.93	1'070.99	0.06	FDC 3
1'071.15	1'071.30	0.15	Fault zone	1'071.15	1'071.30	0.15	FDC 3
1'072.06	1'072.27	0.21	Fault zone	1'072.06	1'072.27	0.21	FDC 3
1'072.62	1'072.65	0.03	Fault zone	1'072.62	1'072.65	0.03	FDC 3
1'073.46	1'073.74	0.28	Fault zone	1'073.46	1'073.74	0.28	FDC 3
1'075.34	1'075.59	0.25	Fault zone	1'075.34	1'075.59	0.25	FDC 3
1'075.97	1'076.07	0.10	Fault zone	1'075.97	1'076.07	0.10	FDC 3
1'077.04	1'077.90	0.86	Fault zone	1'077.04	1'077.90	0.86	FDC 3

Tab. 4-2: continued

Fault zones				**FDC**			
Top [m MD log depth]	**Bottom** [m MD log depth]	**Thickness** [m]	**Type**	**Top** [m MD log depth]	**Bottom** [m MD log depth]	**Thickness** [m]	**FDC**
1'078.61	1'078.70	0.09	Fault zone	1'078.61	1'078.70	0.09	FDC 3
1'078.80	1'078.97	0.17	Fault zone	1'078.80	1'078.97	0.17	FDC 3
1'079.10	1'079.20	0.10	Fault zone	1'079.10	1'079.20	0.10	FDC 3
1'079.45	1'080.70	1.25	Fault zone				
1'083.06	1'086.40	3.34	Fault zone	1'083.06	1'086.40	3.34	FDC 3
1'086.63	1'086.68	0.05	Fault zone	1'086.63	1'086.68	0.05	FDC 4
1'086.99	1'087.18	0.19	Fault zone	1'086.99	1'087.18	0.19	FDC 4
1'088.00	1'089.50	1.50	Fault zone	1'088.00	1'088.38	0.38	FDC 3
1'092.09	1'092.50	0.41	Fault zone	1'092.09	1'092.50	0.41	FDC 3
1'092.66	1'093.20	0.54	Fault zone	1'092.66	1'093.20	0.54	FDC 3
1'093.71	1'096.02	2.31	Fault zone	1'093.71	1'096.02	2.31	FDC 2
1'096.53	1'100.57	4.04	Fault zone	1'096.53	1'100.57	4.04	FDC 2
1'102.12	1'104.78	2.66	Fault zone	1'102.12	1'104.78	2.66	FDC 2
1'106.21	1'106.49	0.28	Fault zone	1'106.21	1'106.49	0.28	FDC 3
1'108.15	1'108.94	0.79	Fault zone	1'108.15	1'108.94	0.79	FDC 2
1'362.15	1'362.25	0.10	Fault zone	1'362.15	1'362.25	0.10	FDC 4
1'362.60	1'362.65	0.05	Fault zone	1'362.60	1'362.65	0.05	FDC 4
1'362.76	1'362.80	0.04	Fault zone	1'362.76	1'362.80	0.04	FDC 4
1'363.08	1'363.14	0.06	Fault zone	1'363.08	1'363.14	0.06	FDC 4

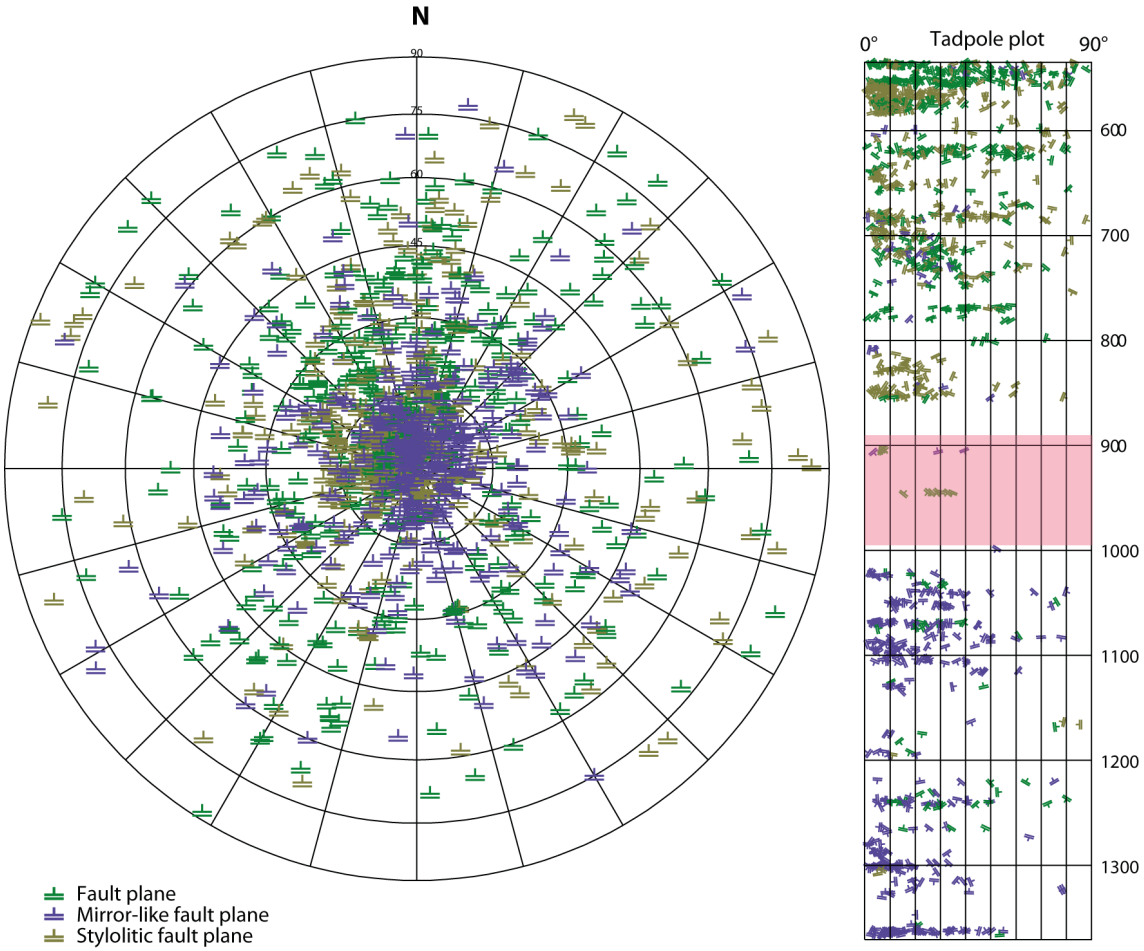

Fig. 4-5: Stereogram and depth plot of fault planes in the entire cored interval

In total, 1'182 fault planes are plotted: fault planes (n = 422), mirror-like fault planes (n = 369) and stylolitic fault planes (n = 391). Depth range is 535 – 1'370.14 m MD log depth. In the tadpole plot, the Opalinus Clay interval is shaded in red.

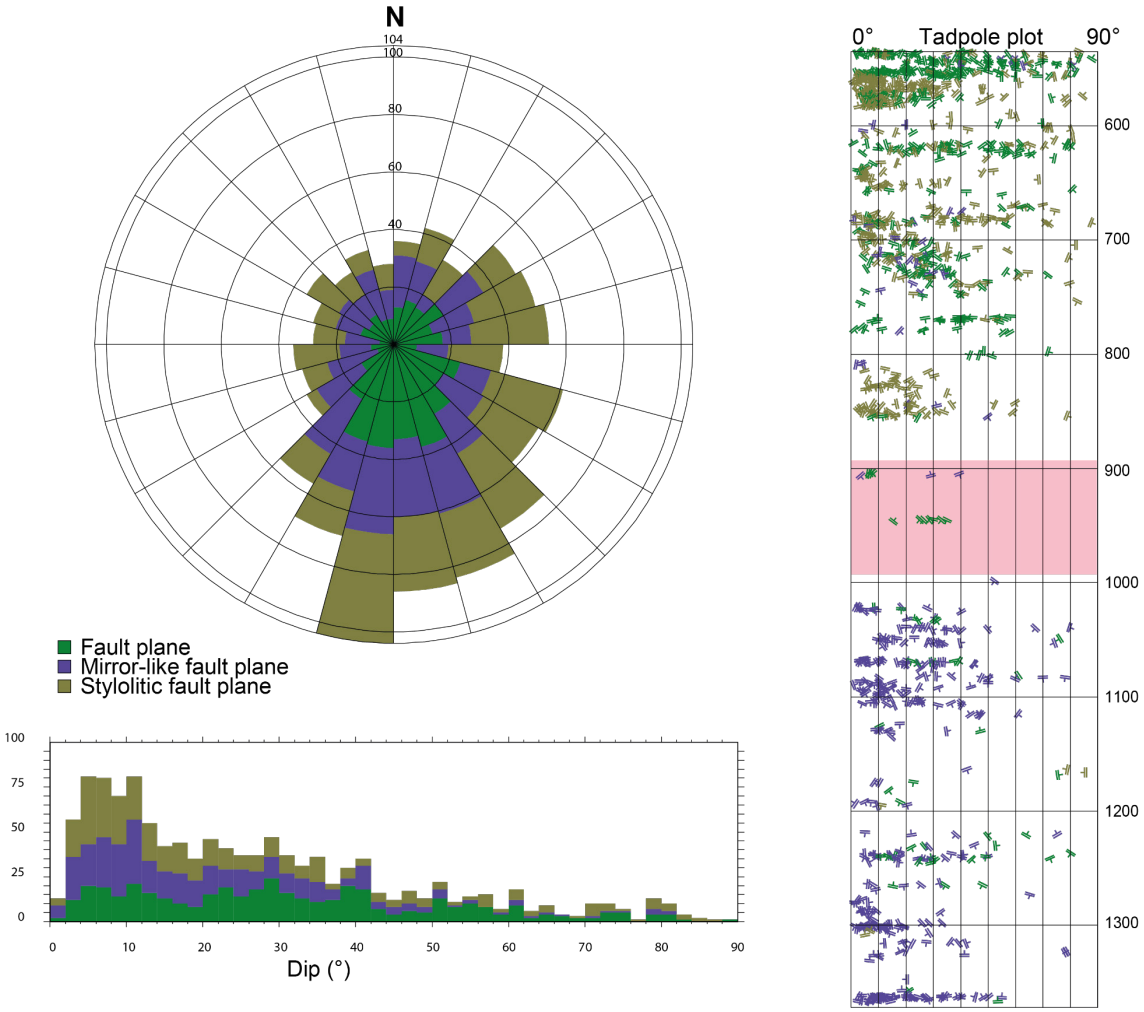

Fig. 4-6: Azimuth rose diagram, dip histogram and depth plot for fault planes in the entire cored interval

In total, 1'182 fault planes are plotted: fault plane (n = 422), mirror-like fault plane (n = 369) and stylolitic fault plane (n = 391). Depth range is 535 – 1'370.14 m MD log depth. In the tadpole plot, the Opalinus Clay interval is shaded in red.

Fractures, joints and tension gashes / veins

This group of structures represents features without shear indicators and comprises tension gashes / veins (n = 233), fractures (n = 39) and joints (n = 37). With a total of 309 individual structures, this represents the smallest group of structural discontinuities. Out of these 309 structures, 283 planes were recorded in oriented cores.

The borehole distribution of tension gashes / veins, fractures and joints is provided in Fig. 4-4 and discussed in Section 4.1.4. Compared to faults they reveal a larger orientation scatter as seen in Figs. 4-7 and 4-8. However, two weakly defined clusters are observed (Tab. 4-1): planes predominantly dipping 1 – 30° E- (mean: 102/05; n = 101) and a subordinate cluster dipping 50 – 90° W- (mean: 270/73; n = 72). They are particularly abundant in the upper borehole interval at depths of 535 – 740 m MD log depth and 1'100 m MD log depth.

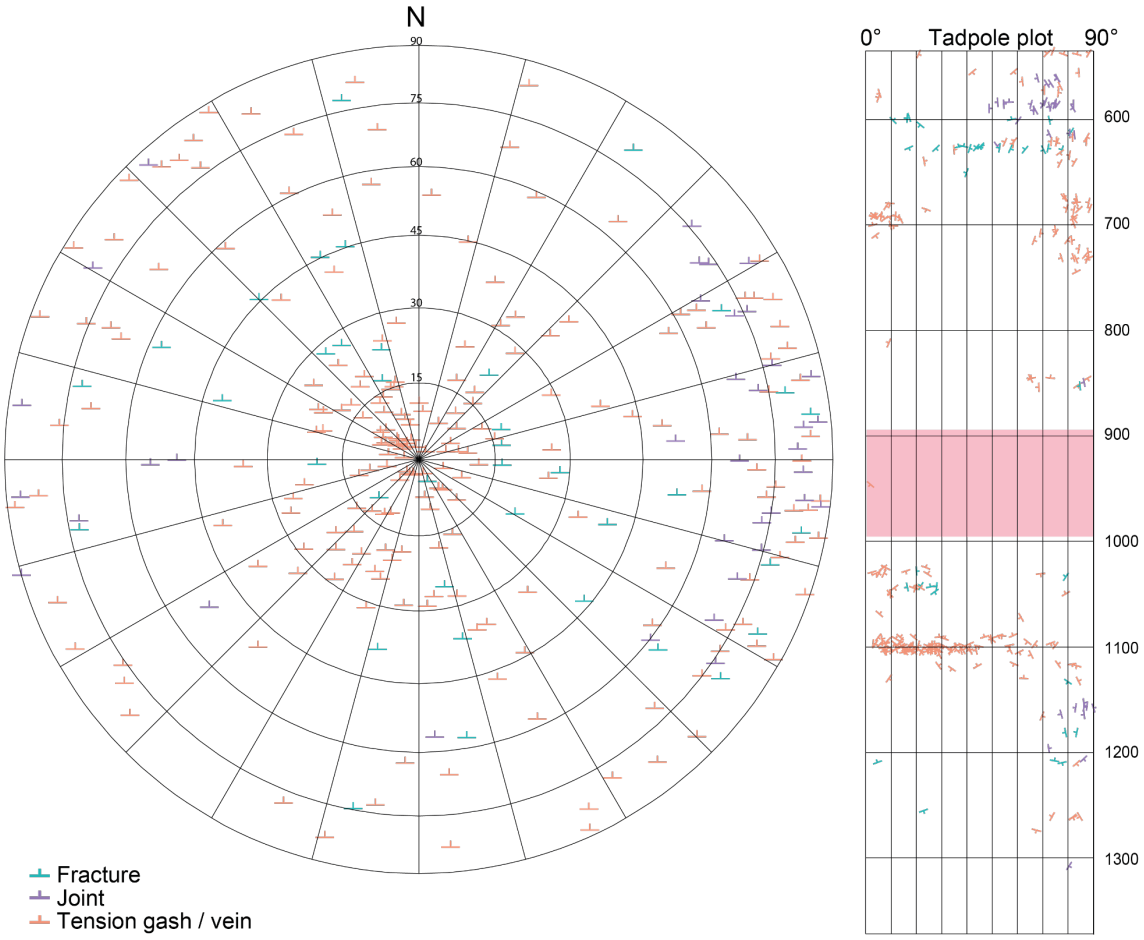

Fig. 4-7: Stereogram and depth plot for tension gashes / veins, fractures and joints in the entire cored interval

In total, 283 structures are plotted: tension gashes / veins (n = 208), fractures (n = 38) and joints (n = 37). Depth range is 535 – 1'370.14 m MD log depth. In the tadpole plot, the Opalinus Clay interval is shaded in red.

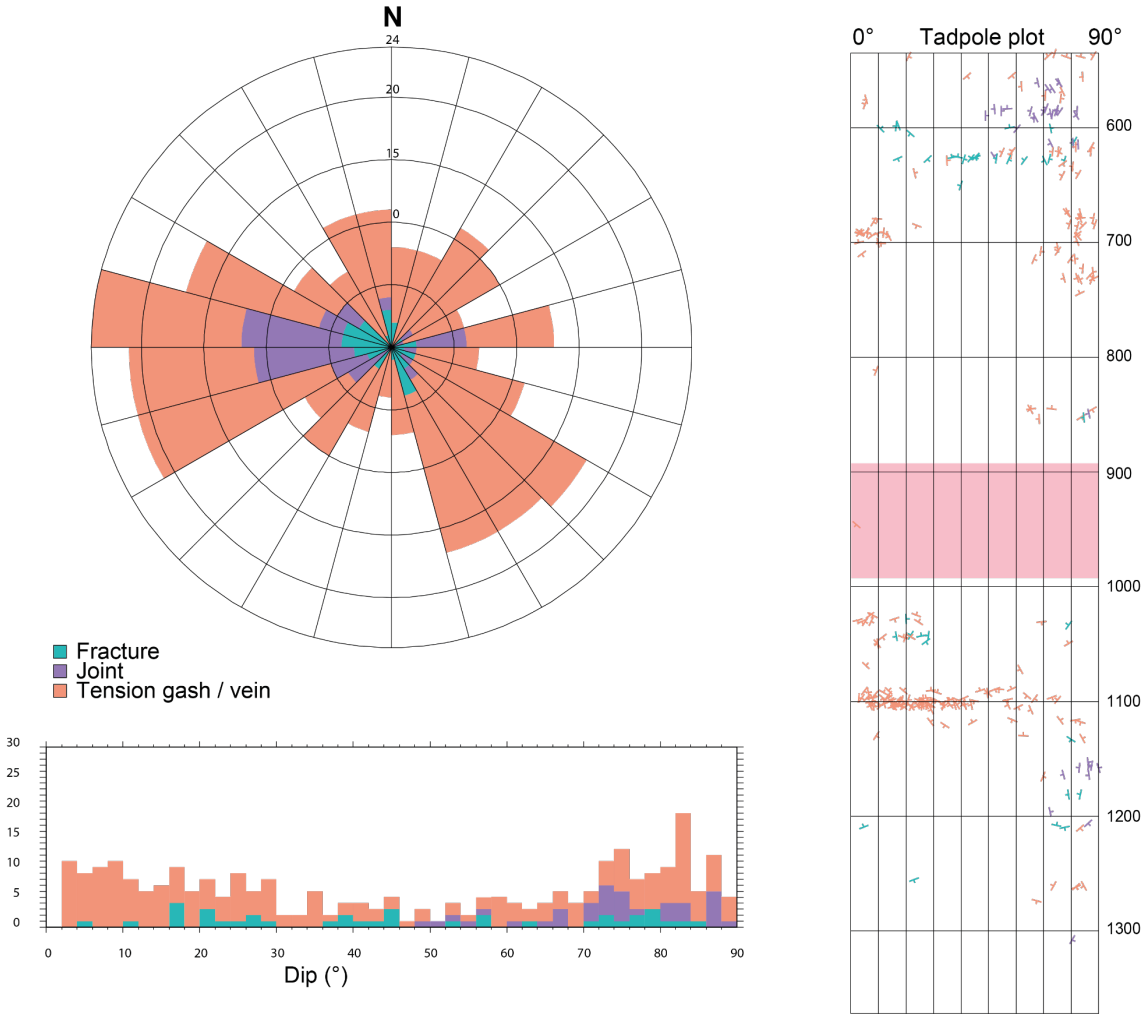

Fig. 4-8: Azimuth rose diagram of tension gashes / veins, fractures and joints in the entire cored interval

Tension gashes / veins (n = 208), fractures (n = 38) and joints (n = 37). Depth range 535 – 1'370.14 m MD log depth. In the tadpole plot, the Opalinus Clay interval is shaded in red.

Stylolites

In total, 755 stylolites were categorised (n = 739 in oriented cores). In stylolite-rich intervals such as the Malm and the Muschelkalk Formation not all stylolites could be picked or documented. It was therefore decided to document and categorise the dominant stylolites which could be picked on core photographs, and otherwise document other stylolitic locations as zones of stylolites. The stylolites depict two well-developed orientation clusters (Figs. 4-9 and 4-10 and Tab. 4-1): a main sub-horizontal to inclined cluster dipping (1 – 20°) S to SE (mean of 127/03; n = 352) and a subordinate steep to sub-vertical cluster striking (60 – 90°) W-E with calculated means of 183/77 (n = 63) and 001/77 (n = 46).

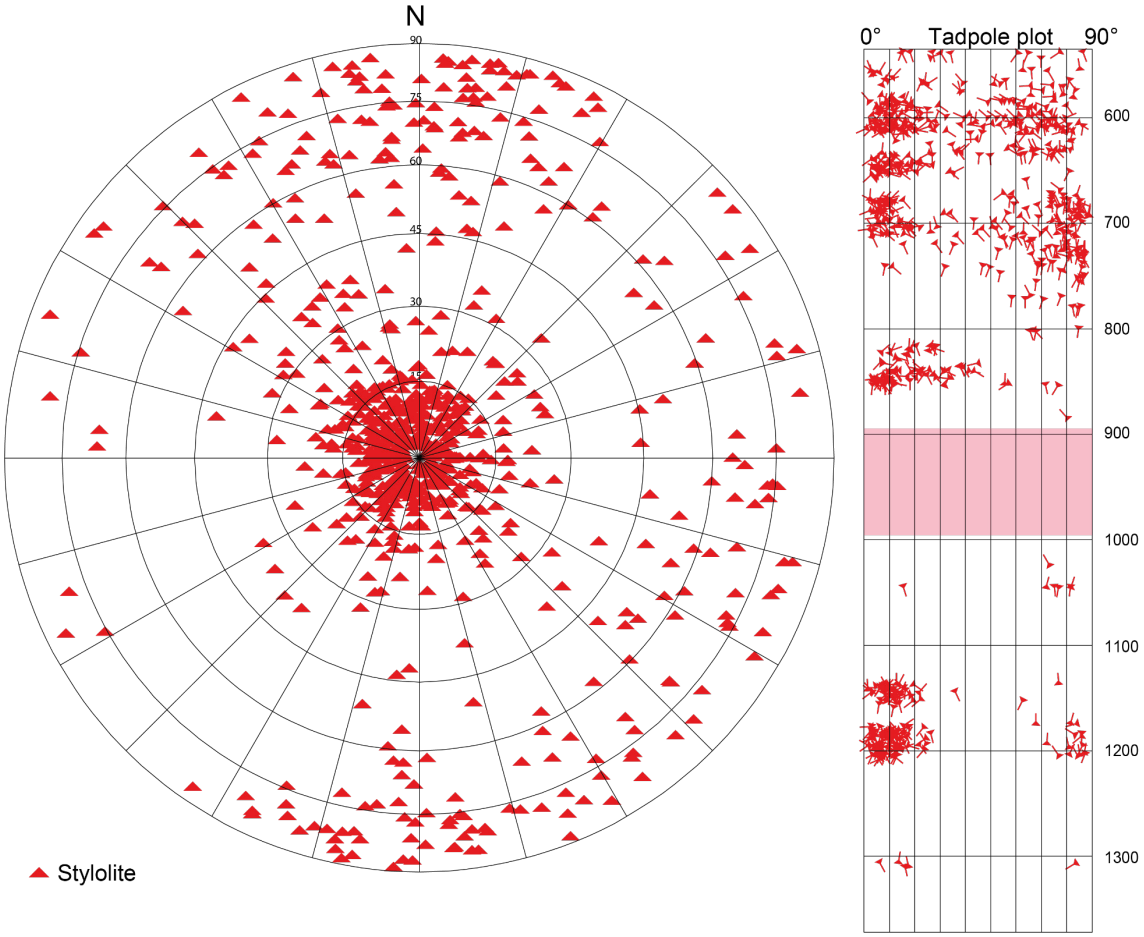

Fig. 4-9: Stereogram and depth plot of stylolites along the borehole in the entire cored interval

Depth range is 535 – 1'370.14 m MD log depth (n = 739). In the tadpole plot, the Opalinus Clay interval is shaded in red.

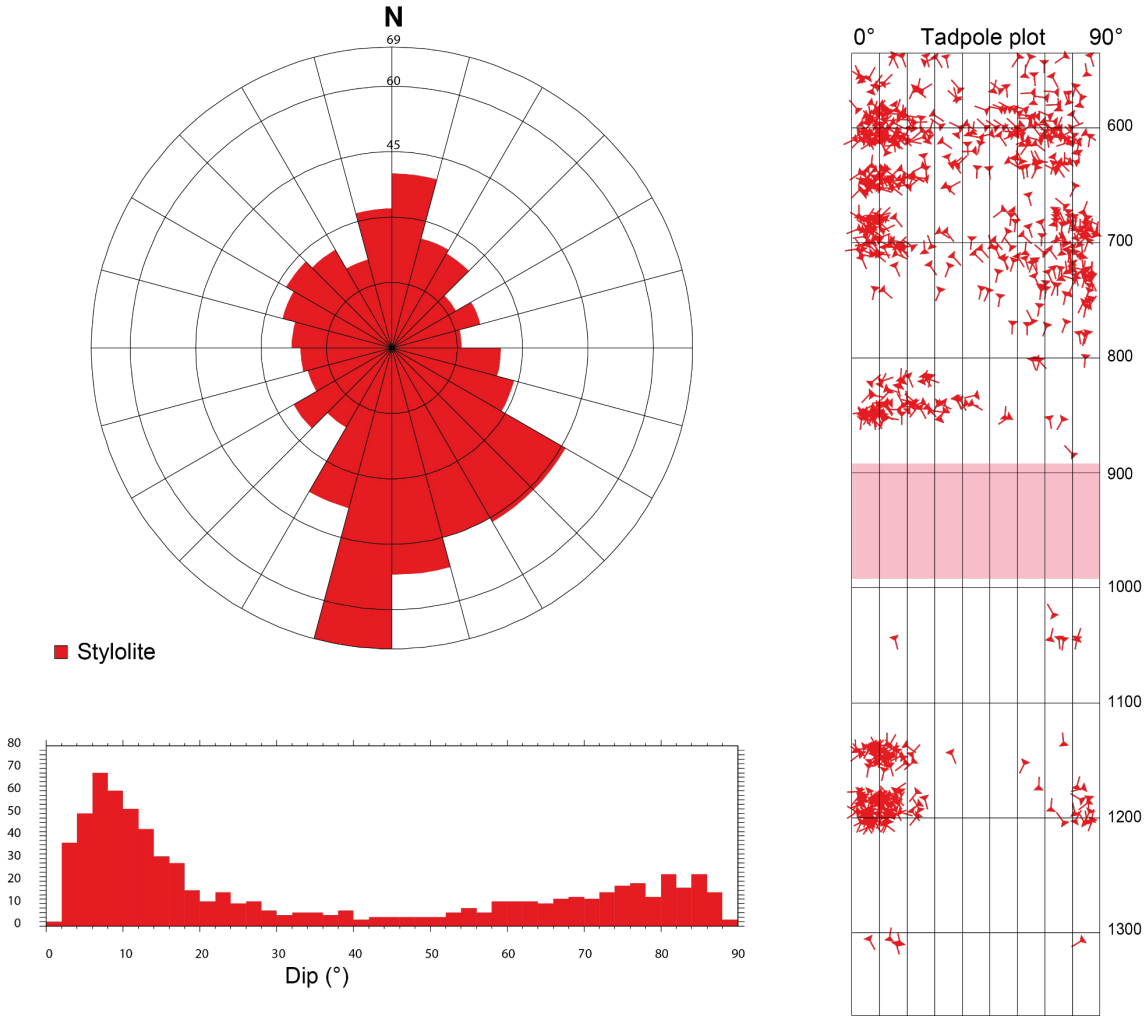

Fig. 4-10: Azimuth rose diagram and depth plot for stylolites in the entire cored interval

Depth range is 535 – 1'370.14 m MD log depth (n = 739). In the tadpole plot, the Opalinus Clay interval is shaded in red.

4.1.3 Fracture density (P32)

Density histograms were prepared in order to evaluate the spatial fracture distribution (Fig. 4-4). As mentioned above, the structural features recorded in non-oriented cores (n = 572) were also considered in the fracture density calculations.

Fault planes were particularly abundant in the uppermost borehole interval from 537.66 to 851 m MD log depth (Malm and uppermost Dogger). In addition, elevated fault counts were found from 1'020 to 1'120 m MD log depth (Klettgau and Bänkerjoch Formation), at 1240 m MD log depth (Zeglingen Formation) and at 1'303 m MD log depth (Kaiseraugst Formation). The highest fault counts were observed within the fault zones from 537.66 to 554 m MD log depth in the «Felsenkalke» / «Massenkalk» and from 1'362.13 – 1'363.05 m MD log depth in the Weitenau Formation (Fig. 4-4).

Increased counts of tension gashes / veins occurred in the Villigen Formation from 670 to 740 m MD log depth as well as in the Bänkerjoch Formation from 1'090 to 1'115 m MD log depth. In contrast, fractures and joints were abundant in the uppermost borehole interval from 560 to 631 m MD log depth («Felsenkalke» / «Massenkalk»). In addition, prominent, wide open, sub-vertical joints up to 4 m long were observed in the Schinznach Formation at 1'158 m MD log depth.

Stylolites revealed an uneven depth distribution and occurred almost exclusively within carbonate-rich lithologies of Malm and Muschelkalk. They were concentrated particularly within three intervals from 535 to 760 m MD log depth, from 820 to 860 m MD log depth and from 1'135 to 1'210 m MD log depth (Fig. 4-4). The highest density of up to 26 stylolites per metre occurred within the Villigen Formation at 692 m MD log depth.

4.1.4 Kinematic indicators

Striations could be measured on 825 fault planes. In total, 87 % of the lineations (n = 715) were collected in oriented cores and are shown in the stereograms below (Tab. 4-3). The orientations of the striations are given in Fig. 4-11 to Fig. 4-16. There is a clear predominance of south-dipping striations. The vast majority has sub-horizontal to inclined (0 – 30°) dip magnitudes.

Three groups of shear sense were distinguished on the analysed drill cores:

up = thrusting / reverse faulting

down = normal faulting

dextral / sinistral = strike-slip faulting

A total of 263 shear indicators were identified as thrusts / reverse fault planes with dominant N-S oriented striations (Fig. 4-13). In contrast, the interpreted normal fault planes (n = 31; Fig. 4-14) and strike-slip fault planes (n = 31; Fig. 4-15) strike roughly in a SW-NE direction. However, the shear sense of most fault planes (n = 499) was uncertain (Fig. 4-16).

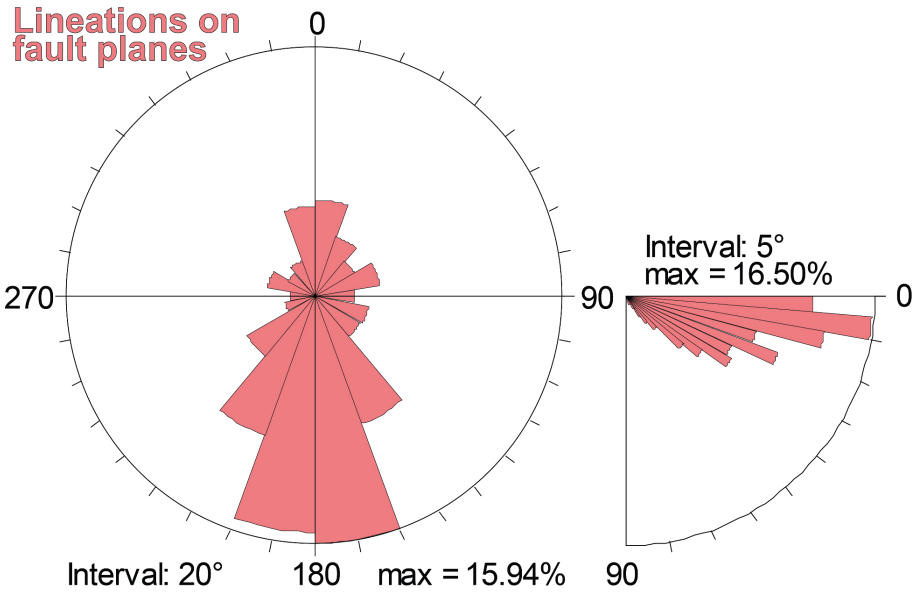

Fig. 4-11: Dip direction of striations along fault planes in the entire cored interval

The lineations (n = 715) from oriented cores of the entire core interval from Malm to Permian are presented. Left: azimuth rose diagram, right: dip histogram. Depth range is 535 – 1'370.14 m MD log depth.

Tab. 4-3: List of all kinematic indicators in oriented and non-oriented cores

Shear sense	**Number**
Up	263
Down	31
Sinistral	19
Dextral	12
Unknown	499
In oriented cores	715
In non-oriented cores	111
Total measured lineations	**825**

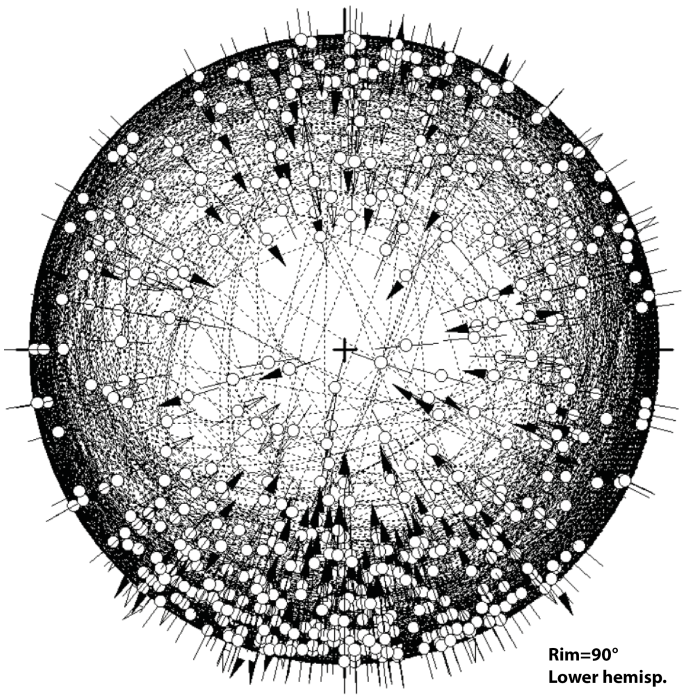

Fig. 4-12: Stereogram with all oriented fault planes and associated kinematic data

Up (n = 232), down (n = 28), dextral (n = 10), sinistral (n = 15) and unknown (n = 430). Depth range is 535 – 1'370.14 m MD log depth.

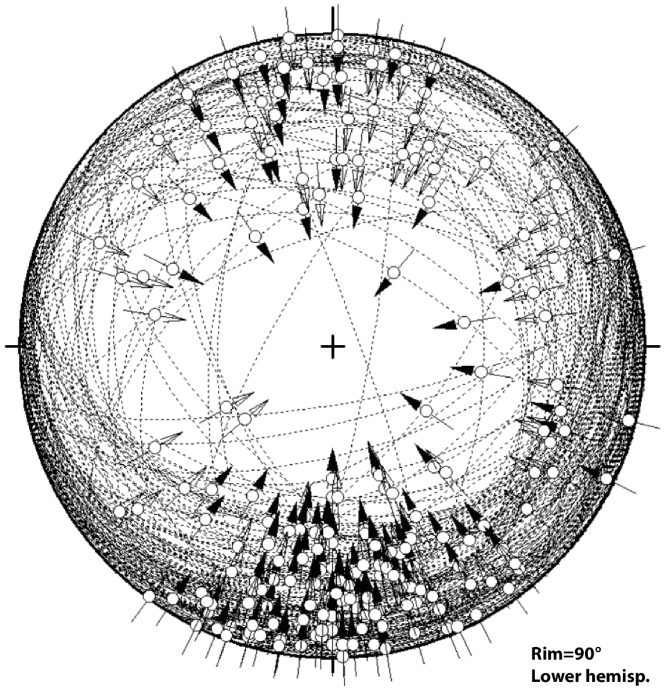

Fig. 4-13: Stereogram with all striations of thrust / reverse fault planes

Up (n = 232). Depth range is 535 – 1'370.14 m MD log depth.

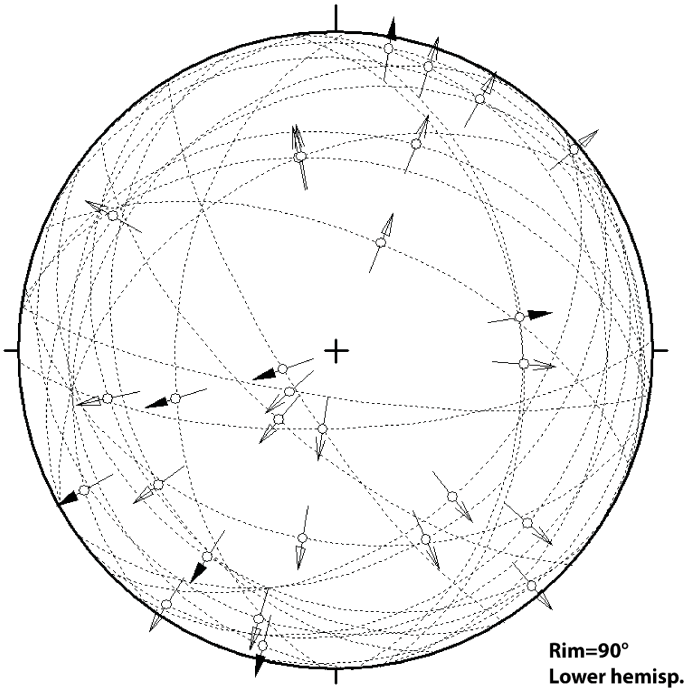

Fig. 4-14: Stereogram with all normal fault planes and associated striations
Down (n = 28). Depth range is 535 – 1'370.14 m MD log depth.

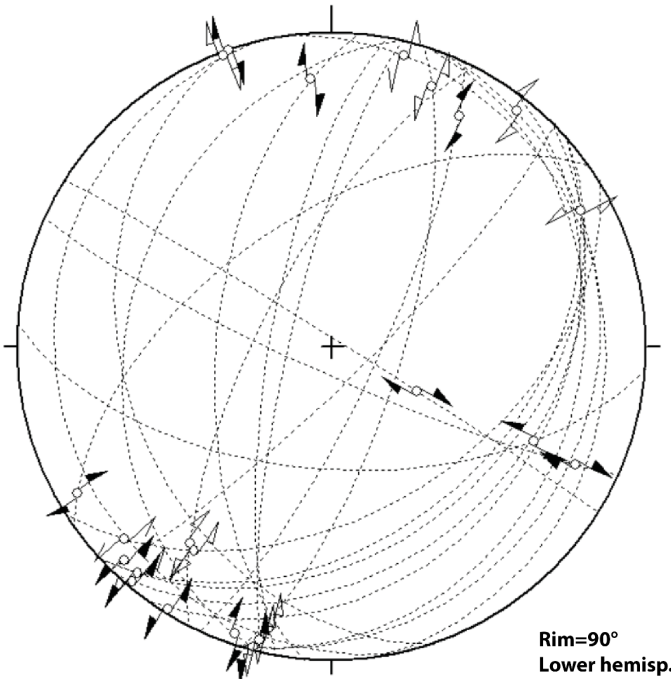

Fig. 4-15: Stereogram with all strike-slip fault planes and associated striations
Dextral (n = 10), sinistral (n = 15). Depth range is 535 – 1'370.14 m MD log depth.

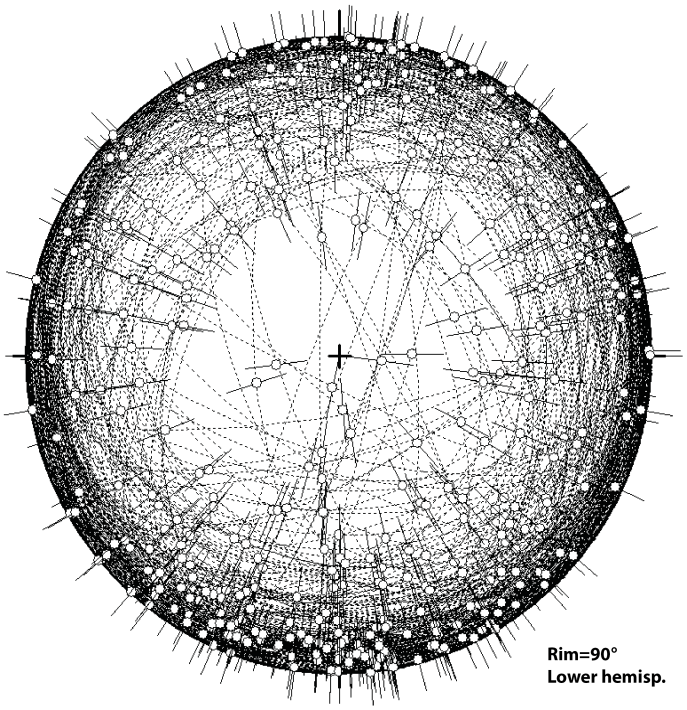

Fig. 4-16: Stereogram for all fault planes with unknown shear sense
Unknown (n = 430). Depth range is 535 – 1'370.14 m MD log depth.

4.2 Malm

The cored Malm interval (535 – 805.38 m MD log depth) showed a strong tectonic overprint and was characterised by abundant fault planes and stylolites. The average fracture density was 3.3 fractures per metre. Within the uppermost «Felsenkalke» / «Massenkalk», a distinct ~ 16.5 m thick fault zone was penetrated (537.5 – 554.0 m MD log depth). This zone was characterised by heavy fracturing and rock disintegration and revealed the highest fracture density calculated for BUL1-1 and BUL1-1B (up to 32 fractures per metre).

For the detailed stereographic evaluation, four lithostratigraphic units were defined within the Malm interval. Only the data for oriented cores are presented.

4.2.1 «Felsenkalke» / «Massenkalk»

The orientation and spatial distribution of structural discontinuities and lineations recorded within the cored interval of the «Felsenkalke» / «Massenkalk» (535 – 653.52 m MD log depth) are visualised in Figs. 4-17 to 4-23.

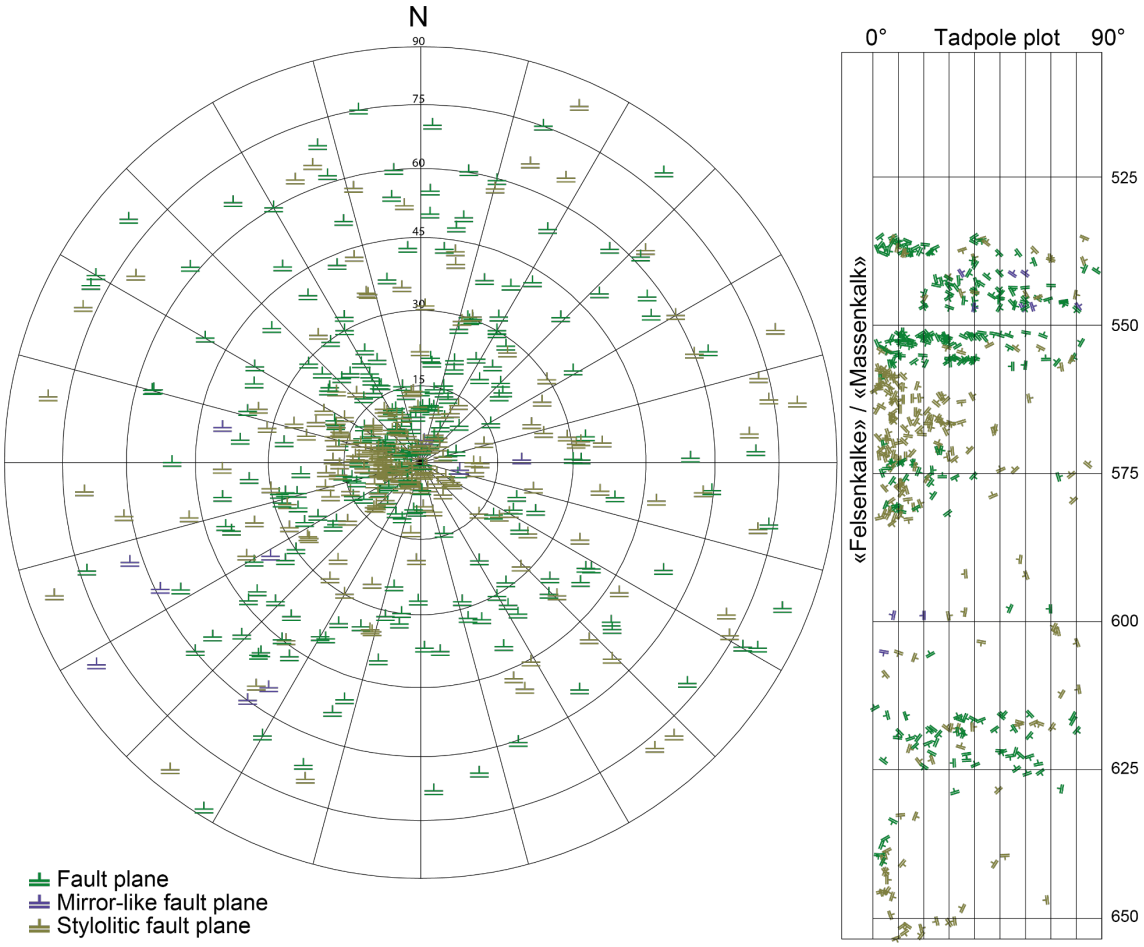

Fig. 4-17: Stereogram and depth plot of fault planes («Felsenkalke» / «Massenkalk»)

Fault planes (n = 248), mirror-like fault planes (n = 10) and stylolitic fault planes (n = 211).

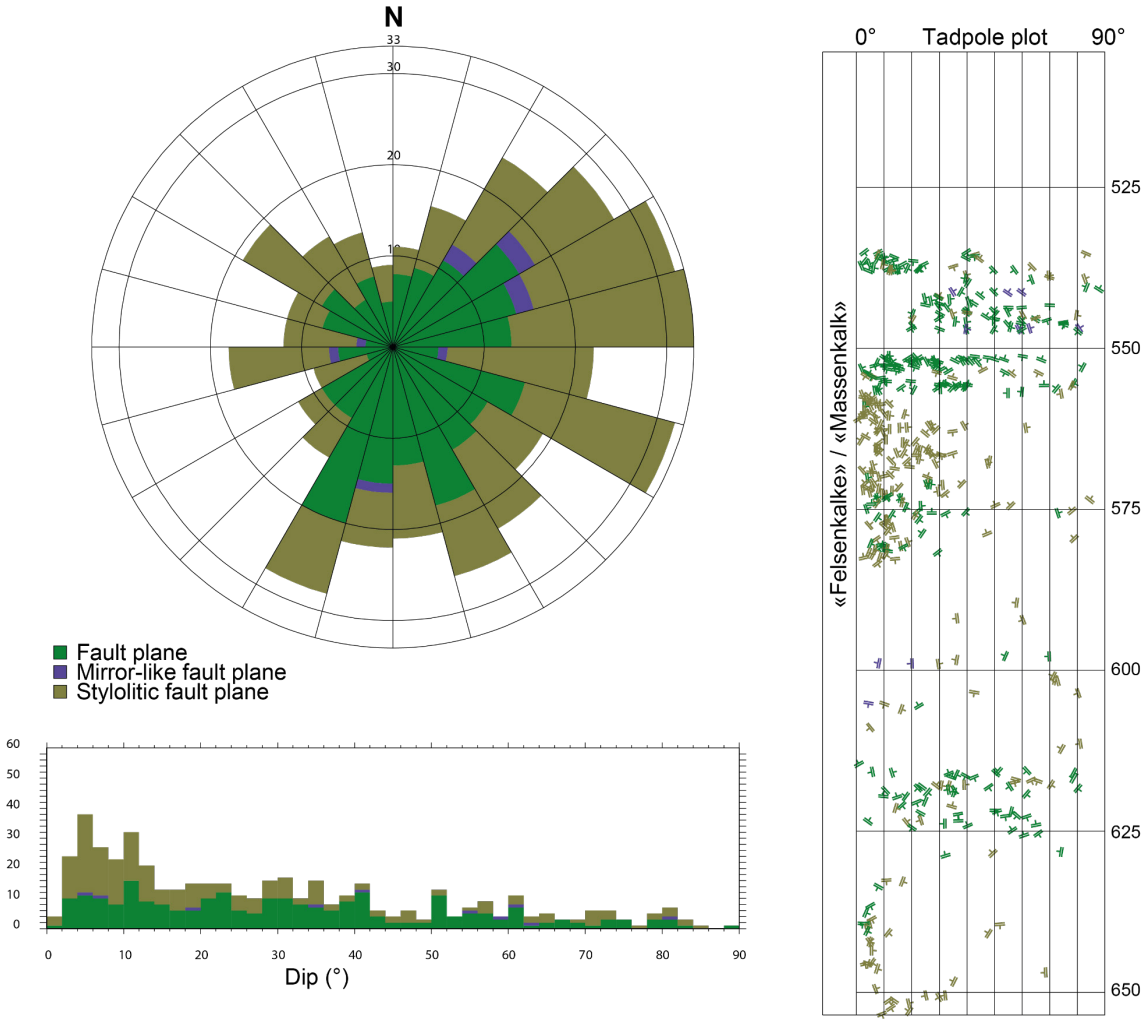

Fig. 4-18: Azimuth rose diagram, dip histogram and depth plot of fault planes («Felsenkalke» / «Massenkalk»)

Fault planes (n = 248), mirror-like fault planes (n = 10) and stylolitic fault planes (n = 211).

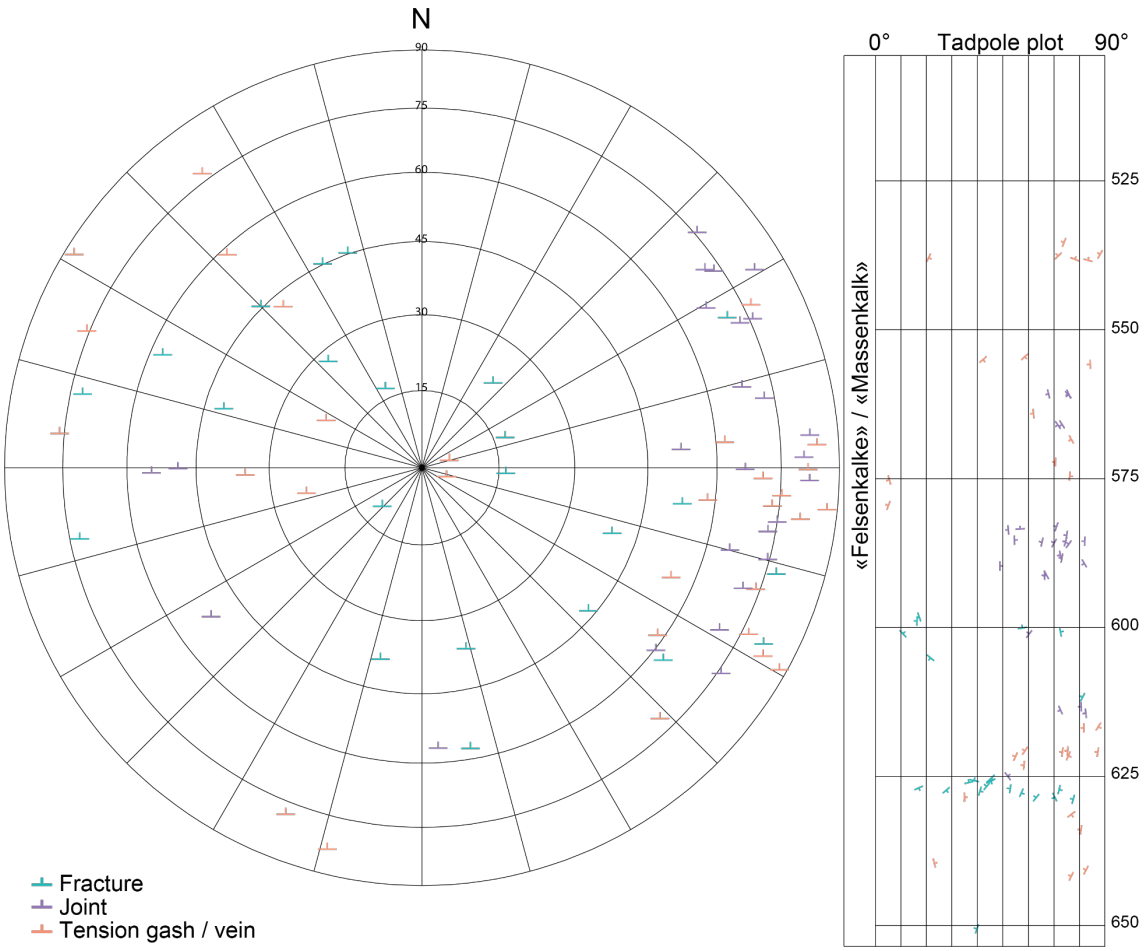

Fig. 4-19: Stereogram and depth plot of fractures, tension gashes / veins and joints («Felsenkalke» / «Massenkalk»)

Fractures (n = 23), joints (n = 26) and tension gashes / veins (n = 30).

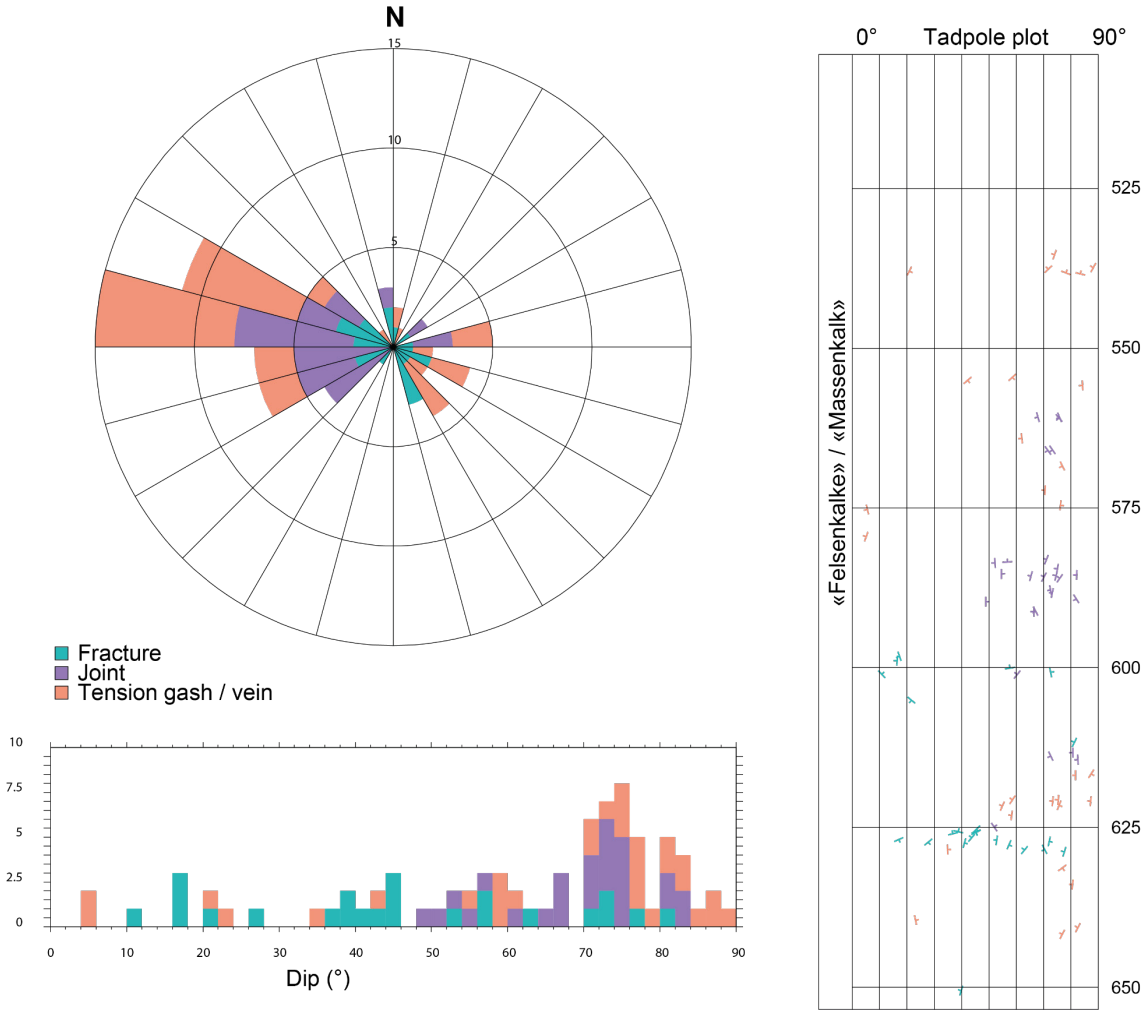

Fig. 4-20: Azimuth rose diagram, dip histogram and depth plot of fractures, tension gashes / veins and joints («Felsenkalke» / «Massenkalk»)

Fractures (n = 23), joints (n = 26) and tension gashes / veins (n = 30).

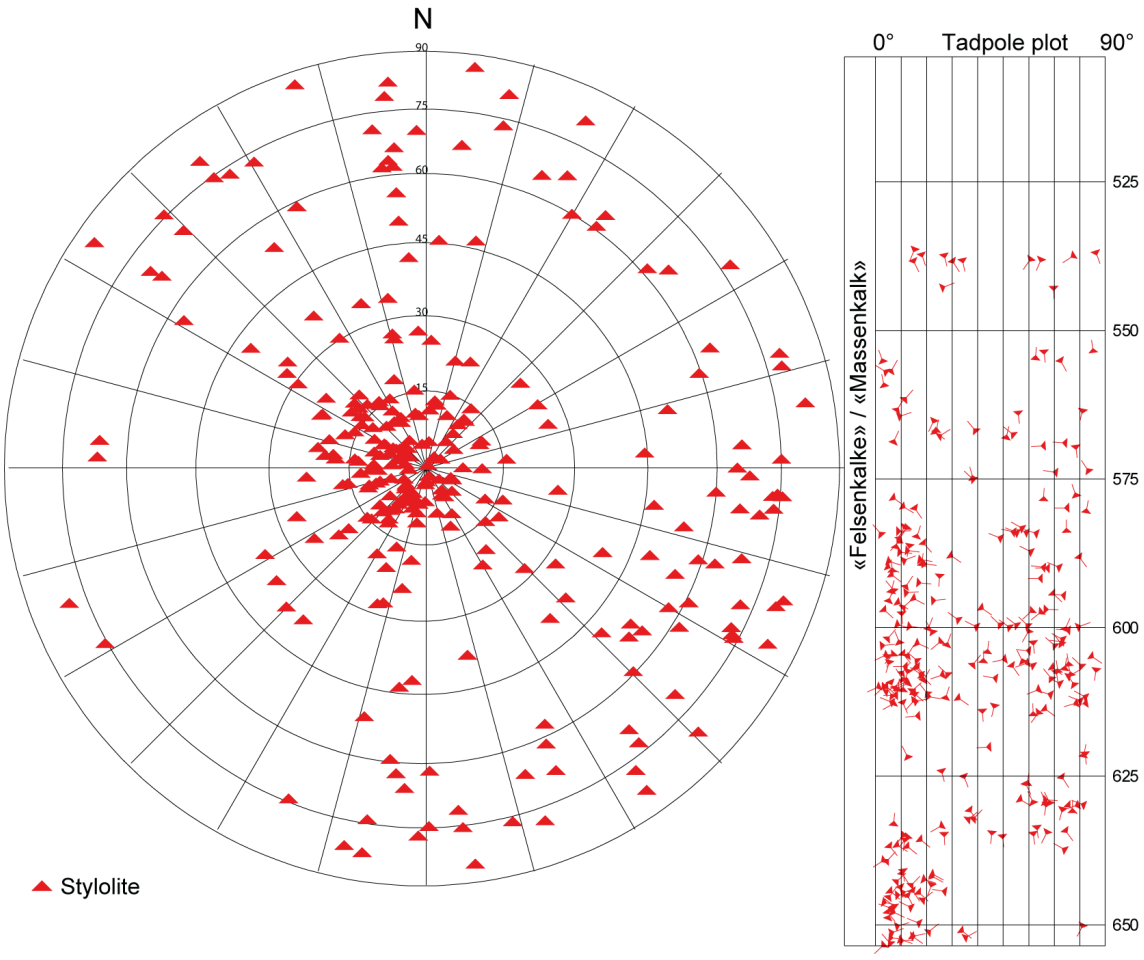

Fig. 4-21: Stereogram and depth plot of stylolites («Felsenkalke» / «Massenkalk», n = 283)

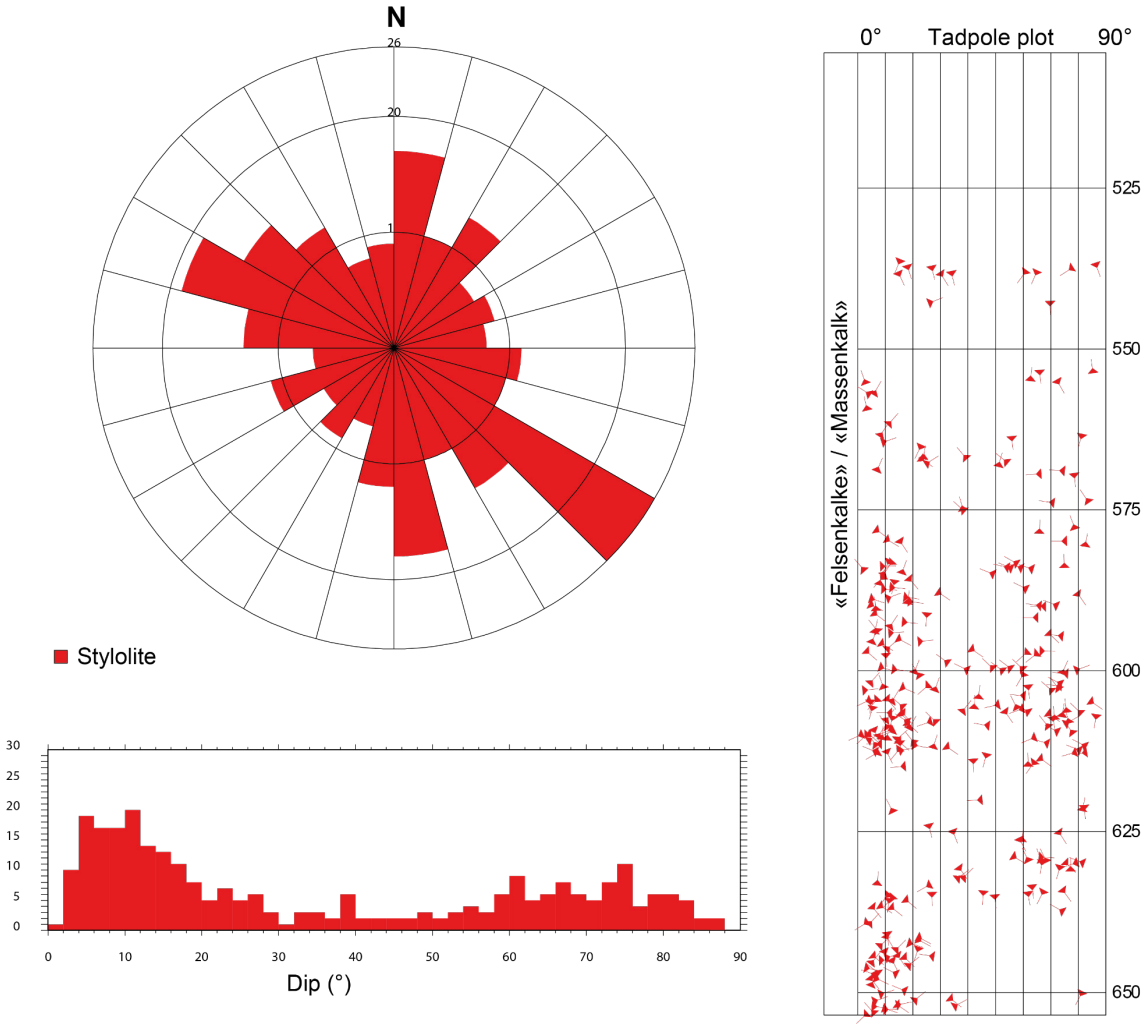

Fig. 4-22: Azimuth rose diagram, dip histogram and depth plot of stylolites («Felsenkalke» / «Massenkalk», n = 283)

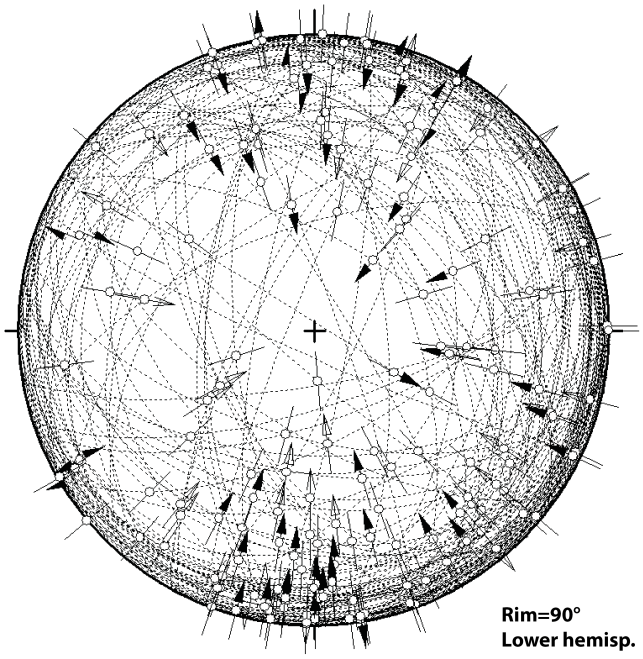

Fig. 4-23: Stereogram of faults («Felsenkalke» / «Massenkalk», n = 173)

4.2.2 Schwarzbach Formation

The structural data for the Schwarzbach Formation (653.52 – 676.51 m MD log depth) are presented in Figs. 4-24 to 4-29. Due to the low number of fractures, joints and tension gashes / veins (n = 3), rose diagram statistics were not calculated.

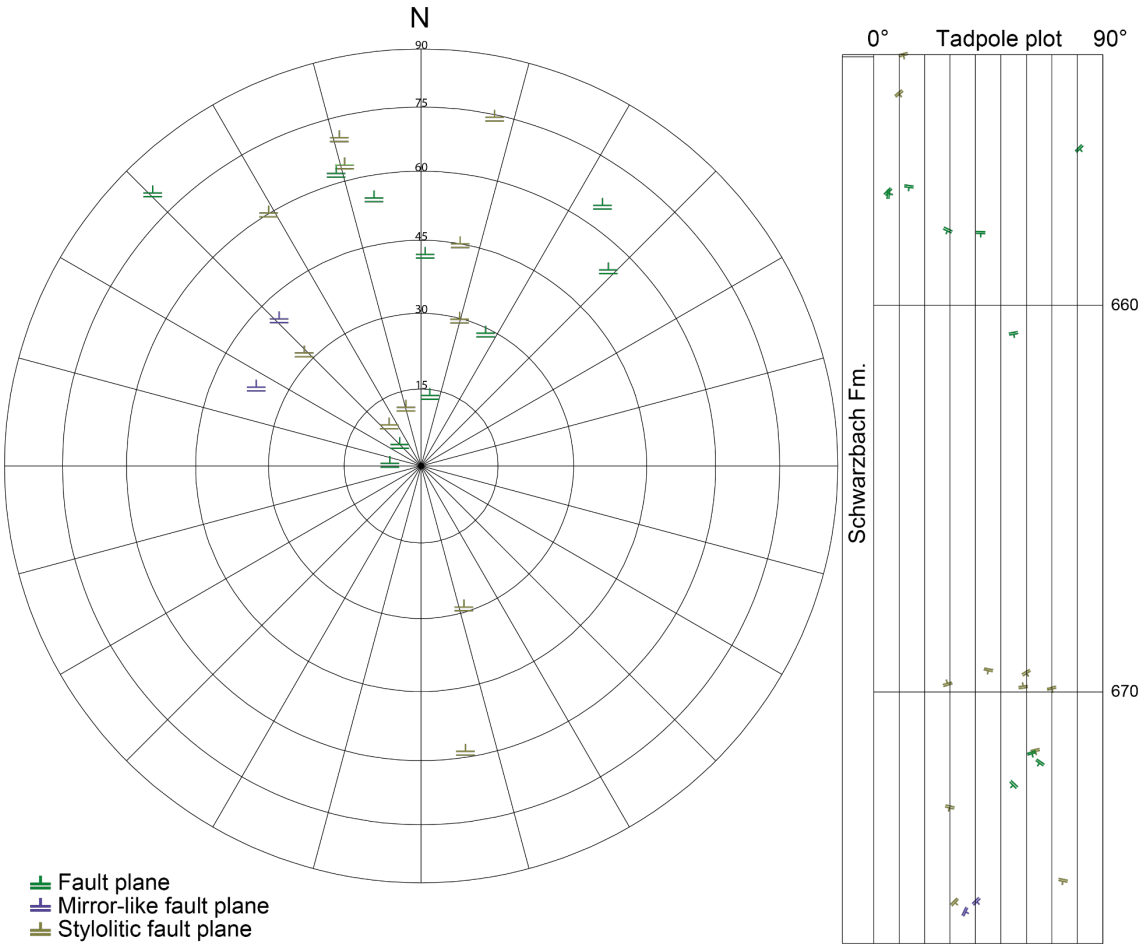

Fig. 4-24: Stereogram and depth plot of fault planes (Schwarzbach Formation)

Fault planes (n = 10), mirror-like fault planes (n = 2) and stylolitic fault planes (n = 11).

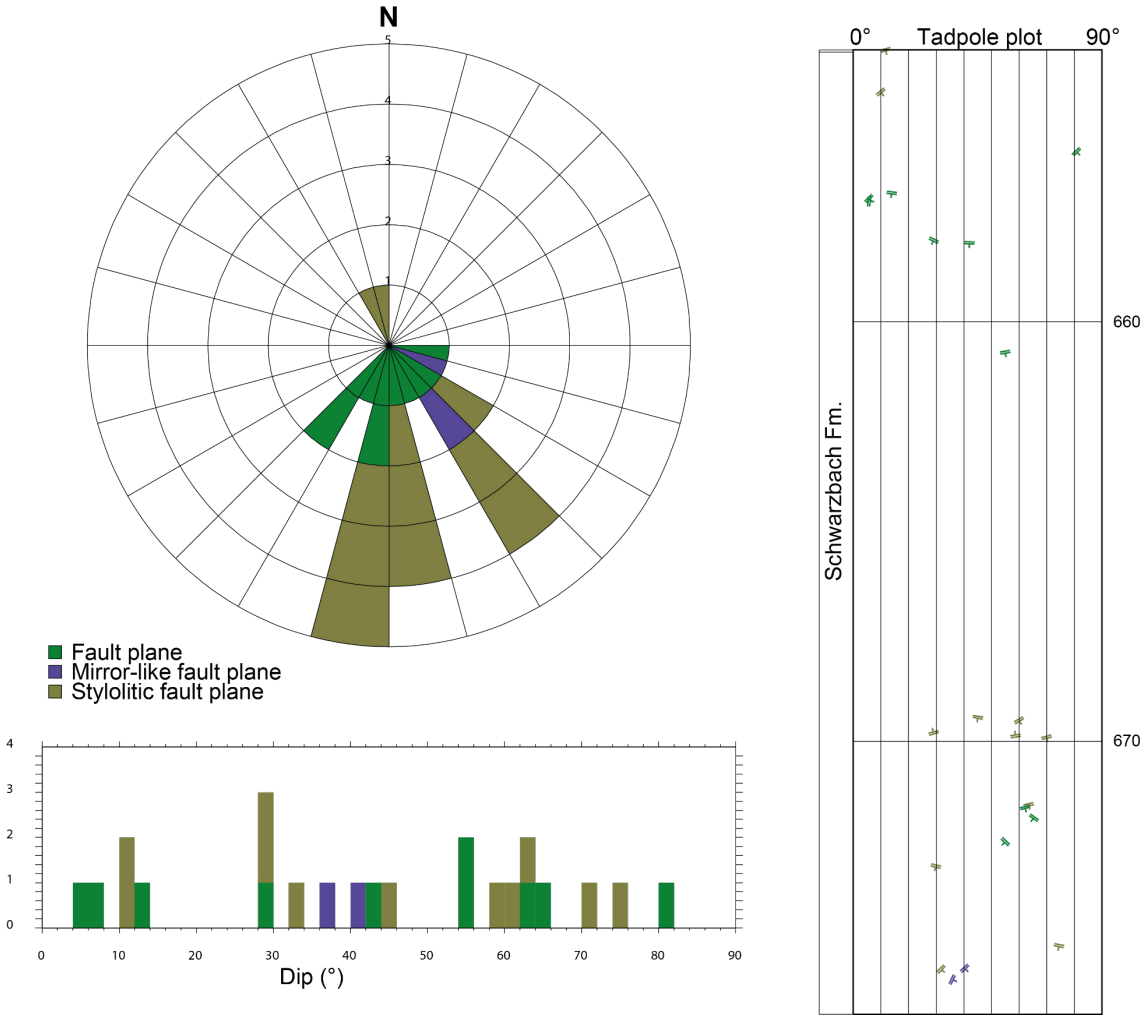

Fig. 4-25: Azimuth rose diagram, dip histogram and depth plot of fault planes (Schwarzbach Formation)

Fault planes (n = 10), mirror-like fault planes (n = 2) and stylolitic fault planes (n = 11).

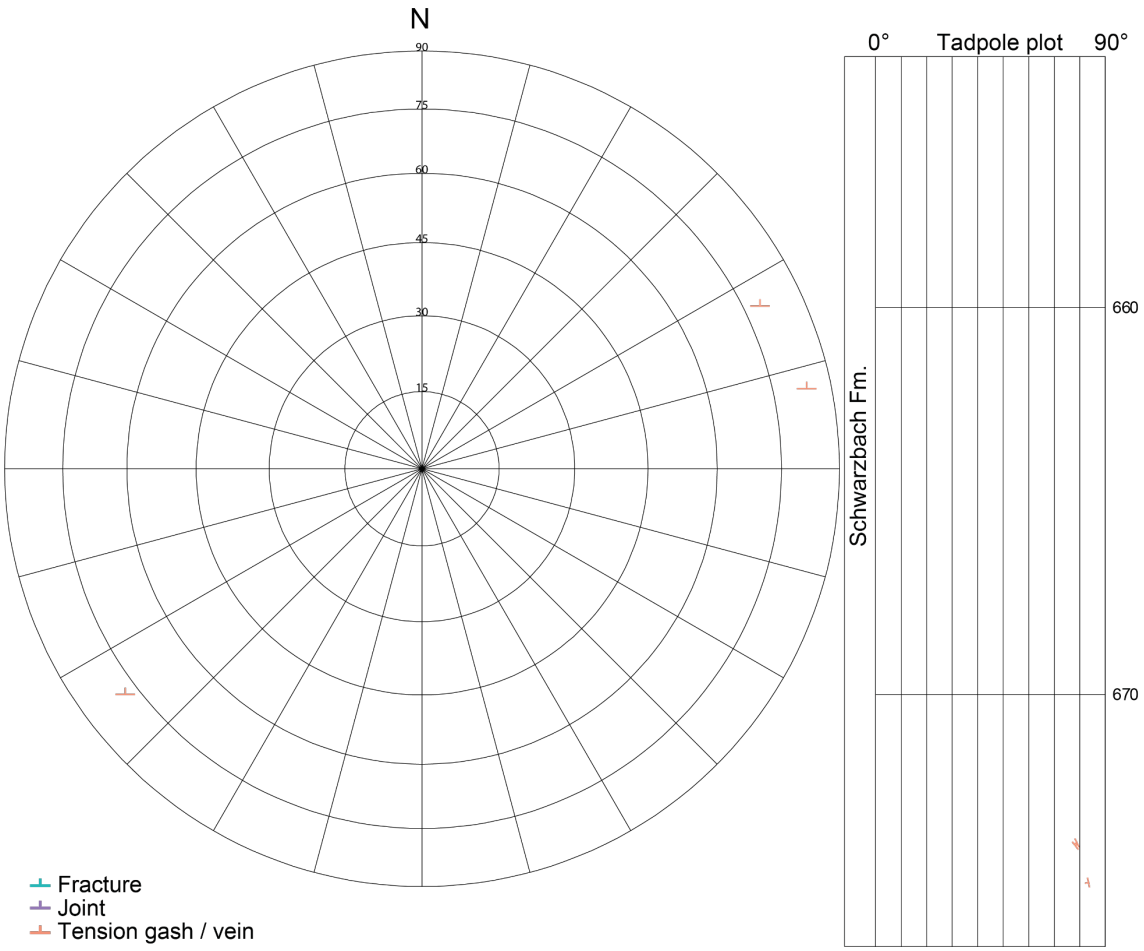

Fig. 4-26: Stereogram and depth plot for fractures, tension gashes / veins and joints (Schwarzbach Formation)

Fractures (n = 0), joints (n = 0) and tension gashes / veins (n = 3).

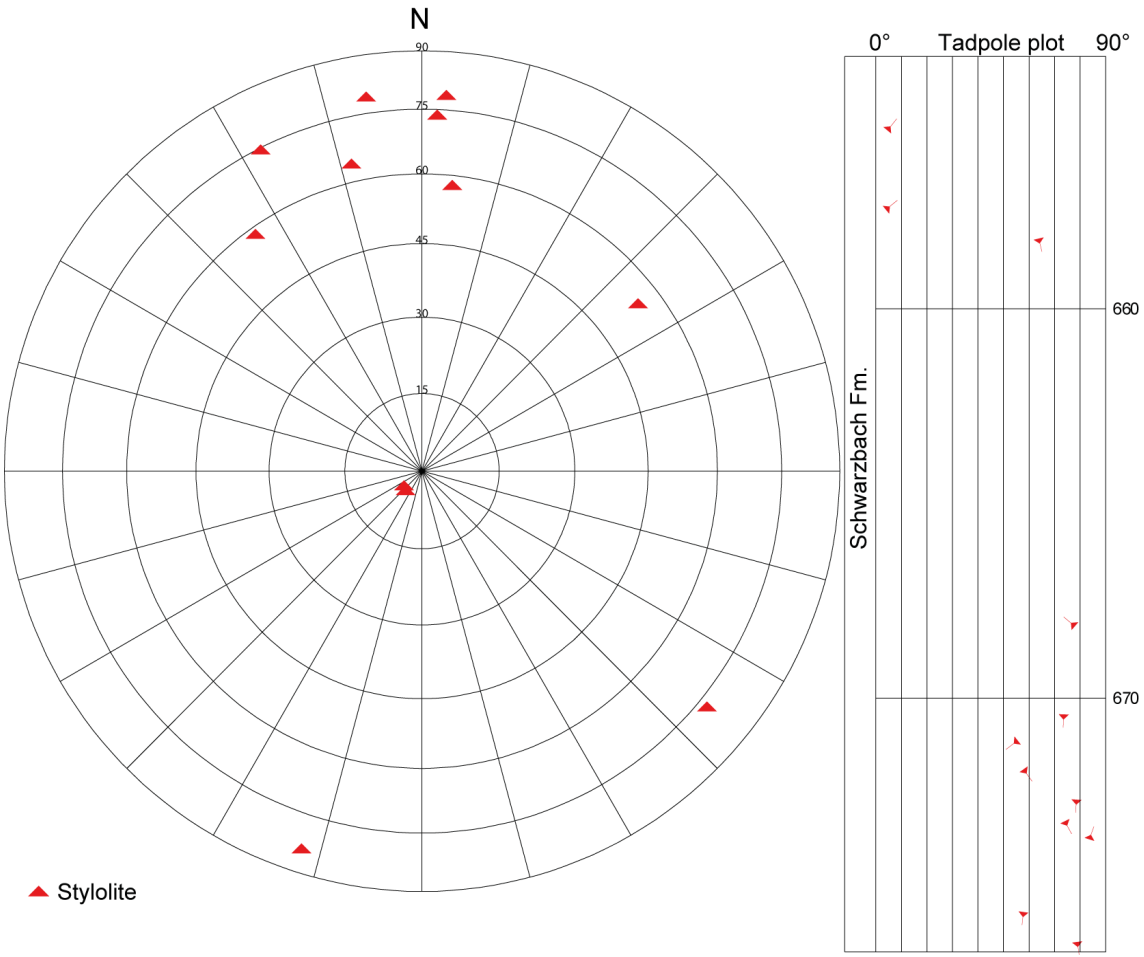

Fig. 4-27: Stereogram and depth plot of stylolites (Schwarzbach Formation, n = 12)

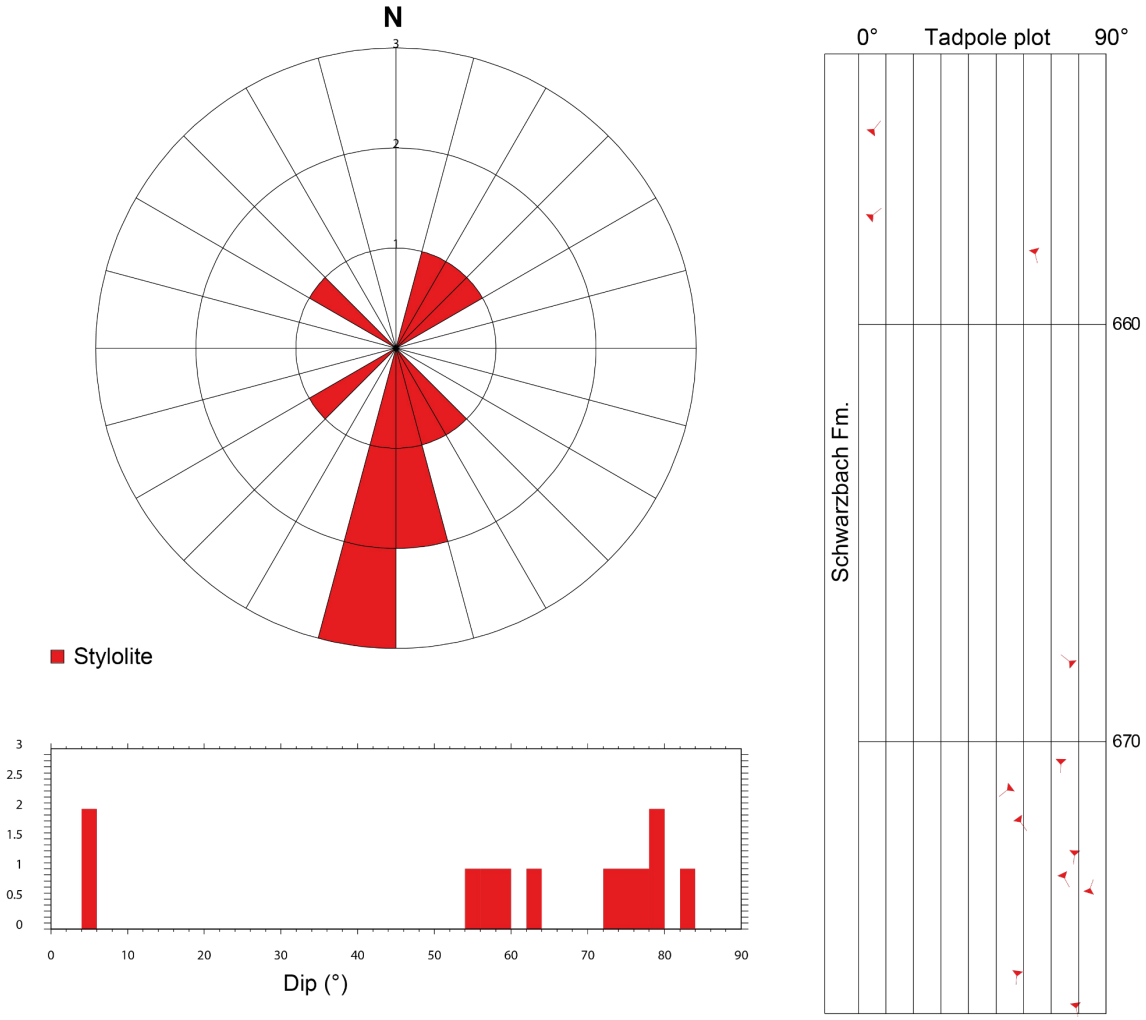

Fig. 4-28: Azimuth rose diagram, dip histogram and depth plot of stylolites (Schwarzbach Formation, n = 12)

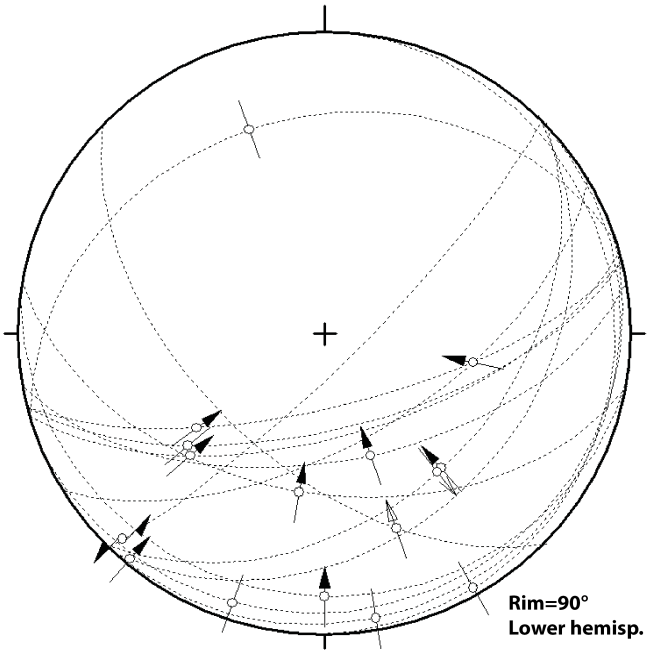

Fig. 4-29: Stereogram of faults (Schwarzbach Formation, n = 15)

4.2.3 Villigen Formation

The orientation and spatial distribution of structural data in the Villigen Formation (676.51 – 751.21 m MD log depth) are visualised in Figs. 4-30 to 4-36.

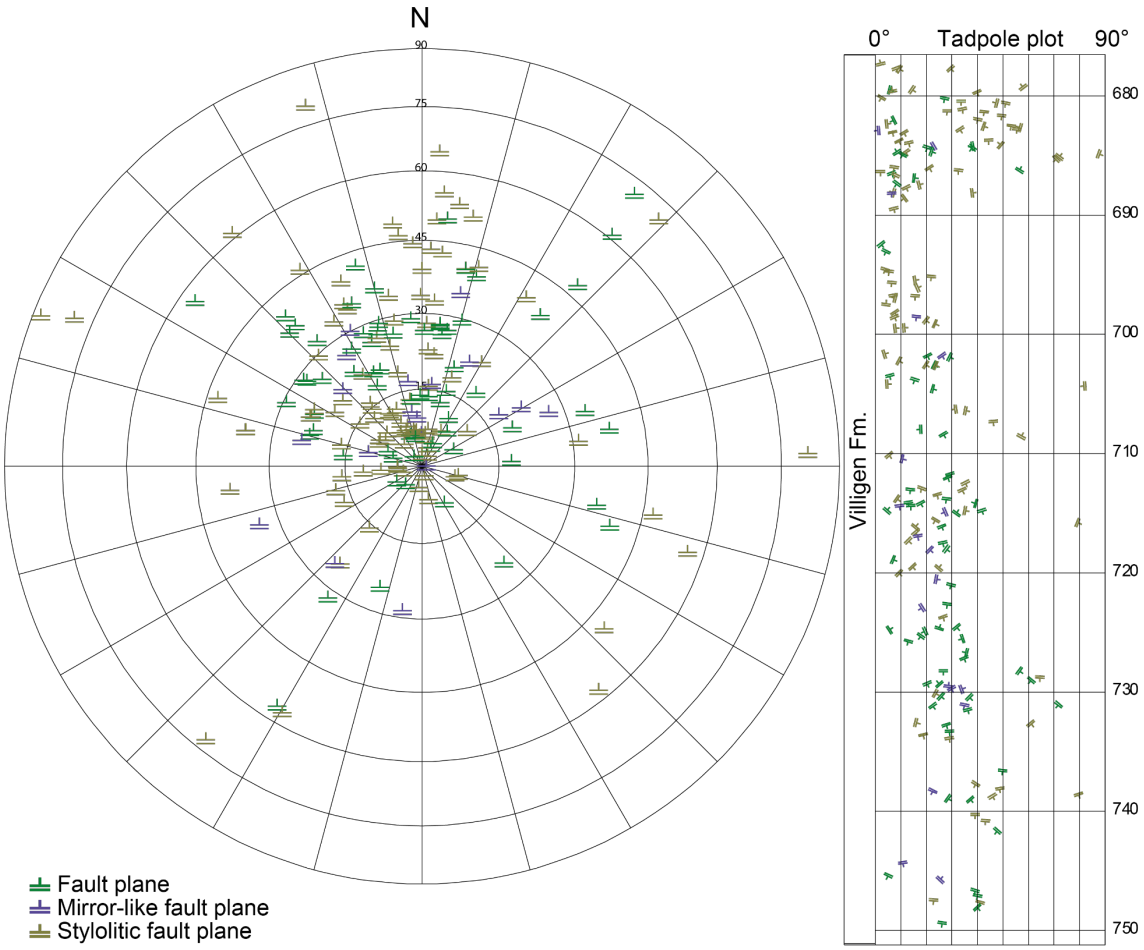

Fig. 4-30: Stereogram and depth plot of fault planes (Villigen Formation)

Fault planes (n = 70), mirror-like fault planes (n = 19) and stylolitic fault planes (n = 100).

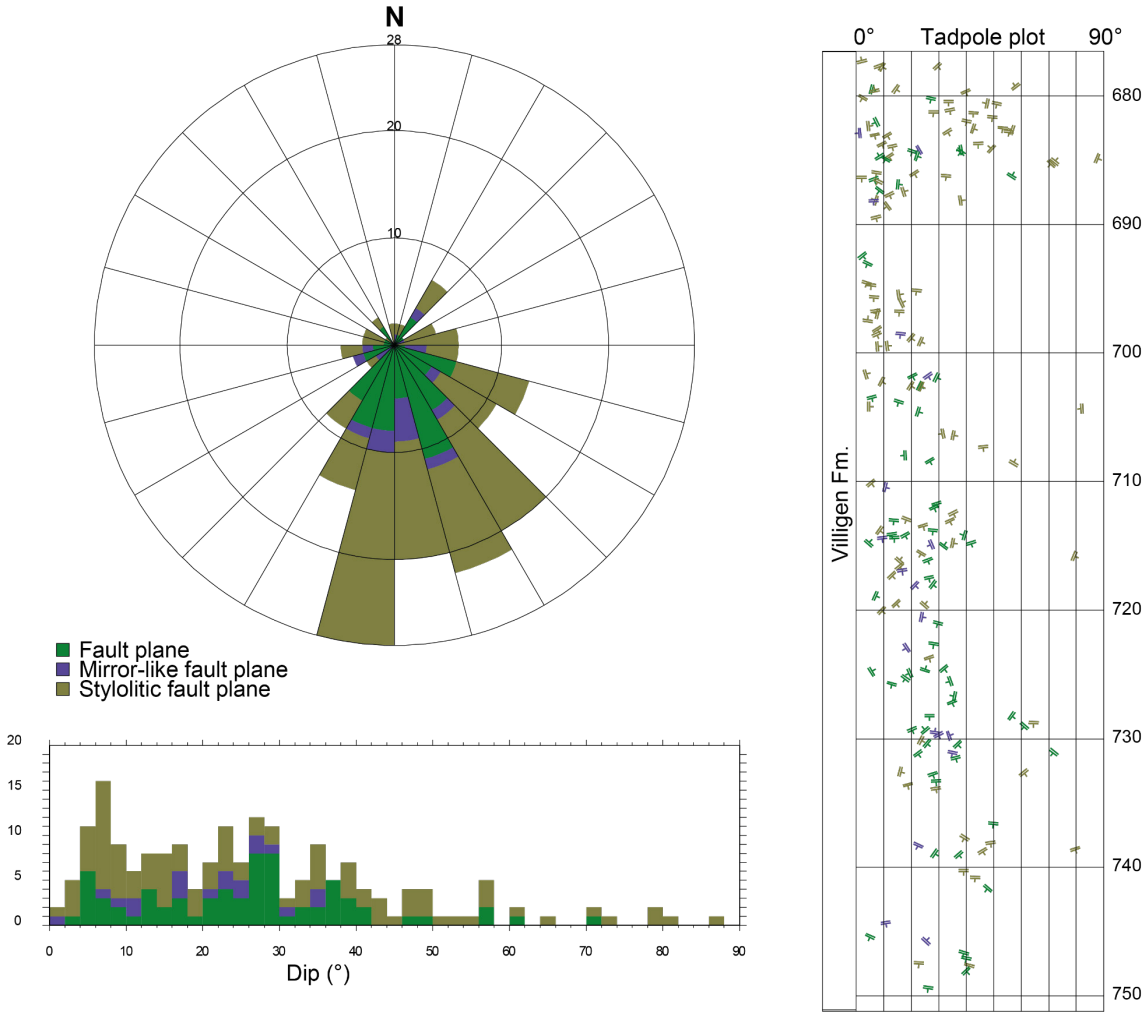

Fig. 4-31: Azimuth rose diagram, dip histogram and depth plot of fault planes (Villigen Formation)

Fault planes (n = 70), mirror-like fault planes (n = 19) and stylolitic fault planes (n = 100).

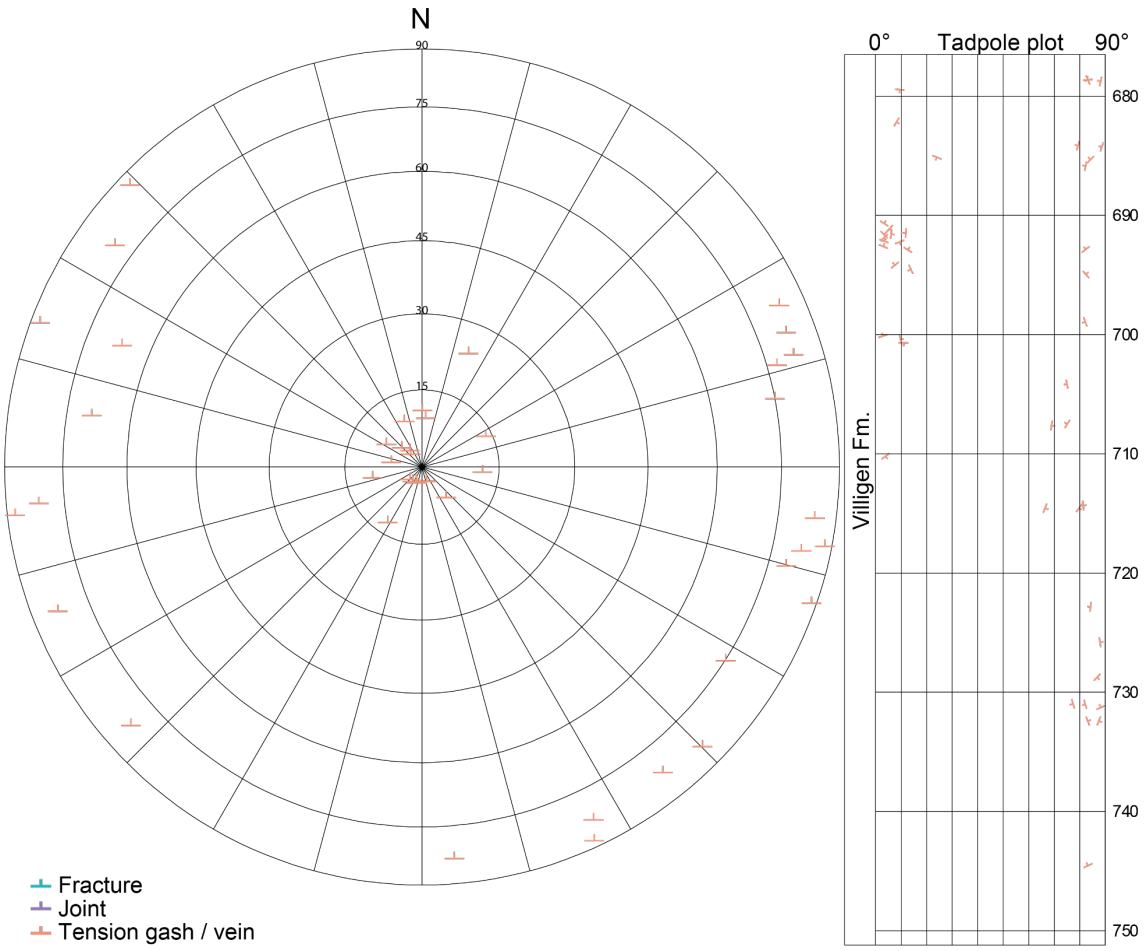

Fig. 4-32: Stereogram and depth plot of fractures, tension gashes / veins and joints (Villigen Formation)

Fractures (n = 0), joints (n = 0) and tension gashes / veins (n = 44).

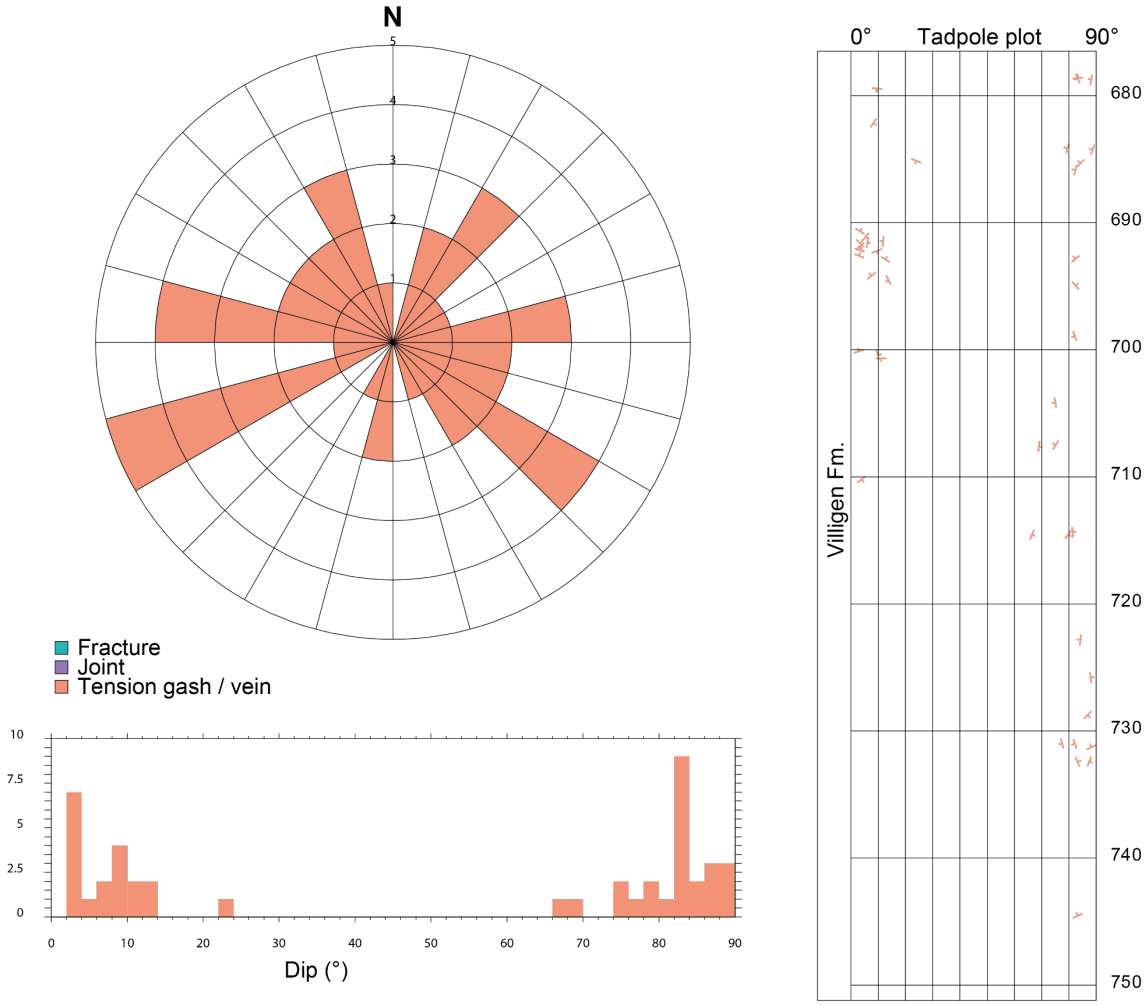

Fig. 4-33: Azimuth rose diagram, dip histogram and depth plot of fractures, tension gashes / veins and joints (Villigen Formation)

Fractures (n = 0), joints (n = 0) and tension gashes / veins (n = 44).

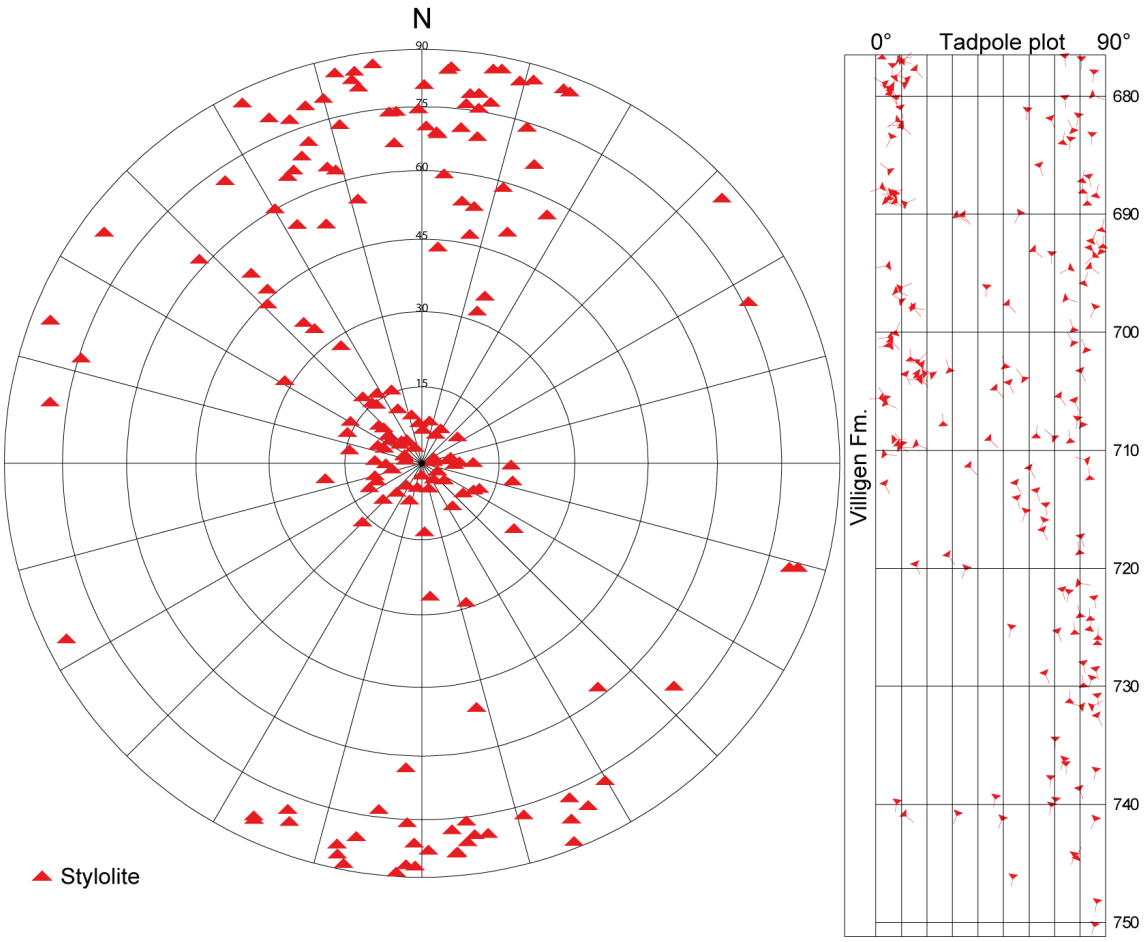

Fig. 4-34: Stereogram and depth plot of stylolites (Villigen Formation, n = 171)

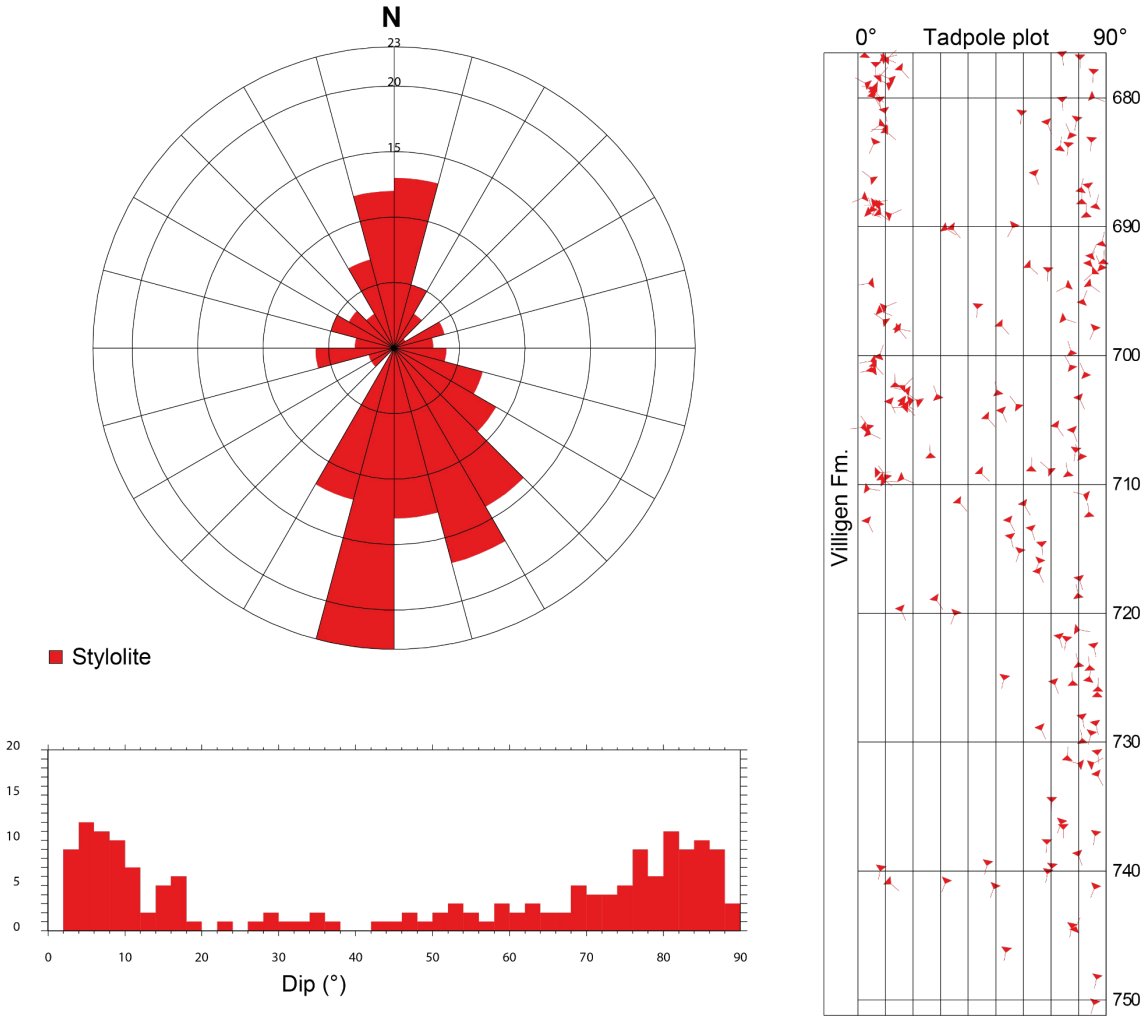

Fig. 4-35: Azimuth rose diagram, dip histogram and depth plot of stylolites (Villigen Formation, n = 171)

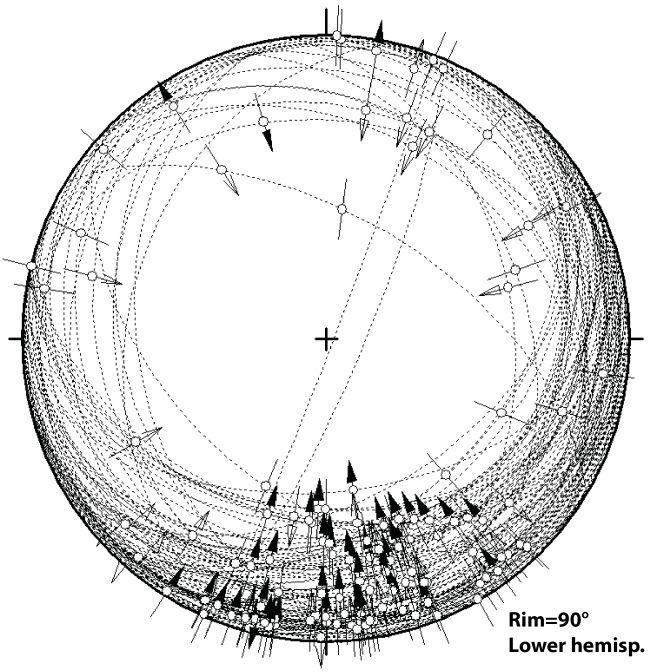

Fig. 4-36: Stereogram of faults (Villigen Formation, n = 130)

4.2.4 Wildegg Formation

The orientation and spatial depth distribution of recorded structures in the Wildegg Formation (751.21 –805.38 m MD log depth) are shown in Figs. 4-37 to 4-41. Fractures, tension gashes / veins and joints are absent in this borehole interval.

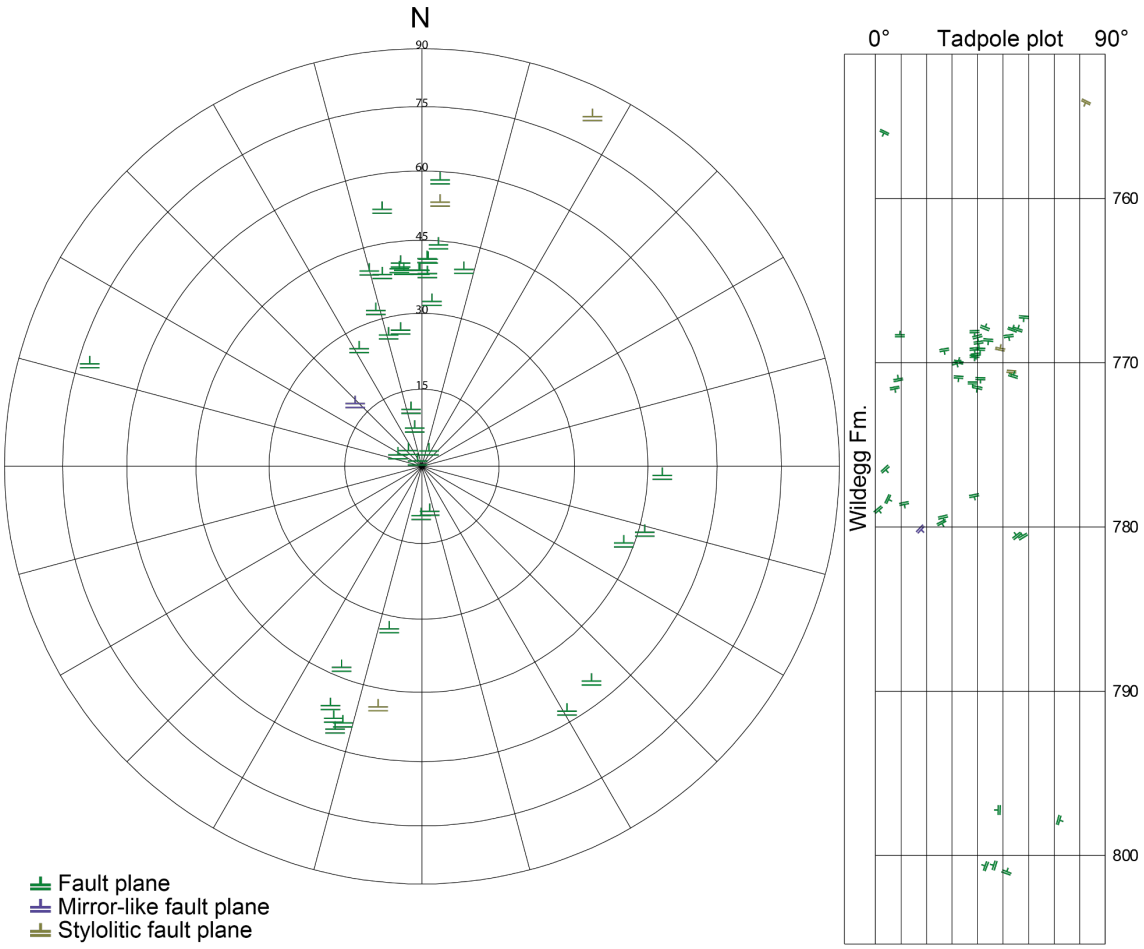

Fig. 4-37: Stereogram and depth plot of fault planes (Wildegg Formation)

Fault planes (n = 39), mirror-like fault planes (n = 1) and stylolitic fault planes (n = 3).

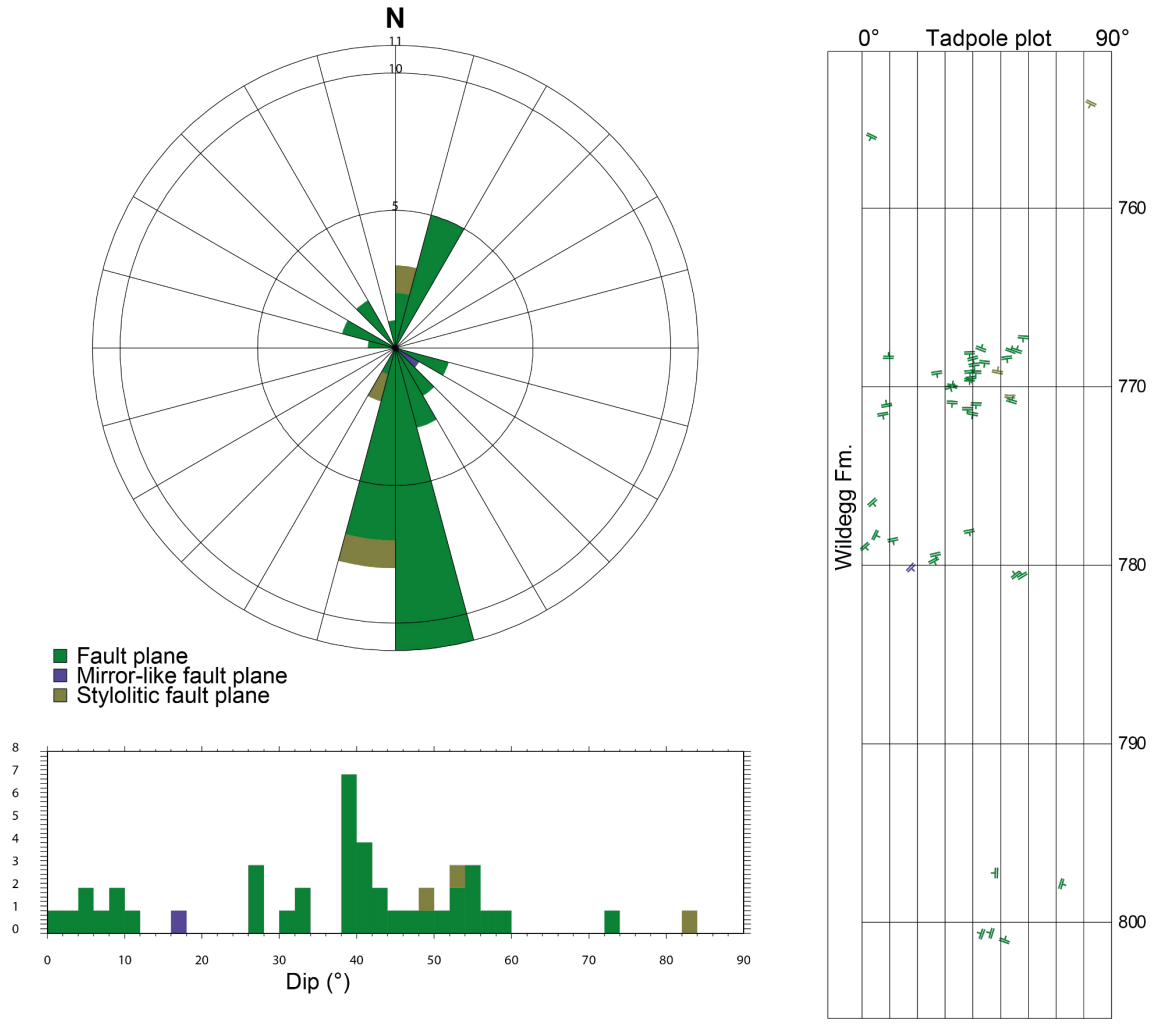

Fig. 4-38: Azimuth rose diagram, dip histogram and depth plot of faults (Wildegg Formation)
Fault planes (n = 39), mirror-like fault planes (n = 1) and stylolitic fault planes (n = 3).

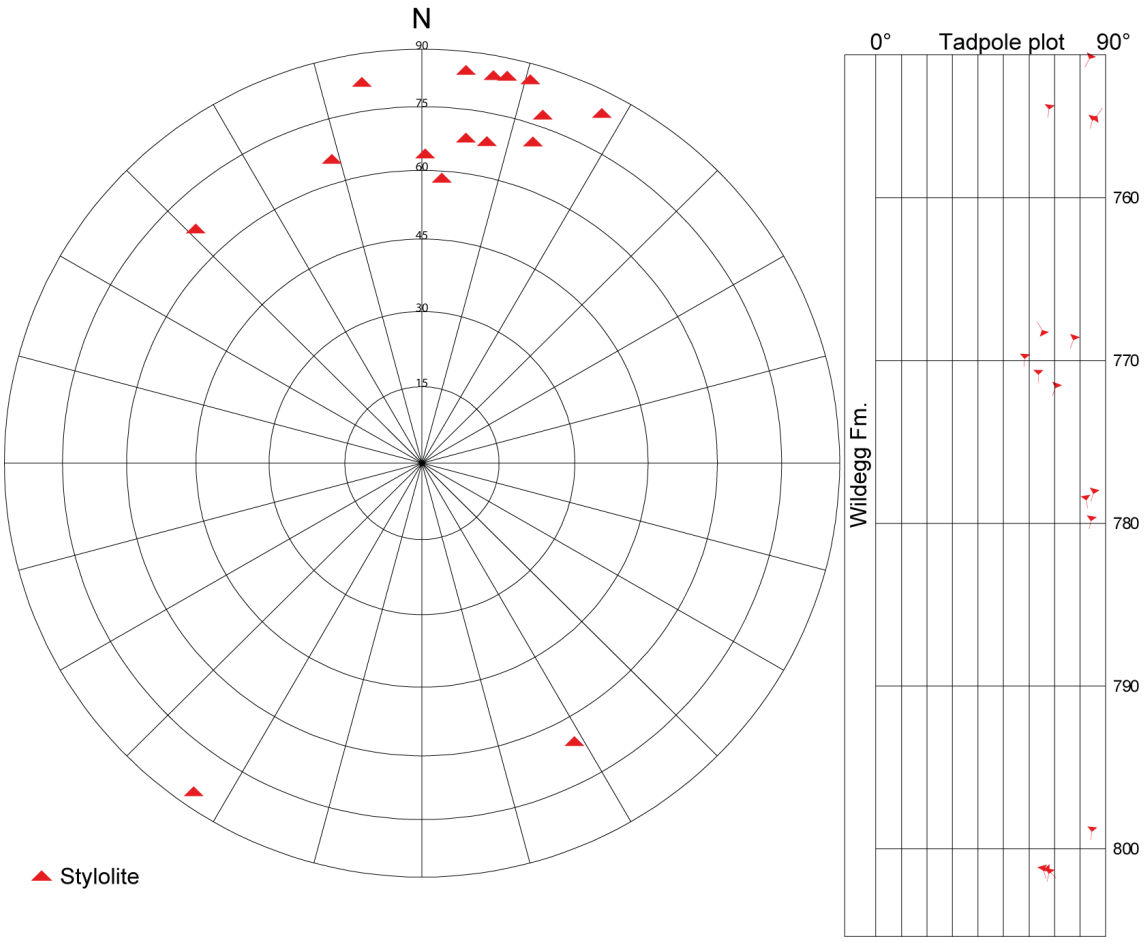

Fig. 4-39: Stereogram and depth plot of stylolites (Wildegg Formation, n = 16)

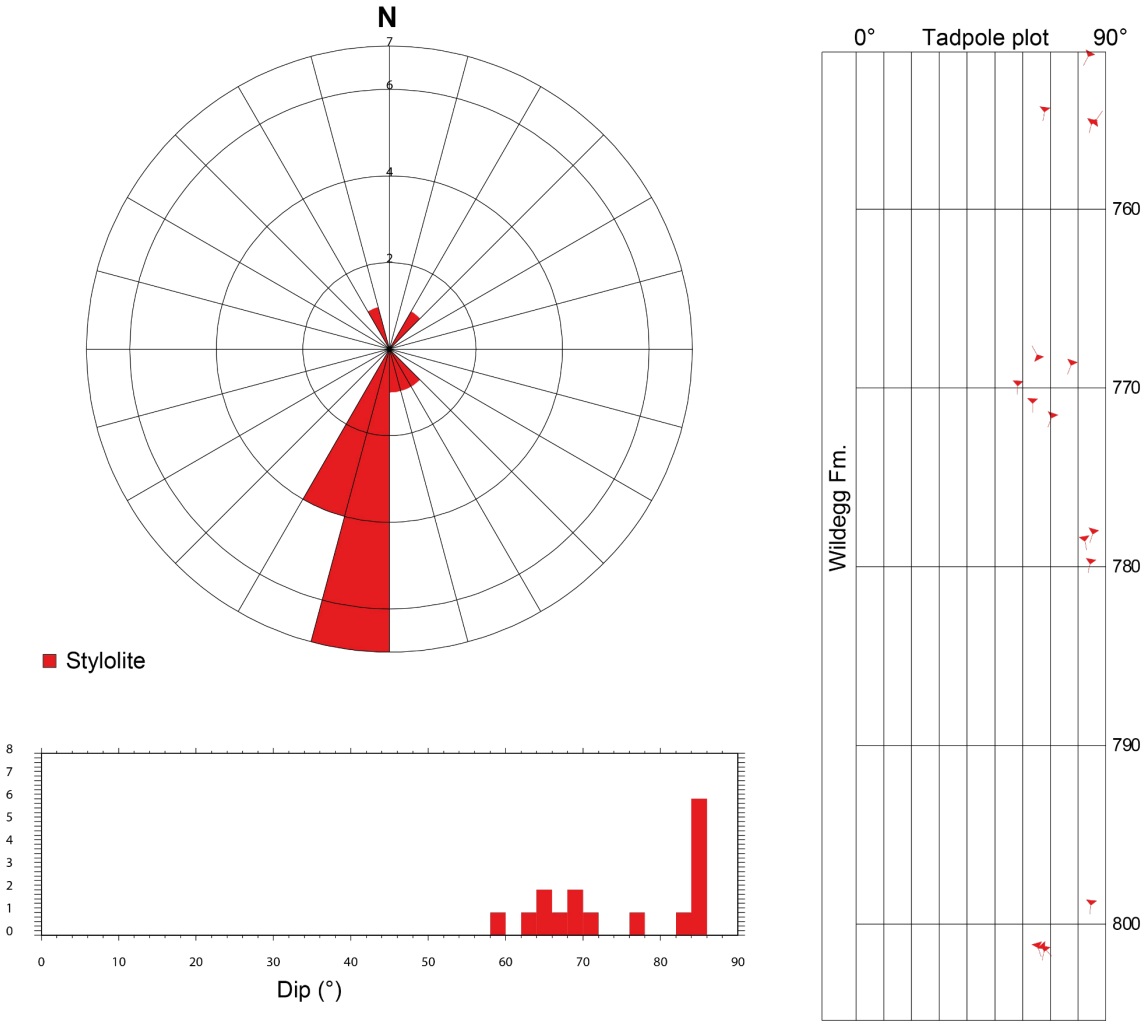

Fig. 4-40: Azimuth rose diagram, dip histogram and depth plot of stylolites (Wildegg Formation, n = 16)

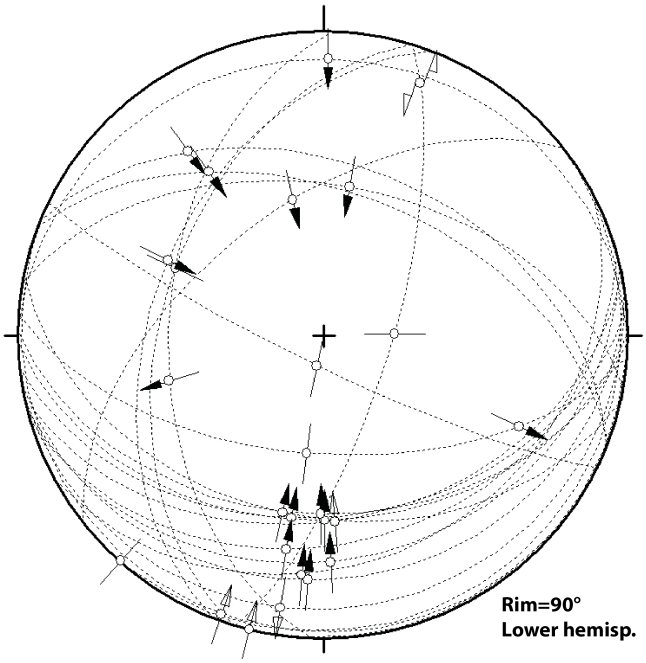

Fig. 4-41: Stereogram of faults (Wildegg Formation, n = 27)

4.3 Dogger

For the detailed stereographic evaluation, the Dogger was subdivided into two units: the 'Brauner Dogger' and the Opalinus Clay. Only the data for oriented cores are presented.

4.3.1 'Brauner Dogger' (Wutach Formation – «Murchisonae-Oolith Formation»)

The 'Brauner Dogger' (805.38 – 891.75 m MD log depth), an informal lithostratigraphic unit summarising predominantly claystone-rich lithologies from the Wutach Formation to the «Murchisonae-Oolith Formation», showed an elevated density of stylolitic fault planes and stylolites in the «Herrenwis Unit» from 813 to 854 m MD log depth. In addition, two fault zones (35 cm and 7 cm thick) were interpreted at the bottom of the 'Brauner Dogger', 1 m above the upper boundary of the Opalinus Clay at a depth of 891.75 m MD log depth. These fault zones were characterised by a complex network of 2 – 25° dipping mirror-like fault planes and fault planes with synkinematic calcite mineralisation. Dip parallel slip was common, which indicates that thrusting / reverse faulting is the main deformation mechanism. The orientation and spatial distribution of structural discontinuities within the 'Brauner Dogger' are visualised in Figs. 4-42 to 4-47. Due to the low number (n = 9) of fractures, joints and tension gashes / veins, rose diagram statistics were not calculated.

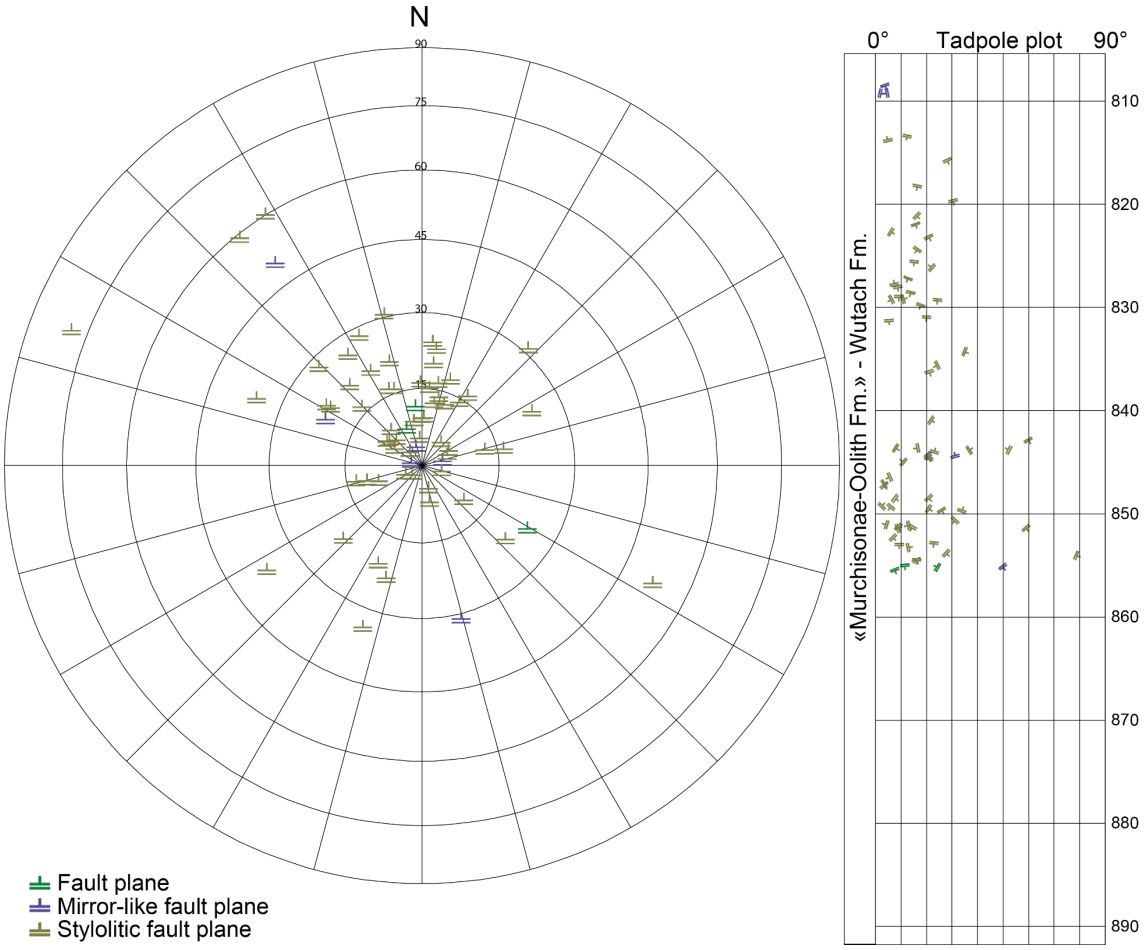

Fig. 4-42: Stereogram and depth plot of fault planes ('Brauner Dogger')

Fault planes (n = 3), mirror-like fault planes (n = 6) and stylolitic fault planes (n = 61).

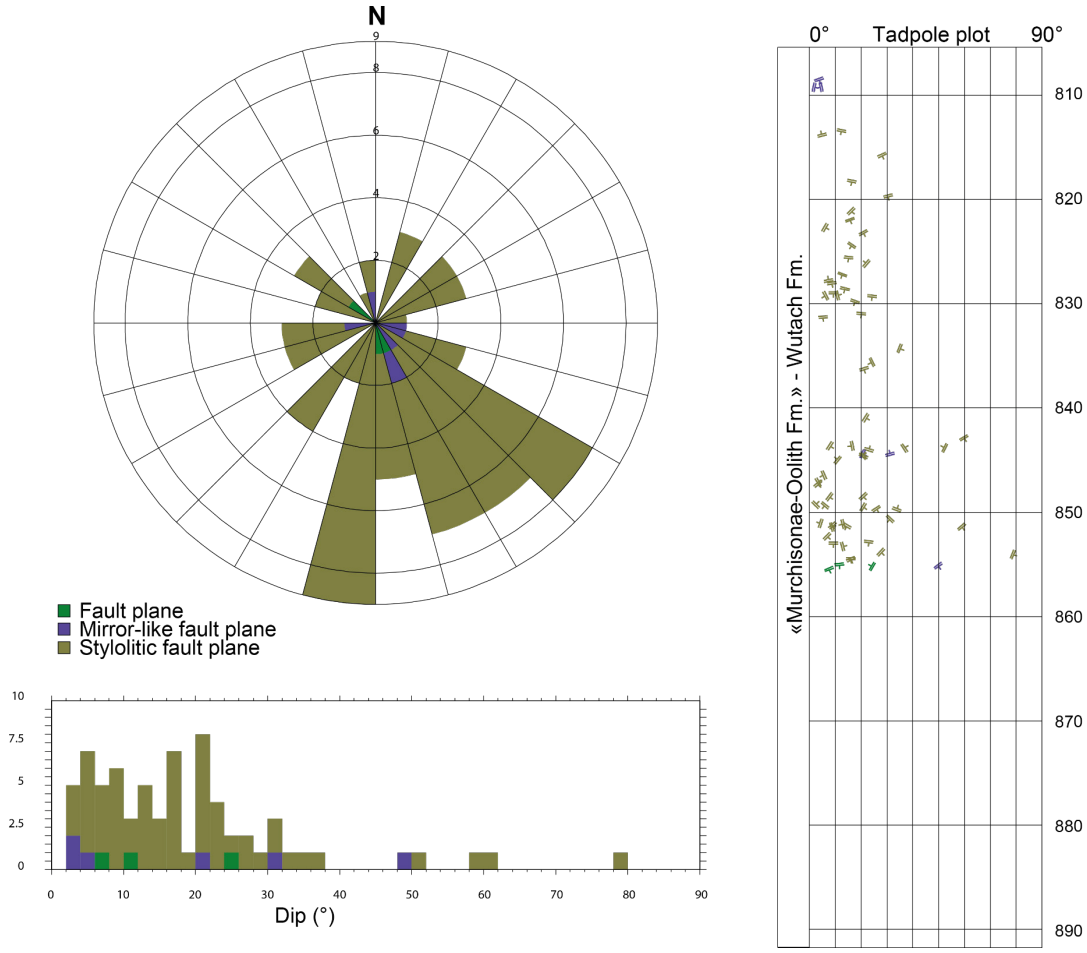

Fig. 4-43: Azimuth rose diagram, dip histogram and depth plot of fault planes ('Brauner Dogger')

Fault planes (n = 3), mirror-like fault planes (n = 6) and stylolitic fault planes (n = 61).

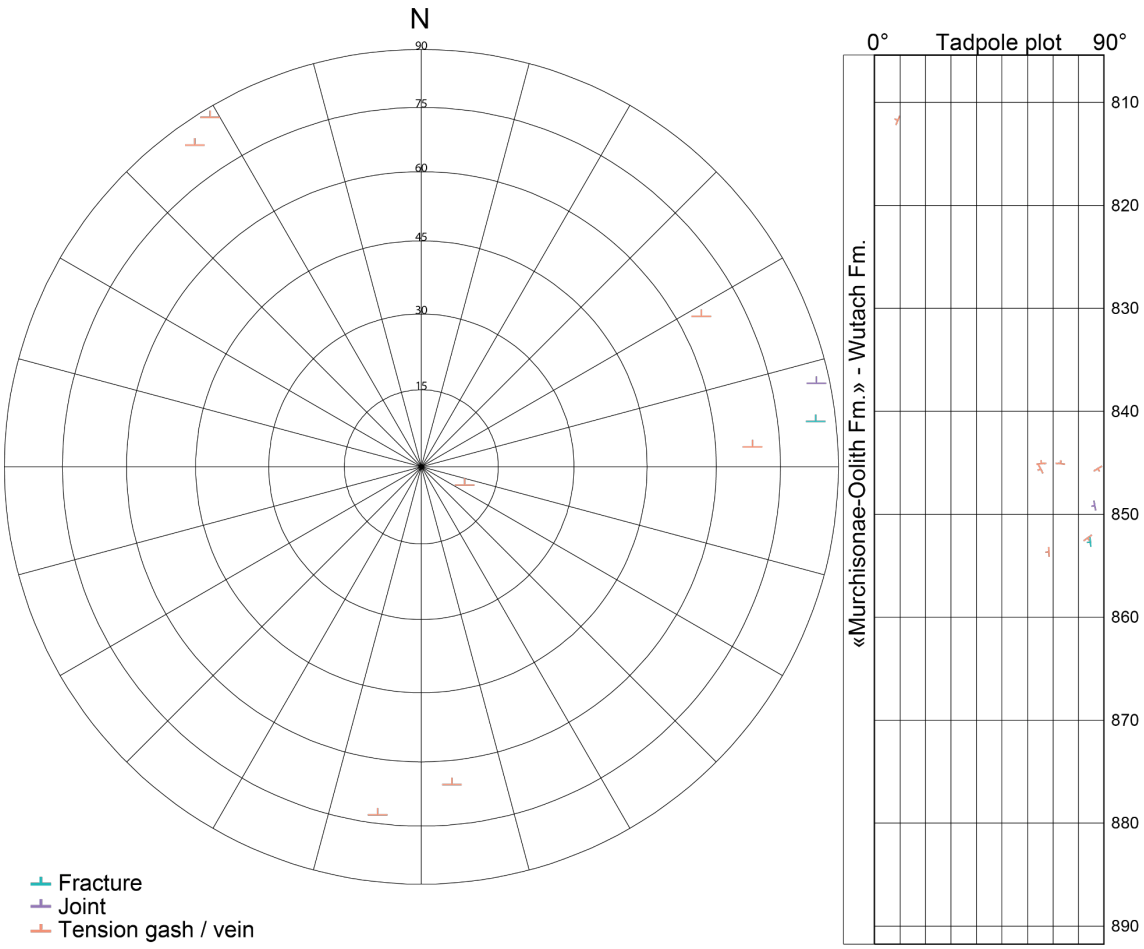

Fig. 4-44: Stereogram and depth plot of fractures, tension gashes / veins and joints ('Brauner Dogger')

Fractures (n = 1), joints (n = 1) and tension gashes / veins (n = 7).

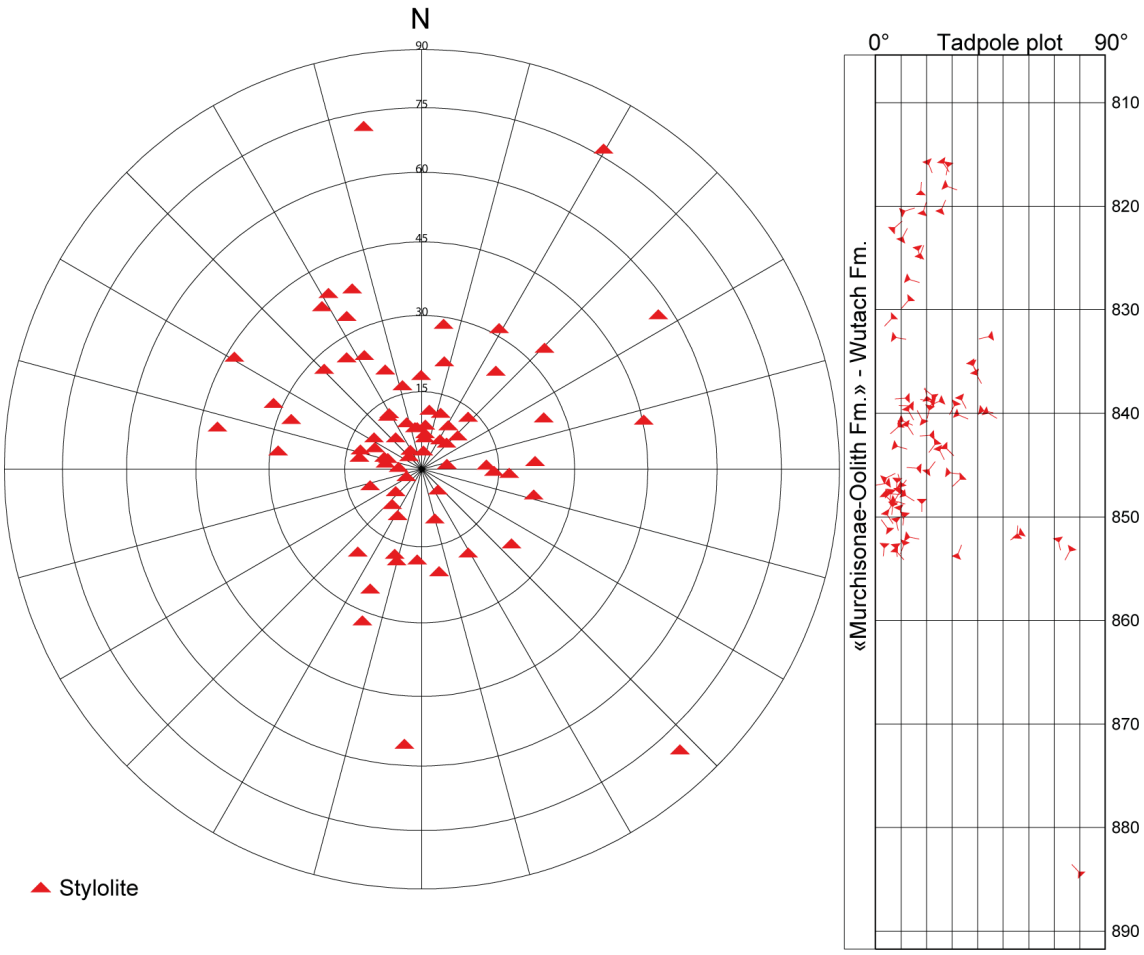

Fig. 4-45: Stereogram and depth plot of stylolites ('Brauner Dogger', n = 76)

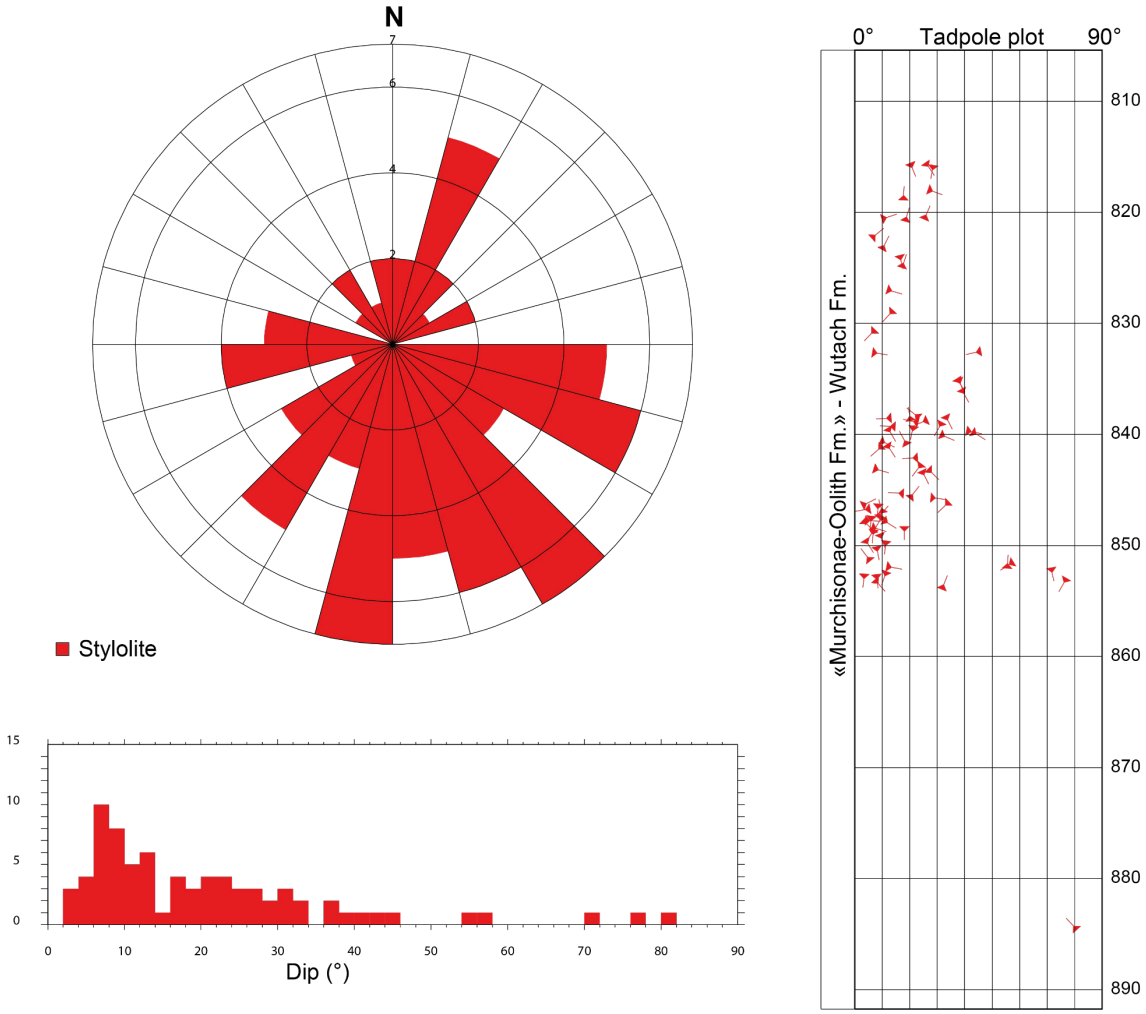

Fig. 4-46: Azimuth rose diagram, dip histogram and depth plot of stylolites ('Brauner Dogger', n = 76)

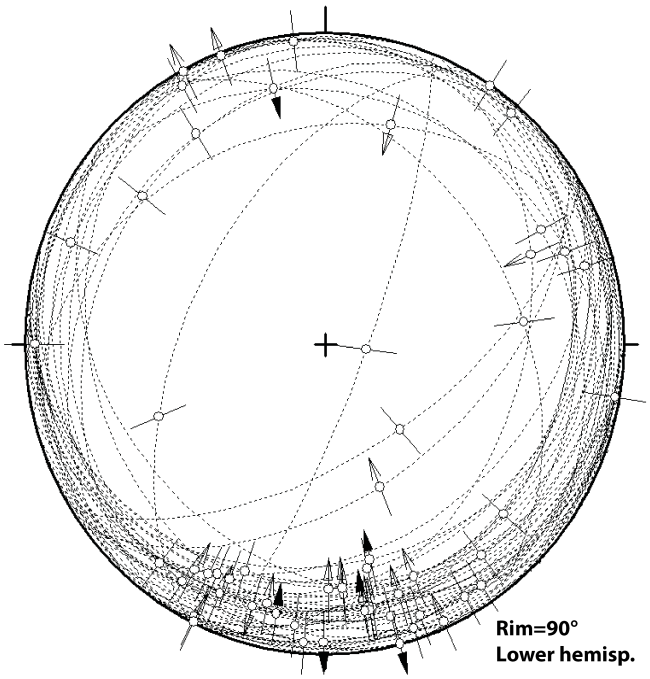

Fig. 4-47: Stereogram of faults ('Brauner Dogger', n = 58)

4.3.2 Opalinus Clay

The 104.26 m thick Opalinus Clay (891.75 – 996.01 m MD log depth) represents a borehole interval with sub-horizontal bedding and only a few structures. It was however strongly affected by core discing. With a total of 26 fault planes and 18 mirror-like fault planes, the Opalinus Clay showed the lowest average natural fracture density. The fault planes have shallow dip angles and variable dip directions.

The structural inventory for the Opalinus Clay is presented in Figs. 4-48 to 4-50, however, only oriented features are visualised in these plots. Fractures, tension gashes / veins, joints and stylolites were not observed in this depth interval.

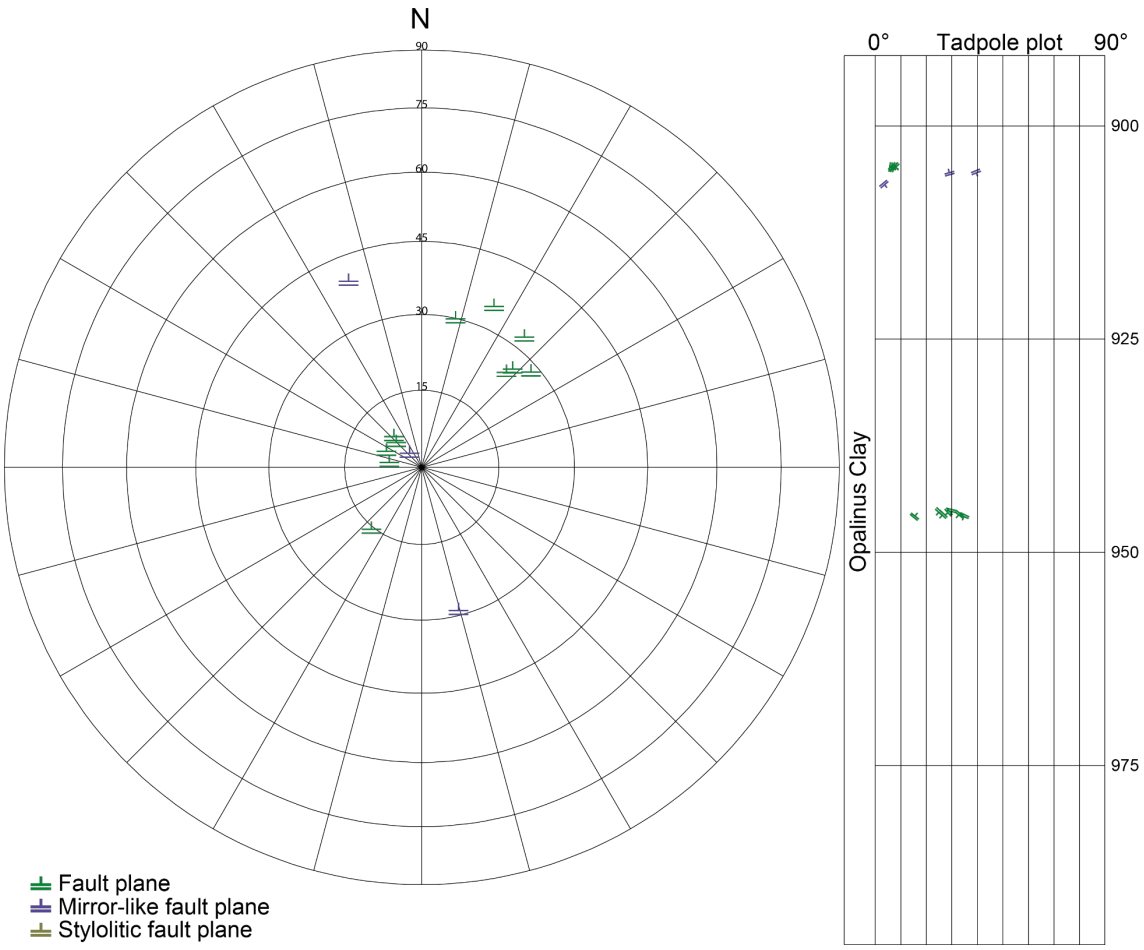

Fig. 4-48: Stereogram and depth plot of fault planes (Opalinus Clay)

Fault planes (n = 11), mirror-like fault planes (n = 3) and stylolitic fault planes (n = 0).

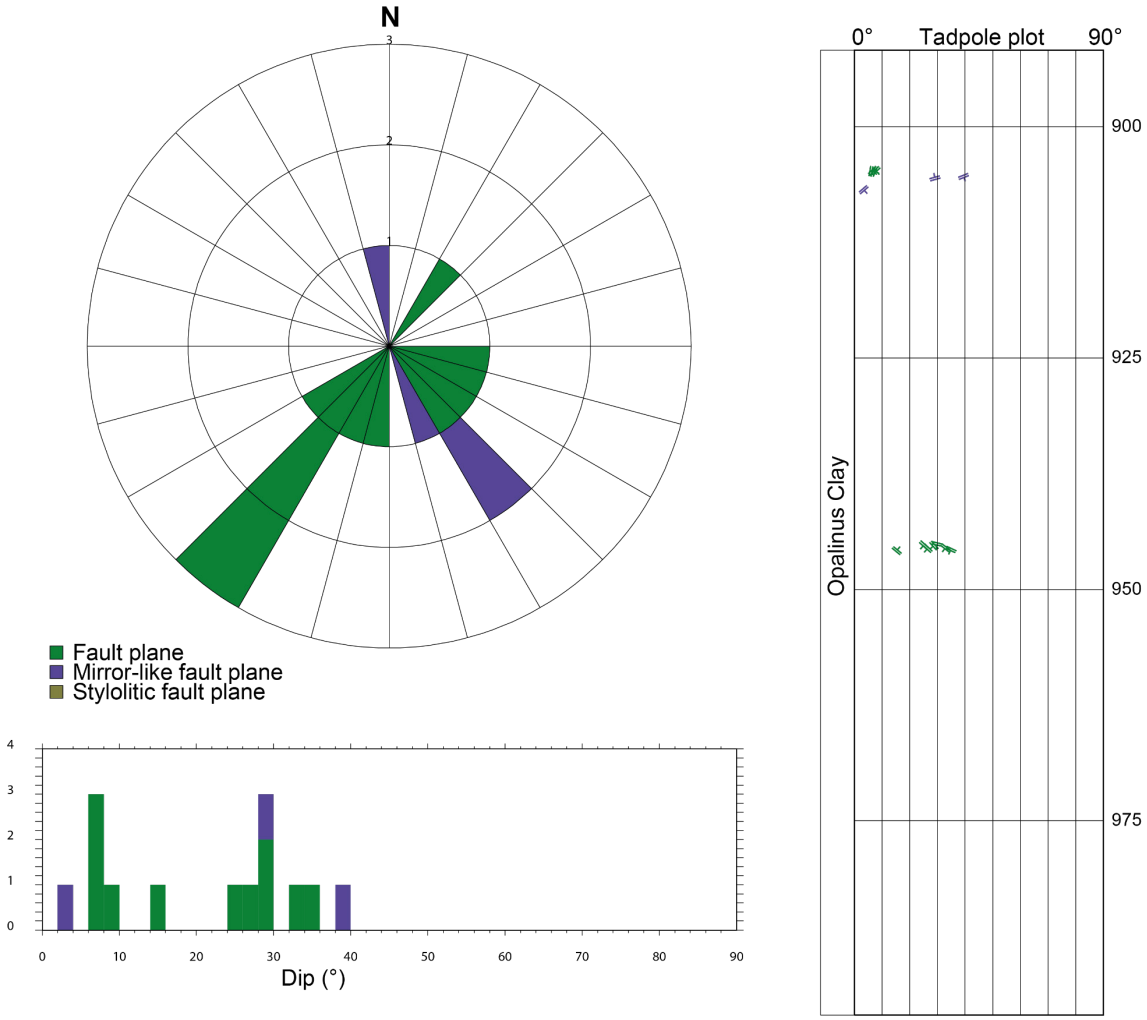

Fig. 4-49: Azimuth rose diagram, dip histogram and depth plot of fault planes (Opalinus Clay)
Fault planes (n = 11), mirror-like fault planes (n = 3) and stylolitic fault planes (n = 0).

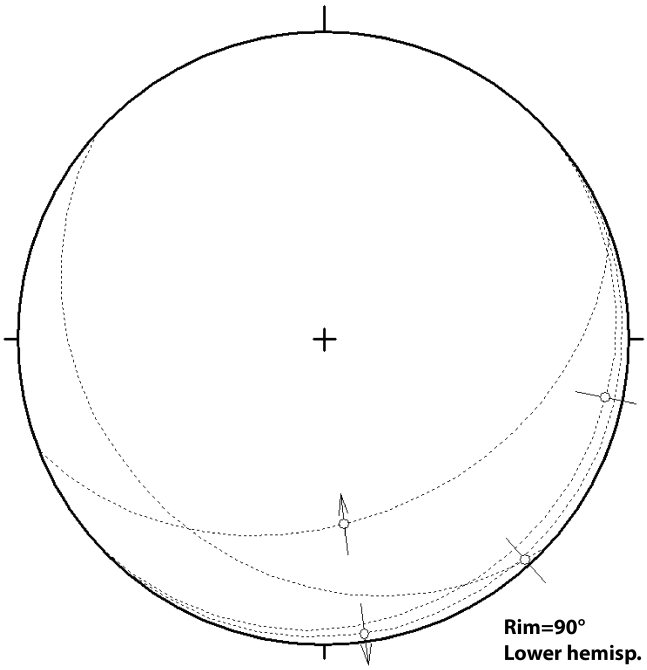

Fig. 4-50: Stereogram of lineations (Opalinus Clay, n = 4)

4.4 Lias (Staffelegg Formation)

As presented in Figs. 4-51 to 4-55, the Lias (996.01 – 1'030.53 m MD log depth) showed a very low number of structural discontinuities. Only the data for oriented cores are presented. Due to the low number of fractures, joints and tension gashes / veins (n = 9) and stylolites (n = 1), rose diagram statistics were not calculated.

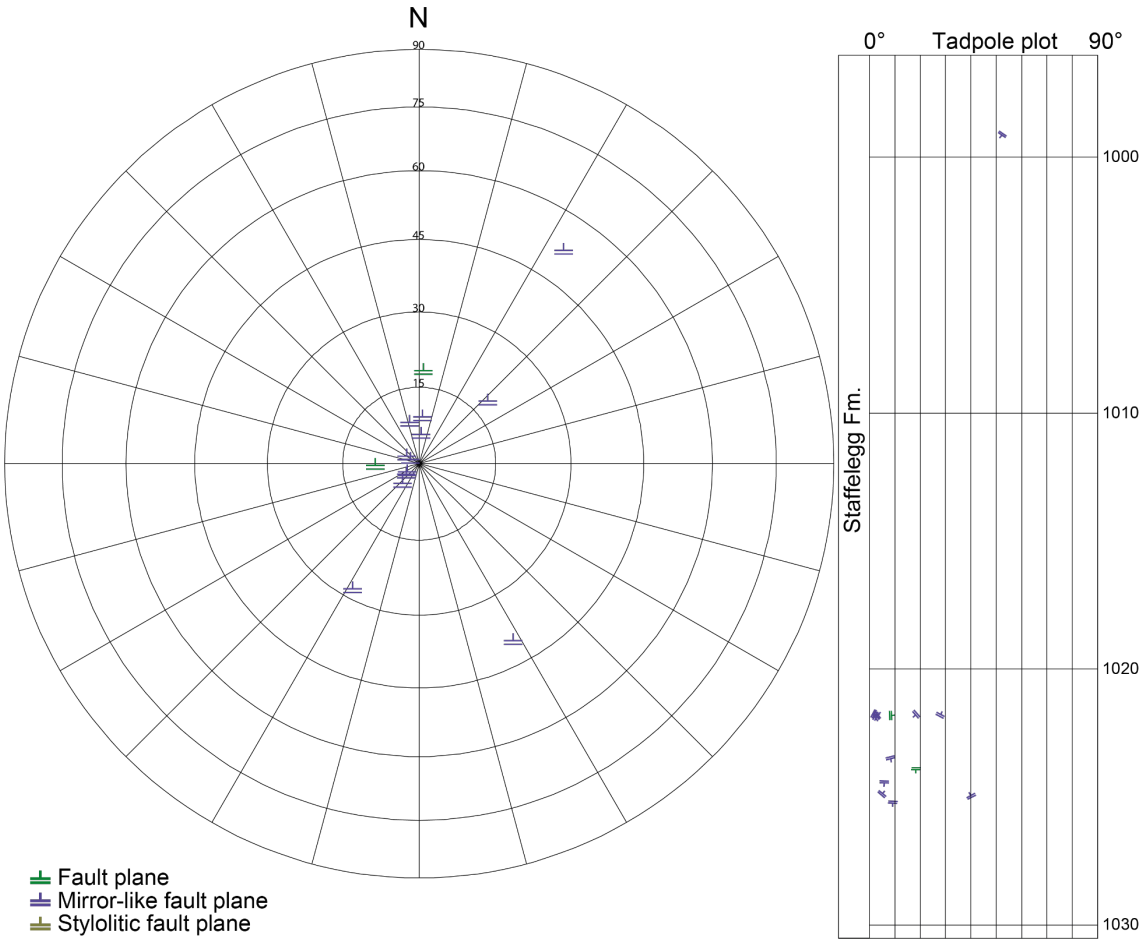

Fig. 4-51: Stereogram and depth plot of fault planes (Lias)

Fault planes (n = 2), mirror-like fault planes (n = 12) and stylolitic fault planes (n = 0).

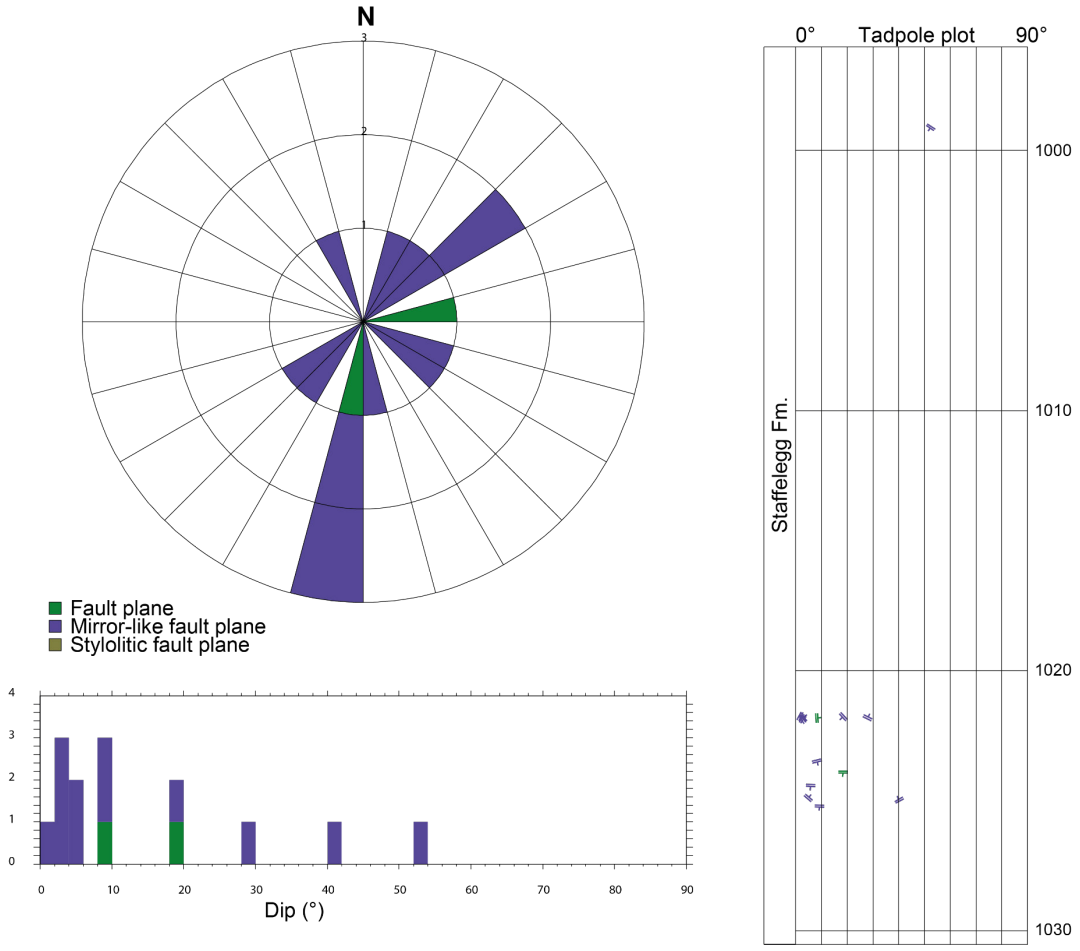

Fig. 4-52: Azimuth rose diagram, dip histogram and depth plot of fault planes (Lias)
Fault planes (n = 2), mirror-like fault planes (n = 12) and stylolitic fault planes (n = 0).

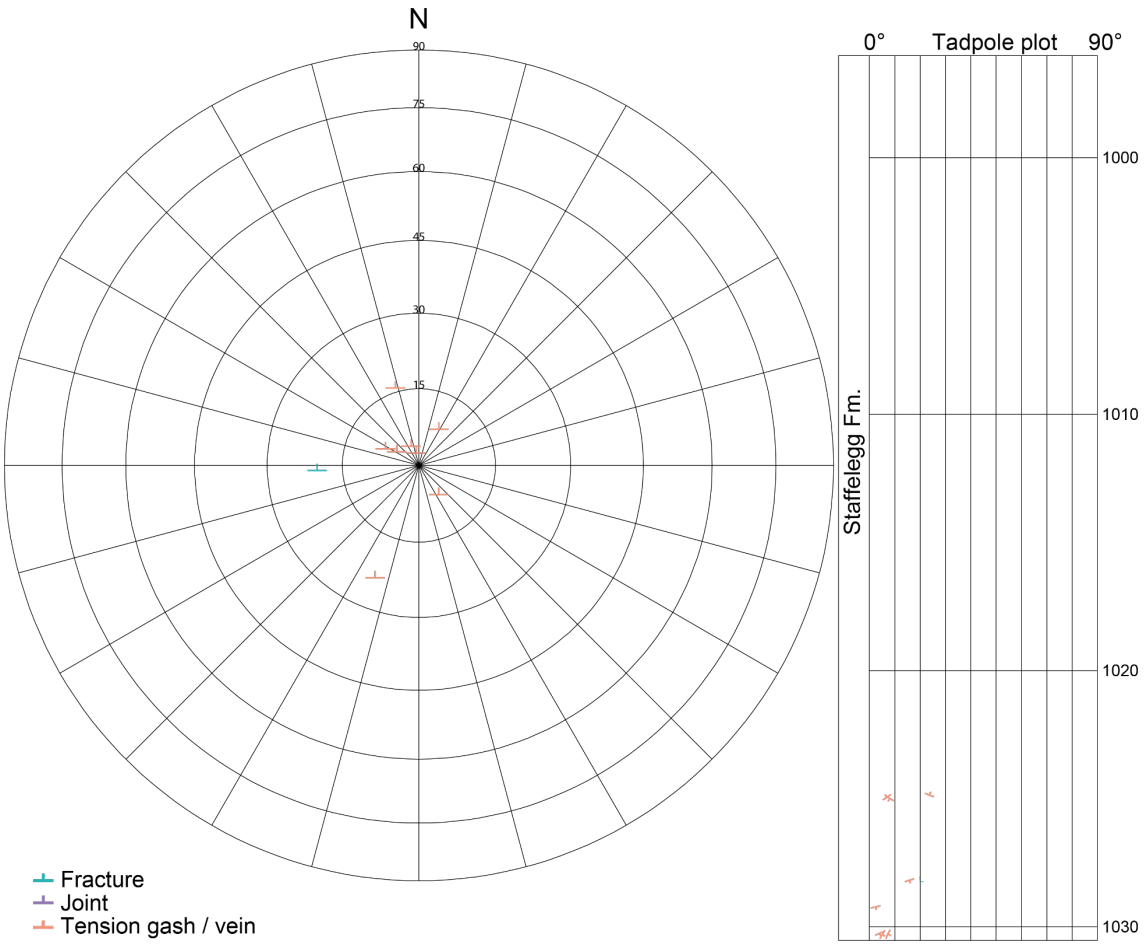

Fig. 4-53: Stereogram and depth plot of fractures, tension gashes / veins and joints (Lias)
Fractures (n = 1), joints (n = 0) and tension gashes / veins (n = 8).

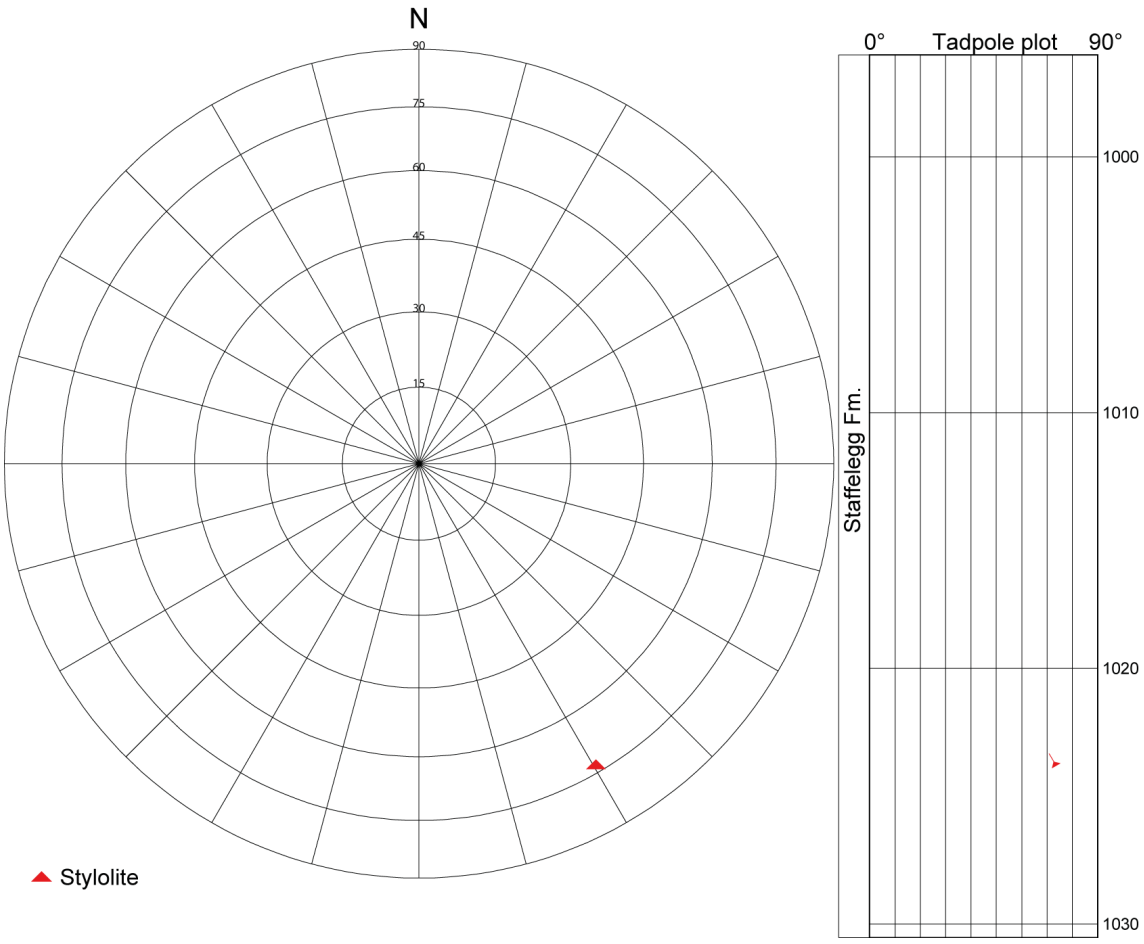

Fig. 4-54: Stereogram and depth plot of stylolites (Lias, n = 1)

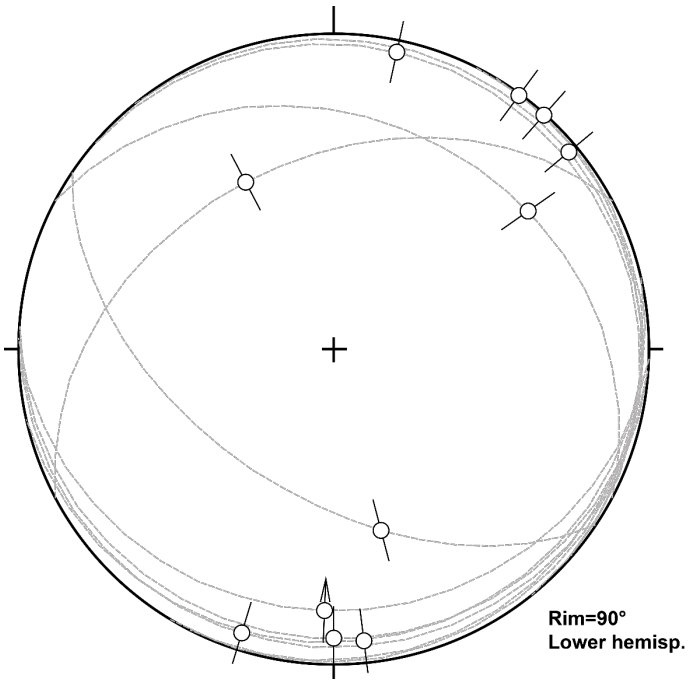

Fig. 4-55: Stereogram of fault planes (Lias, n = 11)

4.5 Keuper

The Keuper (1'030.53 – 1'132.00 m MD log depth) is a structurally rich zone and revealed the highest average fracture density of 4.0 fractures per metre. Mirror-like fault planes and tension gashes / veins prevailed. They were mainly concentrated within the Bänkerjoch Formation. Only the data for oriented cores are presented.

4.5.1 Klettgau Formation

The orientation and spatial distribution of structural discontinuities within the Klettgau Formation (1'030.53 – 1'067.36 m MD log depth) are visualised in Figs. 4-56 to 4-61. Due to the low number of stylolites (n = 6), rose diagram statistics were not calculated.

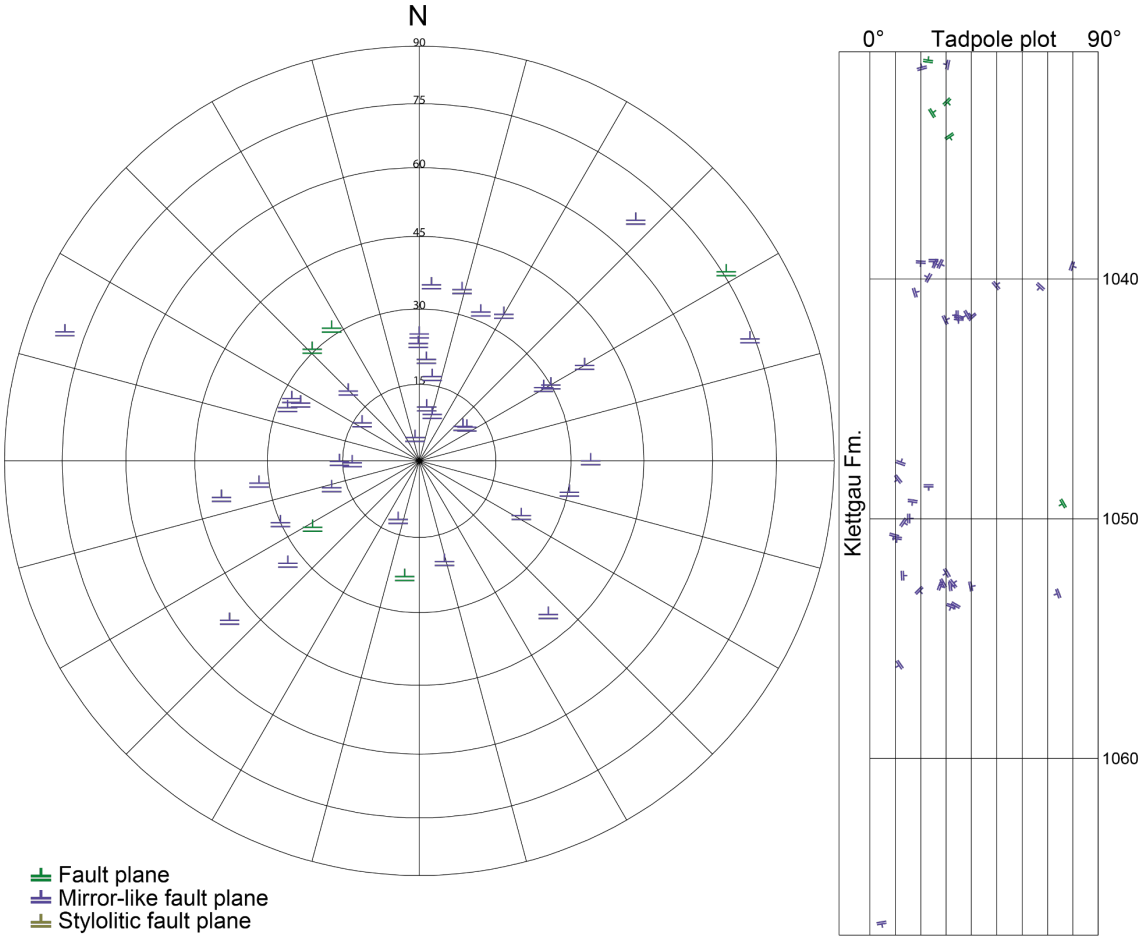

Fig. 4-56: Stereogram and depth plot of faults (Klettgau Formation)

Fault planes (n = 5), mirror-like fault planes (n = 38) and stylolitic fault planes (n = 0).

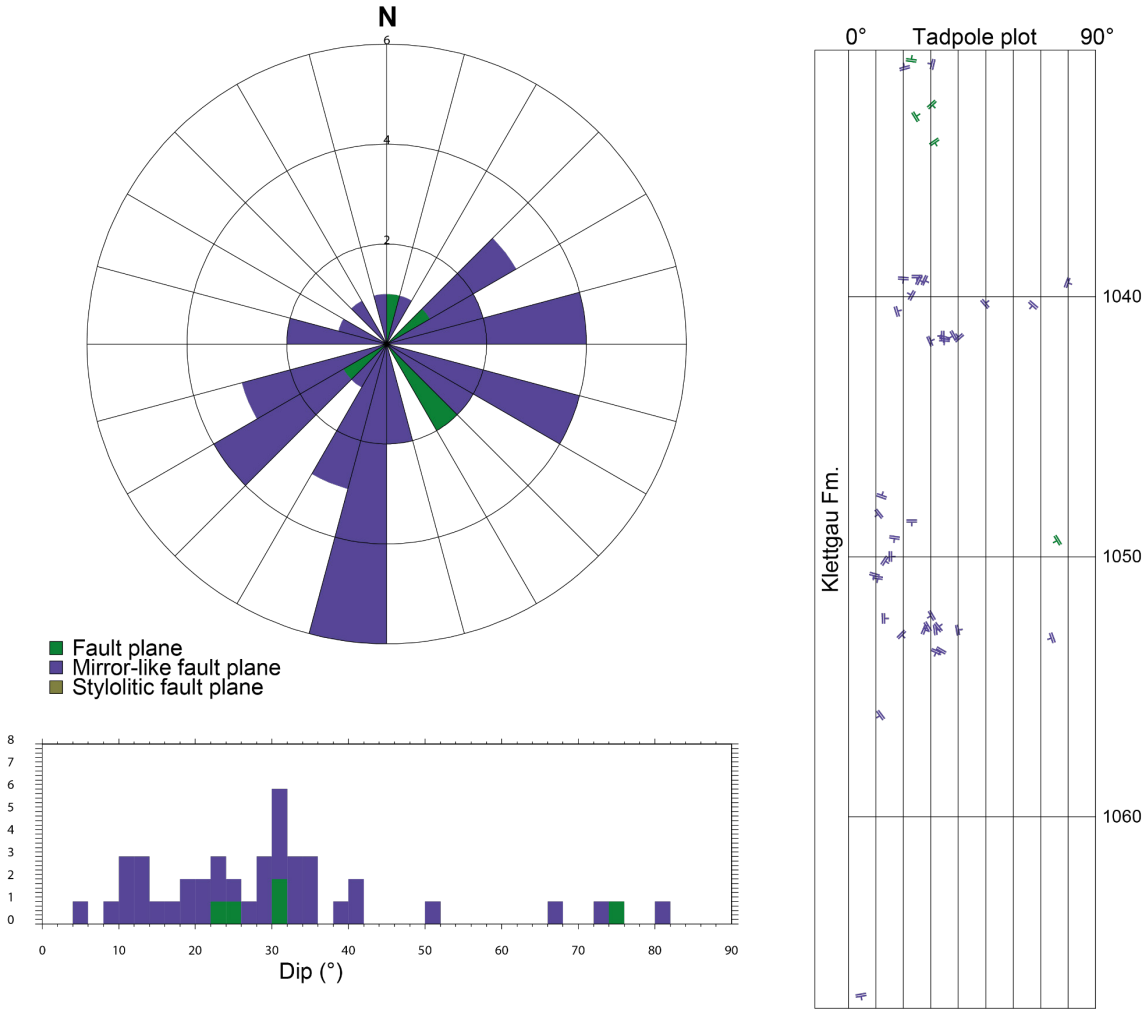

Fig. 4-57: Azimuth rose diagram, dip histogram and depth plot of faults (Klettgau Formation)
Fault planes (n = 5), mirror-like fault planes (n = 38) and stylolitic fault planes (n = 0).

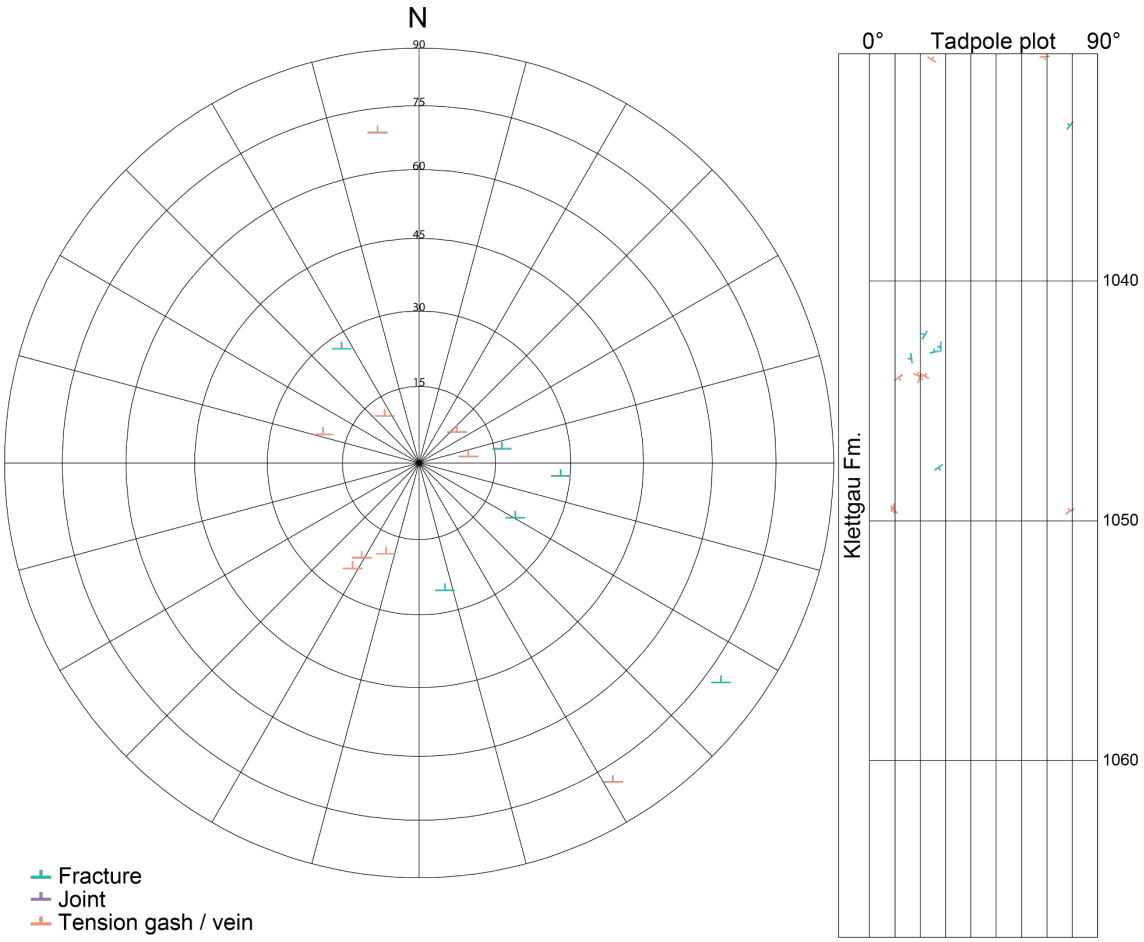

Fig. 4-58: Stereogram and depth plot of fractures, tension gashes / veins and joints (Klettgau Formation)

Fractures (n = 6), joints (n = 0) and tension gashes / veins (n = 9).

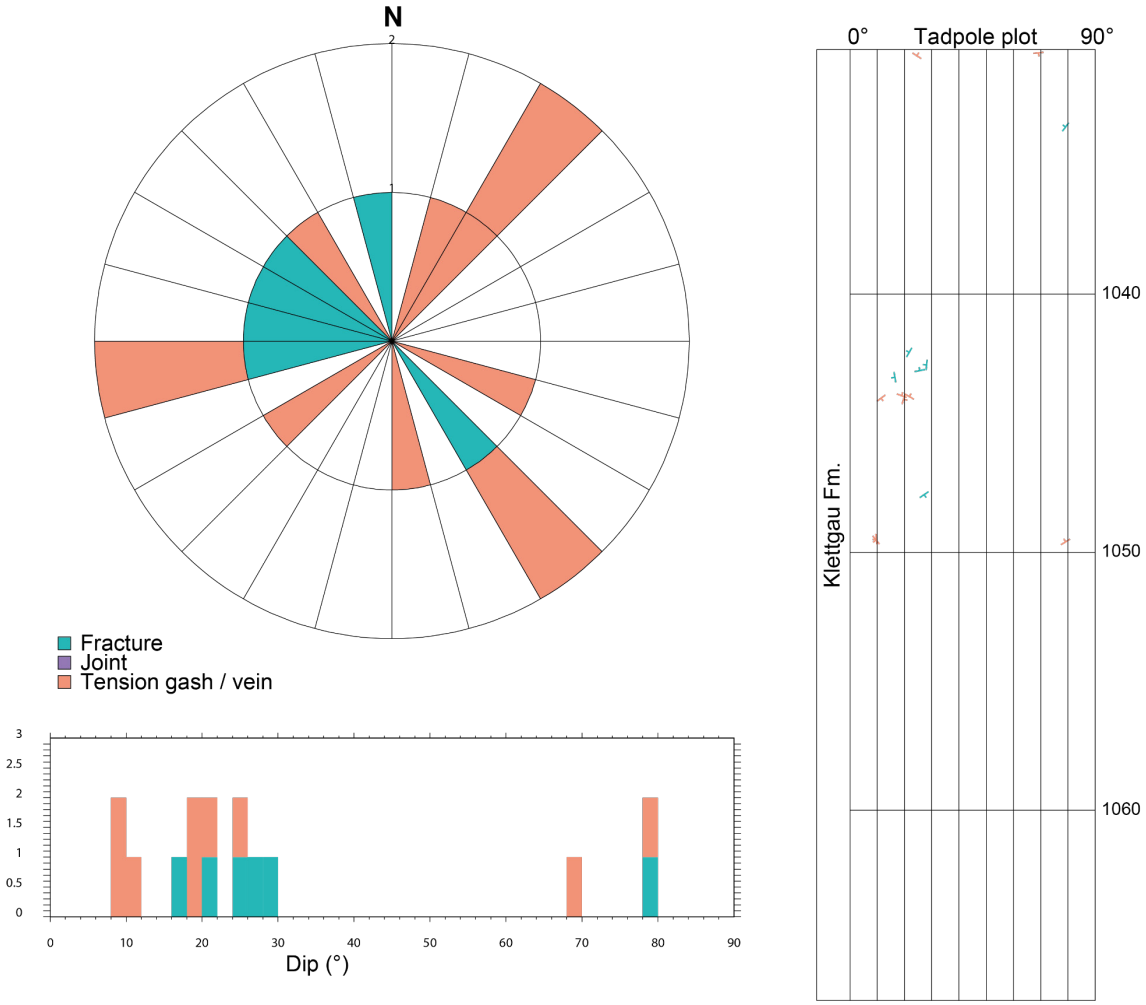

Fig. 4-59: Azimuth rose diagram, dip histogram and depth plot of fractures, tension gashes / veins and joints (Klettgau Formation)

Fractures (n = 6), joints (n = 0) and tension gashes / veins (n = 9).

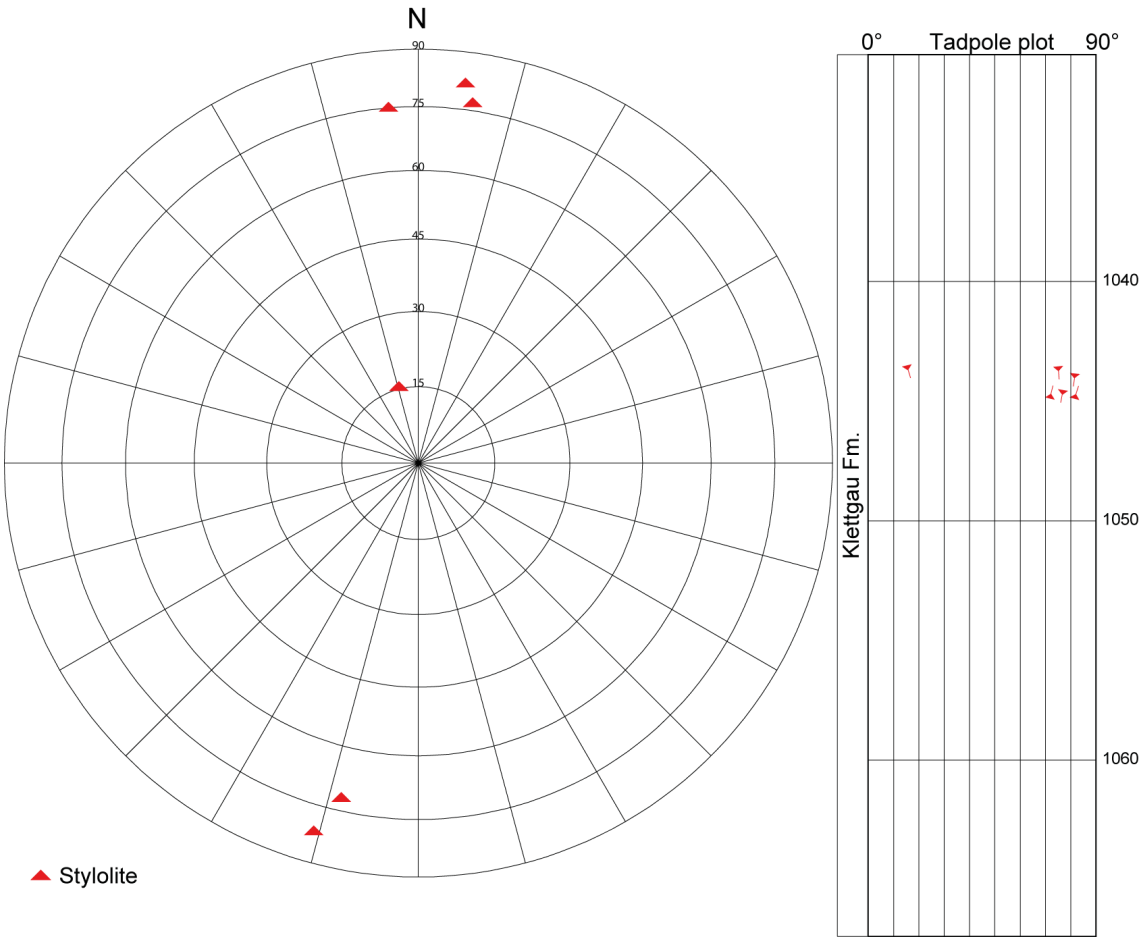

Fig. 4-60: Stereogram and depth plot of stylolites (Klettgau Formation, n = 6)

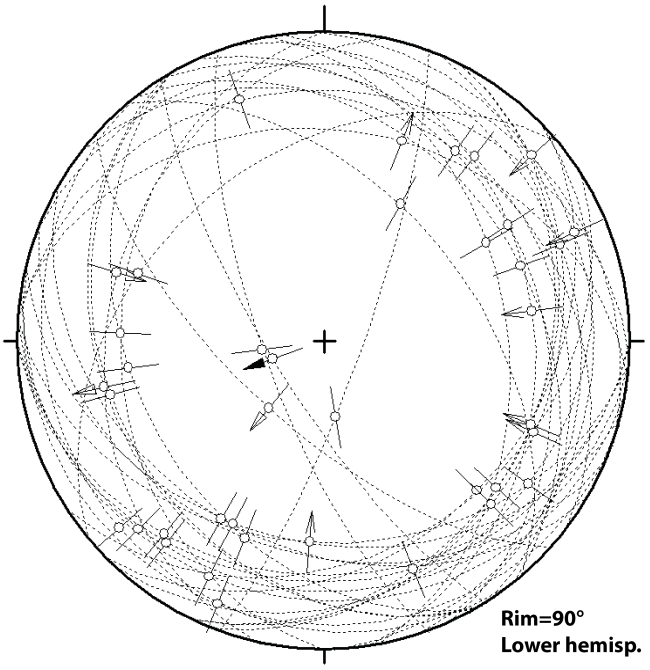

Fig. 4-61: Stereogram of lineations (Klettgau Formation, n = 40)

4.5.2 Bänkerjoch Formation

The orientation and spatial distribution of the structural inventory of the Bänkerjoch Formation (1'067.36 – 1'132.00m MD log depth) are shown in Figs. 4-62 to 4-66. Stylolites were absent in this borehole interval.

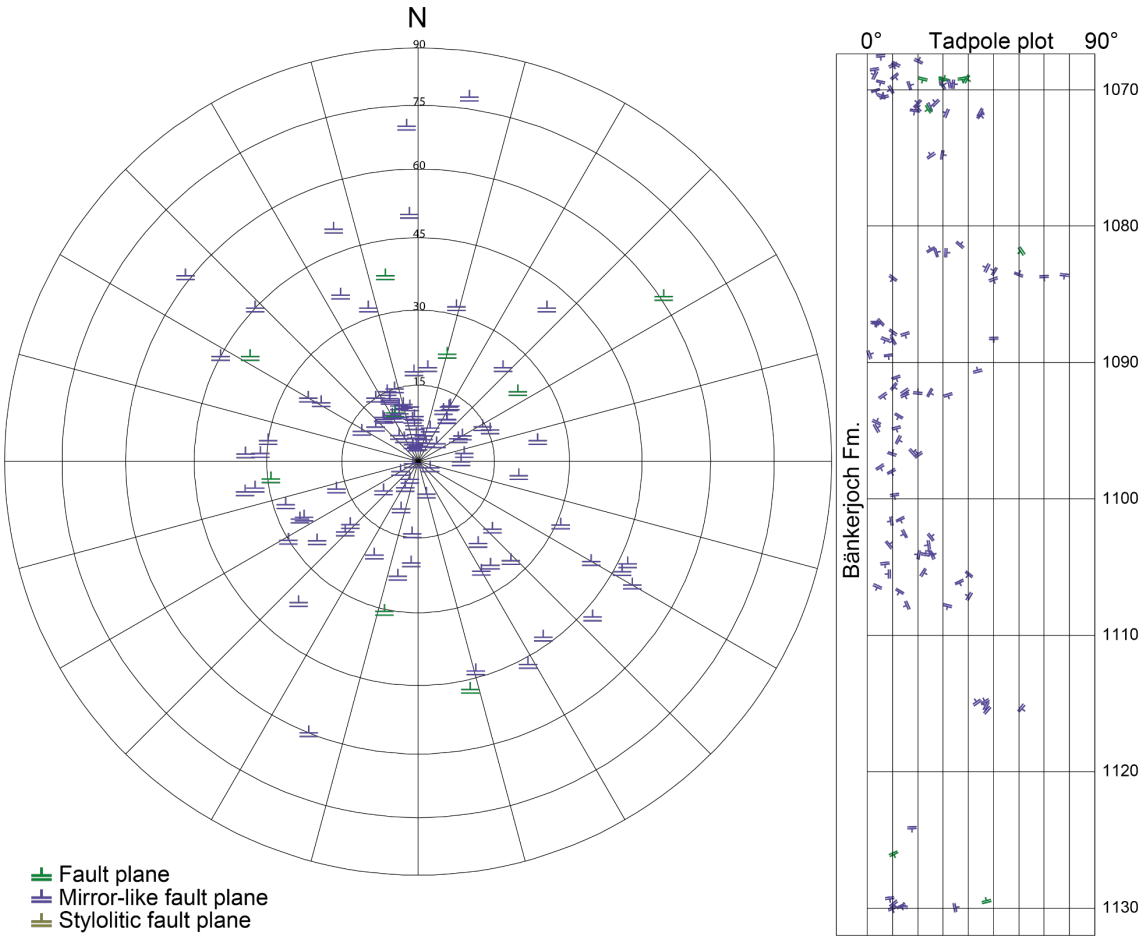

Fig. 4-62: Stereogram and depth plot of faults (Bänkerjoch Formation)

Fault planes (n = 9), mirror-like fault planes (n = 99) and stylolitic fault planes (n = 0).

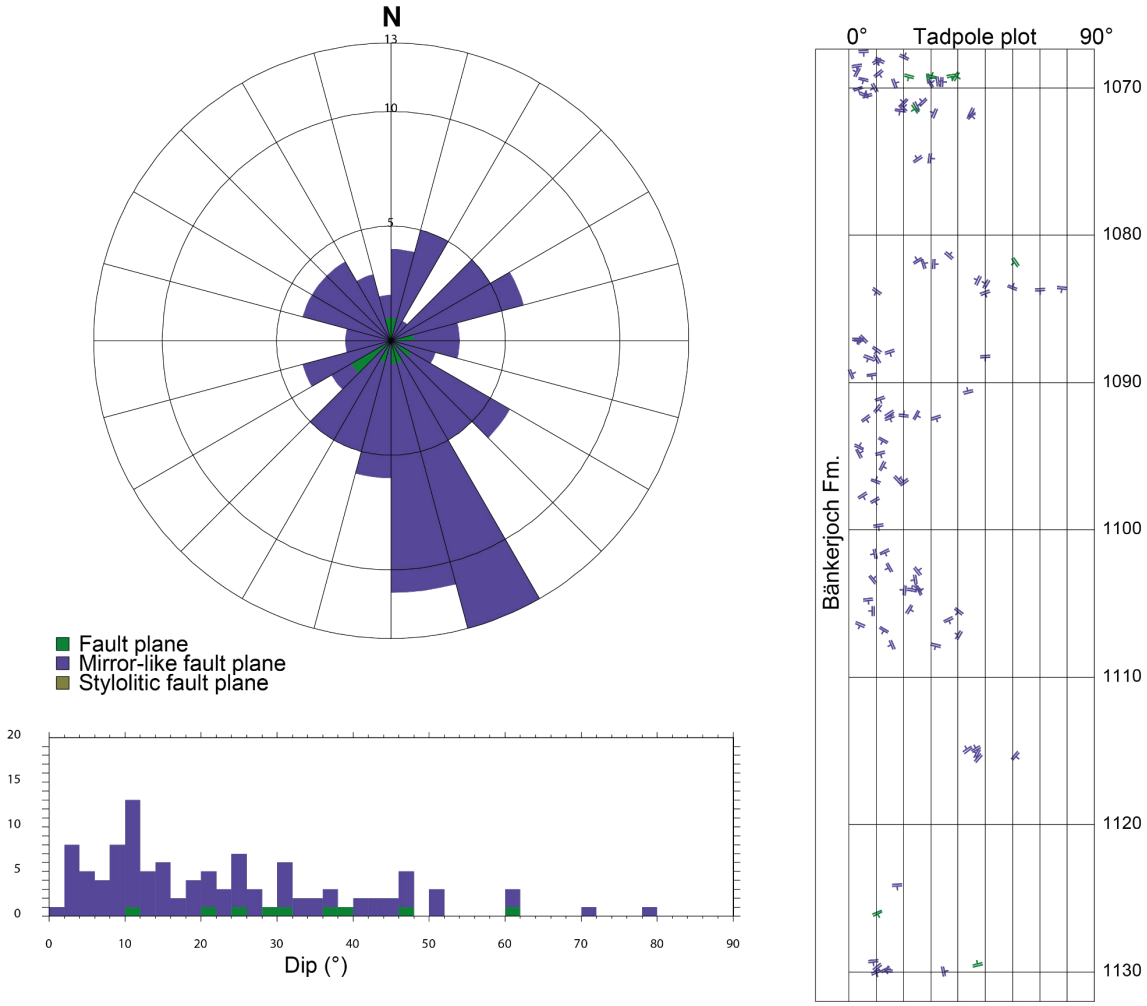

Fig. 4-63: Azimuth rose diagram, dip histogram and depth plot of faults (Bänkerjoch Formation)

Fault planes (n = 9), mirror-like fault planes (n = 99) and stylolitic fault planes (n = 0).

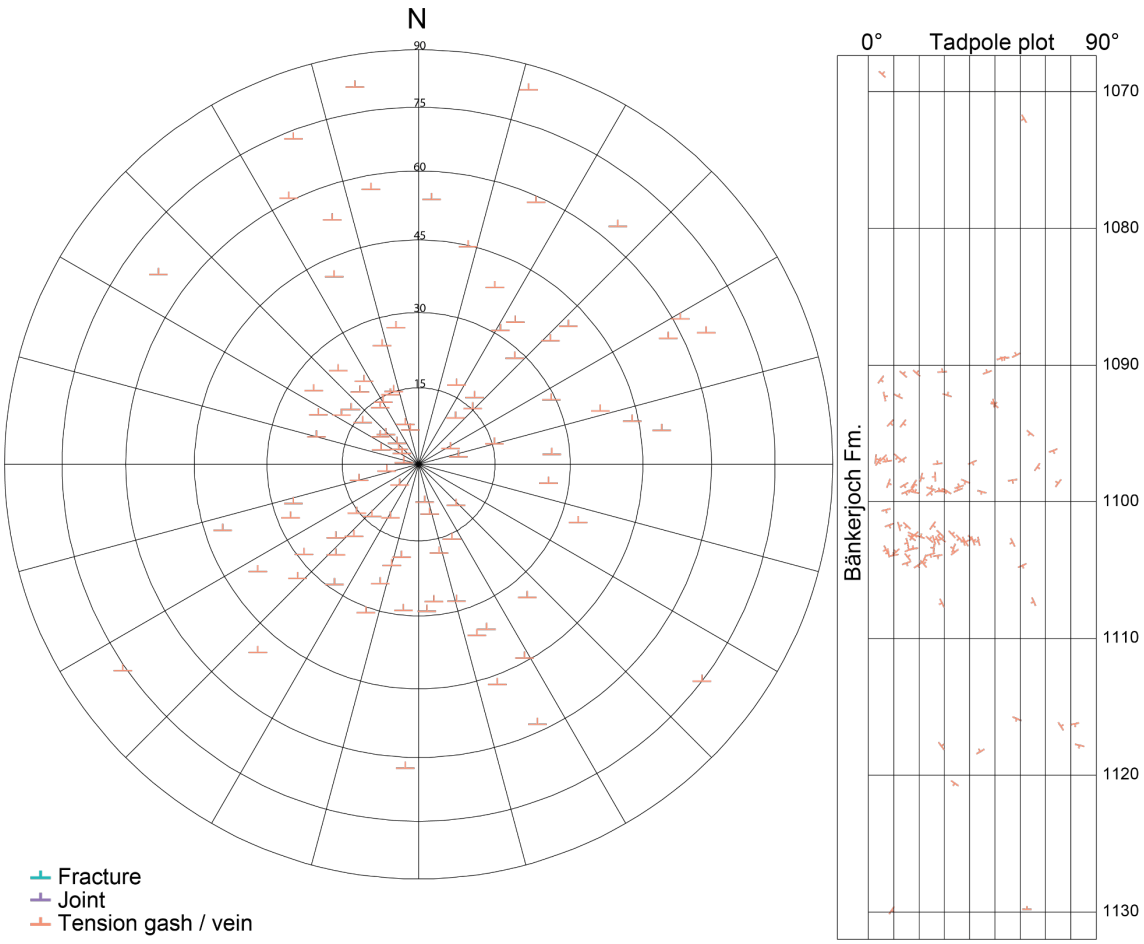

Fig. 4-64: Stereogram and depth plot of fractures, tension gashes / veins and joints (Bänkerjoch Formation)

Fractures (n = 0), joints (n = 0) and tension gashes / veins (n = 98).

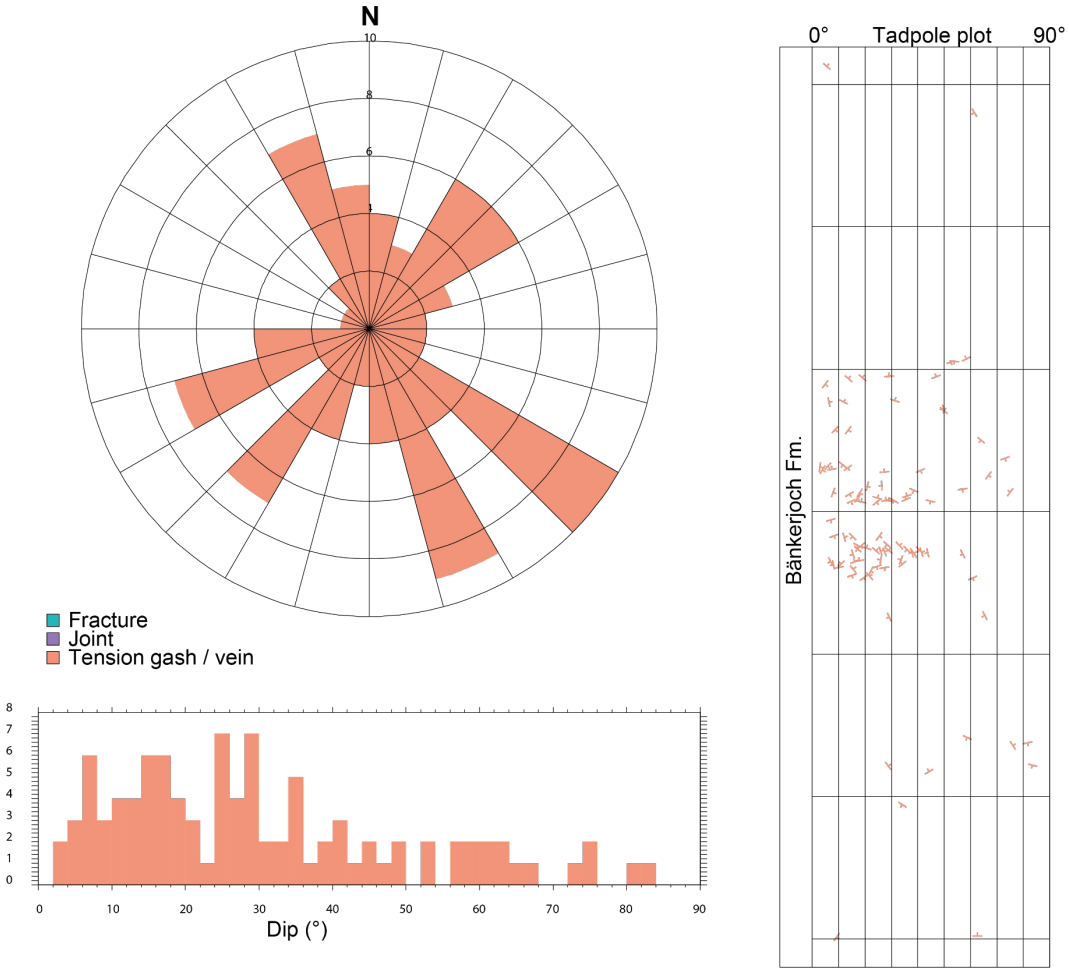

Fig. 4-65: Azimuth rose diagram, dip histogram and depth plot of fractures, tension gashes / veins and joints (Bänkerjoch Formation)

Fractures (n = 0), joints (n = 0) and tension gashes / veins (n = 98).

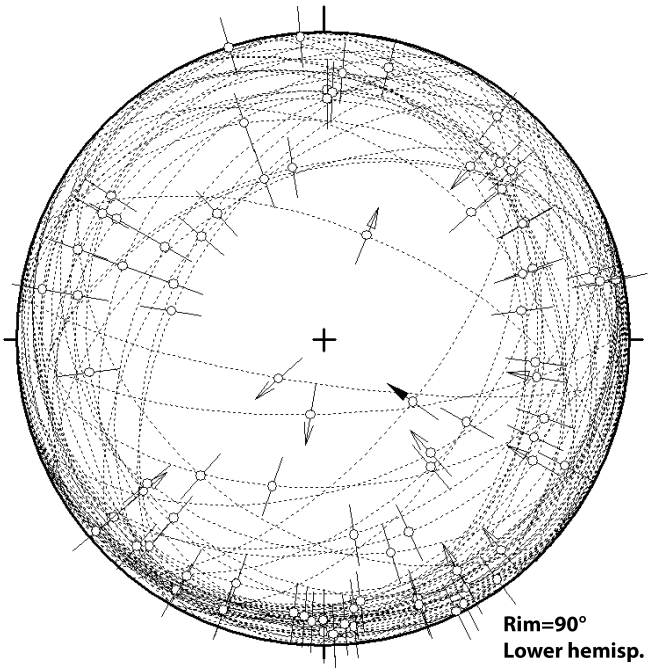

Fig. 4-66: Stereogram of fault planes (Bänkerjoch Formation, n = 85)

4.6 Muschelkalk

The dominant structures within the Muschelkalk (1'132.00 – 1'306.11 m MD log depth) were stylolites followed by mirror-like fault planes. In addition, abundant mm- to cm-sized open pores (vugs) were observed especially within the Schinznach Formation from 1'137 to 1'180 m MD log depth. Indications of small-scale folding, dynamic salt recrystallisation as well as numerous mirror-like fault planes with dip-slip shear senses were found within the «Obere Sulfatzone», «Salzlager» and «Untere Sulfatzone» of the Zeglingen Formation.

The Muschelkalk was subdivided into four lithostratigraphic units for the detailed evaluation. Only the data for oriented cores are presented.

4.6.1 Schinznach Formation

The orientation and spatial distribution of structural observations within the Schinznach Formation (1'132.00 – 1'204.58 m MD log depth) are shown in Figs. 4-67 to 4-73.

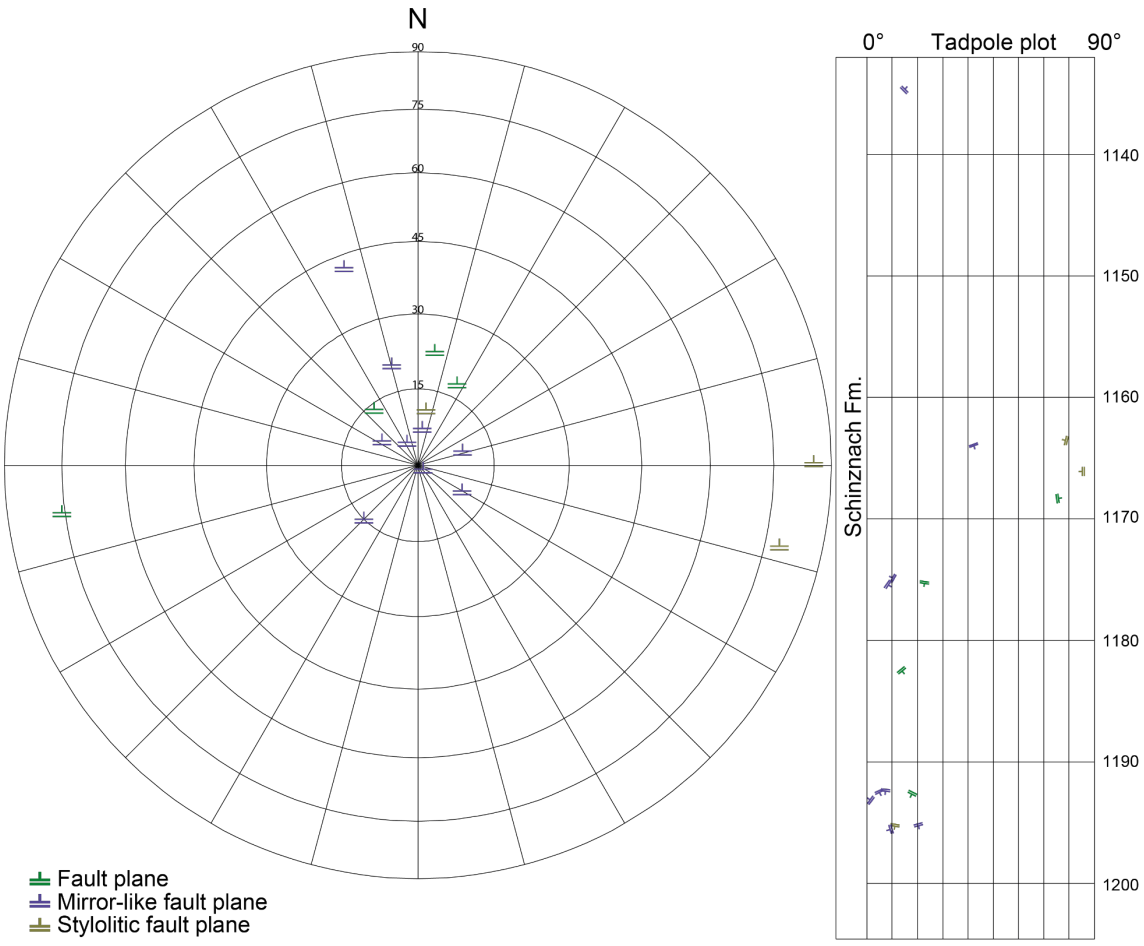

Fig. 4-67: Stereogram and depth plot of fault planes (Schinznach Formation)

Fault planes (n = 4), mirror-like fault planes (n = 9) and stylolitic fault planes (n = 3).

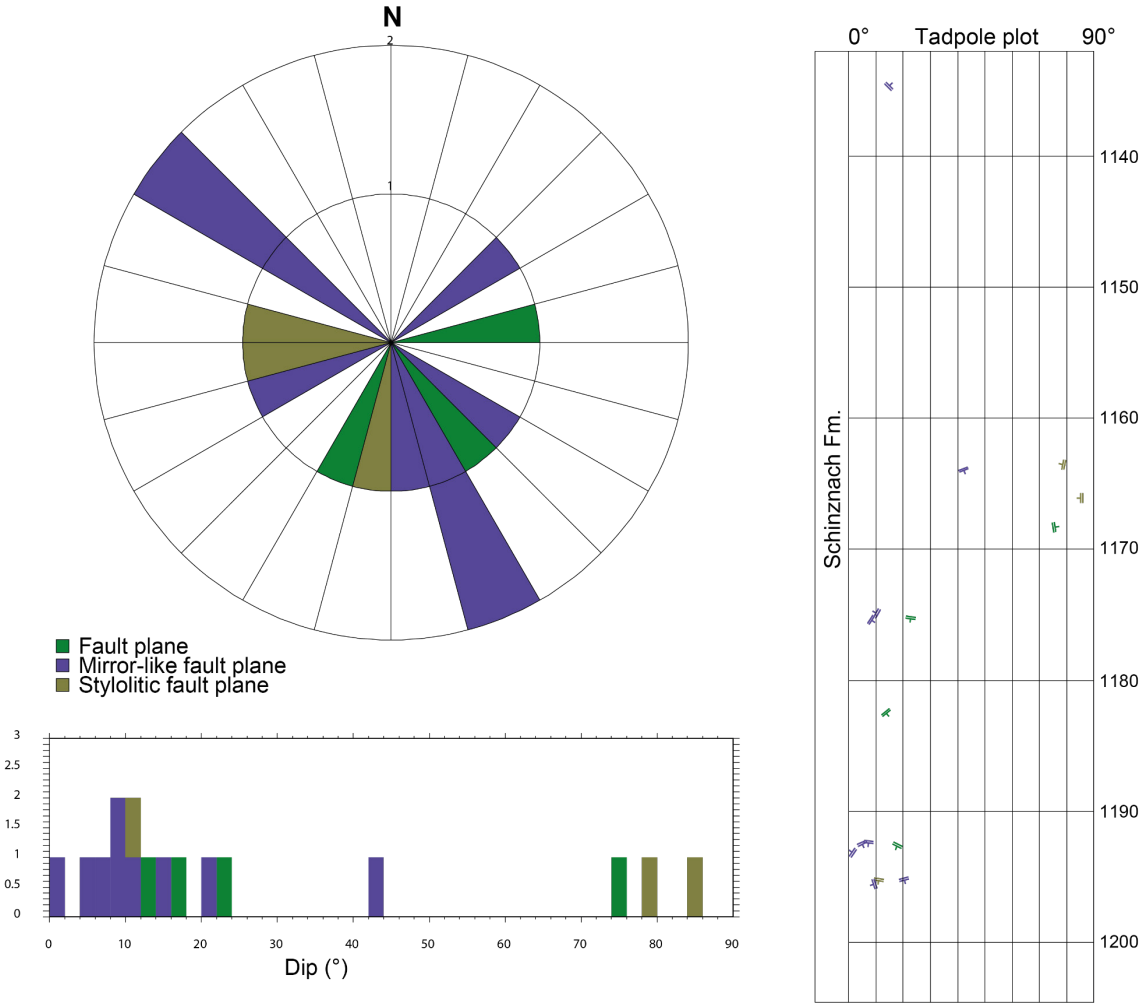

Fig. 4-68: Azimuth rose diagram, dip histogram and depth plot of fault planes (Schinznach Formation)

Fault planes (n = 4), mirror-like fault planes (n = 9) and stylolitic fault planes (n = 3).

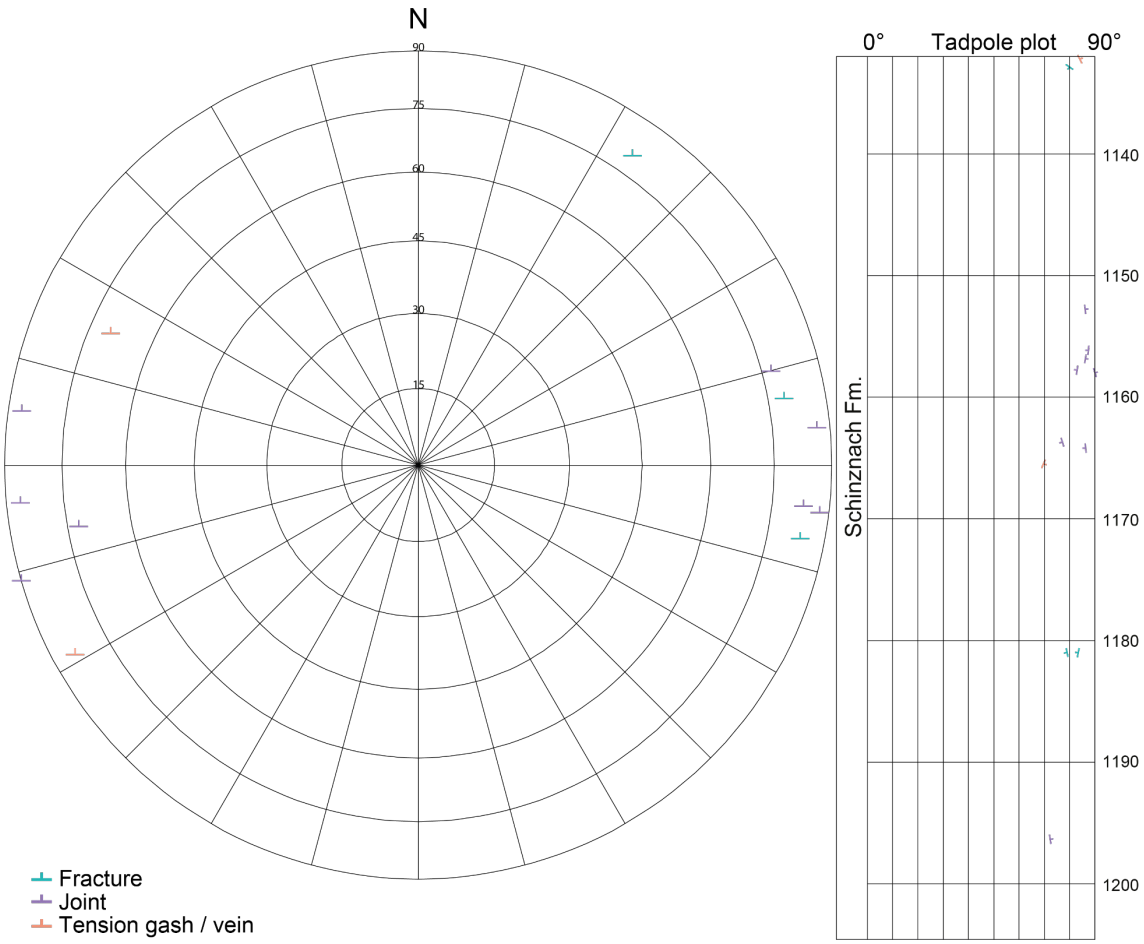

Fig. 4-69: Stereogram and depth plot of fractures, tension gashes / veins and joints (Schinznach Formation)

Fractures (n = 3), joints (n = 8) and tension gashes / veins (n = 2).

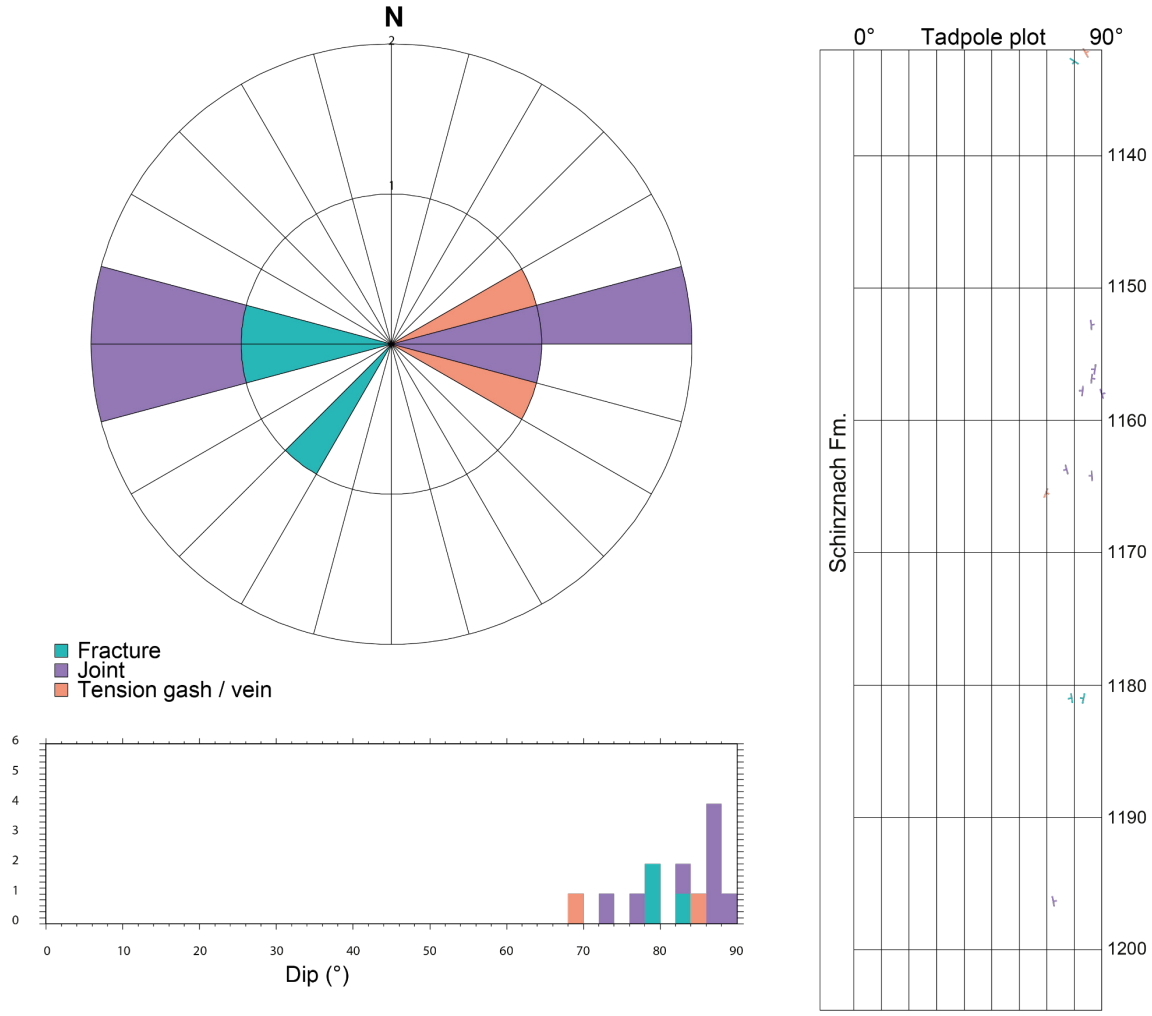

Fig. 4-70: Azimuth rose diagram, dip histogram and depth plot of fractures, tension gashes / veins and joints (Schinznach Formation)

Fractures (n = 3), joints (n = 8) and tension gashes / veins (n = 2).

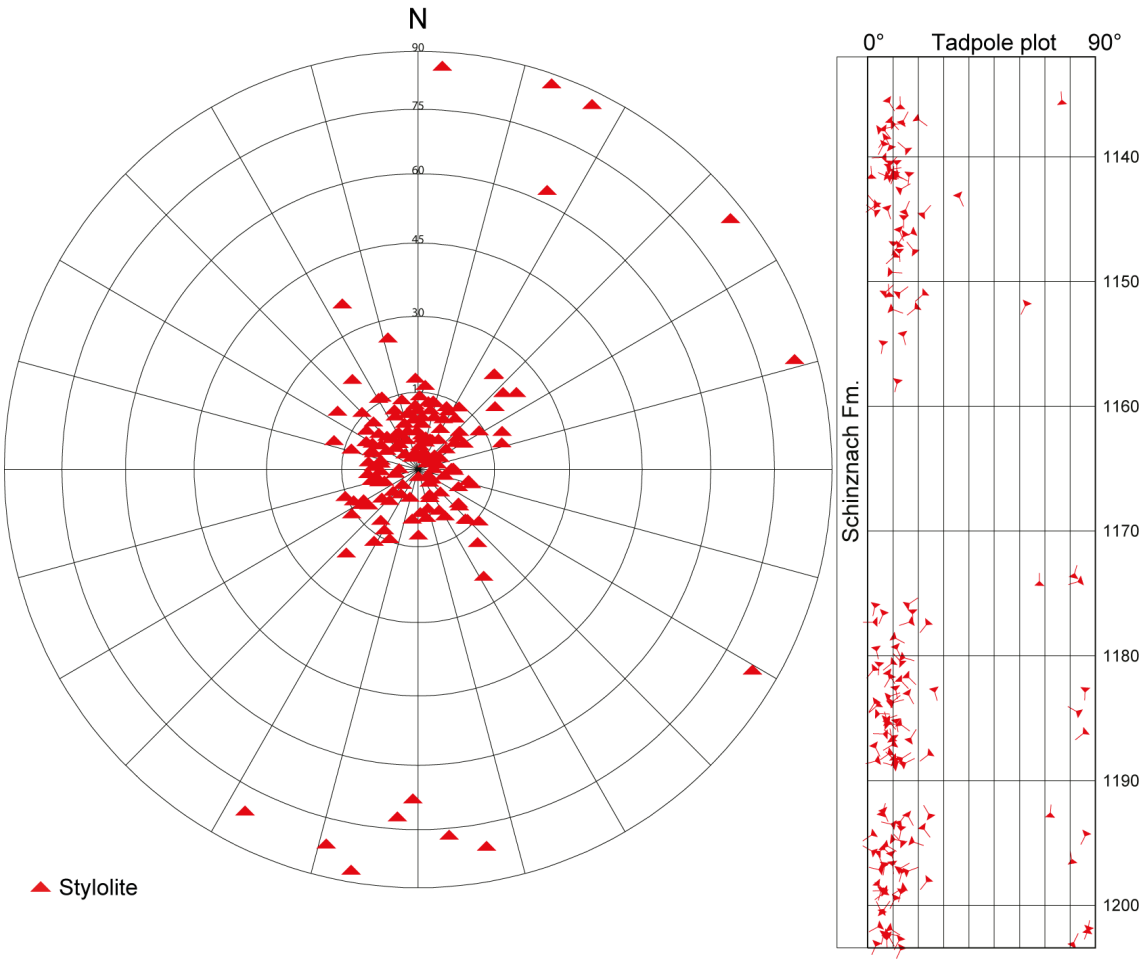

Fig. 4-71: Stereogram and depth plot of stylolites (Schinznach Formation, n = 164)

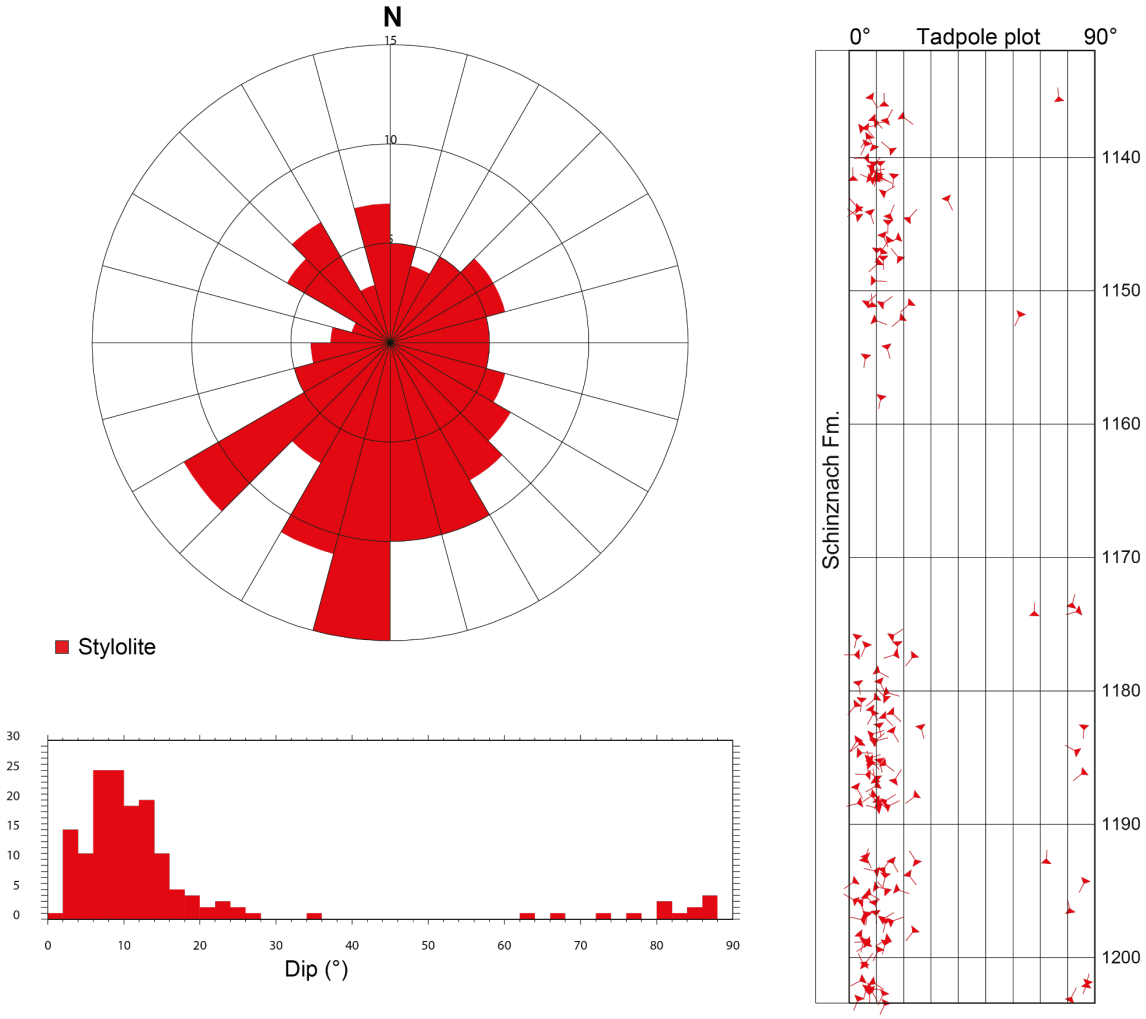

Fig. 4-72: Azimuth rose diagram, dip histogram and depth plot of stylolites (Schinznach Formation, n = 164)

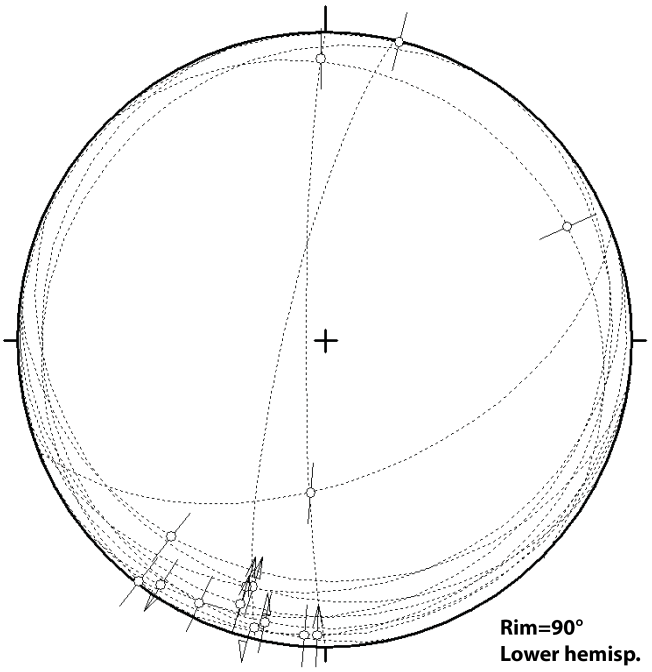

Fig. 4-73: Stereogram of fault planes (Schinznach Formation, n = 15)

4.6.2 Upper and Middle Zeglingen Formation («Dolomitzone» – «Salzlager»)

The orientation and spatial distribution of the structures observed in the «Dolomitzone», «Obere Sulfatzone» and «Salzlager» (1'204.58 – 1'260.37 m MD log depth) are shown in Figs. 4-74 to 4-78. Due to the low number of fractures, joints and tension gashes / veins (n = 6) and Stylolites (n = 5), rose diagram statistics were not calculated for those features.

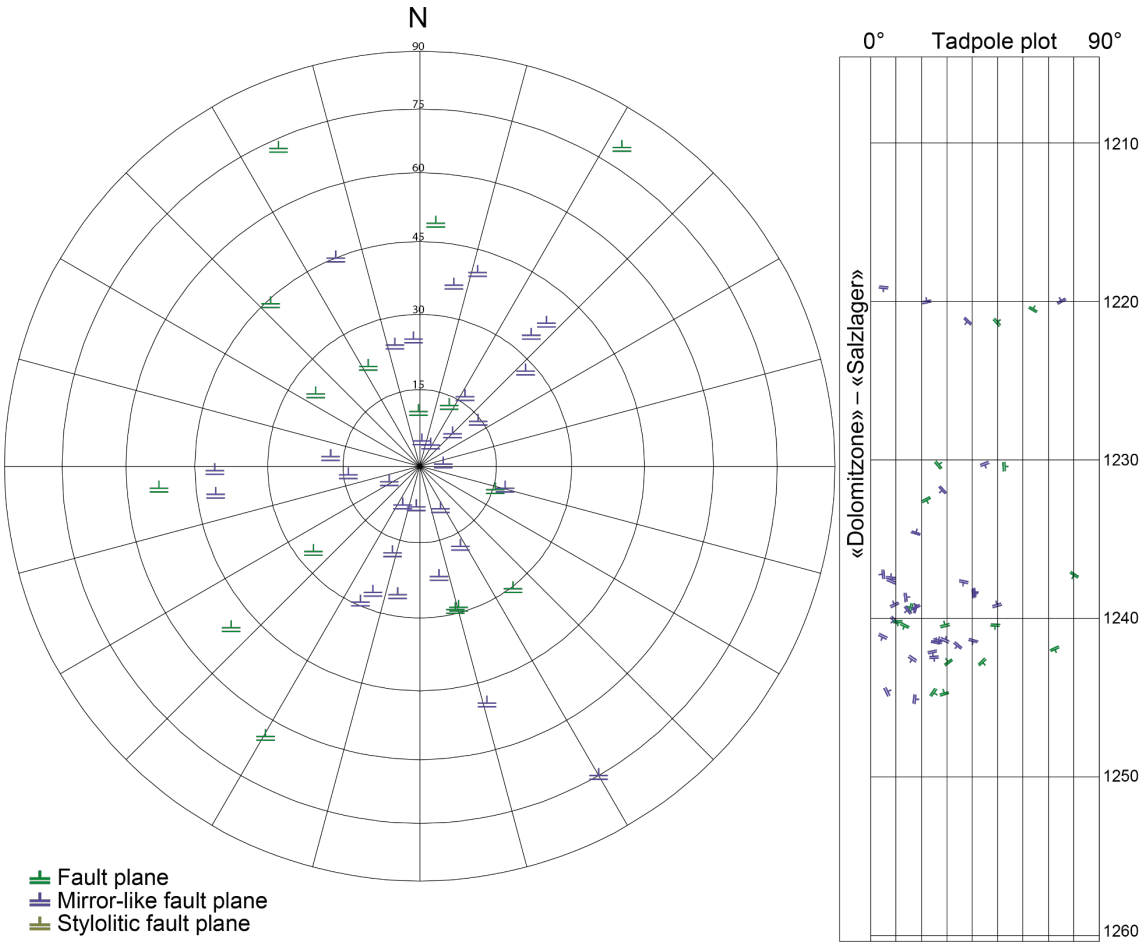

Fig. 4-74: Stereogram and depth plot of fault planes («Dolomitzone» – «Salzlager»)

Fault planes (n = 16), mirror-like fault planes (n = 31) and stylolitic fault planes (n = 0).

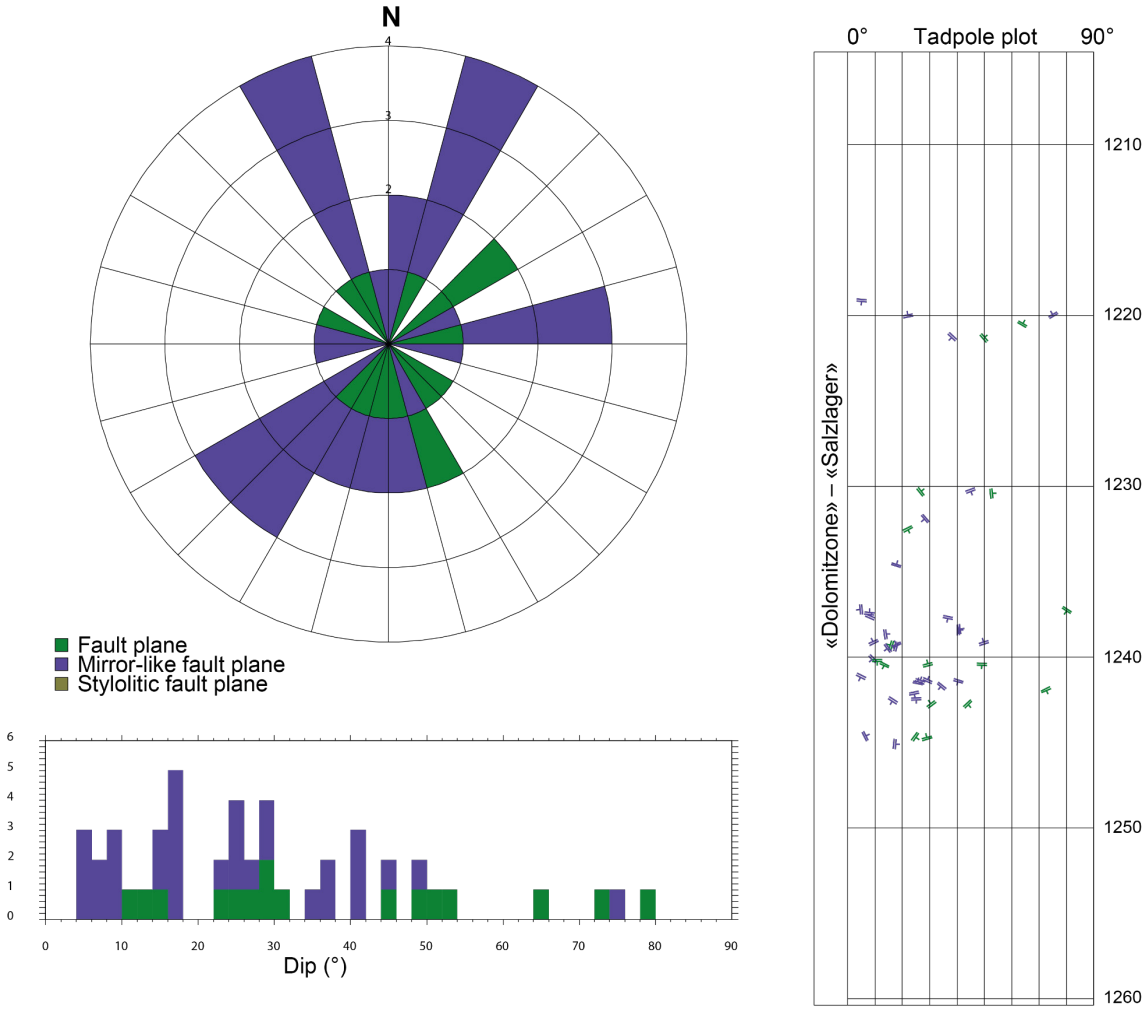

Fig. 4-75: Azimuth rose diagram, dip histogram and depth plot of fault planes («Dolomitzone» – «Salzlager»)

Fault planes (n = 16), mirror-like fault planes (n = 31) and stylolitic fault planes (n = 0).

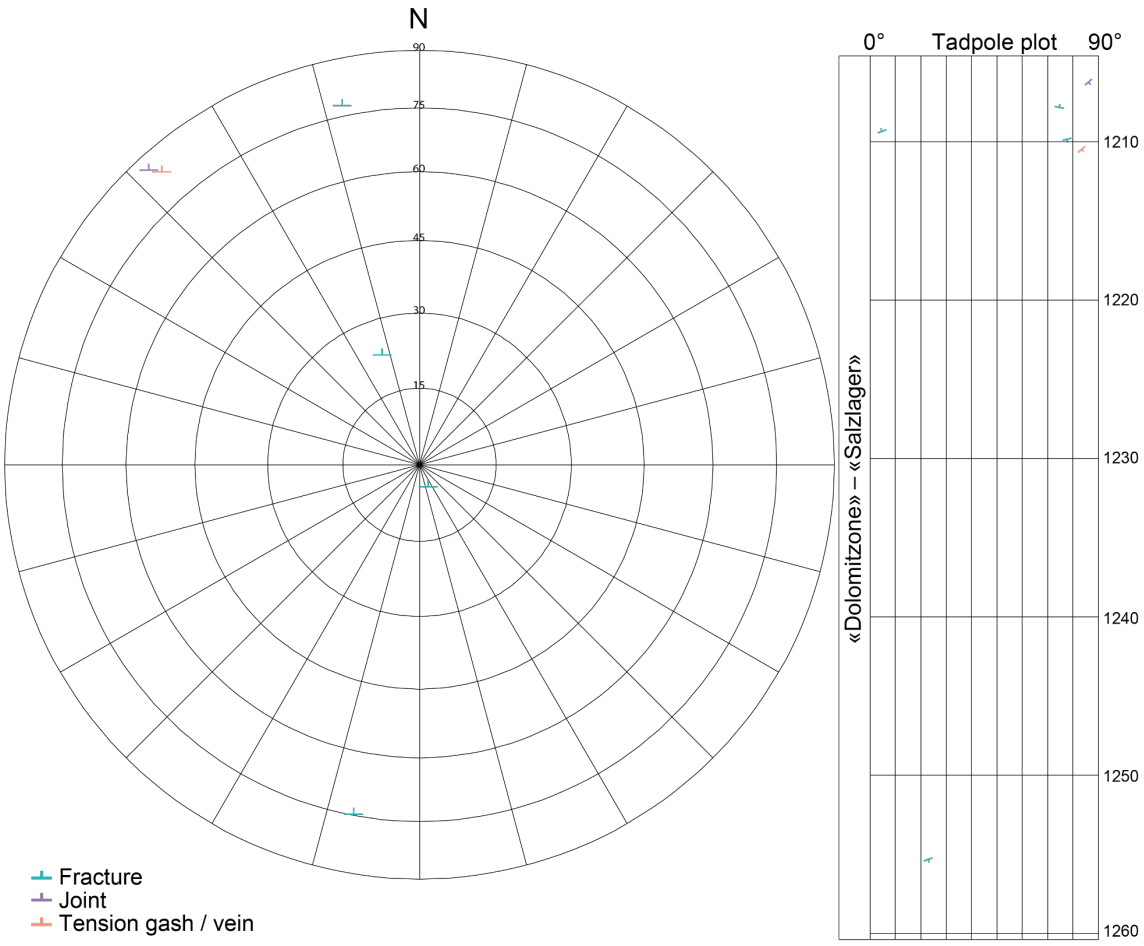

Fig. 4-76: Stereogram and depth plot of fractures, tension gashes / veins and joints («Dolomitzone» – «Salzlager»)

Fractures (n = 4), joints (n = 1) and tension gashes / veins (n = 1).

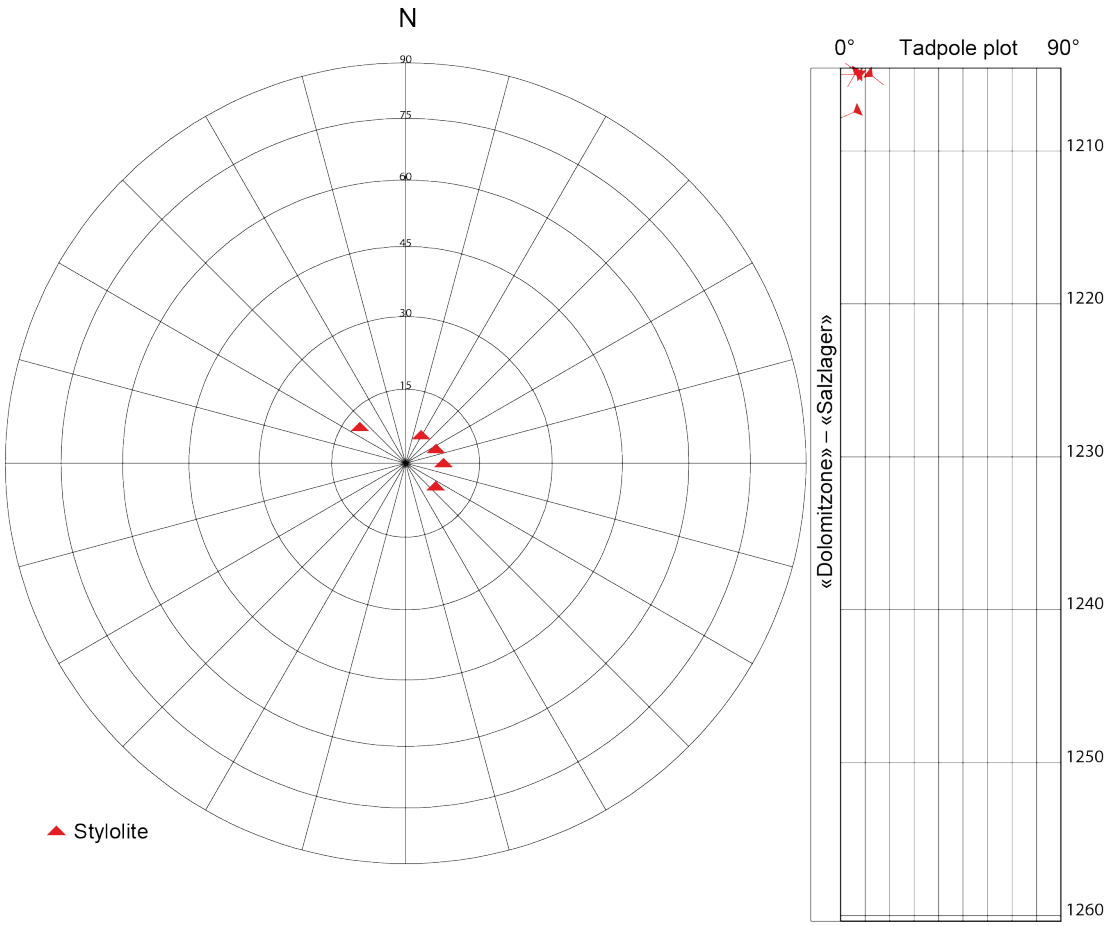

Fig. 4-77: Stereogram and depth plot of stylolites («Dolomitzone» – «Salzlager», n = 5)

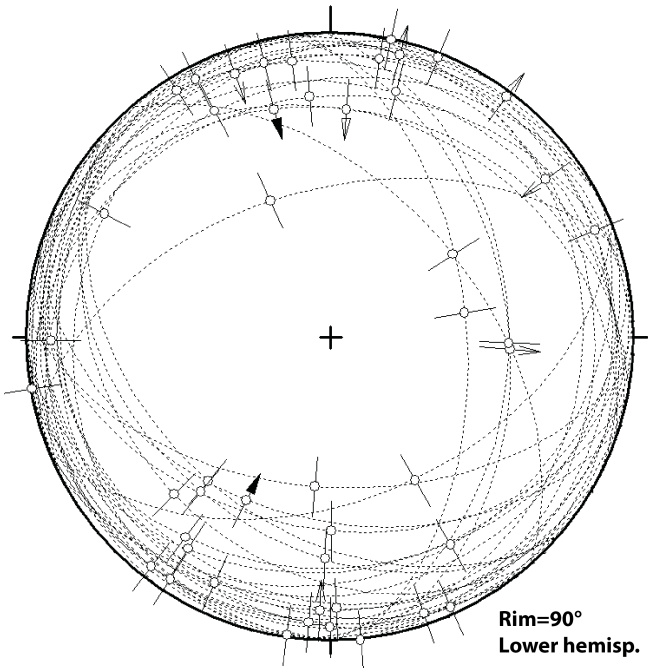

Fig. 4-78: Stereogram of faults («Dolomitzone» – «Salzlager», n = 47)

4.6.3 Lowermost Zeglingen Formation («Untere Sulfatzone»)

The orientation and spatial distribution of structural observations within the «Untere Sulfatzone» (1'260.37 – 1'267.94 m MD log depth) are presented in Figs. 4-79 to 4-81. Stylolites were not observed in this depth interval. Due to the low number of fault planes, mirror-like fault planes and stylolitic fault planes (n = 8) and fractures, joints, tension gashes / veins (n = 4), rose diagram statistics were not calculated.

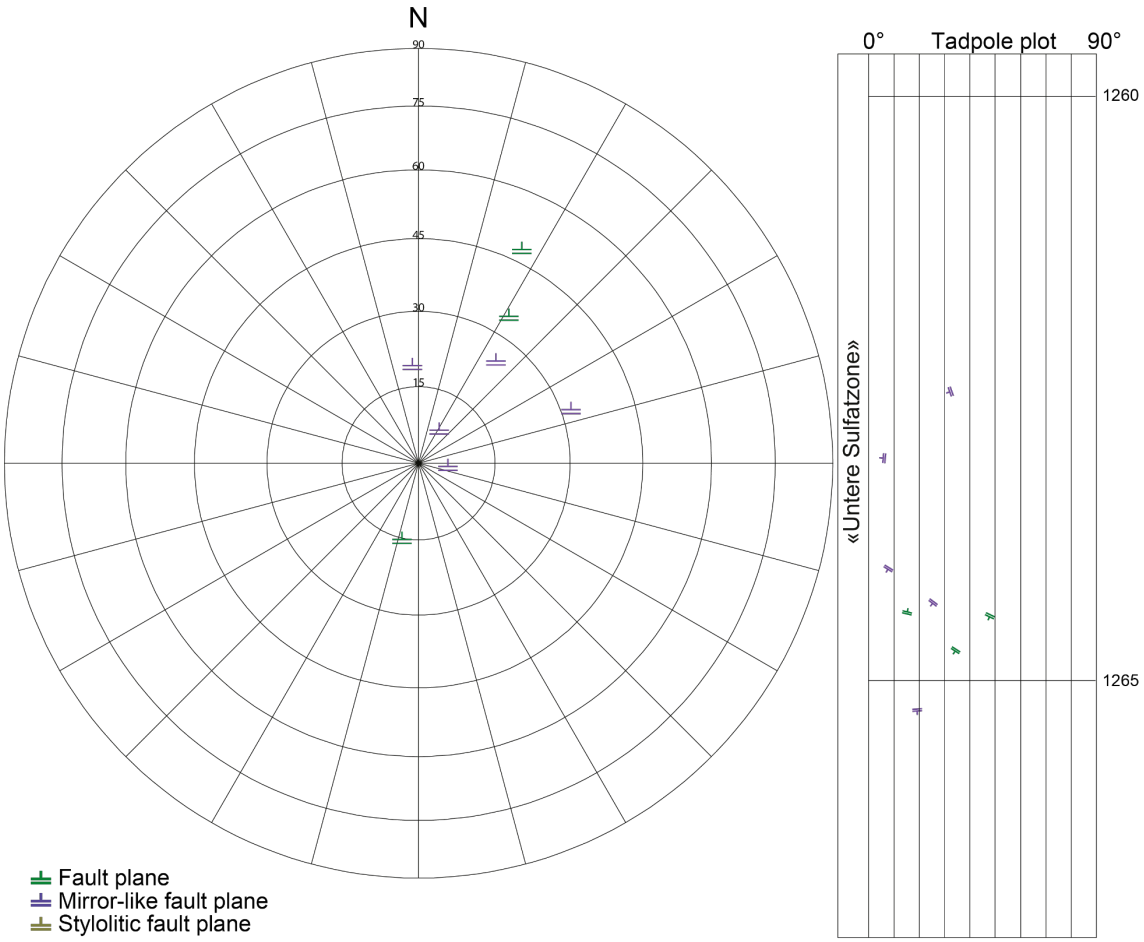

Fig. 4-79: Stereogram and depth plot of fault planes («Untere Sulfatzone»)

Fault planes (n = 3), mirror-like fault planes (n = 5) and stylolitic fault planes (n = 0).

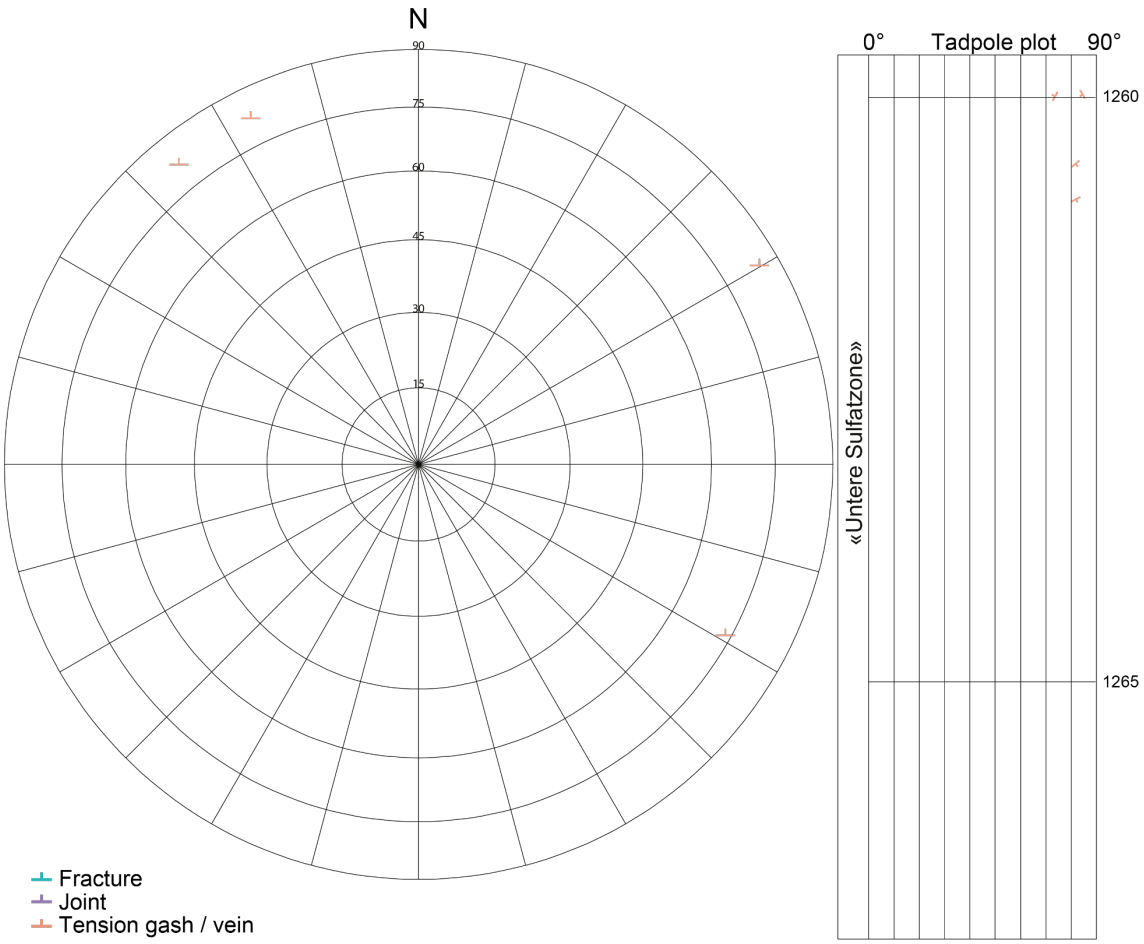

Fig. 4-80: Stereogram and depth plot of fractures, tension gashes / veins and joints («Untere Sulfatzone»)

Fractures (n = 0), joints (n = 0) and tension gashes / veins (n = 4).

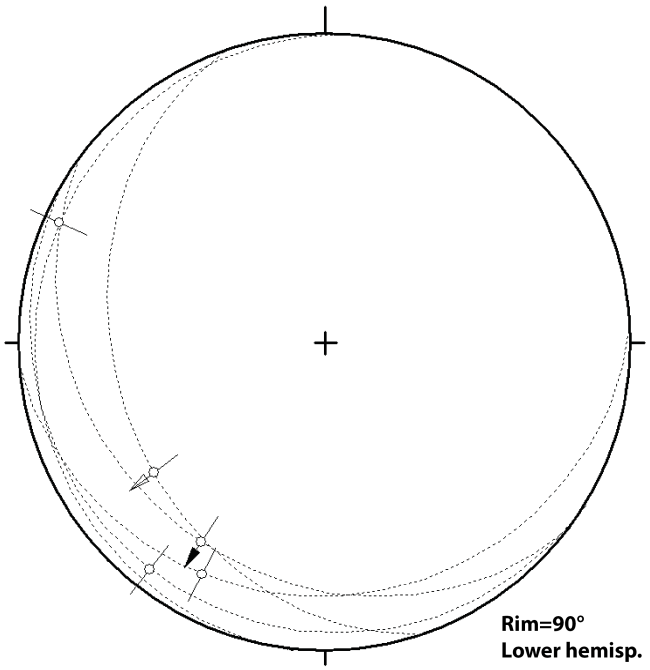

Fig. 4-81: Stereogram of fault planes («Untere Sulfatzone», n = 5)

4.6.4 Kaiseraugst Formation

The orientation and spatial distribution of structural discontinuities within the Kaiseraugst Formation (1'267.94 – 1'306.11 m MD log depth) are shown in Figs. 4-82 to 4-86. Due to the low number of fractures, joints and tension gashes / veins (n = 1) and stylolites (n = 1), rose diagram statistics were not calculated.

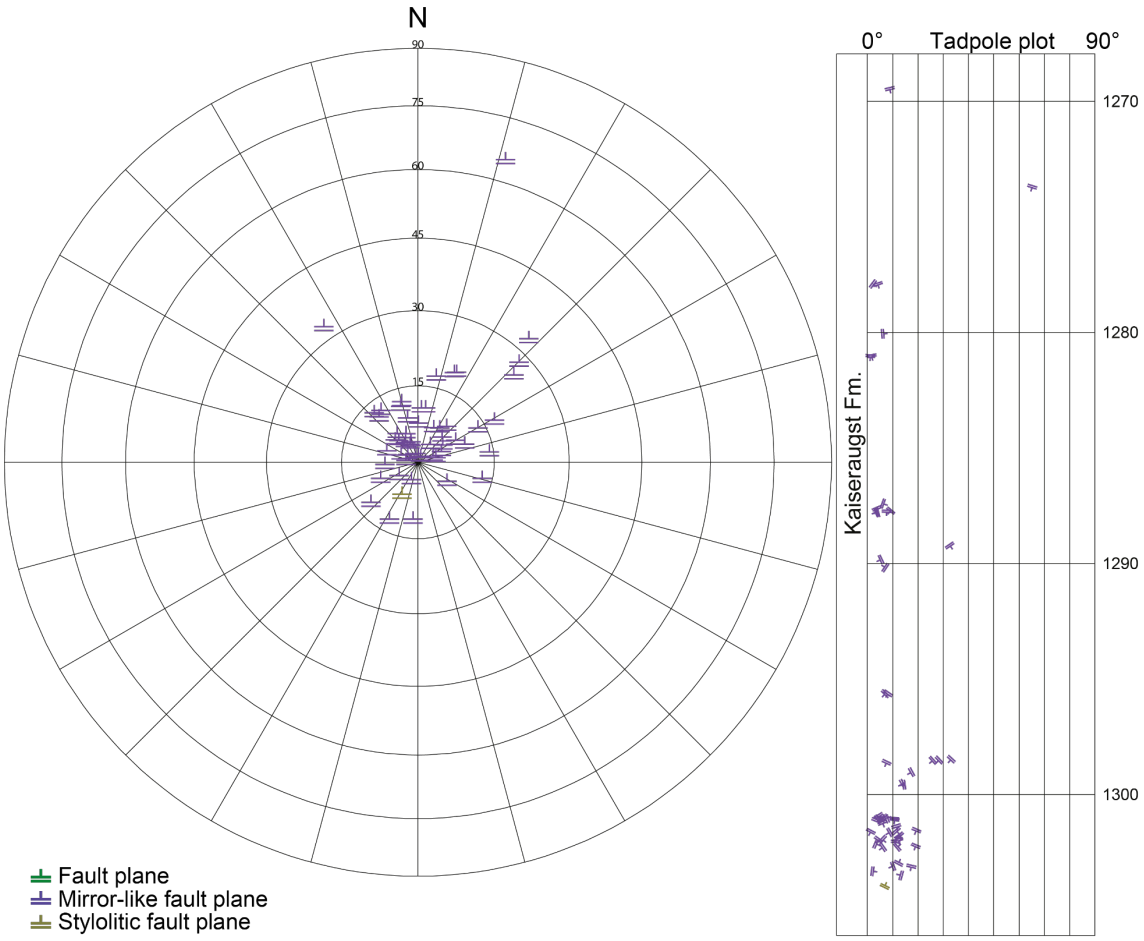

Fig. 4-82: Stereogram and depth plot of fault planes (Kaiseraugst Formation)

Fault planes (n = 0), mirror-like fault planes (n = 54) and stylolitic fault planes (n = 1).

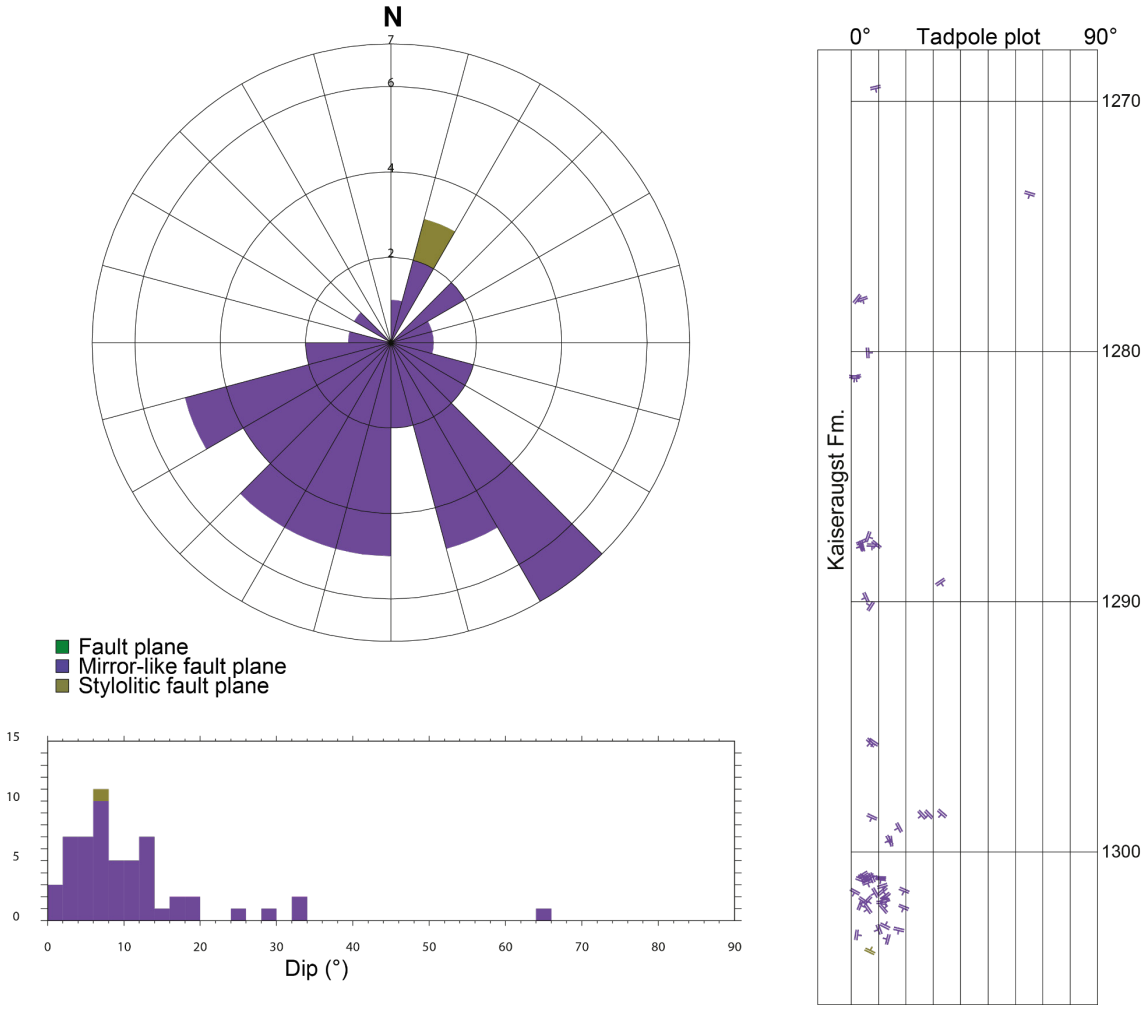

Fig. 4-83: Azimuth rose diagram, dip histogram and depth plot of fault planes (Kaiseraugst Formation)

Fault planes (n = 0), mirror-like fault planes (n = 54) and stylolitic fault planes (n = 1).

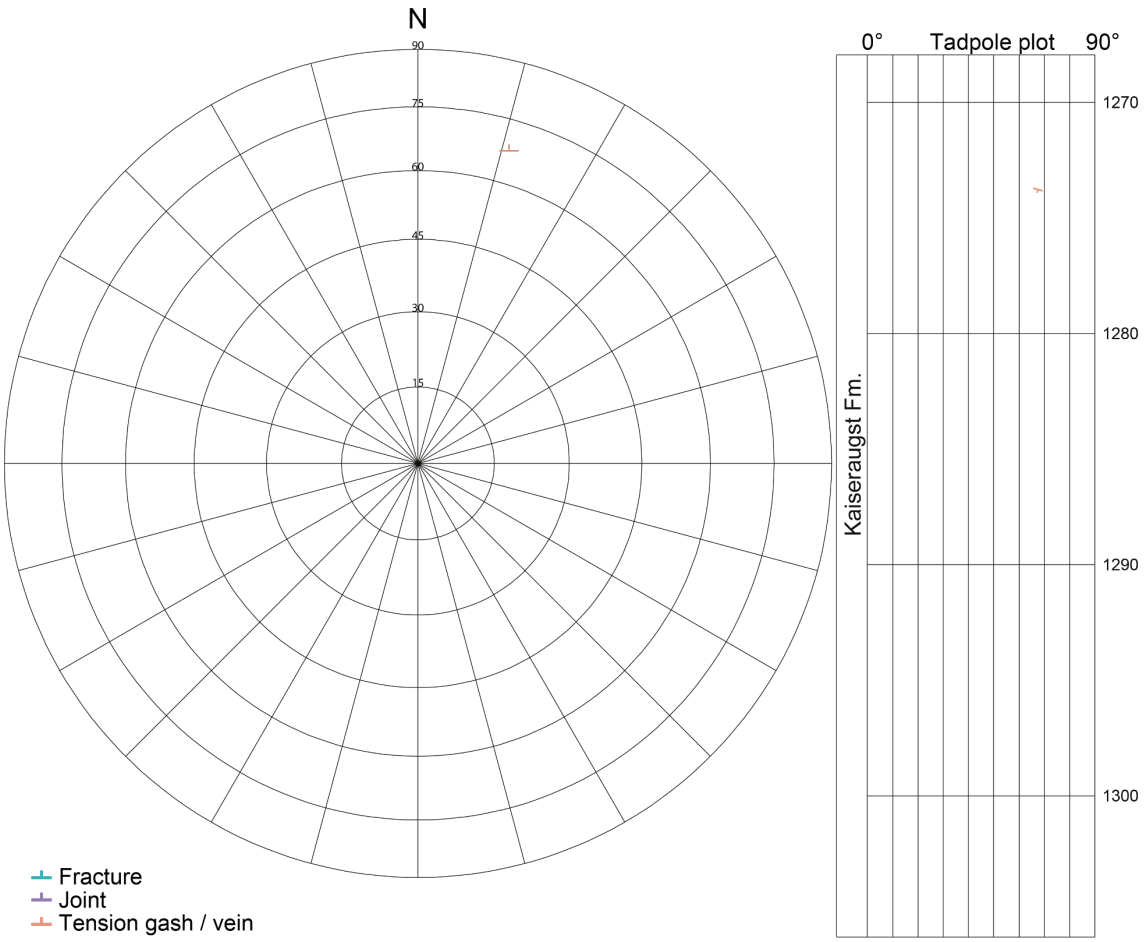

Fig. 4-84: Stereogram and depth plot of fractures, tension gashes / veins and joints (Kaiseraugst Formation)

Fractures (n = 0), joints (n = 0) and tension gashes / veins (n = 1).

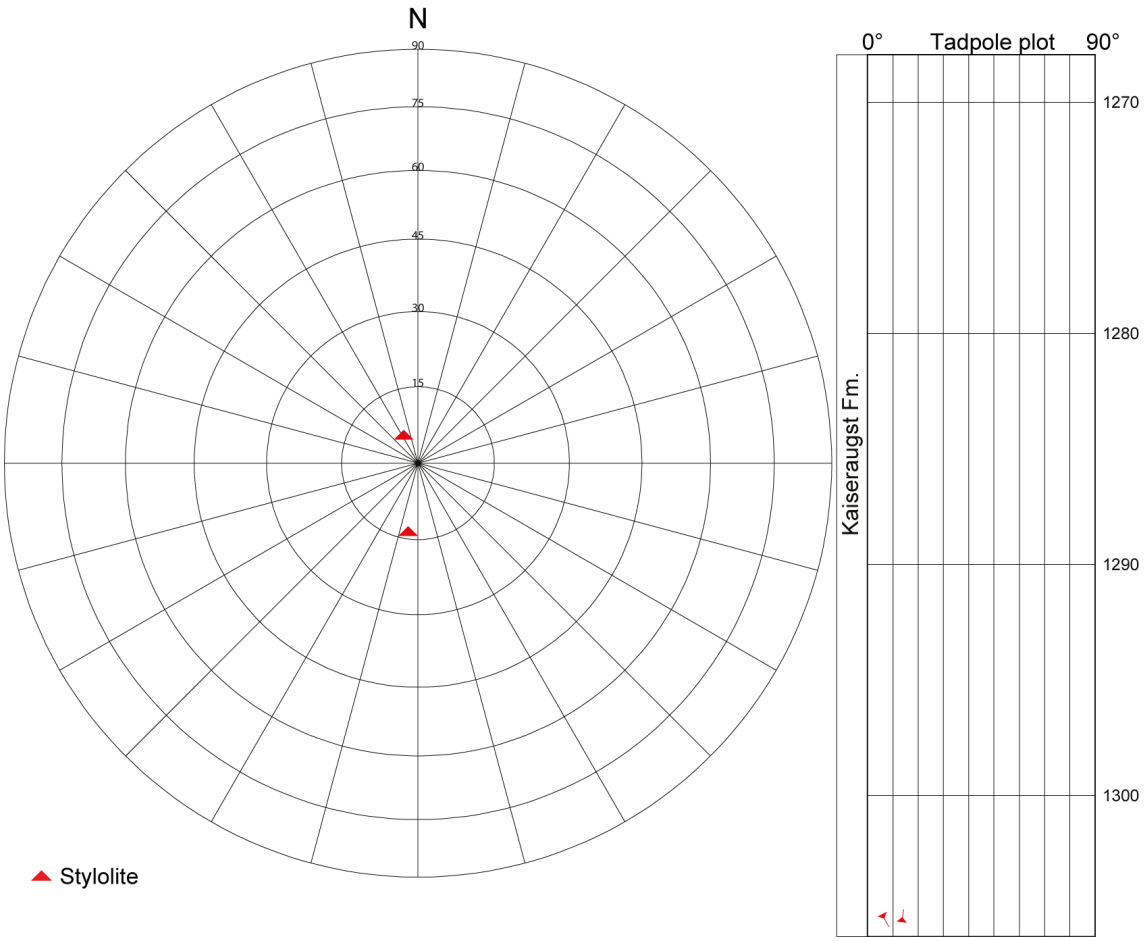

Fig. 4-85: Stereogram and depth plot of stylolites (Kaiseraugst Formation, n = 2)

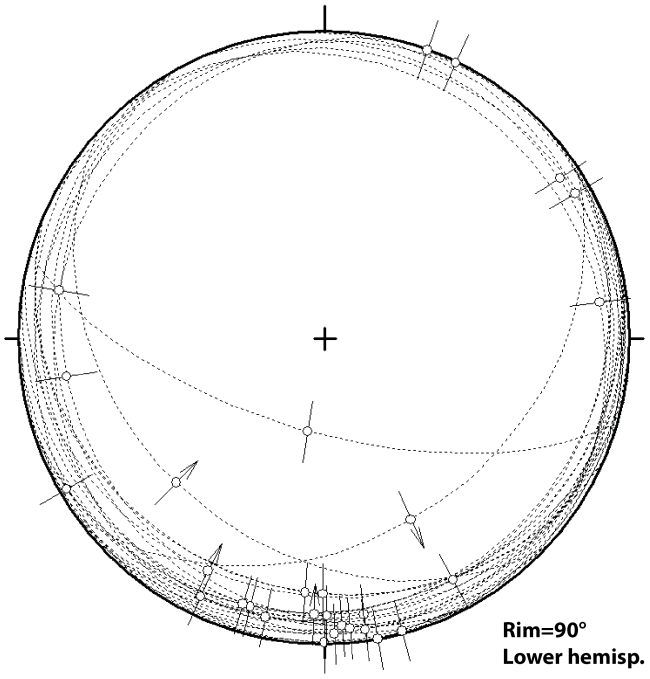

Fig. 4-86: Stereogram of fault planes (Kaiseraugst Formation, n = 29)

4.7 Buntsandstein and Rotliegend (Early Triassic to Permian, Dinkelberg Formation to Weitenau Formation)

The Early Triassic and the Permian (1'306.11 – 1'370.14 m MD log depth) were merged for a detailed stereographic evaluation. They depict borehole intervals with few structures. The Buntsandstein exhibits a horizontal structural dip, whereas the Permian is capped by an angular unconformity at 1'319.46 m MD log depth.

There is a distinct fault zone within the Weitenau Formation from 1'362.13 to 1'363.05 m MD log depth, characterised by almost exclusively mirror-like fault planes associated with 2 – 55° dip angles and dip-parallel slips. Contrary to the Mesozoic, the Triassic and Permian faults mainly dip towards the N and NNW as presented in Figs. 4-87 to 4-91. Only the data for oriented cores are presented. Due to the low number of fractures, joints and tension gashes / veins (n = 1) and stylolites (n = 3), rose diagram statistics were not calculated.

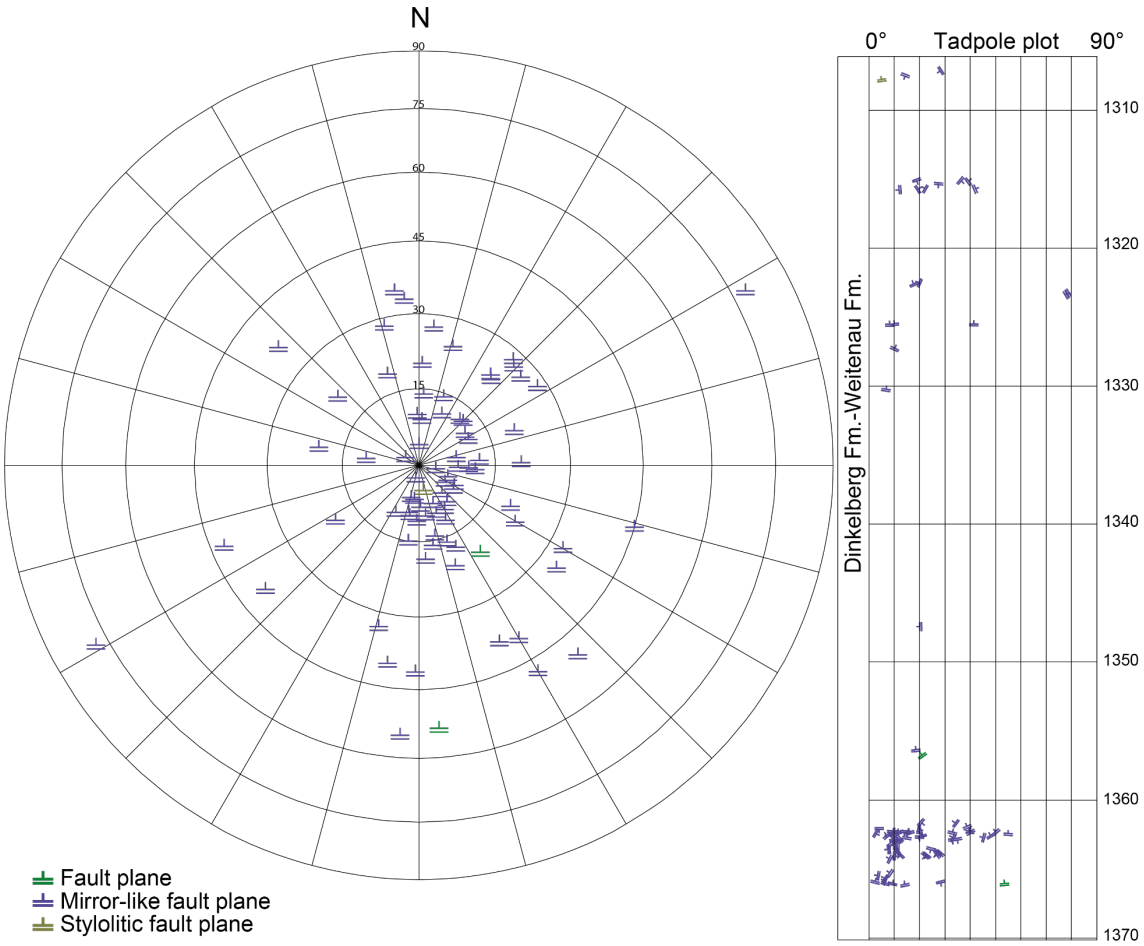

Fig. 4-87: Stereogram and depth plot of fault planes (Dinkelberg Formation to Weitenau Formation)

Fault planes (n = 2), mirror-like fault planes (n = 80) and stylolitic fault planes (n = 1).

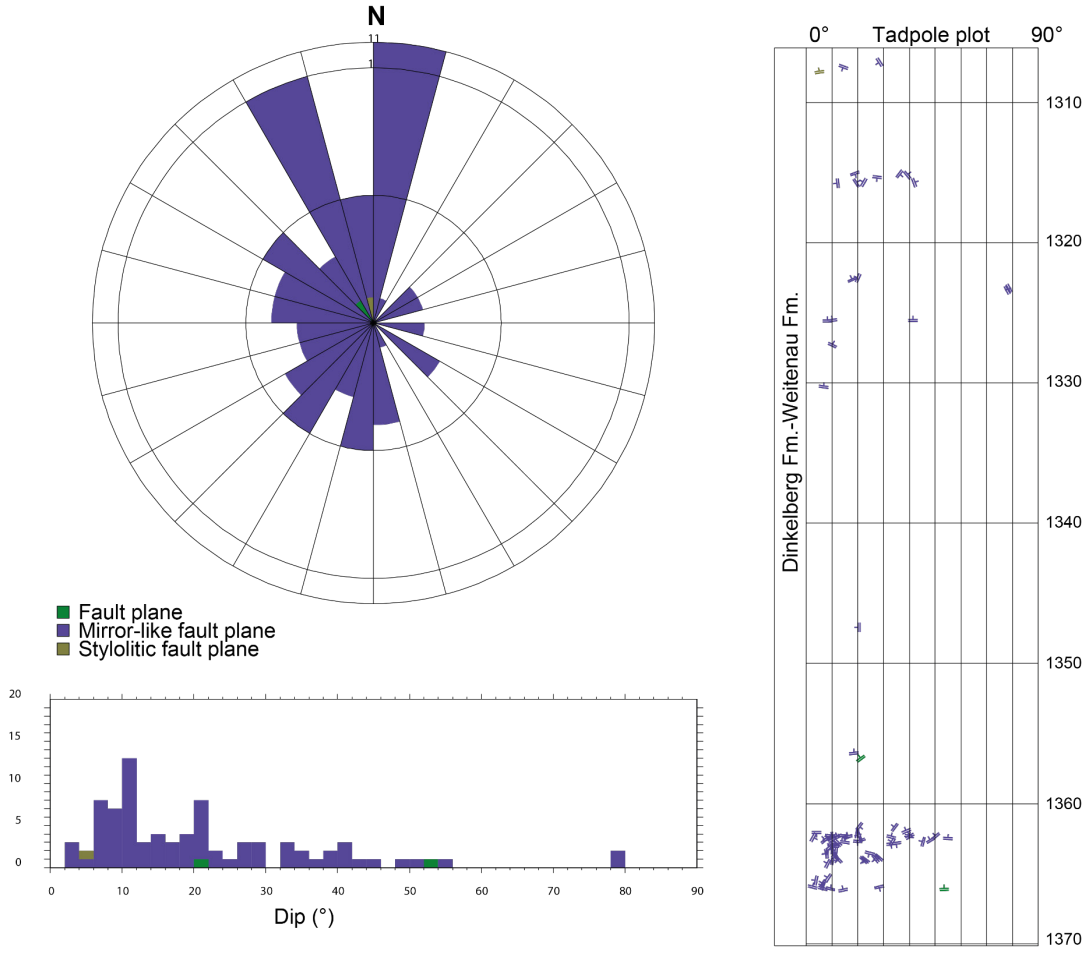

Fig. 4-88: Azimuth rose diagram, dip histogram and depth plot of fault planes (Dinkelberg Formation to Weitenau Formation)

Fault planes (n = 2), mirror-like fault planes (n = 80) and stylolitic fault planes (n = 1).

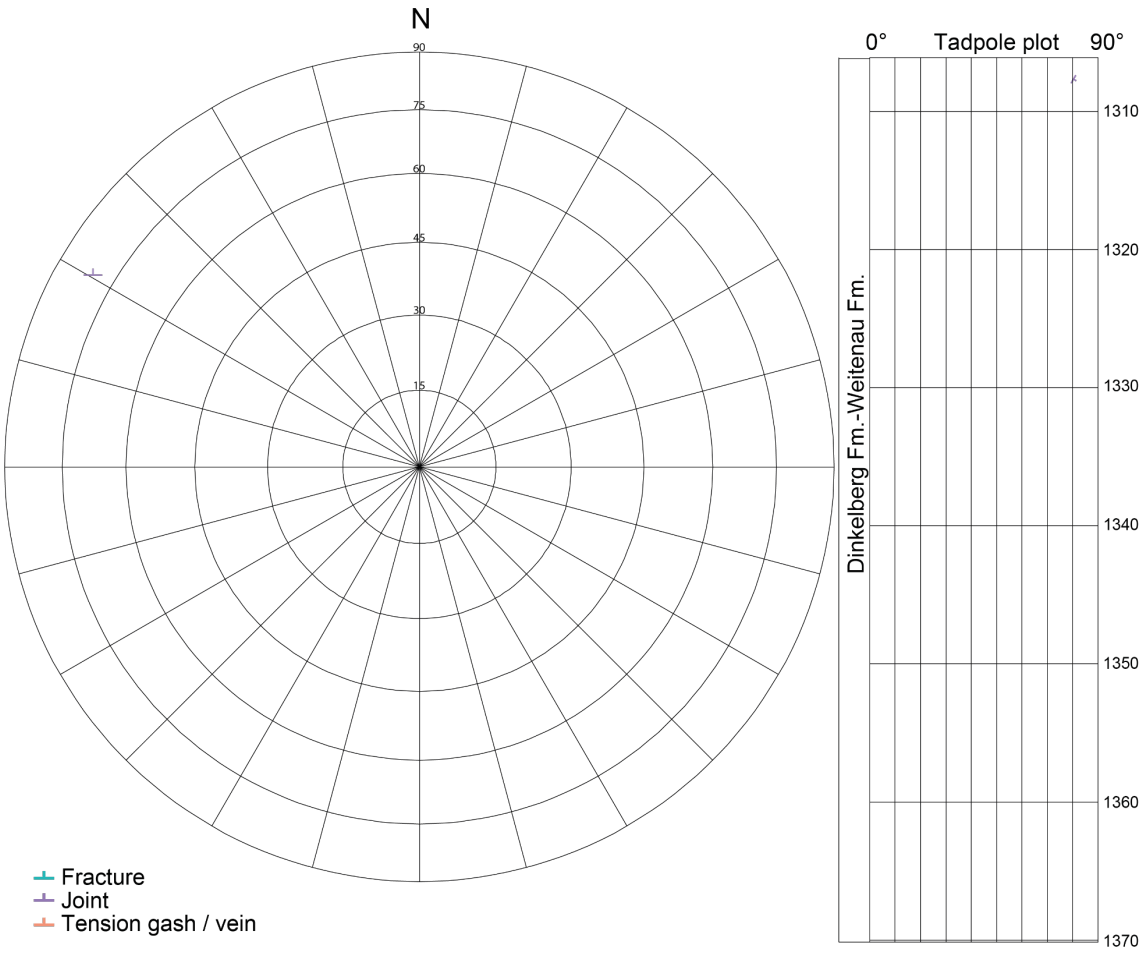

Fig. 4-89: Stereogram and depth plot of fractures, tension gashes / veins and joints (Dinkelberg Formation to Weitenau Formation)

Fractures (n = 0), joints (n = 1) and tension gashes / veins (n = 0).

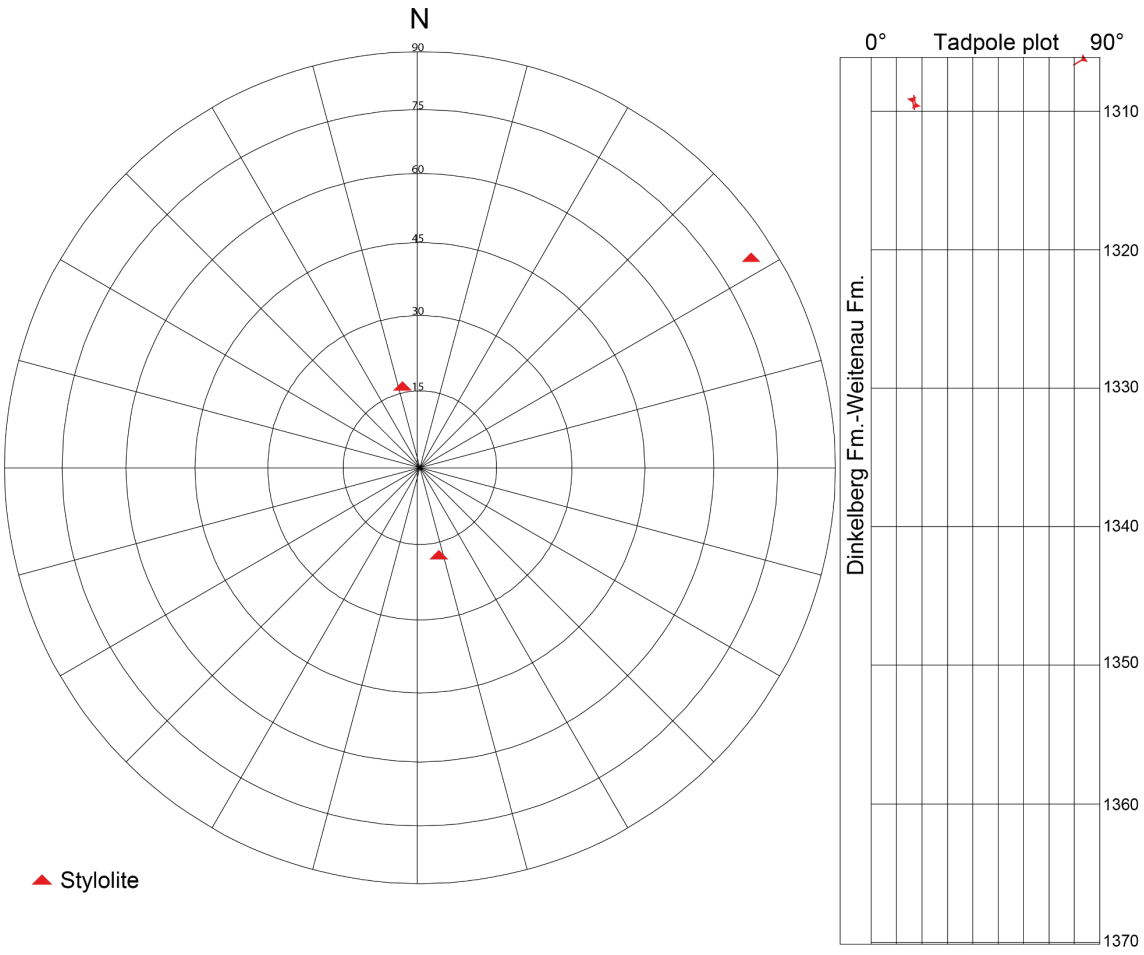

Fig. 4-90: Stereogram and depth plot for stylolites (Dinkelberg Formation to Weitenau Formation, n = 3)

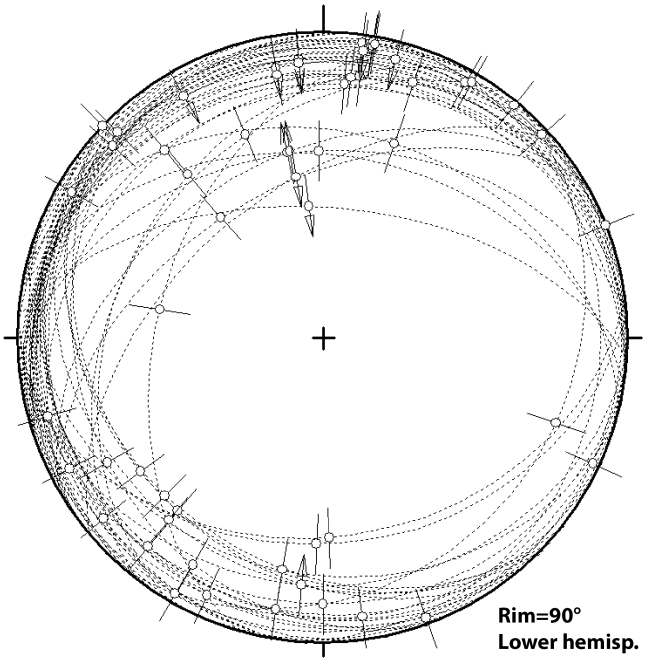

Fig. 4-91: Stereogram of fault planes (Dinkelberg Formation to Weitenau Formation, n = 75).

5 Main structural findings

As presented in Chapters 2 and 4 there were several structural geological features within the interval from 535 to 1'370.14 m MD log depth. Three particularly prominent tectonic zones deserve a more detailed examination and are discussed below.

5.1 Fault zone within the «Felsenkalke» / «Massenkalk»

A distinct fault zone was penetrated in the uppermost borehole interval from 537.66 to 554.0 m MD log depth and clearly correlated with image log data. In drill cores this zone was characterised by dense fracturing on a cm- to dm-scale and partly disintegrated rock with associated fracture density classes 3 and 4 (Fig. 5-1). This interval revealed the highest fracture densities recorded in BUL1-1 and BUL1-1B, with up to 32 faults per metre (P32 = 16.7 m^2/m^3).

Most structures within the fault zone were fault planes (n = 115) followed by stylolitic fault planes (n = 17) and mirror-like fault planes (n = 7). Some observed faults were mineralised with syn-kinematic, often fibrous calcite (up to 1 cm thick; Fig. 5-1). Many faults were detected within the several dm thick, brownish, clayey to silty paleo-karst filling with iron-ooids (Siderolithic; Fig. 5-1). This zone was also associated with brecciated textures. Angular to sub-rounded limestone clasts (cm- to dm-scale) and multi-faced lineations were also common (Fig. 5-1). The limestone walls at the contact to the brownish matrix were smoothly undulating with rough, dissolution-like surfaces and were coated by a fine layer of dark brown clay. This might have been related to dissolution processes (karstification). Some faults were also associated with sub-parallel stylolitic dissolution seams as exemplified in Fig. 5-1.

The upper and lower boundaries of the fault zone showed an abrupt change in fault orientation. While sub-horizontal to inclined (2 – 30°) S-dipping faults occurred at the top and bottom, predominantly moderately inclined to sub-vertical (20 – 80°) NE and SSW dipping faults characterised the fault zone itself (Figs. 5-2, 5-3 and 5-4).

Striations were common along fault planes. In total, 80 kinematic indicators were measured (Figs. 5-5 and 5-6). However, shear senses were determined only for 31 faults and were almost exclusively associated with S- and N-dipping thrusts / reverse faults (n = 30).

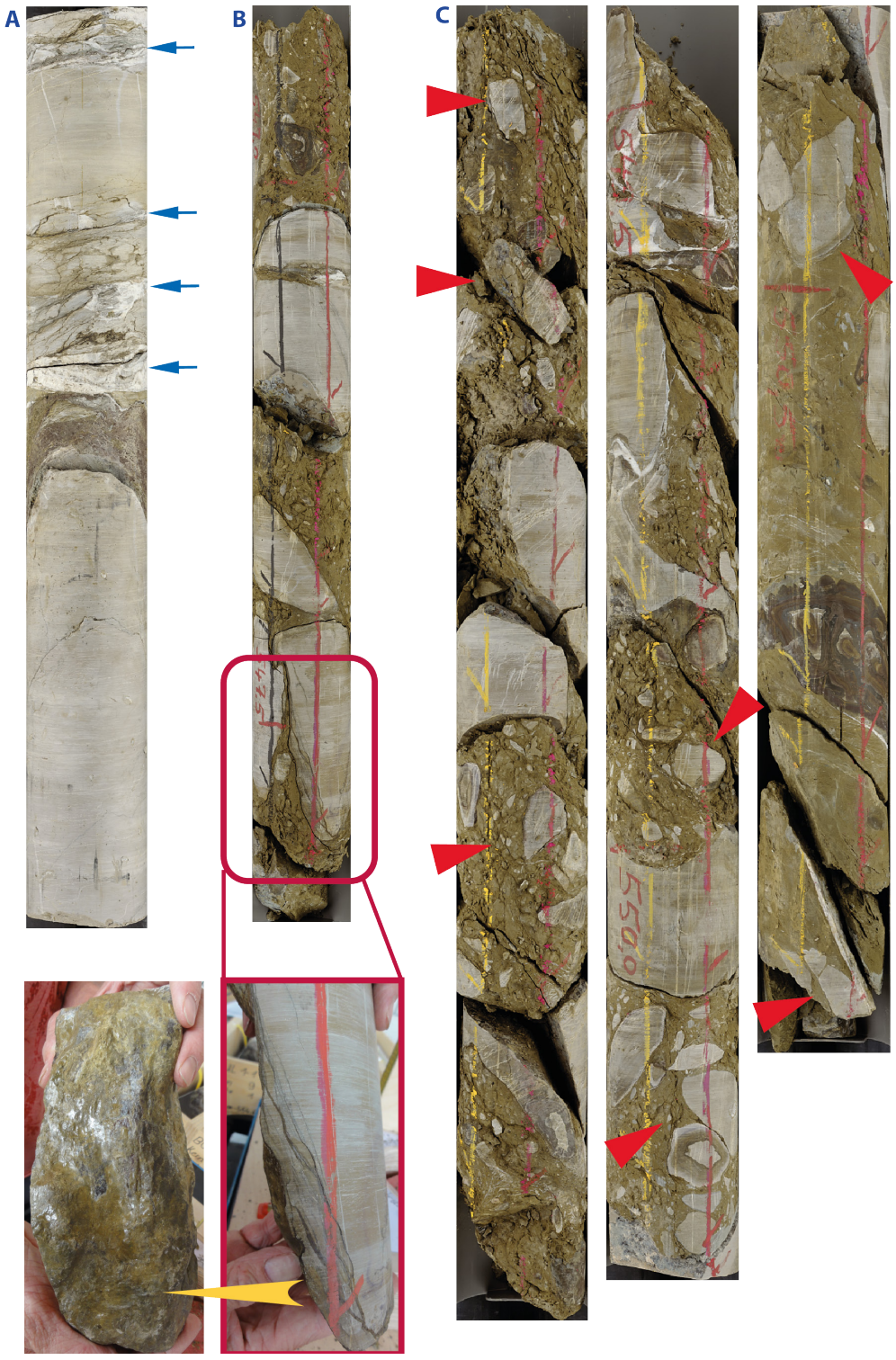

Fig. 5-1: Structures observed in cores within the fault zone

(A) Discrete fault planes (blue arrows) with synkinematic calcite mineralisation (537.62 – 538.32 m MD core depth). (B) Steep fault plane associated with sub-parallel stylolitic reaction seams and undulated surface (546.88 – 547.71 m MD core depth) . (C) Fault gouge and / or Siderolithic with abundant clasts (red arrows) (548.59 – 549.42, 549.42 – 550.31 and 550.31 – 551.00 m MD core depth).

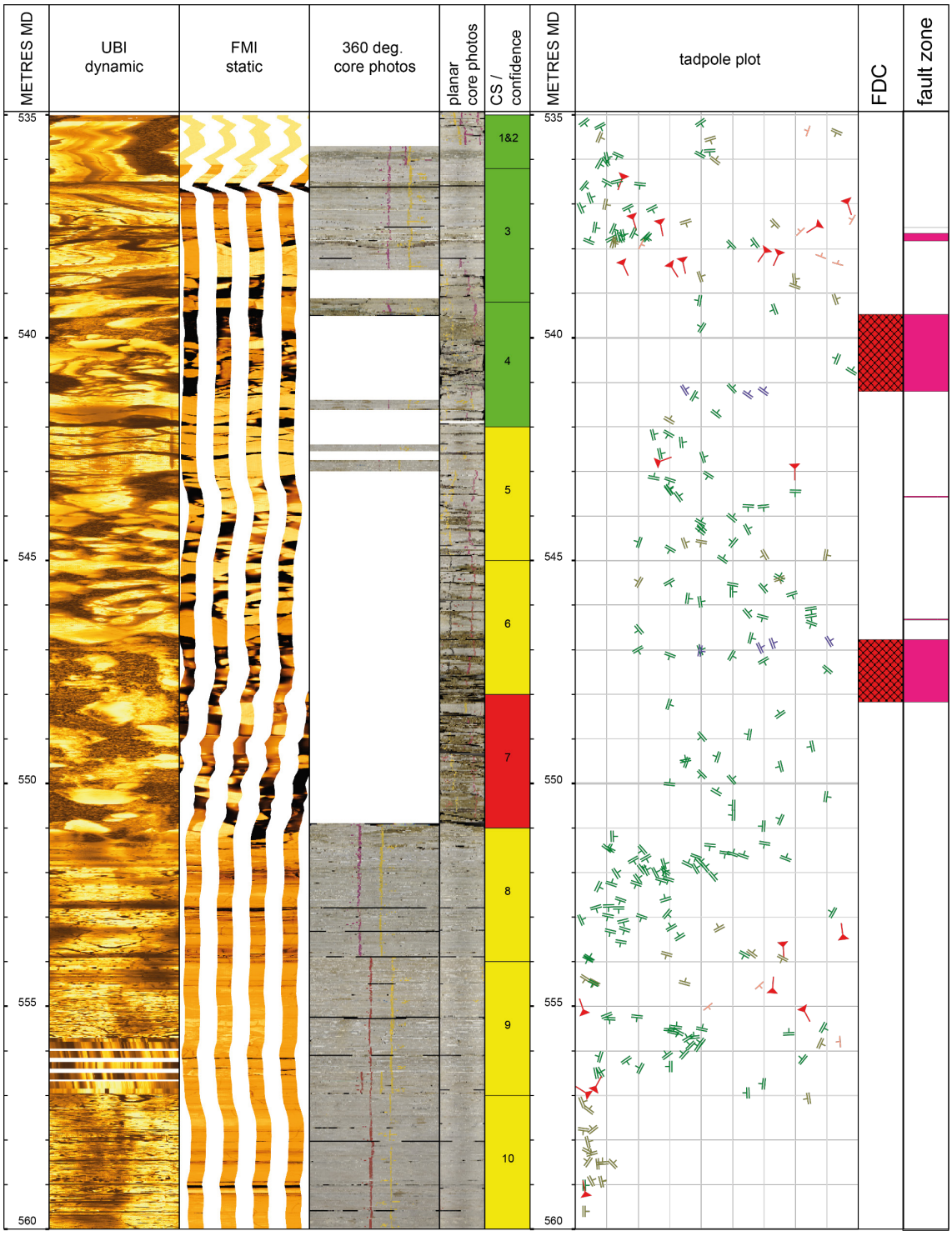

Fig. 5-2: Structural overview plot for the from 535 – 560 m MD log depth

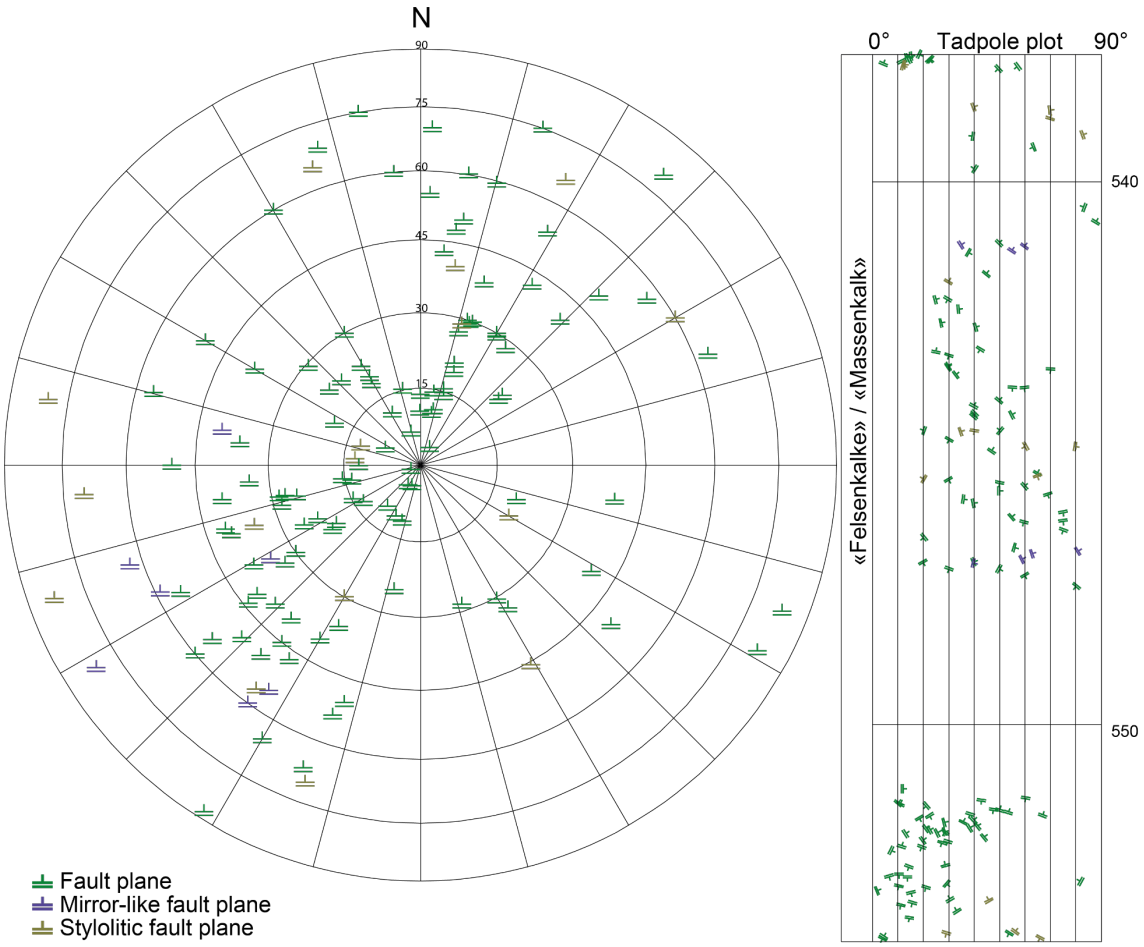

Fig. 5-3: Stereogram and depth plot of fault zone from 537.66 to 554.00 m MD log depth

Fault planes (n = 112), mirror-like fault planes (n = 7) and stylolitic fault planes (n = 17).

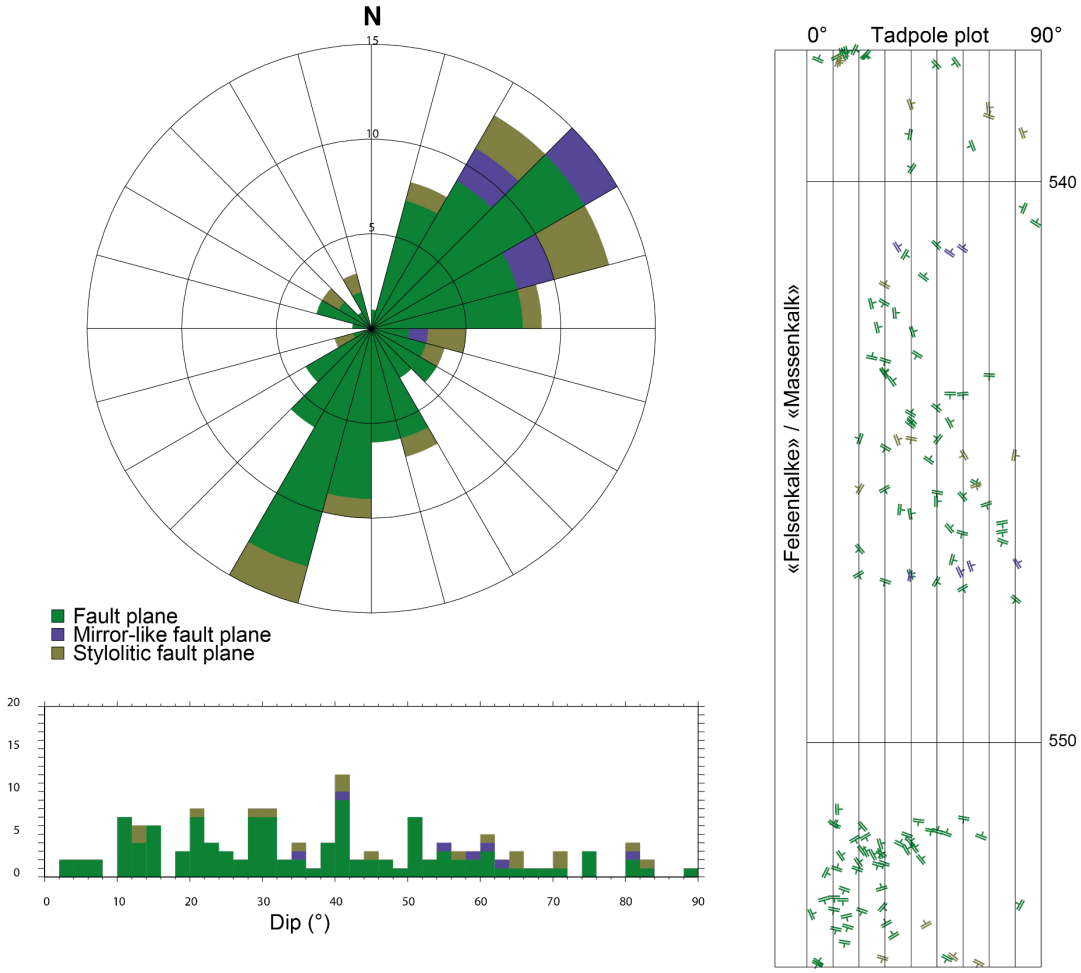

Fig. 5-4: Azimuth rose diagram and dip histogram for the fault zone from 537.66 to 554.00 m MD log depth

Note the predominance of NE and SSW azimuths. Fault planes (n = 112), mirror-like fault planes (n = 7) and stylolitic fault planes (n = 17).

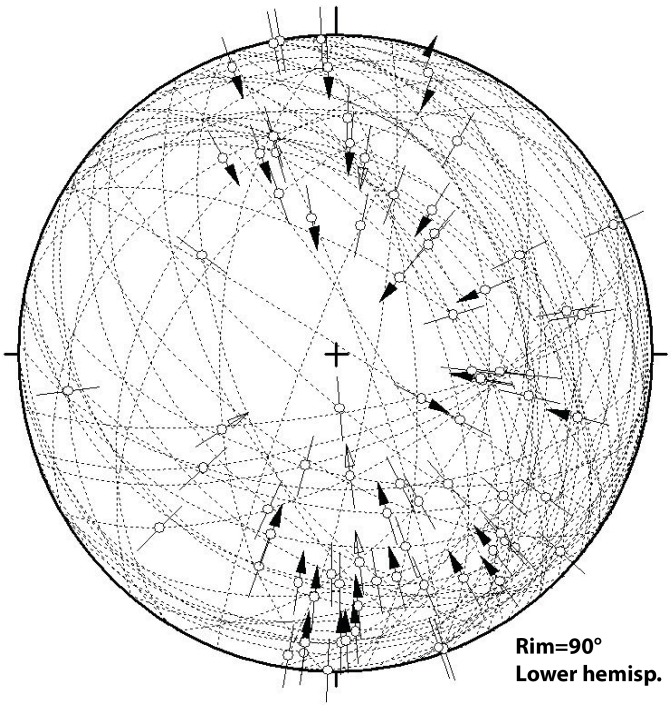

Fig. 5-5: Stereogram of fault planes in the fault zone from 537.66 to 554.00 m MD log depth

Up (n = 30), dextral (n = 1) and unknown (n = 49).

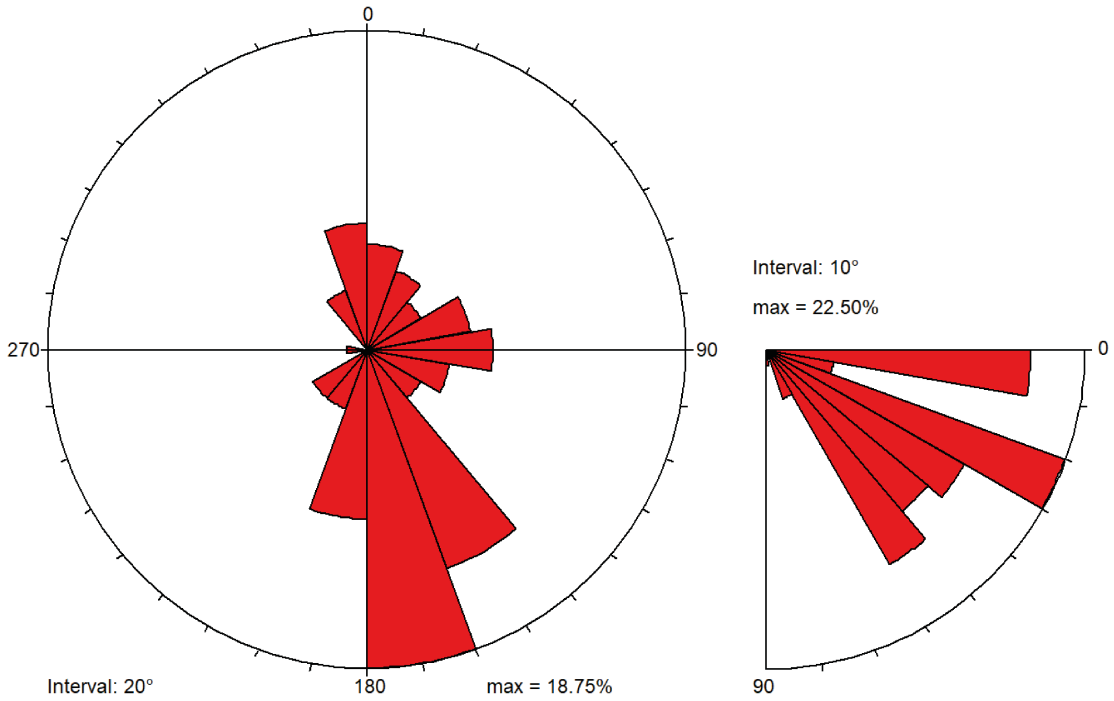

Fig. 5-6: Azimuth rose diagram and dip histogram for striations in the fault zone from 537.50 to 554.00 m MD log depth

Depth range is 537.5 – 554 m MD, n = 80.

5.2 Faulting within the 'Brauner Dogger'

Two thin (35 cm and 7 cm) fault zones were interpreted within the 'Brauner Dogger' from 890.02 to 890.37 m MD log depth and from 890.71 to 890.83 m MD log depth. Despite their small thickness they are relevant due to their proximity to the upper boundary of the Opalinus Clay located 1 m below at 891.75 m MD log depth.

The fault zones were characterised by fracturing and core disintegration corresponding to fracture density classes 2 (Figs. 5-7 and 5-8). The cores showed a complex network of intersecting mirror-like fault planes as well as fault planes associated with synkinematic calcite mineralisation (Fig. 5-8).

The cores could not be oriented at this depth level (Fig. 5-7), thus a directional analysis was impossible. However, the faults had mainly sub-horizontal to shallow (2 – 25°) dip angles and commonly revealed striations with dominant dip parallel slip, most likely linked to a thrusting / reverse faulting stress regime (Fig. 5-8).

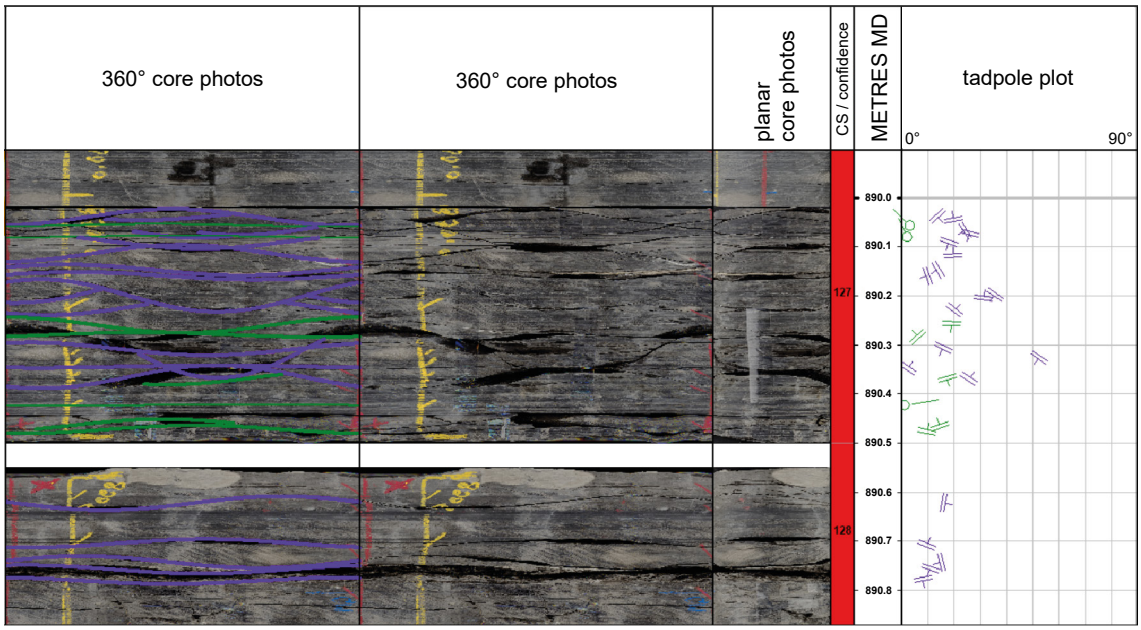

Fig. 5-7: Core scan example for fault zones in the 'Brauner Dogger'

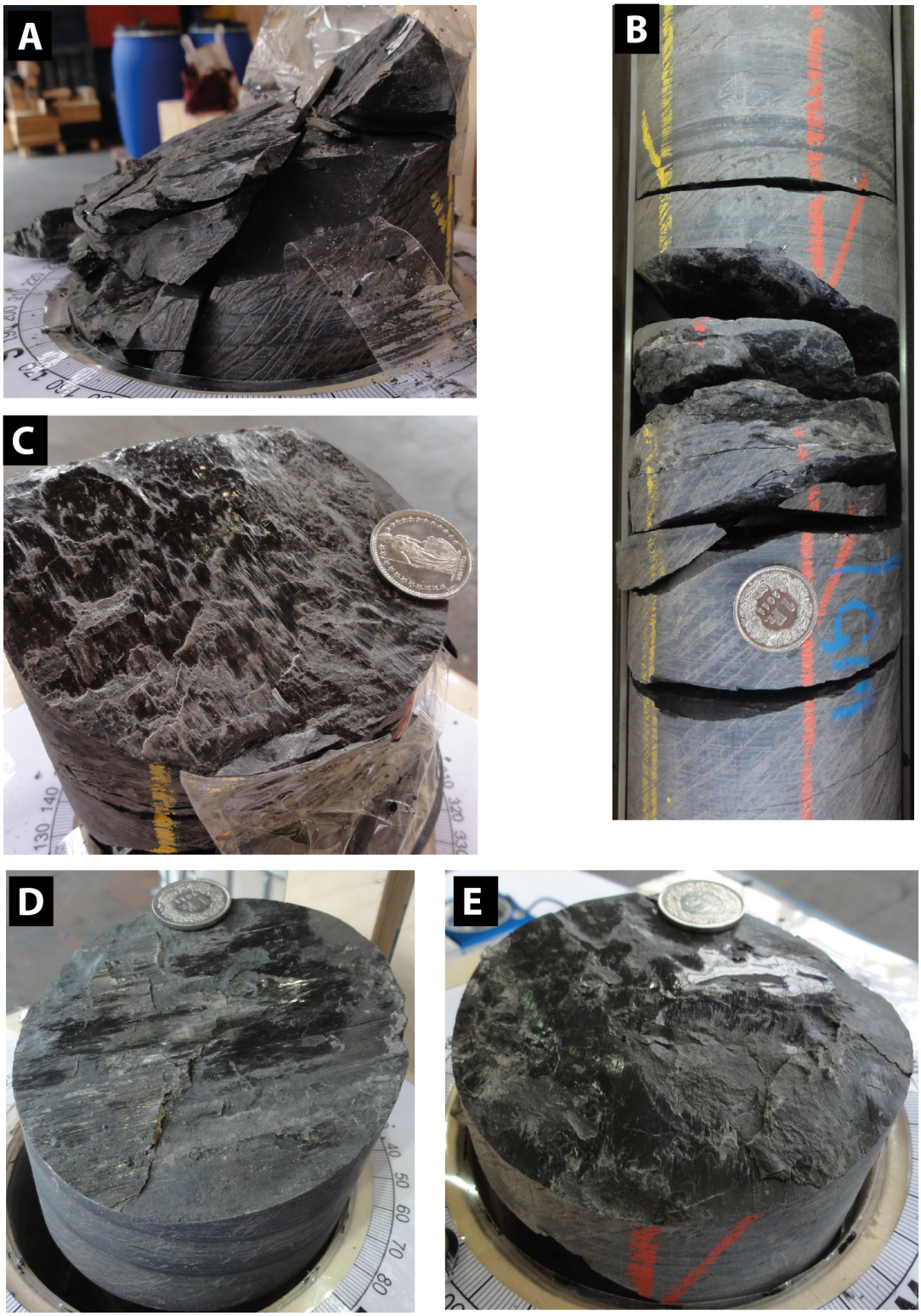

Fig. 5-8: Fault zone within the 'Brauner Dogger' observed in cores

(A and B) Disintegrated core due to abundant fracturing. (C and D) Low-angle faults with synkinematic calcite mineralisation and shear senses suggesting upward movements. (E) Low-angle mirror-like fault.

5.3 The deformed Zeglingen Formation

Indications of a deformation zone were observed within the Zeglingen Formation («Obere Sulfatzone», «Salzlager» and «Untere Sulfatzone») from 1'219 m to 1'267 m MD log depth. The zone mainly comprised anhydrite with thin intercalations of claystone. The zone also hosted a 15 m thick salt layer in the depth interval from 1'245.76 to 1'260.37 m MD log depth. This zone is illustrated in Figs. 5-9 and 5-10 along with graphic representations of the observed structures. However, it is possible that some fault planes may not have been recognised during the structural analysis and are therefore not included in the graphs and data, because the fault planes (in particular mirror-like fault planes) were only recognised on disintegrated cores, and the core was mainly intact in this interval.

Bedding

Adjacent to the deformation zone, the bedding was consistently plane-parallel with dips < 10° and dip directions roughly towards south (SE-SW). In the «Dolomitzone» the bedding was made of stromatolitic lamination.

In the depth interval from 1'223 m to 1'267 m MD log depth, the bedding orientation was variable. Within the anhydrite layers metres-thick sections with a generally sub-horizontal bedding (dipping 5 – 15° towards SE-SW) alternated with up to a few dm-thick layers with steeper and often folded bedding. The latter were characterised by varying dip angles with abrupt changes in dip angles of up to 30° with dominant dip directions to N or S. Currently, it is unclear whether these folds are of synsedimentary or tectonic origin.

The bedding in the salt layer was not visible. However, it cannot be excluded that some layering reflected a kind of "foliation" due to dynamic recrystallisation. In general, the layering of the «Salzlager» was sub-horizontal to moderately inclined (5 – 30°) with variable dip directions (mainly towards the south).

Deformation

A 15 m thick section above the deformation zone was free from deformation structures.

In the depth interval from 1'219 m to 1'237 m MD log depth, 11 fractures were observed. The subsequent section up to the top of the salt layer showed a high fracture density (36 fractures from 1'337 to 1'245 m MD log depth). In both sections, the fractures were either fault planes or mirror-like fault planes. They had variable dip directions with dominant dip angles between 5 – 30°. On nearly all fault planes, lineation (striation or slickenfibres) was present. The striation was dominantly oriented in a N-S direction with a general dip of 5 – 30°. Shear sense was mostly top-to-north. Within the fracture-rich zone, a few cm- to dm-sized folds with sub-horizontal fold axes in N-S and E-W directions were visible. Some of them had shapes of box-folds. Some folds within the anhydrite layers represented fault-propagation folds with reverse fault displacements of around 1 cm and N-S oriented lineation. Dynamic recrystallisation reflects the main deformation mechanism within the salt. It was documented by dm- to m-thick layers of fine and elongated salt grains alternating with partly recrystallised layers with sigma-clasts indicating a northward shear direction. Intercalated, weakly recrystallised layers were represented by cm-sized blocky salt crystals. The long axis of the elongated salt crystals indicated a sub-horizontal lineation facing S-SW. The subsequent anhydrite layer («Untere Sulfatzone») showed similar structural elements to the ones above the salt. However, this layer showed a lower fracture density but a higher variability in orientations of the structures. The fracture planes generally dip from S to W with variable dip angles between 5° and 50°. The «Wellenmergel» showed a lower structural overprint with few sub-horizontal mirror-like fault planes.

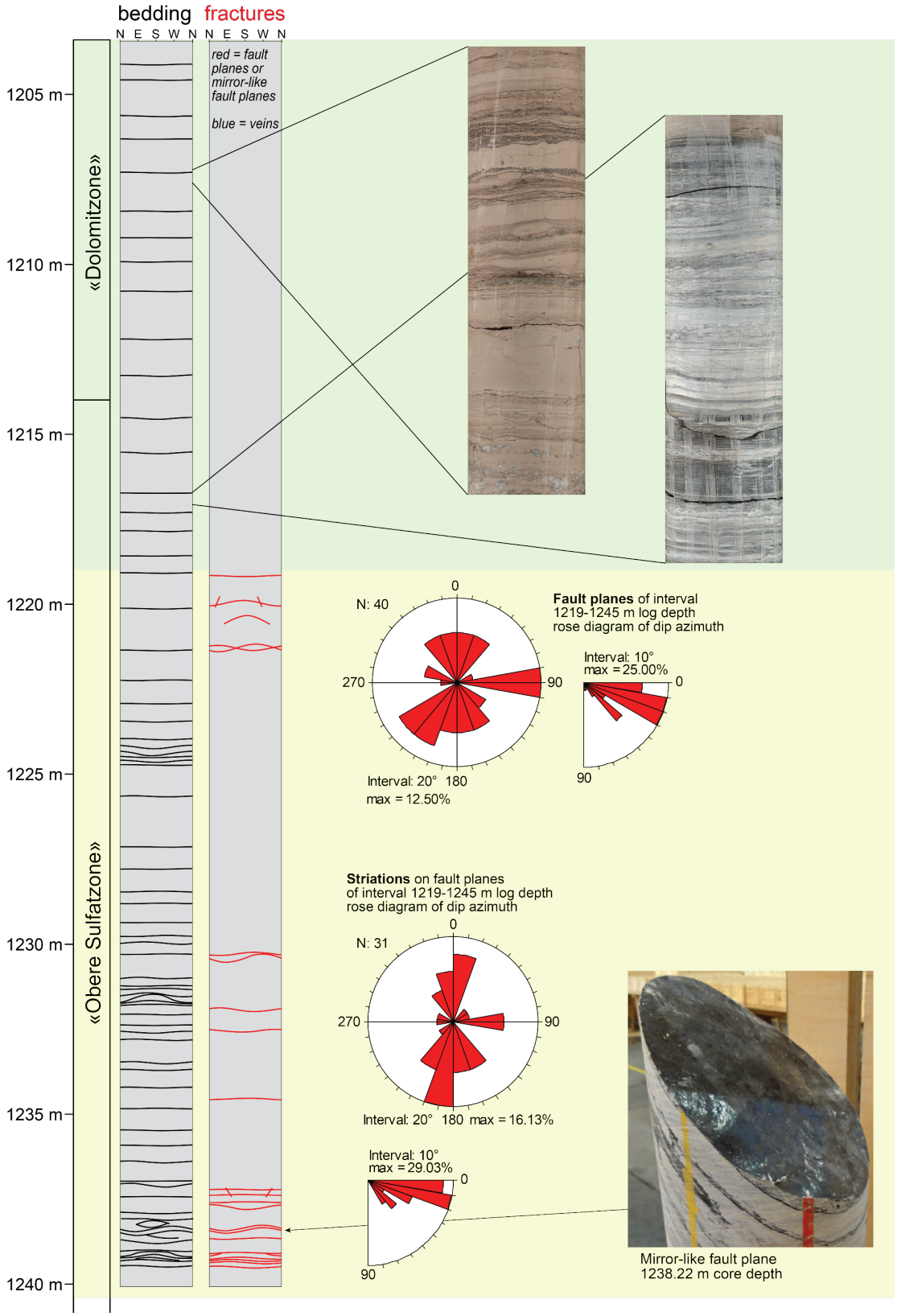

Fig. 5-9: Schematic structural overview of the Zeglingen Formation (1'205 – 1'240 m MD log depth)

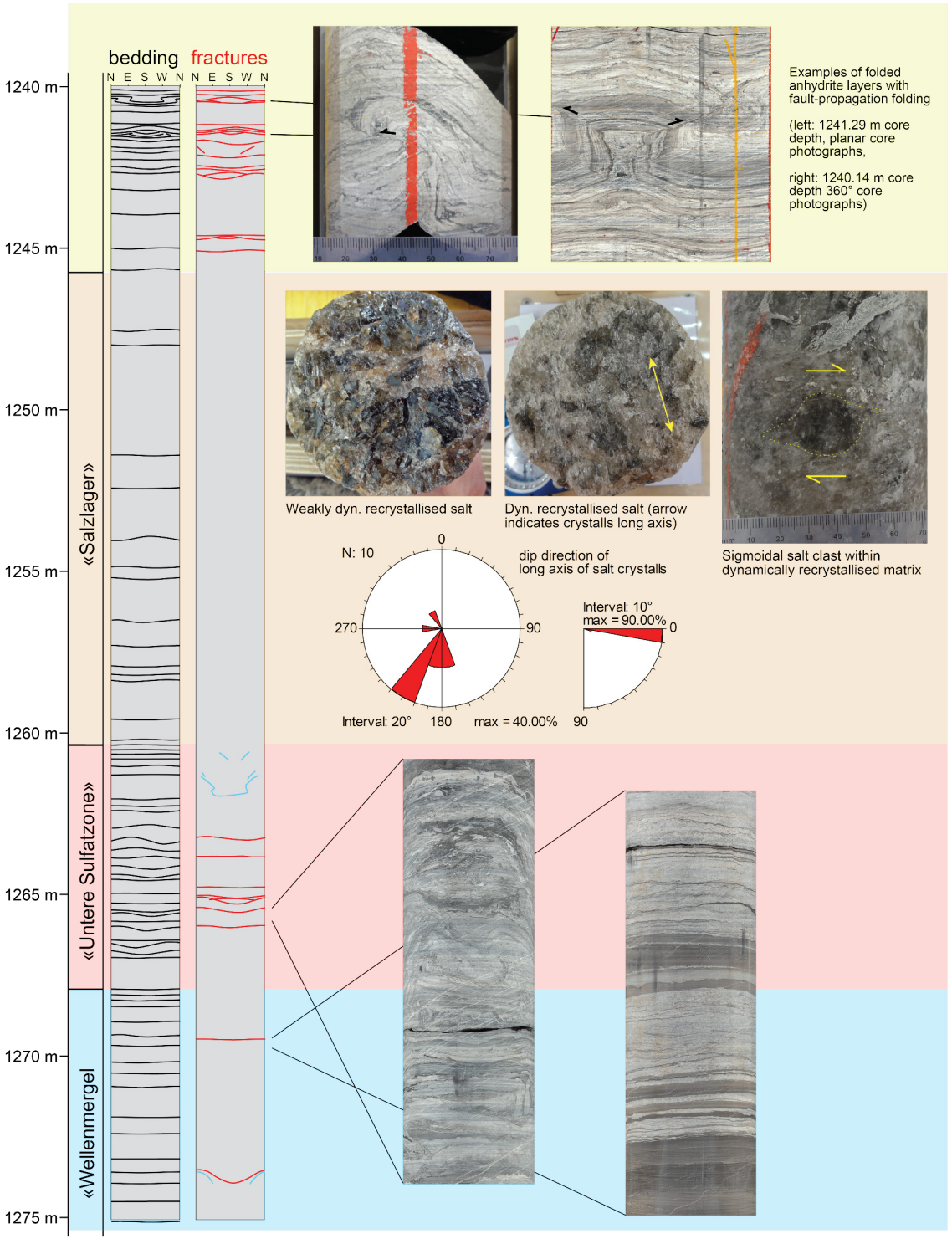

Fig. 5-10: Schematic structural overview of the Zeglingen Formation (1'240 – 1'275 m MD log depth)

6 References

Barton, N. (1976): The shear strength of rock and rock joints. Int J Rock Mech Min Sci & Geomech Abstr 13/9, 255-279.

Barton, N. & Choubey V. (1977): The shear strength of rock joints in theory and practice. Rock mechanics 10/1-2, 1-54.

Bauer, H., Schröckenfuchs, T. & Decker, K. (2016): Hydrogeological properties of fault zones in a karstified carbonate aquifer (Northern Calcareous Alps, Austria). Hydrogeology Journal 24, 1147-1170.

Hancock, P.L. (1985): Brittle microtectonics: Principles and practice. J. Structural Geology 7/3-4, 437-457.

Isler, A., Pasquier, F. & Huber, M. (1984): Geologische Karte der zentralen Nordschweiz 1:100'000. Herausgegeben von der Nagra und der Schweiz. Geol. Komm.

Ebert, A. & Decker, K. (2019): Structural Analysis Manual. Nagra Arbeitsbericht NAB 19-12.

Nagra (2014): SGT Etappe 2: Vorschlag weiter zu untersuchender geologischer Standortgebiete mit zugehörigen Standortarealen für die Oberflächenanlage. Geologische Grundlagen. Dossier II: Sedimentologische und tektonische Verhältnisse. Nagra Technischer Bericht NTB 14-02.

Passchier, C.W. & Trouw, R.A.J. (1996): Microtectonics. Springer, 289 pp.

Peacock, D.C.P. et al. (2016): Glossary of fault and other fracture networks. J. Structural Geology 92, 12-29.

Pietsch, J. & Jordan, P. (2014): Digitales Höhenmodell Basis Quartär der Nordschweiz – Version 2013 (SGT E2) und ausgewählte Auswertungen. Nagra Arbeitsbericht NAB 14-02.